Experimental Characterisation of Body-Centric Radio Channels Using Wireless Sensors

Max O. Munoz Torrico

A thesis submitted to the faculty of the University of London in partial fulfilment of the requirements for the degree of

Doctor of Philosophy

School of Electronic Engineering and Computer Science,
Queen Mary, University of London
London E1 4NS, United Kingdom

September 2012

To my Family

Abstract

Wireless sensors and their applications have become increasingly attractive for industry, building automation and energy control, paving the way for new applications of sensor networks which go well beyond traditional sensor applications. In recent years, there has been a rapid growth in the number of wireless devices operating in close proximity to the human body. Wearable sensor nodes are growing popular not only in our normal living lifestyle, but also within healthcare and military applications, where different radio units operating in/on/off body communicate pervasively. Expectations go beyond the research visions, towards deployment in real-world applications that would empower business processes and future business cases.

Although theoretical and simulation models give initial results of the antenna behaviour and the radio channel performance of wireless body area network (WBAN) devices, empirical data from different set of measurements still form an essential part of the radio propagation models. Usually, measurements are performed in laboratory facilities which are equipped with bulky and expensive RF instrumentation within calibrated and controllable environments; thus, the acquired data has the highest possible reliability. However, there are still measurement uncertainties due to cables and connections and significant variations when designs are deployed and measured in real scenarios, such as hospitals wards, commercial buildings or even the battle field.

Consequently, more flexible and less expensive measurement tools are required. In this sense, wireless sensor nodes offer not only easiness to deploy or flexibility, but also adaptability to different environments. In this thesis, custom-built wireless sensor nodes are used to characterise different on-body radio channels operating in the IEEE 802.15.4 communication standard at the 2.45 GHz ISM band. Measurement results are also compared with those from the conventional technique using a Vector

Network Analyser. The wireless sensor nodes not only diminished the effect of semi-rigid or flexible coaxial cables (scattering or radiation) used with the Vector Network Analyser (VNA), but also provided a more realistic response of the radio link channel. The performance of the wireless sensors is presented over each of the 16 different channels present at the 2.45 GHz band.

Additionally, custom-built wireless sensors are used to characterise and model the performance of different on-body radio links in dynamic environments, such as jogging, rowing, and cycling. The use of wireless sensors proves to be less obstructive and more flexible than traditional measurements using coaxial cables, VNA or signal generators. The statistical analysis of different WBAN channels highlighted important radio propagation features which can be used as sport classifiers models and motion detection.

Moreover, specific on-body radio propagation channels are further explored, with the aim to recognize physiological features such as motion pattern, breathing activity and heartbeat. The time domain sample data is transformed to the frequency domain using a non-parametric FFT defined by the Welch's periodogram. The Appendix-Section D explores other digital signal processing techniques which include spectrograms (STFT) and wavelet transforms (WT). Although a simple analysis is presented, strong DSP techniques proved to be good for signal de-noising and multi-resolution analysis.

Finally, preliminary results are presented for indoor tracking using the RSS recorded by multiple wireless sensor nodes deployed in an indoor scenario. In contrast to outdoor environments, indoor scenarios are subject to a high level of multipath signals which are dependent on the indoor clutter. The presented algorithm is based on path loss analysis combined with spatial knowledge of each wireless sensor.

Acknowledgements

First and foremost I would like to express my gratitude to my supervisor, Prof. Yang Hao for his supervision, advice and guidance throughout this research project. His encouragement and support has enabled me to grow as a student as well as a researcher. Without his constant help and motivation this thesis would not have been possible. Also thanks to Mr. John Dupuy for his patience and assistance with RF instrumentation and antenna fabrication.

Additionally, I would like to thank to Prof. Clive Parini and the School of Electronic Engineering and Computer Science for giving me the opportunity to complete my Ph.D. studies in the antenna research group in Queen Mary, University of London.

I would also like to thank my colleagues Dr. Anestis Katsounaros, Dr. Robert Foster and Dr. Andrea Sani for their friendship, willingness to help and their input from a very early stage of my Ph.D., as well as for their fruitful comments which has been a vital part of this work not only research wise, but also every aspect of my Ph.D.

Throughout my Ph.D. studies, I have been surrounded by, not only colleagues, but also valuable friends: Dr. Rhiannon Mitchell-Thomas, Mr. Jiefu Zhang and Ms. Berit Greinke. My deepest gratitude to you all for making our office a comfortable place to work!

Above all, I would like to thank my family (Schirley and Andrew), and especially my parents, Faustino and Alejandrina, for all their love, encouragement and spiritual support. It is maybe the best place to say thank you for all that they have given up for me to be and study in the United Kingdom.

Contents

Abstract ..... **i**

Acknowledgements ..... **iii**

Contents ..... **iv**

List of Figures ..... **vii**

List of Tables ..... **xvi**

Abbreviations ..... **xviii**

Publication List ..... **xx**

Introduction **21**

1.1. Research Scope and Applications 22
1.2. Research Objectives 25
1.3. Thesis Outline 27

Wireless Technologies for Body-Centric Networks **29**

2.1. WPAN Standards 30

2.1.1. Bluetooth 32
2.1.2. Bluetooth Low-Energy (BLE) 33
2.1.3. ZigBee 33

2.2. BLE or ZigBee for WBAN Applications 35
2.3. IEEE 802.15 Task Group 6 (TG6) – WBAN standard 37
2.4. Radio Propagation and Antennas for WBAN communications 40
2.5. Fundamental Parameters of Propagation Models 40

2.5.4. On-Body Radio Channel Modelling 43

2.6. Electromagnetic Properties of the Human Tissues 45
2.7. Antennas for Body-Centric Communications 49
2.8. Optimised Antennas for WBAN operation 52
2.9. Discussion and Conclusion 54

Design and Development of Body-Centric Wireless Sensors using the IEEE 802.15.4 Standard **56**

3.1. Understanding the IEEE 802.15.4 standard 57
3.2. Engineering wearable sensors for WBAN communications 60

3.2.1. Antenna Impedance Matching 63
3.2.2. Antenna Design and Manufacturing 65
3.2.3. Spectral Response of the transceiver modules and Performance of the wireless sensor nodes 68

3.3. Discussion and Conclusion 75

On-Body Channel Measurement using Wireless Sensors 76

4.1. On-Body Communications and Related Work 78
4.2. Measurement Procedures 80

4.2.1. First Measurement Setup 83
4.2.2. Second Measurement Setup 84

4.3. Data Processing 85

4.3.3. Path Loss Analysis 85
4.3.4. Cumulative Distribution Function 92

4.4. Discussion and Conclusion 95

Exploring Dynamic On-Body Radio Channels for Physiological Features 97

5.1. Measurement Procedure 98
5.2. Data Analysis 102

5.2.1. Characterisation of On-body Radio Channels for dynamic scenarios 102

5.3. Exploring On-Body Radio Channels for Embedded Physiological Features 108

5.3.2. Physiological Information Parameters 110
5.3.3. Frequency Analysis of Time-Domain Channel Data 113

5.4. Discussion and Conclusion 121

RF Positioning using Body-Centric Low-Power Wireless Sensors 122

6.1. Review of Wireless Positioning 123
6.2. Localization Techniques and Algorithms 125
6.3. RSS-based indoor location using low-power wireless sensors 128

6.3.1. First Experiment - Feasibility study using custom-built wireless sensors 128
6.3.2. Second Experiment using Commercial Wireless Modules Telos-B 132

6.4. Discussion and Conclusion 144

Conclusions and Future Work 145

7.1. Discussion and Conclusion 145
7.2. Key Contributions 147
7.3. Future Work 148

References.....150

Appendix A 160

Prototyping a Wireless Sensor Node 160

A.1. The microstrip patch antenna 160
A.2. CC2420 from Texas Instruments 162
A.3. Microcontroller board design and manufactured module 162
A.4. Radio transceiver (CC2420) board design and manufactured module. 163
A.5. Simulation models for the impedance matching network 164

Appendix B 165

The IEEE 802.15.4 MAC Frame Format 165

B.1. The IEEE 802.15.4 MAC Frame Format 165
B.2 Steps to Configure CC2420 in transmitting mode 166
B.3 Steps to Configure CC2420 in receiving mode 166

Appendix C 167

Short-Time Fourier Transform for Non-Stationary Signals 167

Appendix D 171

Wavelet Transform 171

List of Figures

Fig. 1.1.System integration and development of 3D stacking technology, flex materials and full wafer-scale for magnitude reduction in volume and enable smart unobtrusive autonomous sensor systems [3]. 22

Fig. 1.2.Photograph of (a) Google's Project Glass [8], (b) Electronic Paper [9] and (c) flexible OLED display [10]. 23

Fig. 2.1.Schematic representation of the IEEE 802.15 which is a working group of the Institute of Electrical and Electronics Engineers (IEEE) IEEE 802 standards committee. The working group specifies Wireless Personal Area Network (WPAN) standards and it is sub-divided in seven task groups.[22, 24, 25]. 30

Fig. 2.2.The concept of WBAN communications and its possible components [14, 23, 38]. Sensing and gathering data from individual wireless sensor nodes distribute around the human body. The collected information is transmitted to a healthcare server via the main gateway which can be a smart phone. 38

Fig. 2.3. Elements of a simple Wireless Communication System [43]. 42

Fig. 2.4.An example of a received signal envelope with both the short-term and long-term fading (dotted line follows the long-term variation). Long-term fading is caused by the change in path length due to the motion of transmitter and/or receiver relative to each other. Short-term fading is caused by the superposition of multiple copies of the received signal. 44

Fig. 2.5.Relative permittivity (ε_r) and conductivity (σ) for specific human body tissues at different frequencies obtained from a compilation presented in [24, 58-60]. The results can help in producing modelling equation to determine the appropriate dielectric values at each desired frequency. 47

Fig. 2.6.A three layer Gel Phantom used to mimic electrical properties of the human body for the characterisation of implantable RFID tags [67]. 49

Fig. 2.7.Simulation results of a commercial chip antenna, Antenova's Rufa 2.4 GHz SMD Antenna module [70, 71]. (a) Design model of the Rufa antenna implemented in CST Microwave Studio; (b) Effects of different

PCB lengths on the reflection coefficient of the Rufa antenna; (c) 3D radiation pattern of the Rufa antenna with a maximum radiation pointing. 51

Fig. 2.8.Wearable Antennas designed for the radio channel characterisation of different WBAN links. (a) HMMPA antennas consist of a ground-plane and patch metallization on a dielectric substrate with εr = 2.33 (Taconic TLY-3, PTFE woven glass)[61]; (b) Printed-F antenna is constructed on 0.6 mm thick CER 10 substrate. The wearable integrated antenna (WIA) consists of a 3 mm diameter copper element embedded in a tapered Taconic CER 10 dielectric substrate (εr = 10.2). Dimensions for each antenna can be found in [73]; (c) monopole with a small ground plane, (d) coil with small ground plane, (e) microstrip patch on a small ground plane, (f)Two element patch array with beam at 30 to give a broadside beam. Further details for figures (c)-(f) can be found in [48, 74]. 53

Fig. 3.1.Relation between the ZigBee Alliance specification and IEEE 802.15.4 standard when is compared to the OSI Communication Model. 57

Fig. 3.2.Photograph of commercial wireless modules found in the consumer electronics market: (a) ultra-compact 2.4GHz ZigBee Module from MeshNetics [98]; (b) JN5139 wireless microcontroller from Jenic [94]; (c) SPZB260-ZigBee module from ST [95]; (d) Pixie from FlexiPanel Ltd. [97] and (e) Crossbow's TelosB mote (TPR2400) IEEE 802.15.4/ZigBee compliant platform [96]. 59

Fig. 3.3.Frequency bands and channel structure for the IEEE 802.15.4 standard. 60

Fig. 3.4.The main concept of Wireless Body Area Networks (WBANs) defined under the IEEE 802.15.6 standard [23]. 61

Fig. 3.5.Wireless Sensor prototypes for on-body communications manufactured by Phillips Research Laboratory [100]. 61

Fig. 3.6.Design and implementation of the Microcontroller module that houses a low power Microchip component, the PIC18LF2620 [102]. 63

Fig. 3.7.Block diagram representation of the impedance matching network placed between the transceiver output impedance and the 50 Ω input impedance of the antenna. 63

Fig. 3.8.Simulation results of the 50 Ω Matching Network using lossless connections implemented in Advanced Design System (ADS) software from Agilent. 64

Fig. 3.9.Simulation results of the 50 Ω matching network using transmission lines at the 2.45 GHz ISM band. 65

Fig. 3.10.Antenna used for custom-built wireless sensors and the characterisation of WBAN channels: (a) design layout of a microstrip patch antenna implemented in CST Microwave Studio; (b) manufactured microstrip patch antenna using FR-4 as a base substrate. 66

Fig. 3.11.Simulation and measured results for a pair of patch antennas, one for the Tx. node and the second for the Rx. node. (a) simulated and measured reflection coefficient, S11, for both microstrip patch antennas; (b) 3D free-space radiation pattern of the microstrip patch antenna implemented in CST Microwave Studio 67

Fig. 3.12.Power spectrum response measured using the *max-hold* function of the Rohde & Schwarz FSP 40 Spectrum Analyser for: (a) custom-built wireless sensor node of a Rx. node, (b) Texas Instrument (TI) evaluation modules; (c) custom-built wireless sensor nodes transmitter and receiver nodes, respectively. 69

Fig. 3.13.Wireless sensor modules used for WBAN measurements and Data Logging units: (a) internal wireless sensor structure; (b) implemented custom built wireless sensor node using a microstrip patch antenna; (c) custom-built wireless sensor node showing the battery placement; (d) alternative commercial wireless node using CC2420 evaluation modules from TI. 71

Fig. 3.14.Measurement setup of a pair of microstrip patch antennas separated 30 cm in Queen Mary's Anechoic Chamber Environment. 72

Fig. 3.15.Measurement structure set up for the acquisition of radiation patterns of custom-built wireless sensor nodes. The measurement was performed in Queen Mary's Anechoic Chamber. The wireless node, with dimensions of 50x40x30 mm, was positioned on top a rotational table. The rotational table and data acquisition was controlled by a computer which was synchronized with a Rohde & Schwarz FSP 40 Spectrum Analyser. 73

Fig. 3.16.Measured radiation patterns of custom-built wireless sensor nodes and when placed on-body. The measurements were taken in an Anechoic Environment in Queen Mary's Antenna Lab using a Rohde & Schwarz FSP 40 Spectrum Analyser. 74

Fig. 4.1.Fibre-Optic system (a) a PIFA antenna connected directly to the electro-optic Field Sensor (OEFS); (b) a typical measurement set-up using a coaxial cable for body-worn antennas; (c) free-space fibre-optic measurement set-up (close up of antenna taped to underside of foam block); (d) on-body fibre optic measurement set up at the NPL's SMART range facility [35, 105]. 77

Fig. 4.2.Location of transmitter and receiver antennas used for each on-body measurement in an anechoic environment. 81

Fig. 4.3.On-body absolute frequency detuning and return loss deviation of the receiver antenna at each point on the trunk section, compared with free-space measurements. Both sets of measurements were taken using a Hewlett Packard 8720ES Vector Network Analyser. 82

Fig. 4.4.Measurement of the microstrip patch antenna using a Hewlett Packard 8720ES Vector Network Analyser: (a) stand-alone antenna; (b) antenna with close proximity to the in-house wireless node. Note that the PCB SMA is not connected to SMA connector of the antenna (passive SMA). 83

Fig. 4.5.Custom-built wireless sensor node used for WBAN channel characterization. The design and development descriptions are presented in Chapter 3. 84

Fig. 4.6.Anechoic Chamber Measured Path and Power Loss values on the trunk section using LS linear fitting for: Stand Alone Antenna (see Fig. 4.4a), Antenna with close proximity to the in-house wireless sensor node (see Fig. 4.4b), in-house wireless sensor node with patch antenna (operating at a single frequency, see Fig. 4.5) and alternative wireless node using Texas Instruments evaluation modules (see Fig. 3.13d). 86

Fig. 4.7.Channel performance of receiving node located at the largest distance (position 6), from the transmitter module. The mean value (line-plot) and standard deviation (red error bars plot) shows the variation of antenna radiation properties is related to long term fading effects, the motion produced by breathing process which also produces movements on the antenna orientation. 88

Fig. 4.8.Different locations used for custom-built wireless sensor nodes to characterize the operation of the sensors at each carrier frequency. The

receiver node was moved around trunk locations highlighted in red. The transmitter node was positioned at waist position. 90

Fig. 4.9.Average Power Loss values using LS linear fitting for each frequency carrier at 2.45 GHz ISM band: (a) response of the first 8 channels; (b) response of the last 8 channels; (c) summary of statistical parameters of each frequency carrier. 91

Fig. 4.10. Comparison of average path and power loss of: stand-alone antenna, antenna with close proximity to wireless boards, both measured using VNA equipment, and custom-built wireless sensor nodes operating at a single frequency, and the mean across the 16 channels which was recorded individually and mean was calculated after all channels were recorded. 93

Fig. 4.11.Deviation of measurement from the average path and power loss acquired with VNA and custom-wireless sensor nodes, respectively. A wireless sensor node operating at a single frequency has different radio channel characteristics from a stand-antenna measured by a VNA and characterised over the whole bandwidth of operation. 94

Fig. 5.1.Location of custom-built wireless sensors nodes used for dynamic WBAN radio channel characterization for each athletic activity. 99

Fig. 5.2. Medical Sport Equipment used for the characterization of dynamic WBAN channels using custom-built wireless sensors. (a) WOODWAY ELG treadmill machine [147]; (b) Lode Excalibur Sport bike with pedal force measurement [148], and (c) Rowperfect RP3 rowing ergometer [149]. 100

Fig. 5.3. The plot shows the variation of the resonant frequency of the transmitting antenna while the test subject is resting, jogging and in a recovery process. 101

Fig. 5.4.Recorded received signal strength (RSS) for a waist-to-chest channel recorded by custom-built wireless sensor nodes when the test subject is jogging and motionless in Queen Mary's Human Performance Laboratory. 103

Fig. 5.5.Power loss for different on-body radio channels estimated from recorded RSS while test subject is under physical workout. The spacing between

the different parts of the box indicates the degree of dispersion and skewness of the data. 104
Fig. 5.6.Probability Distribution Function (PFD) for a waist-to-back channel recorded by custom-built wireless sensor nodes operating at 2.45 GHz while the test subject was jogging at a constant speed of 5km/h. 107
Fig. 5.7.Probability Distribution Function (PFD) for a waist-to-ankle channel recorded by custom-built wireless sensor nodes operating at 2.45 GHz while the test subject was rowing at a constant speed of 5km/h. 107
Fig. 5.8.Simulation results of the EM wave propagation alongside the trunk section of the Hugo model implemented in CST Microwave Studio. The radiating element was the designed microstrip patch antenna from Chapter 3 109
Fig. 5.9.Received Signal Strength (RSS) for waist-chest channels recorded with custom-built wireless sensor nodes from three different activities: (a) jogging; (b) rowing and (c) cycling. The measurements were performed in Queen Mary's Human Performance Laboratory 110
Fig. 5.10.Queen Mary's Human Performance Laboratory, (a) integrated Cortex System synchronized with a treadmill machine and electrocardiograph, (b) 12-Lead electrocardiograph system Cardio-Collect 12. 111
Fig. 5.11.Heartbeat signal of the test subject while is: (a) standing on the treadmill machine (resting stage). The average heartbeat was 86 BPM; (b) jogging at a constant speed of 5 km/h. The heartbeat rate was 106 BPM. 112
Fig. 5.12.Power spectral response recorded by WSNs for five different positions alongside the trunk section while the test subject is resting (standing on the treadmill machine). 114
Fig. 5.13.Power spectral density response using Welch’s method for RSS signals while the test subject is (a) jogging; (b) rowing and (c) cycling. All the activities are performed at a constant speed of 5 km/h. 115
Fig. 5.14.Snapshot sequence of the human body movement during a jogging exercise, modelled in POSER: (a), (b), (c) represent the initial forward step and (d), (e), (f) correspond to the next forward pace. 116
Fig. 5.15.A common sequence during a rowing process: (a) the catch, (b) the drive, (c) the finish, (d) the recovery and (e) the return to catch. 117

Fig. 5.16.Cycling at a constant speed of 5 km/h, (a)-(c) Snapshots of main movements of the human body while (Images are for illustration purposes only) and (d) normalized spectrum response of the received signal. 118

Fig. 5.17.Power spectral density response using Welch's method for recorded ECG signals while the test subject is (a) standing on the treadmill machine (resting stage); (b) jogging at a constant speed of 5 km/h. 119

Fig. 6.1.Commercial RFID tags for indoor location (a) SpotON [21]; (b) LANDMARC [175]. 125

Fig. 6.2.A functional block diagram of positioning system using some location metric parameters which include Time of Arrival (ToA), Angle of Arrival (AoA), RSS for indoor location estimation. 126

Fig. 6.3.Popular Localization techniques used for tracking and positioning systems (a) trilateration; (b) triangulation; (c) Maximum Likelihood Estimation 126

Fig. 6.4.Theoretical and empirical model used to translate the difference between the transmitted signal strength and the received signal into a range estimate for the object's positioning. The positioning is based on RSS, where PL1, PL2, and PL3 denote the measured path loss. 127

Fig. 6.5. (a) Implemented wireless nodes using a microstrip patch antenna; (b) simplified floor-plan of the Body-Centric Lab, with node positions and separations shown. Note the assumed orientations of the body along the path. 129

Fig. 6.6 Smoothed received power in dBm for each node: x in blue; y in red; z in green. Sampling period was 14 ms; window-size for moving average filter was 50 samples. 130

Fig. 6.7 (a) The Telos B sensor board, with integrated printed IFA, battery-pack, USB connector, and temperature and humidity sensors [96]; (b) simplified CST model of the TelosB wireless sensor. 132

Fig. 6.8. Free-space radiation patterns from CST Microwave Studio: (a) Gθ plane and (b) Gφ plane. 133

Fig. 6.9. Second experiment setup based on commercial wireless sensor nodes, TelosB. (a) Experimental arrangement: the blue circles denote the positions of the fixed wireless sensor nodes; the green circles denote the

positions of the on-body nodes; (b) wireless sensor nodes on the test subject 134
Fig. 6.10.Representative RSS time-series plots (a) node 1-to- node 2; (b) node 1-to-node 10 135
Fig. 6.11.Mean Path Loss values for off-body links in transmit and receive modes. (a) Path loss from the human body, (b) path loss from the wall mounted wireless sensors. 136
Fig. 6.12.Path loss comparison plots for an empty and occupied environment while sensor nodes 3, 7, 11 and 15 are transmitting. 139
Fig. 6.13.Standard deviation for transmitting nodes 3, 7 11 and 15 (the remaining nodes are operating as receivers). 139
Fig. 6.14.Representation of (a) monitoring area layout; (b) distance matrix between neighbour nodes in cm and (c) interpolated distances. 141
Fig. 6.15.Estimated path loss values acquired from pre-calculated distances (a) empty room and (b) occupied room. 141
Fig. 6.16.Colour map contour plots of estimated path loss values. (a) empty indoor environment; (b) a test subject standing in the centre of the monitoring area. 142
Fig. 6.17.Measured Path values for an empty and occupied room using LS linear fitting 142
Fig. 6.18.Updated path loss matrix using information from the fitted path loss curves (a) empty room; (b) occupied indoor environment. 143
Fig. 6.19.Colour map contour for calculated path loss values. (a) empty indoor environment; (b) a test subject in the centre of the monitoring area. 144
Fig. A.1 Microstrip Patch Antenna on an FR-4 substrate 160
Fig. A.2. CC2420 core transceiver pin out [101]. 162
Fig.A.3.Design and implementation of the Microcontroller module that houses a low power Microchip component, the PIC18LF2620. 162
Fig.A.4.Design and implementation of the RF radio transceiver boar module that houses a Texas Instruments transceiver, the CC2420. (a) design implemented using Ultiboard software from National Instruments; (b) manufactured and assembled module 163
Fig.A.5. (a) Implemented design using ideal transmission lines (losless) modelled and simulated in Advanced Design System (ADS) software from Agilent;

(b)implemented design using transmission lines model between passive components. 164
Fig. B.1.Schematic view of the IEEE 802.15.4 Frame Format. 165
Fig. B.2.Format of the Frame Control Field (FCF). 165
Fig.B.3.Sequential steps for a successful configuration of the CC2420 in transmitting mode. 166
Fig.B.4.Sequential steps for a successful configuration of the CC2420 in receiving mode. 166
Fig. C.1. Spectrogram results while exercising at a constant speed of 5 km/h: (a) ECG recording, (b) jogging, (c) rowing and (d) cycling using a window size of (a) 256 and (b)-(d) 128 169
Fig. D.1.De-noising of the received signal using a one dimensional wavelet function for a) jogging, b) rowing, c) cycling. 173

List of Tables

2-1 Frequency Bands Allocated for WBANs and WPANs around the world [22, 24, 25, 27] 31
2-2 Comparison of Bluetooth Communication Technology Core Specification and Blueetooth Low-Energy [32, 33] 34
2-3 ZigBee Maximum Transmit Power Levels [34] 34
2-4 Comparison of Different Low Power WBAN Communication Standards – Bluetooth and Zigbee [25, 32-34, 36, 37] 37
2-5 Compliant Frequency Bands for the IEEE 802.15.6 [38] 39
2-6 Electric Properties of Specific Human Body tissues used for the Visible Man Model Project at 2.45 Ghz. The values were taken at body 48
temperature using an Impedance Analyser[57, 58, 60]. 48
2-7 Antenna Design Topologies for Microwave Frequencies 50
2-8 Effects of Size Reduction on Antenova's Rufa 2.4 GHz SMD Antenna Module 52
2-9 Antenna Topologies and their Physical Dimensions for WBAN Communications extracted from Body-centric Literature. The listed body-worn antennas are designed to operate at ISM band 2.45 GHz [48, 61, 73, 74] 53
3-1 Low Power Wireless Ssystems Operating at the 2.45 GHz ISM Band 58
3-2 Parametric Comparison between Antenna Designs in Free Space Simulation and Measurements in an Anechoic Environment in Queen Mary's Antenna Laboratoy 68
3-3 Measurement of the Power Spectrum Response of Individual Custom-Built Wireless Sensor Nodes Used for On-Body Measurements 70
3-4 Response Of The Wireless Sensors In A Free Space Environment at a Distance of 30 cm 72
4-1 Deviation of Antenna parameters when placed on-body 82
4-2 Statistical Parameters of Measured On-Body Path Loss at 2.42 GHz for an Anechoic Environment 86

4-3 Mean and Standard deviation for each of the 16 channels in the 2.45 GHz ISM band using in-house Wireless Nodes for on-body locations 89
4-4 Summary of Statistical Parameters of 16 Different Channels Using Low Power Sensors 92
4-5 Summary of Statistical Parameters for Path and Power Loss Measured by: the VNA (2.45 GHz ISM band) and in-house wireless nodes (single channel 2.42GHz and average of all 16 channels)..... 93
4-6 Average Value and Standard Deviation of Lognormal Distribution Applied to Path and Power Loss for measurements taken with the VNA (2.45 GHz ISM band) and in-house wireless nodes (single channel 2.42GHz and average of all 16 channels)..... 95
5-1 Variation of the S_{11} Recorded Prior the Selection of the Communication Channel of the Custom-Built Wireless Sensor Nodes..... 102
5-2 Statistical Summary of the Power Loss Variation Recorded by Custom-Built Wireless Sensor Nodes..... 105
5-3 ML Estimated Distribution Parameters for different mobile WBAN channels and Distributions 106
5-4 Heart Rate Variability for a Resting and Jogging Scenarios Calculated from a 5 Minute Segment Frame 112
5-5 Summary of Main Harmonics for each Performed Activity and the Recorded ECG..... 120
6-1 Summary of information for the first experiment (Feasibility Study)..... 130
6-2 Summary Of calculated Path-Loss Exponents and Estimated Positions (Note: Negative Errors Indicate Under-Estimates; Positive Errors Indicate Over-Estimates.)..... 131
6-3 Mean Path Loss and Standard Deviation for Node 1 when it is operating in a receiving mode 138
6-4 Mean Path Loss and Standard Deviation for Node 1 when it is operating in a Transmitting mode 138
6-5 Statistical Parameters of Measured Path Loss at 2.42 GHz for an indoor Environment..... 143

Abbreviations

BAN	Body Area Networks
BER	Bit Error Rate
ISM	Industrial, Scientific and Medical
dBm	Decibels Relative to 1mW
Rx	Receiver
FR4	Flame resistant 4
EM	Electromagnetic
LOS	Line of Sight
ITU	International Telecommunications Union
MS	MicroStrip
RSSI	Receive Signal Strength Indication
Tx	Transmitter
RF	Radio Frequency
UWB	Ultra Wide Band
WBAN	Wireless Body Area Network
WPAN	Wireless Personal Area Network
VNA	Vector Network Analyser
PCB	Printed Circuit Board
IEEE	Institute of Electrical and Electronics Engineers
BWCS	Body Centric Wireless Communication Systems
API	Application Interface
OSI	Open Systems Interconnection
MAC	Media Access Control
CSMA-CA	Carrier Sense Multiple Access, Collision Avoidance
MMCX	Micro-Miniature Coaxial Connector
SMA	Sub Miniature version A connector
WIA	Wearable Integrated Antenna
HMMPA	Higher Mode Microstrip Patch Antenna
PAM	Pulse Amplitude Modulation

PPM	Pulse Position Modulation
OFDM	Orthogonal frequency-division multiplexing
ISI	Inter-symbol Interference
FFT	Fast Fourier Transform
STFT	Short-Time Fourier Transform
CEPT	Conference of European Posts & Telegraphs
ETSI	European Telecommunications Standards Institute

Publication List

BOOK CHAPTER

- ✓ Robert Foster, Tuba Yilmaz, **Max Munoz**, and Yang Hao, Chapter 5: Wearable Sensors in "*Autonomous Sensor Networks: Collective Sensing Strategies for Analytical Purposes*", Springer, 2013, ISBN: 3642346480.

JOURNAL AND CONFERENCE PUBLICATIONS

- ✓ **M.O. Munoz**, R Foster, L. Zhang, M. Gillot, Y. Hao, " Building Material and Indoor Radio Propagation Characteristics for Sustainable Houses", to be submitted in *IEEE Transactions on Antennas and Propagation.*
- ✓ **M.O. Munoz**, E. Nagijew, R Foster, R. Shipman,M. Gillot, Y. Hao, "Indoor localization using IEEE.802.15.4-based sensors", to be submitted in *IEEE Transactions on Antennas and Propagation.*
- ✓ **M. O. Munoz**, R. Foster, and Y. Hao, "Exploring Physiological Parameters in Dynamic WBAN Radio Channels", accepted to *IEEE Transactions on Antennas and Propagation*, 2013
- ✓ **M. Munoz** Torrico, R. Foster, and Y. Hao, "Identifying Physiological Features from the Radio Propagation Signal of Low-Power Wireless Sensors," in *Wireless Mobile Communication and Healthcare*. vol. 61, B. Godara and K. Nikita, Eds., ed: Springer Berlin Heidelberg, 2013, pp. 341-350.
- ✓ T. Yilmaz, **M. Munoz**, R. N. Foster, and Y. Hao, "Wearable wireless sensors for healthcare applications," in *Antenna Technology (iWAT), 2013 International Workshop on*, 2013, pp. 376-379.
- ✓ Y. Hao, A. Brizzi, R. Foster, **M. Munoz**, A. Pellegrini, and T. Yilmaz, "Antennas and propagation for body-centric wireless communications: Current status, applications and future trend," in *Electromagnetics; Applications and Student Innovation (iWEM), 2012 IEEE International Workshop on*, 2012, pp. 1-2.
- ✓ **M. O. Munoz**, R. Foster, and Y. Hao, "Physiological Features from an On-Body Radio Propagation Channel," in *Wearable and Implantable Body Sensor Networks (BSN), 2012 Ninth International Conference on*, 2012, pp. 52-57.
- ✓ **M. O. Munoz**, R. Foster, and Y. Hao, "On-Body Channel Measurement Using Wireless Sensors," *Antennas and Propagation, IEEE Transactions on*, vol. 60, pp. 3397-3406, 2012.
- ✓ F. Yifeng, K. Z. Rajab, **M. Munoz**, and Y. Hao, "Electrically small half-loop antenna design with non-foster matching networks," in *Antennas and Propagation (EUCAP), 2012 6th European Conference on*, 2012, pp. 126-129.
- ✓ N. Fontana, A. Monorchio, **M. O. Munoz Torrico** , Y. Hao, "A Numerical Assessment of the Effect of MRI Surface Coils on Implanted Pacemakers", in *International Symposium (APS/URSI 2012), IEEE Antennas and Propagation Society*, July, 2012, Chicago.
- ✓ **M. O. Munoz**, R. Foster, Y. Hao, "On-Body performance of Wireless Sensor Nodes using IEEE 802.15.4", *European Conference on Antennas and Propagation (EUCAP 2011)*, Rome, Italy, April 2011.
- ✓ R. Foster, **M.O. Munoz**, Y. Hao, "RF positioning using Body-Centric Wireless Systems", *Loughborough Antenna and Propagation Conference*, 14-15 November, 2011,UK

Chapter 1

Introduction

The integration and connectivity of different electronic devices, such as home entertainment systems, using inter-operability guidelines of the Digital Living Network Alliance (DLNA), smart phones and even domestic appliances (intelligent refrigerators, microwaves, smart washing machines), have become part of our daily life. As a result, current devices offer not only human interaction, but also the inter-connectivity of each of them. The electronic devices process and control unique applications which are transmitted through seamless wireless channels creating independent networks that operate at exclusive radio frequencies. As a result, wireless personal area networks (WPANs) are formed.

In a similar way, different groups are taking advantage of these technological trends. For example, military institutions start using body-worn equipment to control and monitor soldier battlefield positioning [1]. In the case of the medical scenario, real-time monitoring systems for biological and biomechanical signals, such as

heartbeat variability, breath rhythm, blood pressure, perspiration and temperature, are testing the potential and reliability of current technologies [2].

1.1. Research Scope and Applications

Next generation wearable sensors are expected to be autonomous self-powered systems stacked in fractional volumes of $0.1cm^3$ [3] (Fig. 1.1). They will also be equipped with a type of piezoelectric transducer for energy scavenging transforming mechanical energy, such as pressure, force, vibration and physiological processes and physical quantities of the human body for example kinetic, sound, thermal and internal acid fluids into a source of power [3-5].

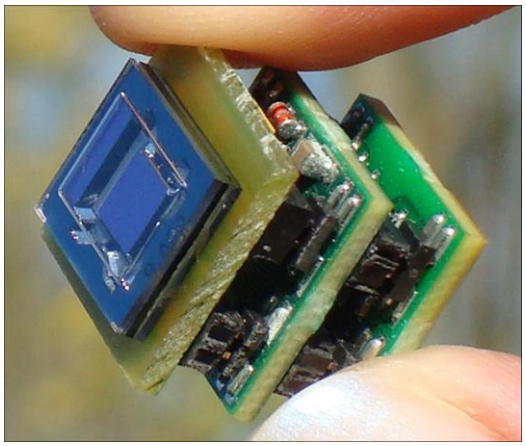

Fig. 1.1.System integration and development of 3D stacking technology, flex materials and full wafer-scale for magnitude reduction in volume and enable smart unobtrusive autonomous sensor systems [3].

Moreover, the design and manufacturing process of forthcoming chips are evolving from the classical 2D manufacturing process (28 nm) to 3D implementations (22 nm) where the number of transistors is increased, thus increasing the computational speed and reducing the power consumption.

A recent report made by ABI research predicts that over the next five years the market for wearable wireless sensors is set to grow to more than 400 million devices by 2014 [6]. These figures show the popularity of wearable sensors; but, at the same time pushes current technology trends towards new manufacturing designs where the integration of biocompatible and biodegradable materials together with flexible and organic electronics [7] will become a common standard for body-centric devices. Furthermore, recent implementations made use of conductive polymers, commonly carbon-based, to create light and flexible materials, where the traditional

combination of copper and silicon dioxide (silica) is unsuitable [7]. These materials will be used on a new set of wearable functions and thus extending the frontiers of current on-body applications. Such conductive polymers are expected to play an important role in emerging applications not only for body-centric environments but also for future building structures. Some examples of such technologies are the Google's project glass [8] (Fig. 1.2a), electronic paper [9] (Fig. 1.2b), the flexible displays (OLED) [10] and the smart window (Eglass) [11] (Fig. 1.2c).

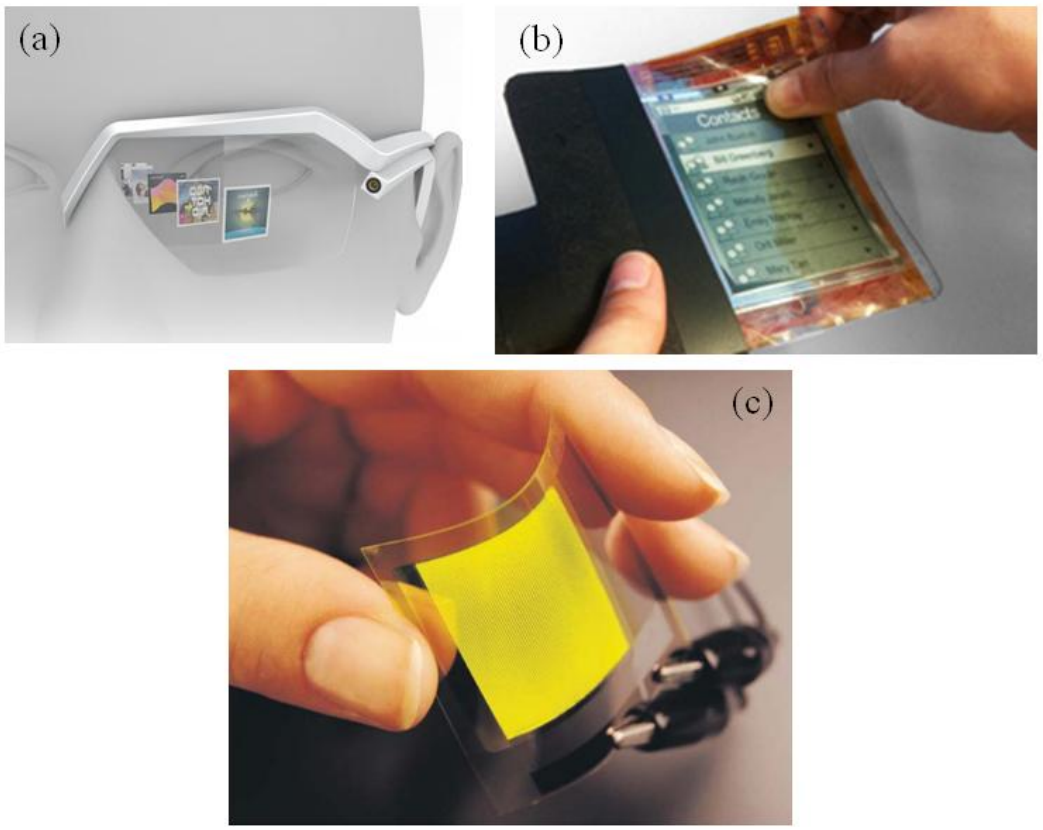

Fig. 1.2.Photograph of (a) Google's Project Glass [8], (b) Electronic Paper [9] and (c) flexible OLED display [10].

In the case of human microchip implants [12, 13], the electronic components will be made from biocompatible materials. Accordingly, implants that need to reside for short periods of time could be broken down and absorbed by the human tissues thus eliminating the need for additional surgery for the implant removal. Furthermore, new implantable devices will also include smart drug-release subsystems that enclose compact RF sub-sections for the wireless communication which empower the continuous monitoring of the patient during the recovery process.

It is evident that new technological trends will lead to new body-centric environments bringing about new areas of investigation, not only to control and monitor human physiology, but also to understand and model the behaviour of current and future designs when placed on-body. Moreover, wearable devices will become autonomous devices that are compact and conformal to the body and capable to harvest energy, sense physiological parameters and communicate between body-worn nodes.

The reliability of each on-body radio link depends on power constraints, body location, application environment and the wireless sensor architecture. Compact and conformal lightweight wearable devices usually house miniature antennas that have low gain, narrow bandwidth and low efficiency; thus, the on-body radio link is degraded [14]. Forthcoming body-worn antennas, including those with a greater coverage area, high efficiency, enhanced behaviour to the proximity of the human body and operation at different frequencies, are current topics of active research [14, 15].

Currently, most of the Wireless Body Area Networks (WBAN) literature characterises on/off-body radio channels using standalone antennas (either single or multiple radiating elements) [14]. Even though the size of such antennas is large and non-conformal to the human body, they help to understand and model the electromagnetic wave propagation around the body using a combination of EM solvers and measurements of the scattering parameters. Traditionally, the scattering parameters of WBAN communication channels are measured with the aid of Vector Network Analysers (VNAs) or Spectrum Analysers (SA). Measured data is further post-processed in order to define propagation models for different on-body radio links.

In contrast, the characterisation of WBAN communication channels using compact wireless sensor nodes is still limited and needs to be explored. At lower frequencies, the effects of active and passive elements barely influence the communication channel, but at high frequencies, the electromagnetic propagation properties alongside the human body are highly perturbed by external factors (e.g., the lossy tissues of the human body).

1.2. Research Objectives

The reliability of body-centric communication networks is highly influenced by the behaviour of the transmission path. The radiating element of an on-body wireless node radiates electromagnetic waves that propagate in free space and alongside the body surface where they are absorbed by the lossy human tissues. The latter and the inhomogeneous composition of the human body counteract the electromagnetic wave propagation and radiation of body-worn antennas, thus hindering the radio communication performance of functional prototypes.

In order to design wearable devices, a thorough investigation on the causes of inefficiency in WBAN channels, due to antenna performance and the effect of full sensor structures (including ICs and lumped elements) on the wireless sensor operation, is required. For example, wireless modules that exclude the ground metallization underneath the antenna (e.g., designs using chip antennas) are drastically affected by the human tissue proximity. However, the radio efficiency of WBAN sensors is affected not only by the type or size of the antenna, but also by the body location, the posture, the user and the application itself.

The thesis aims to understand, from simulation and empirical models, how body centric wireless communication (BCWC) parameters may change from the design of the antenna to the development process of the wireless sensor node. The study also introduces a new measurement technique to characterise on-body radio channels, using wireless sensor nodes. The data collected from on-body measurements are compared with traditional measurement techniques used in different WBAN studies, where VNA's are connected through flexible or semi-rigid coaxial cables.

On the other hand, it is also important to understand and model the variations of the radio propagation channels within dynamic WBAN environments which severely affect the received signal (i.e., fading effects), thus degrading the radio communication performance. The research work presented in this thesis describes the radio propagation characteristics of different dynamic scenarios, with respect to body position, through measurement campaigns using low-power wireless sensors. Additionally, statistical models are used to characterise and provide a framework of the on-body propagation channel and its behaviour with regards to dynamic environments.

Many studies have shown the potential of contactless sensors for the retrieval of different physiological signals for example breathing, heartbeat, gait pattern [16-18]. The biomechanical features are embedded in the reflected waves which present shifts on frequency and phase when compared to the transmitted signal, similar to the Doppler Effect. Although microwave sensors literature showed different contactless sensor prototypes, different sources of electromagnetic signals are propagating within the environment (e.g., Wi-Fi, GSM, GPS, Bluetooth, ZigBee) and hence human bodies are greatly exposed to them. Consequently, the radio propagation signal from each source can be used as a potential contactless sensing method. The thesis investigates the latter and the possibility of introducing an alternative sensing method by means of the recorded received signal strength (RSS) of low-power wireless sensors. The received signal of a particular on-body location is further analysed implementing frequency domain techniques with the aim to retrieve additional information embedded in the wave propagation.

The interest in biomedical research is directed toward continuous monitoring and quantification of physiological body signals as well as on development of personalized healthcare devices [19, 20]. Tele-monitoring and tele-diagnostics systems in smart home environments provide a large amount of health related information from strategically placed body-worn sensors which sample, process, and transmit vital signs such as heart-rate, blood pressure, skin temperature, pH, respiration, oxygen saturation.

Since people spend most of their time in indoor environments and as part of the monitoring system itself, indoor tracking service is in great public demand [21]. In outdoor environments, the global positioning system (GPS) can provide very accurate positioning. However, in the indoor environments, the radio signal of GPS satellite is too weak to penetrate most of the buildings, and thus GPS cannot provide desirable positioning accuracy. Based on this observation, the study takes advantage of the recorded RSS to introduce the concept of indoor RSS-based location tracking using the IEEE 802.15.4 standard. The proposed method combines the results of empirical indoor path loss models measured by custom-built WBAN sensors and TelosB which is a commercial wireless module. The radio propagation models are built from the received signal of individual sensors enabling the determination of the user location within indoor environments.

The analysis and interpretation of simulation and measurement campaigns form an essential part for the validation of the gathered data. Some of the important steps carried out in the following study are:

- design of standard printed antennas for 2.45 GHz ISM band;
- design and manufacturing of wireless sensor nodes for WBAN applications;
- analysis of the antenna performance with/without the presence of passive and active elements;
- evaluation of the wireless sensor node performance with/without the human body;
- study of different on-body radio channels of different on-body locations, channel of operation, transmitted power;
- comparison of WBAN measurements techniques:
    - using VNA with coaxial cables,
    - employing wireless sensor nodes;
- measurement and characterisation of different dynamic WBAN scenarios using custom-built wireless sensor nodes;
- post-processing and interpretation of recorded data using different digital signal techniques for the extraction of bio-mechanical features.
- analysis of the radio propagation models for indoor location tracking
    - using custom-built wireless sensors,
    - using commercial wireless nodes (i.e., TelosB).

1.3. Thesis Outline

Following this introductory chapter, the rest of the thesis is organised as follows:

Chapter 2 introduces the different wireless technologies for Body-Centric Networks. The IEEE 802.15 Working Group is introduced, including the different task groups for WPAN and WBAN communications. A summary of low-power wireless standards, such as Bluetooth, Bluetooth-LE, ZigBee, is given, highlighting their main operational characteristics. The chapter also describes the newly published WBAN communication standard, the IEEE 802.15.6, which considers the effects on portable antennas due to the presence of a person.

Furthermore, fundamental theory for radio propagation characterisation and modelling of WBAN environments is discussed and analysed. A brief introduction of the interaction of human tissues with electromagnetic waves is also described, in addition to different methods to model and implement human phantoms which are used for EM studies.

The last section presents a comprehensive literature review of wearable antennas highlighting the antenna topologies and their operation for WBAN applications at 2.45 GHz ISM band.

Chapter 3 compares the ZigBee specification with the IEEE 802.15.4 standard and reviews advances and developments of different commercial wireless nodes operating at 2.45 GHz. The chapter defines rigorously the design, development and performance of in-house wireless sensor nodes for WBAN applications. The chapter explains the antenna design, the performance of matching network and ultimately custom-built wireless sensor nodes using IEEE 802.15.4 standard as a communication protocol.

Chapter 4 provides an extensive and detailed literature review of different measurement techniques used to characterise the radio propagation properties of different WBAN channels.

The chapter also introduces and defines a new measurement technique for body-centric channels using wireless sensors. The results are compared with traditional methods using the Vector Network Analyser.

Chapter 5 outlines dynamic on-body radio channel measurements. Three different scenarios are considered and it is shown that dynamic on-body radio channels contain rich biomechanical information. It is demonstrated that some physiological features, such as motion pattern and breathing process can, therefore, be identified using Fast Fourier techniques.

Chapter 6 presents preliminary results for passive user tracking using the received signal strength of low-power wireless sensors for indoor scenarios. The chapter considers path loss models acquired from empirical scenarios which are commonly used in WBAN radio channel analysis. The study is mainly focused in a motionless subject.

The conclusions of the study are drawn in **Chapter 7**. It also highlights the future research including the planned work for measurement campaigns using more compact wireless sensors embedded with different antenna topologies.

Chapter 2

Wireless Technologies for Body-Centric Networks

The IEEE 802.15 working group is responsible for the development of consensus WPAN and WBAN standards [22, 23], in order to have reliable wireless networks for wide market applicability. The group has established seven task groups, which are shown in Fig. 2.1, each working on specific components of the 802.15 specification. Each task-group defines standards for the coexistence of different communication platforms and the improvement of signal mitigation and network sustainability. Thus, different low power wireless systems, such as portable devices, home appliances and body sensor networks can establish communication links, while they interact between each other, at different spectrum frequencies.

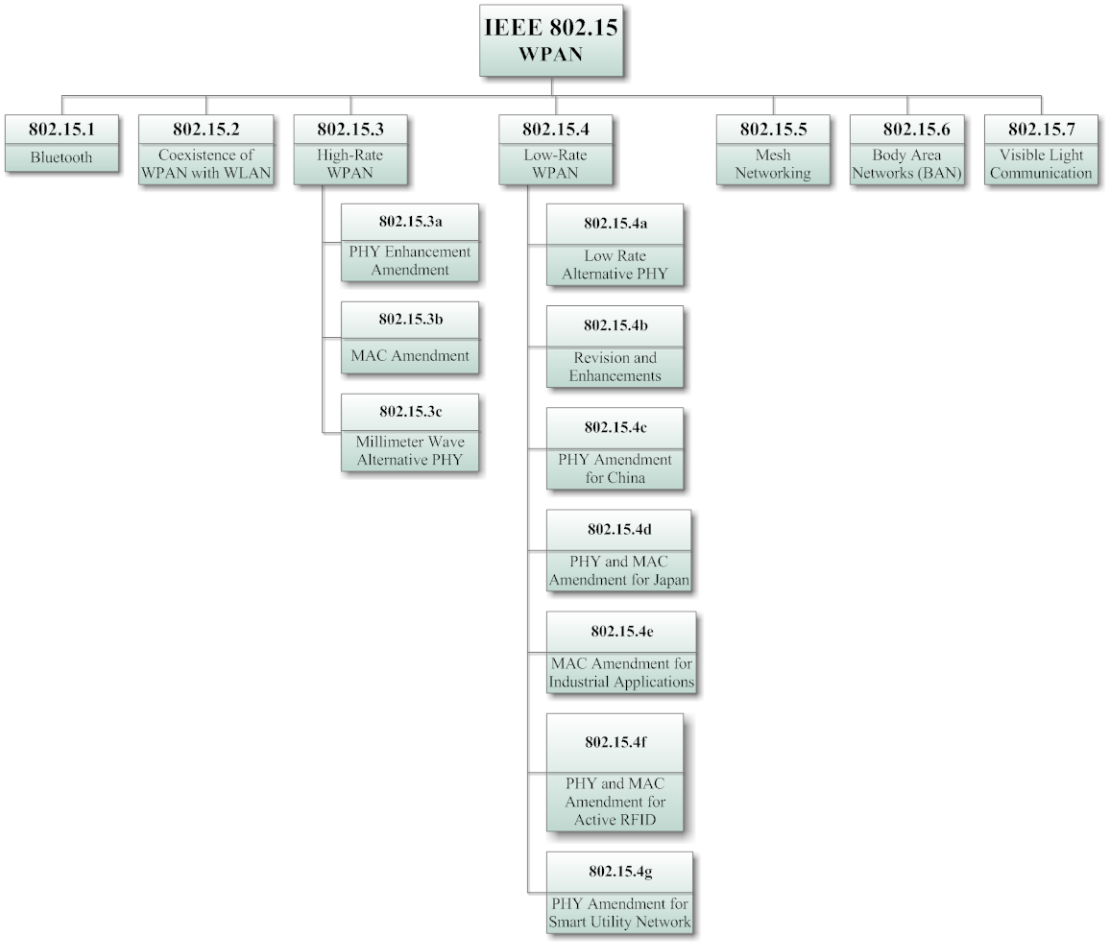

Fig. 2.1.Schematic representation of the IEEE 802.15 which is a working group of the Institute of Electrical and Electronics Engineers (IEEE) IEEE 802 standards committee. The working group specifies Wireless Personal Area Network (WPAN) standards and it is sub-divided in seven task groups.[22, 24, 25].

A different specification, defined by FCC and ETSI [26], is the Medical Implanted Communication Service (MICS), which is defined at 402 - 405 MHz. MICS rules apply to ultra-low power transmissions that support the diagnostic and/or therapeutic functions associated with implanted medical devices.

The operation of different wireless systems at unlicensed frequency portions of the spectrum are not the same around different geographical areas. A summary of the frequency bands allocated for WBANs and WPANs around the world is listed in Table 2-1.

2.1. WPAN Standards

A WPAN is a network of interconnected devices which are centred on an individual user workspace. Each device is connected wirelessly and allows

communication links within 10-100 meters range [22]. Moreover, WPANs enable electronic devices to communicate with other nearby equipment and exchange digital information.

TABLE 2-1
FREQUENCY BANDS ALLOCATED FOR WBANS AND WPANS AROUND THE WORLD [22, 24, 25, 27]

Specification	Freq. Band MHz	Max. Tx. Power dBm	Location
MICS	402.0 - 405.0	-16	Worldwide
ISM	433.1 - 434.8	+7.85	Europe
ISM	868.0 - 868.6	+11.85	Europe
ISM	902.8 - 928.0	+36 w/ spreading[1]	Not in Europe
MBAN	2360.0 - 2400.0	+36 w/ spreading	US only
ISM	2400.0 - 2483.5	+36 w/ spreading	Worldwide
WMTS	1395.0 - 1400.0	+22.2	US only
UWB	3100.0 - 10600.0	see [28, 29]	US, Europe and Asia

Wireless communication around the user's body or with other WBANs may be based on microwave radio links and even near-field communications [30, 31]. WBANs may communicate externally with other fixed networks, using one of a range of available wireless technologies. For short and medium communications, Bluetooth, ZigBee, UWB, Wireless LAN (Wi-Fi) and Wi-MAX communication are available, allowing a wide coverage area and offering the possibility of ubiquitous worldwide wireless mobility [25].

Short-range devices and networks operate mainly in stand-alone configurations either in home and office environments or large enclosed public areas, while their integration into the wireless wide-area infrastructure like the cellular WANs or WiFi is still nearly non-existent; therefore, extensive work is targeting the capability for seamless coexistence, interoperability, and integration among different communication technologies. When designing future short-range wireless systems, the increasing pervasive nature of technology and computing must be accounted for.

[1] Spectral spreading is accomplished by digital modulation at a high data rate or by direct sequence spread spectrum technique.

Bluetooth, Bluetooth Low Energy (BLE) and ZigBee (see Fig. 2.1) communications technologies are introduced and described in the next section. BLE and ZigBee are regarded as the most promising technology for WBAN applications and specially for their low-power consumption.

2.1.1. Bluetooth

Bluetooth foundation core v1.1, also known as the IEEE 802.15.1 standard, is a wireless communication technology designed and optimised for power-conscious, battery-operated, low cost and lightweight personal devices communicate within short-range through point-to-point and point-to-multi-point connections (i.e. piconets or scatternet networks).

The core structure is composed by: a radio unit, a link control unit, a support unit for link management and the host controller interface (HCI) functions. The latter provides the means for a host device to access Bluetooth hardware capabilities. The radio layer operates in the 2.4 GHz ISM band and uses frequency hopping spread spectrum (FHSS) for the coding; thus, a transmitter will use 79 individual, randomly chosen frequencies (each channel of 1 MHz bandwidth) within a designated range.

The modulation methods implemented are: Gaussian Frequency-Shift Keying (GFSK), for Basic Rate (BR); and both Differential quadrature phase-shift keying (π/4-DQPSK) and Differential phase-shift keying (8-DPSK), for Enhanced Data Rate (EDR). The two modes of Bluetooth, BR and EDR, can sustain data rates of 1 Mbps and 2-3 Mbps, respectively. Moreover, the output power levels are classified into three different classes [25, 32]:

- Class 1 devices broadcast using 100 mW (20 dBm) of power, the maximum range is approximately 100 m;
- Class 2 devices broadcast using 2.5 mW (40 dBm) of power, the maximum range is approximately 10 m;
- Class 3 devices broadcast using up to 1 mW (0 dBm) of power, and a maximum range of approximately 5 m.

Bluetooth eliminates the need for cable attachments and provides support to a wide variety of short range applications, such as: audio, data, graphics and even video,

which are seamlessly connected to other portable or stationary Bluetooth devices as soon as they come into range forming ad-hoc networks [32, 33].

2.1.2. Bluetooth Low-Energy (BLE)

One of the most recent versions of Bluetooth wireless technology is Bluetooth Low-Energy (BLE), also called Bluetooth v4.0 [32]. BLE introduces a new communication method, which is optimized for small packet sizes, integrating low energy and low latency features to the Bluetooth Core Specification. It targets short range communications for devices that do not need streaming data or high data throughput; thus, battery operated sensor nodes could last for months or even years [32].

Although the BLE specification keeps the frequency hopping transceiver through many FHSS carriers, albeit fewer than in the standard modes, which combat interference and fading, the lack of Direct Sequence Spread Spectrum (DSSS) on the modulation scheme results in a radio lacking in robustness and vulnerable to jamming and interference; thus, mesh network topologies are unavailable. The highlights of the main differences of Bluetooth wireless communication Core Specification and BLE are shown in Table 2-2.

The new technology features of BLE, such as the infrequent sending of small data packets to a mobile phone and /or to a web service, are creating new opportunities for developers, manufacturers and applications, bringing to life entirely new markets for devices that are low-cost and operate with low power wireless connectivity.

2.1.3. ZigBee

ZigBee technology is a low data rate, low cost and low power consumption wireless mesh network protocol targeted towards automation and remote control applications. The ZigBee stack protocol enables the connectivity of multiple wireless nodes using low data rates and long battery life [25, 34]. In addition, wireless mesh networks using ZigBee specification can be larger than Bluetooth networks. ZigBee compliant wireless devices are expected to hold communication links within 10 to 75 meters, depending on the RF environment, and they operate in the unlicensed RF spectrum, as shown in Table 2-3.

TABLE 2-2
COMPARISON OF BLUETOOTH COMMUNICATION TECHNOLOGY CORE SPECIFICATION AND BLUEETOOTH LOW-ENERGY [32, 33]

Technical Specification	**Core Bluetooth Technology**	**Bluetooth LE technology**
Distance/Range	100 m	50 m
Over the air data rate	1 - 3 Mbit/s	1 Mbit/s
Application throughput	0.7 - 2.1 Mbit/s	0.26 Mbit/s
Active slaves	7	Not defined; implementation dependent
Security	56/128-bit and application layer user defined	128-bit AES with Counter Mode CBC-MAC and application layer user defined
Robustness	Adaptive fast frequency hopping, FEC, fast ACK	Adaptive frequency hopping, 24-bit CRC, 32-bit Message Integrity Check
Latency	Typically 100 ms	6 ms
Total time to send data	100 ms	6 ms , < 3ms
Voice capable	Yes	No
Network topology	Piconet, Scatternet	Star-bus
Power consumption	1 as the reference	0.01 to 0.5 (depending on use case)
Peak current consumption	< 30 mA	< 20 mA (max. 15 mA to run on coin cell battery)
Service discovery	Yes	Yes

TABLE 2-3
ZIGBEE MAXIMUM TRANSMIT POWER LEVELS [34]

Frequency band (MHz)	**Geographical Region**	**Maximum conductive power/ radiated field limit**
2400	Japan	10 mW/MHz
	Europe (except Spain and France)	100 mW EIRP or 10 mW/MHz peak power density
	United States	1000 mW
	Canada	1000 mW (with some limitations on installation location)
902–928	United States	1000 mW
868	Europe	25 mW

Zigbee's physical layer, defined in the IEEE 802.15.4 standard, uses DSSS coding to minimize data loss due to noise and interference [34]. The low band (868/915 MHz) physical layer uses Binary Phase-Shift Keying (BPSK) modulation, whereas the 2.4 GHz physical layer uses Offset Quadrature Phase Shift Keying (O-QPSK).The transmission data rate is 250 kbps at 2.4 GHz, 40 kbps at 915 MHz and 20 kbps at 868 MHz [34].

Parallel Sequence Spread Spectrum (PSSS) using Amplitude Shift Keying (ASK) and DSSS employing O-QPSK are optional modulation techniques at the low band (i.e., 868 and 915 MHz) [35]), thereby achieving data rates of:

- 250 kbps when operating in the 868 MHz and 915 MHz bands if PSSS and ASK is implemented,
- 250 kbps when operating in the 915 MHz band if DSSS and O-QPSK is used,
- 100 kbps when operating in the 868 MHz band if DSSS and O-QPSK is used.

ZigBee is built using the IEEE 802.15.4 standard and follows strict IEEE guidelines to ensure long-term sustainability and reliable operation. The IEEE 802.15.4 standard mainly focuses in the bottom two layers of the protocol, physical layer and media access control (MAC) layer respectively. Moreover, the IEEE 802.15.4 protocol can implement different communication network topologies such as star, mesh, and cluster tree; however, routing strategy mechanisms are not supported [34]. The top layers are driven by the ZigBee stack, where power conservation, low latency, radio link redundancy (elimination of single points of failure in mesh routing schemes) and security services are implemented.

The specification is designed to provide smart network solutions not only to facilitate the interoperability of different multi-vendor devices, but also to improve the efficiency, security and reliability of different ZigBee applications assisting from building automation and smart energy control to health care and fitness.

2.2. BLE or ZigBee for WBAN Applications

Both technologies offer many advantages with respect to Bluetooth Core v1.1, such as less power consumption, higher data rate, and scalability.

In the case of BLE, a quite simple network topology is usually implemented, a star network which is designed around portable devices like a smart phone (good for on-body communications). This simple network topology causes the end of a communication or coming onto the network dynamically as they (or the central device) move in and out of range. It should be easy to add nodes, since they all connect to the central device.

ZigBee, by contrast, is designed to operate in a mesh network. The latter has two main characteristics: ZigBee sensor nodes can have a large coverage network area which is good for many off-body communications, and secondly it permits flexible routing to deal with situations where routing nodes may become unavailable for some reason.

An advantage for Bluetooth core v1.1 and the new BLE is the huge installed infrastructure base of Bluetooth devices. Therefore, it is easier to implement the application and the communication with a device that already includes Bluetooth (mobile phone, PC, PDA, notebook).

Power-wise, BLE devices use a synchronous connection for its connections; meaning that both master and slave wake up synchronously, which helps to keep power on both sides low. On the other hand, WBAN applications using ZigBee specification employ an asynchronous scheme which means that the routers stay awake all the time. The power consumption of the routers is then relatively high, but the end-nodes can wake up at any time, send their data and not have to wait for a specific time slot.

Both standards are relatively similar in terms of complexity but wearable devices using BLE technology tend to have a longer battery life primarily due to the use of short packet overhead and faster data rates, and reduced number of packet exchanges for a short discovery/connect time, while body-worn sensor nodes with the Zigbee specification benefit from a longer range and better reliability with the use of a Direct Sequence Spread Spectrum with orthogonal coding [36, 37] as a modulation scheme and a mesh-like clustered star networking technology. The latter creates a robust and scalable network of different WBAN applications for both on body and off the body communications.

It is evident that ZigBee and Bluetooth are quite different; nonetheless, the power consumption or energy saving is dependent on the type of application and usage

scenario. A comparison of each low power wireless communication technology is shown in Table 2-4.

TABLE 2-4
COMPARISON OF DIFFERENT LOW POWER WBAN COMMUNICATION STANDARDS – BLUETOOTH AND ZIGBEE [25, 32-34, 36, 37]

Property	Bluetooth	ZigBee
IEEE Standard	802.15.1	802.15.4
Frequency Band -(GHz)	2.4	0.868 / 0.915 / 2.4
Max. Tx. Rate	1 - 3 Mbps	20 / 40 / 250 Kbps
Nominal Range-(m)	10	10-100
Nominal Tx. Power-(dBm)	0-10	-25 - 0
Number of RF Channels	79	1 / 10 / 16
Channel BW-(MHz)	1	0.3 / 0.6 / 2
Modulation Type	GFSK / DPSK	BPSK / BPSK / O-QPSK
Spreading	FHSS	DSSS
Coexistence Mechanism	Adaptive Freq. Hopping	Dynamic Freq. Selection

2.3. IEEE 802.15 Task Group 6 (TG6) – WBAN standard

The advances in communication and electronic technologies have enabled the development of compact and intelligent devices which can be deployed in and around the human body. A network of wearable sensors distributed along a person's body and wirelessly connected defines the concept of WBAN platforms. Different wireless sensors deployed around the user's body offer routine diagnostic testing, such as EEGs (electroencephalogram), ECGs (electrocardiogram) and control, and monitoring of vital signals such as temperature, heart rate, oxygen, and blood pressure. It may also find use in automated drug delivery systems for treatment of chronic conditions such as diabetes, to interconnect a wearable or implanted glucose sensor. As an extension to these sensors, base units are deployed on or close to the

human body to collect information and relay command signals to the various sensors in order to perform specific tasks. The concept of WBAN communication systems and its applications is depicted in Fig. 2.2.

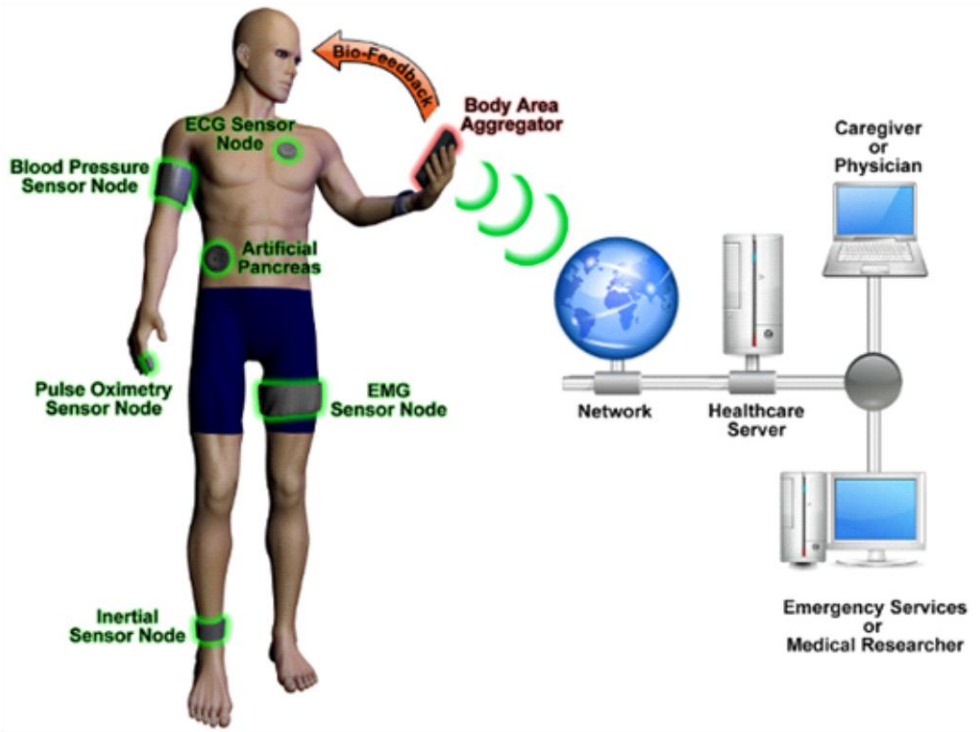

Fig. 2.2.The concept of WBAN communications and its possible components [14, 23, 38]. Sensing and gathering data from individual wireless sensor nodes distribute around the human body. The collected information is transmitted to a healthcare server via the main gateway which can be a smart phone.

However, the radio communication between peer devices depends on the geographical region which allocates different frequency portions of the spectrum for specific body-centric communications (see Table 2-1 and Table 2-3). Consequently, the interoperability of WBANs among other available on-body wireless nodes is not plausible (i.e., restrictions of the communication protocol).

In order to create an international standard to serve a variety of applications, including medical and personal entertainment, the IEEE has designed and published the IEEE 802.15.6-2012 standard (approved on the 6th of February 2012) [38]. IEEE 802.15.6 is designed to support:

- short-range communications,
- extremely-low-power consumption,
- data rates up to 10 Mbps,

– discovery and quality of service (QoS),
– high reliable and re-configurable wireless networks,

which are implemented in close proximity to, or inside, the human body (i.e., in/on/off the body wireless communication systems). The standard uses existing industrial scientific medical (ISM) bands as well as frequency bands approved by national medical and/or regulatory authorities [23, 24, 38, 39]. The frequency bands, the effective isotropic radiated power (EIRP) for non-low-power low-duty-cycle (LP/LDC) and the channel bandwidth of compliant devices that are able to support transmissions and reception using the IEEE 802.15.6 standard are listed in Table 2-5.

TABLE 2-5
COMPLIANT FREQUENCY BANDS FOR THE IEEE 802.15.6 [38]

Frequency Band MHz	**Number of channels N**	**EIRP[2] for non LP/LDC dBm**	**Channel Bandwidth MHz**	**Information Data Rate kbps**
402 - 405	10	-16	0.3	75.9
420 - 450	12	-10	0.32	151.8
863 - 870	14	-10	0.4	303.6
902 - 928	60	-10	0.4	455.4
950 - 958	16	-10	0.4	75.9
2360 - 2400	39	-10	1	151.8
2400 – 2483.5	79	-10	1	187.5

The standard also includes the effects of the human body on portable antennas (which varies with male, female, skinny, heavy, etc.), radiation pattern shaping to minimize the specific absorption rate (SAR) into the body, and changes in characteristics as a result of the user motions. The main focus of the Task Group is low power devices which work at low data rates.

Nonetheless, WBAN sensors can also be applied to other fields which include [40]:

[2] Effective Isotropic Radiated Power (EIRP) is expressed in decibels. It is the power needed by an ideal antenna (one that radiates uniformly in all directions) to generate the same electrical field strength that the actual device produces at a particular distance.

- Military applications, including soldier location, tracking, image and video transmission,
- Access & identification systems by using individual peripheral devices.
- Navigation and support in the car or while walking, for example, access to emergency services, such as police, paramedics, fire fighters.

2.4. Radio Propagation and Antennas for WBAN communications

The evolution of current and future wearable devices towards the use of radio frequency communications, instead of wired systems, has become popular on the design of compact antennas integrated into small body-worn modules. Each wireless sensor not only monitors specific physiological parameters [40, 41], but also enables the data exchange with a central unit. The communication channel may consist of a standard wireless technology that can be ZigBee or Bluetooth or a combination of both, and hence taking advantage of individual features such as network topology or high data rates.

In order to establish on-body radio links, individual sensor nodes are dependent on antenna design, power consumption and body location. In terms of antennas and propagation, efficient design requires both good understanding of the properties of the propagation channel involved, and the development of small, lightweight antennas conformal to the human body. Therefore, individual antennas placed around the human body need to be electromagnetically characterised through numerical and experimental techniques.

2.5. Fundamental Parameters of Propagation Models

Antennas are an essential part of any wireless communication system. An antenna is: *part of a transmitting or receiving system that is designed to radiate or receive electromagnetic wave* [42]. The topology of the antenna defines the wave propagation characteristics of a given wireless system; it also determines the frequency of operation and the reliability of individual radio links. In contrast with normal wireless systems, where the antenna's output impedance tend to be real, antennas for on-body applications present a highly reactive component inherit from the small design and the proximity to the lossy human tissues.

For the case of a simple transmitting antenna (without any lossy dielectric), the maximum power radiated is defined by (3.1). The terms R_r and R_L in (2.1) represent the radiation resistance and the loss resistance of the antenna, respectively [42]. The $V_{Output\text{-}Trans.}$ is the maximum voltage generated by the source. In order to achieve maximum power transfer, the input impedance of the antenna has to be equal to the conjugate impedance of the output impedance of the RF transceiver which is generally highly reactive [42, 43].

$$P_r = \frac{\left|V_{Output\text{-}Trans.}^2\right|}{8}\left[\frac{R_r}{\left(R_r + R_L\right)^2}\right] \qquad (2.1)$$

In a free-space environment, the radio channel is modelled by the Friis transmission equation which is mathematically represented by (2.2) where:

- P_t and P_r are the transmit power and received power, respectively;
- G_t and G_r are the antenna gains (with respect to an isotropic radiator) of the transmitting and receiving antennas, respectively;
- d is the separation distance;
- λ is the wavelength at the frequency of operation.

$$P_r = \frac{P_t G_t G_r \lambda^2}{(4\pi)^2 d^2} \qquad (2.2)$$

The latter not only estimates the received signal strength, but also the range of the wireless system. Since the power is spread over the surface area of the sphere, which increases as d^2, the available power at the receiver antenna decreases in proportion to d^2 [42, 43]. The elements of a simple wireless communication system are illustrated in Fig. 2.3.

The predicted received power decays as a function of the separation distance d, where $d \geq 2D^2/\lambda$ (D is the largest dimension of either antenna. Beyond $d=2D^2/\lambda$ lies

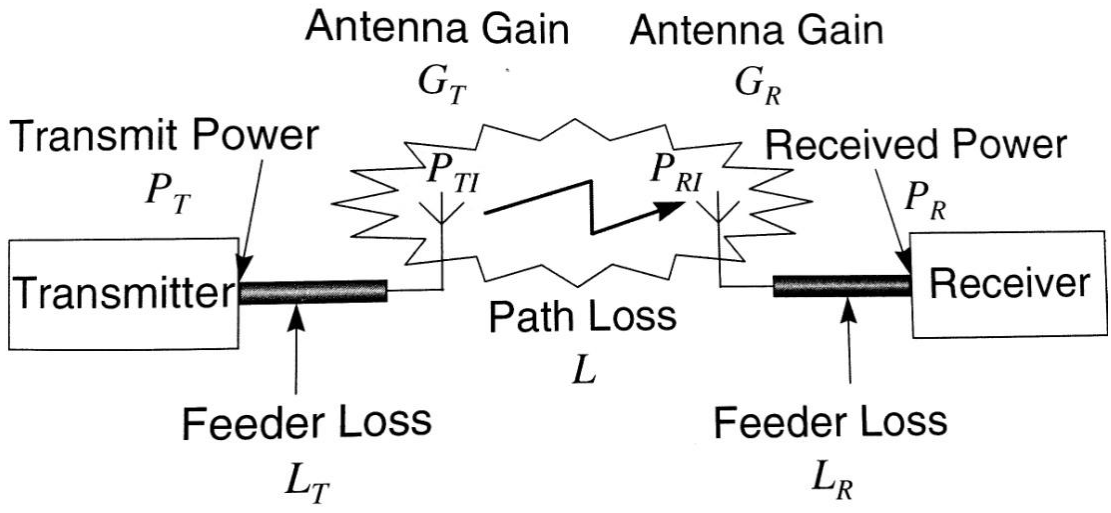

Fig. 2.3. Elements of a simple Wireless Communication System [43].

the far-field region). For antennas using the same polarization, aligned to their maximum directional radiation and placed within a Line-of-Sight (LOS), (2.2) is still applicable.

However, common radio channels do not necessarily meet these conditions; therefore, all these factors previously mentioned need to be considered. A complete transmission formula is given by (2.3) where:

- Γ_t and Γ_r are the reflection coefficients at the input of the transmitting and receiving antennas, respectively;
- $\left|\hat{\rho}_t \times \hat{\rho}_r\right|^2$ is the polarisation[3] matching factor between Tx. and Rx. antennas.

$$\frac{1}{PL} = \frac{P_r}{P_t} = (1-\left|\Gamma_t\right|^2)(1-\left|\Gamma_r\right|^2)\left|\hat{\rho}_t \times \hat{\rho}_r\right|^2 G_t G_r \left(\frac{\lambda}{4\pi d}\right)^2 \qquad (2.3)$$

The signal attenuation as a positive quantity is represented by the path loss (PL), which is defined in decibels (dB) as the difference between the effective transmitted power and the received power $PL_{(dB)}=P_{t(dB)} - P_{r(dB)}$.

[3] The alignment of the electric field vector of a plane wave relative to the direction of the propagation defines the polarization of the wave. Linearly polarized antennas have the electric field vector in the same direction along the whole propagation.

2.5.4. On-Body Radio Channel Modelling

Analytical and empirical propagation models have been well covered in the literature [14, 44]. Measurements, for both indoor and outdoor environments, have shown that the average received signal is best characterised and modelled by lognormal distributions [14, 44]. The mathematical approximation of power loss as a function of distance is defined by:

$$P_{rdBm} = P_{tdBm} - \left[PL(d_0)_{dB} + 10\gamma \log\left(\frac{d}{d_0}\right) + \chi_\sigma \right] \qquad (2.4)$$

The term χ_σ in (2.4) represents distributed random variables modelled by a zero-mean Gaussian function, γ defines the path loss exponent which indicates the rate at which the path loss increases with distance and $PL_{(d_0)dB}$ is the initial path loss at reference distance d_0 including antenna gains [45, 46]. Generally, the reference distance should always be in the far field of the antenna so that the near-field effects do not alter the reference path loss $PL_{(d_0)dB}$. The latter is calculated using the free space path loss formula given by equation (2.2) or through field measurements at distance d_0. For the case of on/off-body communications (2.4) includes not only antenna characteristics, but also human body properties (shadowing which depends on the user) and average channel attenuation, which is defined by surrounding environment [47, 48].

In order to encompass a detailed description of the wave propagation environment, path loss models have to be combined with other multiplicative and time-variant processes, which are categorised as short-term fading and long-term fading (see Fig. 2.4). Long-term fading, often called shadowing, is caused by the change in path length due to the motion of transmitter and/or receiver relative to each other or due to an obstruction or shadowing in the propagation path. Some paths will suffer increased loss, while others will be less obstructed and have an increased signal strength.

On the other hand, short-term fading is mainly caused by the superposition of multiple copies of the received signal, which are different in magnitude, phase and time. These happen due to a very common phenomenon in wireless communications

called multipath propagation where the signal from the transmitter to the receiver travels via more than one path, each having a different phase and attenuation factor. The received signal levels change so rapid that it can only usefully be predicted by statistical means.

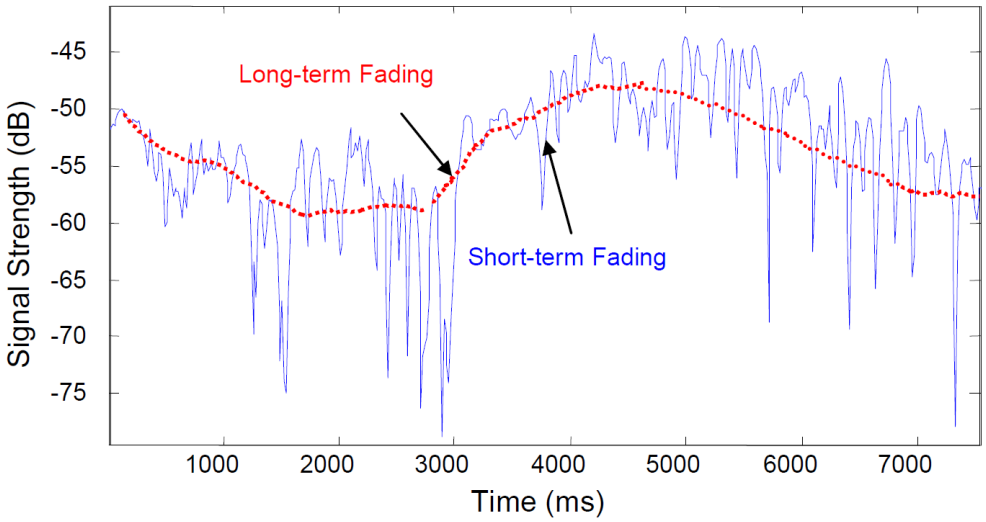

Fig. 2.4.An example of a received signal envelope with both the short-term and long-term fading (dotted line follows the long-term variation). Long-term fading is caused by the change in path length due to the motion of transmitter and/or receiver relative to each other. Short-term fading is caused by the superposition of multiple copies of the received signal.

The contribution of each of these processes is frequently characterised by empirical methods, based on fitting curves (statistical distribution models), and deterministic propagation models, based on theoretical and computational models, such as ray tracing, method of moments (MoM) or full wave electromagnetic numerical techniques like the finite-difference time-domain (FDTD).

In mobile communication, shadowing happens in large areas due to presence of buildings. However, in the case of on-body propagation channels, not only shadowing by the body but also changes in antenna direction and distance variation may contribute to the fading. Different statistical distributions have been fitted to model the WBAN path loss variation on data collected for a diverse set of activities [14, 47, 49-52]. It has been shown that a mobile WBAN radio link (dynamic channel with strong fast fading) is best characterised by Rician and Nakagami distributions, whereas a long term fading (often referred to as slow fading-shadowing) is best described by a Log-normal and Gamma distribution [53, 54].

A procedure for statistical model identification, which is free from the ambiguities inherent in the application, is the Akaike information criterion (AIC)

[55]. The Akaike's Information Criterion (AIC) score model is used to compare and evaluate the goodness of the fitting distribution for each sport activity. Most of the studies use the second order AIC (AIC_c) model, which is given by (2.5), because the collected sample size is finite. The term $\ln\left(l(\hat{\theta}|\text{data})\right)$ in (2.5) is the value of the maximized log-likelihood over the unknown parameters θ, given the data and the model, K is the number of parameters estimated for that distribution and *n* is the sample size.

$$AIC_c = -2\ln\left(l(\hat{\theta}|\text{data})\right) + 2K + \frac{2K(K+1)}{(n-K-1)} \qquad (2.5)$$

The criterion has been applied to evaluate the goodness of five different distributions commonly used in WBAN communications: normal, lognormal, Nakagami, Weibull, and Rayleigh that seem to provide the best fitting for the measurements. They are all two parameter distributions (K=2), except the Rayleigh (K=1). A smaller value of AIC_c means a better statistical model, and the criterion is used to classify the models from the best to the worse; to facilitate this process, the relative AIC_c (shown in (2.6)) is considered and results are normalized to the lowest value obtained where a zero value indicates the best fitness.

$$\Delta_i = AIC_{c,i} - \min\left(AIC_c\right) \qquad (2.6)$$

2.6. Electromagnetic Properties of the Human Tissues

The wave propagation alongside the human body is not influenced only by the antenna design topology, the environment or the application, but also by the lossy dielectric tissues, which produce changes on the antenna's input impedance, distortion-fragmentation of the radiation pattern, reduced gain and degradation of the radiation efficiency [24, 56].

Therefore, it is necessary to characterise the electromagnetic response of the antenna when operates in close proximity to the human tissue. The rate of change of the electrical properties (conductivity and relative permittivity) of the latter needs to be quantified and hence the effects towards the antenna's radiation performance are

understood. Human body tissues are generally lossy materials and their complex relative permittivity ($\hat{\varepsilon}$) is defined by (2.7):

$$\hat{\varepsilon} = \varepsilon' - j\varepsilon'' \tag{2.7}$$

where:

- ε' is the relative permittivity (ε_r) of the material,

$$\varepsilon' = \varepsilon_r \tag{2.8}$$

- ε'' is the out-of-phase loss factor associated with the tissue such that

$$\varepsilon'' = \frac{\sigma}{\omega\varepsilon_o} \tag{2.9}$$

In [57], measured values for a wide range of frequencies (10 Hz to 20 GHz) has been intensively studied and characterised. The frequency dependence of the complex permittivity of different biological tissues has been estimated using (2.10), which is a four-pole Cole-Cole model expression where:

- ε_∞ is the permittivity at field frequencies where $\omega\tau \gg 1$ (i.e., the high frequency permittivity);
- $\Delta\varepsilon_n$ is the magnitude of the dispersion, described as $\Delta\varepsilon = \varepsilon_s - \varepsilon_\infty$ (ε_s is the permittivity at $\omega\tau \ll 1$);
- τ_n is the relaxation time;
- α_n is a measure of the broadening of the dispersion;
- σ_i is the conductivity due to ionic drift and the lower frequency polarization mechanisms (i.e., static ionic conductivity).

$$\varepsilon_r = \varepsilon_\infty + \sum_{n=1}^{4} \frac{\Delta\varepsilon_n}{1+(j\omega\tau_n)^{(1-\alpha_n)}} + \frac{\sigma_i}{j\omega\varepsilon_o} \tag{2.10}$$

The results show that relative permittivity at low frequencies (lower than 100 Hz) can reach values up to 10^6-10^7, but the permittivity decreases at high frequencies with respect to three main relaxation factors, known as:

- α dispersion, in the high frequency region, due to the polarization of water molecules;

– β dispersion, in the hundreds of kilohertz region, a consequence of the polarization of cellular membranes;
– γ dispersion, in the low frequency region, associated with ionic diffusion processes at the site of the cellular membrane.

The measured permittivity and conductivity values for a number of human tissues for a frequency range of 0.5 GHz to 20 GHz are depicted in Fig. 2.5a and Fig. 2.5b. The results are obtained from a compilation presented in [58-60] which covers a wide collection of different body tissues and it also provides the appropriate dielectric values at a desired frequency. It can be seen that at lower frequencies, the permittivity is relatively high and the conductivity low; hence, the EM wave can propagate through the human body. At higher frequencies, the lossy effect is higher, so the skin depth decreases.

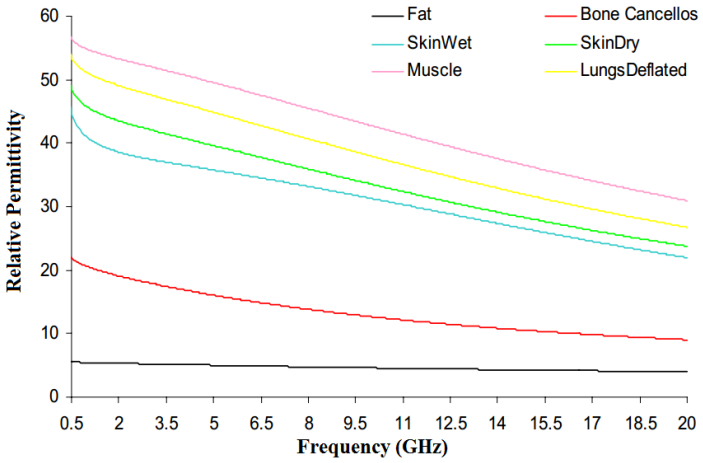

(a)

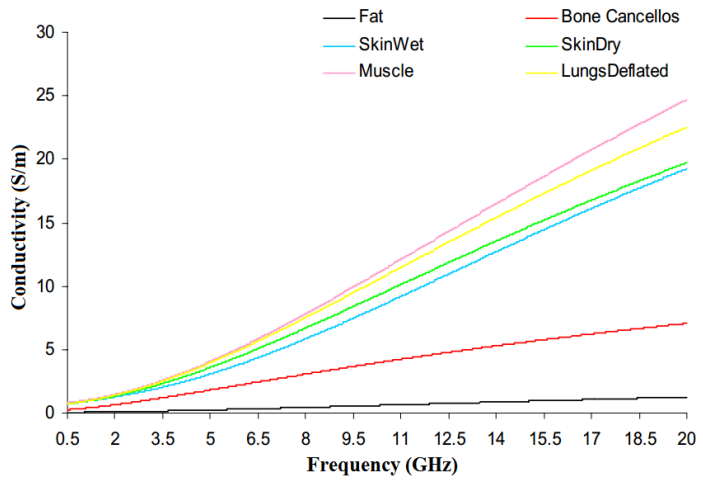

(b)

Fig. 2.5.Relative permittivity (ε_r) and conductivity (σ) for specific human body tissues at different frequencies obtained from a compilation presented in [24, 58-60]. The results can help in producing modelling equation to determine the appropriate dielectric values at each desired frequency.

The current study is focused on the thoracic section of the human body, as it represents the main area for a variety of healthcare applications, such as cardiac monitoring, respiratory sensors, pacemakers, gastric band controllers, bladder implants and others. The trunk not only includes a great variety of organs, but is also anticipated to be the most complex and irregular environment for electromagnetic modelling and, hence, for on-body radio links.

A summary of the electrical properties for human tissues at 2.45 GHz is described in Table 2-6 [57, 58, 60]. It can be seen that the human anatomy presents heterogeneous tissues with different electrical properties.

TABLE 2-6
ELECTRIC PROPERTIES OF SPECIFIC HUMAN BODY TISSUES USED FOR THE VISIBLE MAN MODEL PROJECT AT 2.45 GHZ. THE VALUES WERE TAKEN AT BODY TEMPERATURE USING AN IMPEDANCE ANALYSER [57, 58, 60].

Tissue Name	Conductivity S/m	Relative Permittivity	Loss Tangent
Blood	2.56	58.23	0.32
Body Fluid	2.49	68.19	0.27
Bone Marrow	0.096	5.29	0.13
Fat	0.105	5.28	0.14
Muscle	1.75	52.70	0.24
Nerve	1.09	30.12	0.26
Skin Dry	1.47	37.98	0.28

In order to derive a generic on-body radio propagation model (either analytical or empirical), the human body anatomy is usually replaced by simplified phantom models which have the same electromagnetic properties of specific human tissues [61-67]. Most of the empirical, numerical and theoretical studies use a three layer model made of skin, fat and muscle. This type of phantom has shown good results for on/off-body communications; however, some particular studies such as in-body communications (implants) need to use specific body tissues for the EM modelling.

Different phantoms with different characteristics have been presented in the literature, from liquid [63, 65] and gel [64, 67], to semi-hard and solid [66, 68] models. An example of a three layer gel phantom used for the characterisation of implanted RFID tags [67] is displayed in Fig. 2.6.

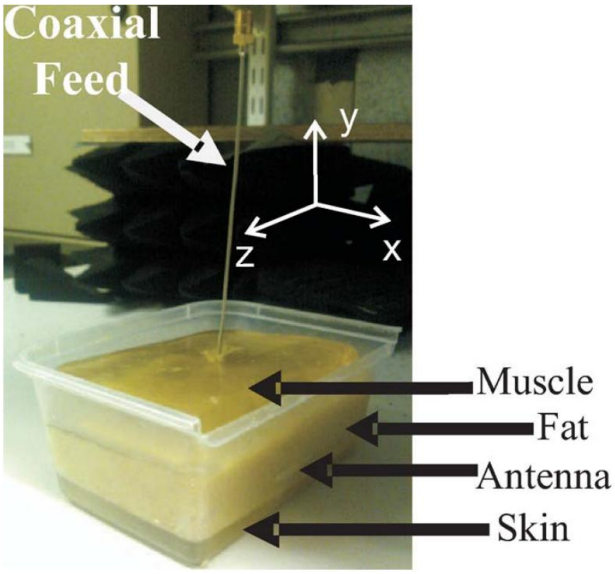

Fig. 2.6.A three layer Gel Phantom used to mimic electrical properties of the human body for the characterisation of implantable RFID tags [67].

A homogeneous liquid phantom, made of a glycol solution that has the same electric properties of the human muscle at 2.45 GHz, was used to evaluate antenna performance and characterise over-the-body-surface communications using a variety of higher mode microstrip patch antennas (HMMPA) in [61, 62]. Although the empirical phantom model only used a single dielectric layer, the results showed that over-the-body communications are plausible if the antenna's maximum gain is tangential to the body surface, thus maximising propagation through creeping waves.

On the other hand, a theoretical study was presented in [69] for a 2D, three-layer human model (skin-fat-muscle) for over-the-body or surface communications. Their analytical study showed that TE waves are highly attenuated and TM Zenneck (non-radiating energy) propagates for short distances, preventing the transmission and reception.

2.7. Antennas for Body-Centric Communications

A wide variety of antenna designs can be found in the consumer market. Most of these radiating elements are integrated in commercial wireless systems such as the Wi-Fi hubs. Nonetheless, they still face constraints when on-body radio links are part of the applications. Antennas for on-body communications need to be further characterised taking into account the effects of the human tissue. Wearable antennas

also need to follow compact and lightweight designs that are conformal to the human shape. Different antenna models and the effects of the human body on their radiation properties are described in Table 2-7.

TABLE 2-7
ANTENNA DESIGN TOPOLOGIES FOR MICROWAVE FREQUENCIES

Antenna Types	Pros	Cons	On-Body Scenario
PCB antenna	▪ Low cost involved ▪ Good performance for frequencies above 868 MHz ▪ Small designs at high frequencies ▪ Standard design antennas widely available	▪ Difficult to design small and efficient PCB antennas for frequencies below 433 MHz ▪ Potentially large size at low frequencies	▪ If a ground plane is present alongside the human surface, they offer good performance. ▪ Antenna radiation parameter do not change a lot
Chip antenna	▪ Very small in size ▪ Solutions available on the consumer market ▪ Very Low cost	▪ Medium to Low performance ▪ Depending on the substrate used the cost may varies	▪ Most of them are fitted with coplanar ground planes. The non-presence of ground underneath the chip affects the antenna radiation response.
Whip antenna	▪ Good performance ▪ Solutions available on the consumer market	▪ High cost ▪ Difficult to fit in many applications (large in size)	▪ Too large for on-body applications ▪ Difficult to wear them
Wire antenna	▪ Very low cost ▪ Easy to manufacture	▪ Mechanical manufacturing of Antenna	▪ Low efficiency, higher losses ▪ Large and uncomfortable to wear
Customise antenna	▪ Custom based design ▪ (Intellectual Property-IP)	▪ High cost involved compared to PCB antenna designs.	▪ Good performance and reliable.

Frequently, PCB antennas with ground planes facing the human body surface counteract the effects of lossy tissues producing strong electromagnetic fields around the antenna ground plane. The use of an antenna with a ground plane, for example a microstrip patch, reduces the interaction of the human tissue and the radiating element thus minimizing the absorption from the human tissues. If the size of the ground plane is $\lambda/4$ larger than the maximum length of the radiating element, the return loss (S_{11}) of the antenna has less fluctuations, and hence good radiation performance; but, if the ground plane is smaller than $\lambda/4$, the radiating antenna

couples high reactive near fields which interact with the human body surface, thus producing significant energy losses.

In contrast to the aforementioned design, antennas without a (significant) ground plane tend to be highly affected by the human body, which includes chip antennas. Although the antenna itself is compact in size, the designs are fitted with extended coplanar ground sections which form an essential part of the radiating antenna. The simulation results of a commercial chip antenna, the Antenova's 'Rufa' antenna, and the effects of size reduction are described in Fig. 2.7 and Table 2-8 [24, 70, 71].

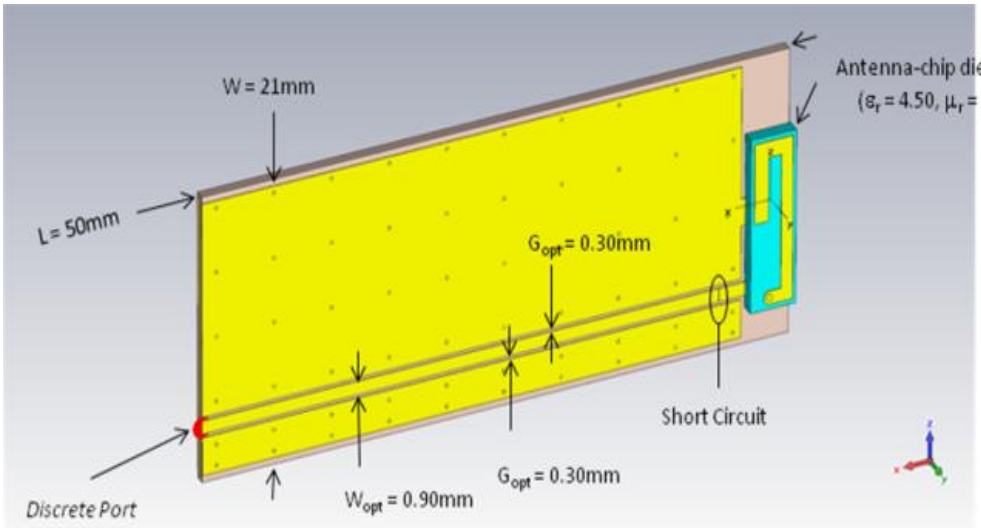

(a)

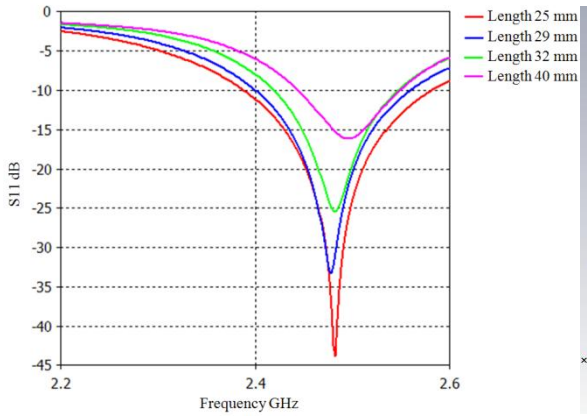

(b)

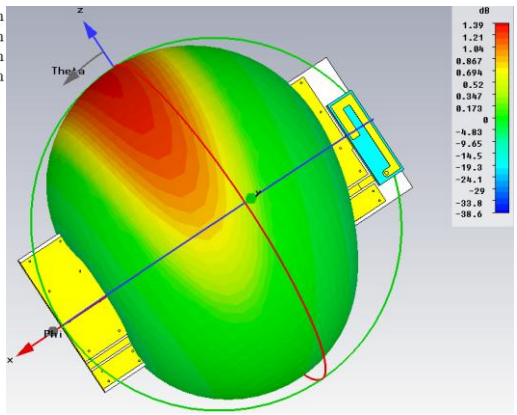

(c)

Fig. 2.7.Simulation results of a commercial chip antenna, Antenova's Rufa 2.4 GHz SMD Antenna module [70, 71]. (a) Design model of the Rufa antenna implemented in CST Microwave Studio; (b) Effects of different PCB lengths on the reflection coefficient of the Rufa antenna; (c) 3D radiation pattern of the Rufa antenna with a maximum radiation pointing.

TABLE 2-8
EFFECTS OF SIZE REDUCTION ON ANTENOVA'S RUFA 2.4 GHZ SMD ANTENNA MODULE

Length mm	Freq. GHz	S11 dB	Gain dBi	Effic. %
50	2.44	-22.04	1.38	68.73
40	2.41	-21.84	0.68	64.61
30	2.45	-10.02	-1.30	41.68
25	2.46	-6.97	-2.18	31.93

2.8. Optimised Antennas for WBAN operation

The on-body communication literature includes several antenna topologies, from the simplest designs (printed monopole and printed dipole antennas) to more complex models (PIFAs, HMMPA, WIA antennas). Some of these antenna designs for WBAN applications are shown in Fig. 2.8 and Table 2-9 lists the layout dimensions for a couple of them [48, 61, 62, 72-74].

Many studies have been done on the operation of antennas located in close proximity of the body [72, 75, 76], as well as on the SAR [77, 78] and on the propagation on and off the body, for use in cellular networks [79]. In [72] a parametric study to evaluate how the antenna-body spacing affects the antenna performance has been presented. The farther the antenna is from the body, the lower is the absorption from the human body. The use of a lossy material to keep this spacing is beneficial, as it leads to SAR reduction because part of the radiating power is dissipated in the lossy material rather than in the body tissues.

To enable the integration of wireless devices in garments, antennas made out of textile materials have been proposed [80-82]. In [80], a patch antenna integrated into protective clothing for fire-fighters was introduced. The antenna was printed on a flexible pad of foam, which is commonly used in protective clothing.

In [83-85] narrowband antennas are printed above Electromagnetic Band Gap (EBG) structures to reduce the radiation towards the human body, and minimize the detuning effect. In [84], Langley et al. proposed a flexible dual-band patch antenna (2.45 and 5.5 GHz) printed on an EBG textile substrate made of felt. Results demonstrated that, introducing the EBG, the radiation into the body is reduced by

over 10 dB, and the antenna gain is improved by 3 dB. However, the antenna is big in size (120 mm x 120 mm).

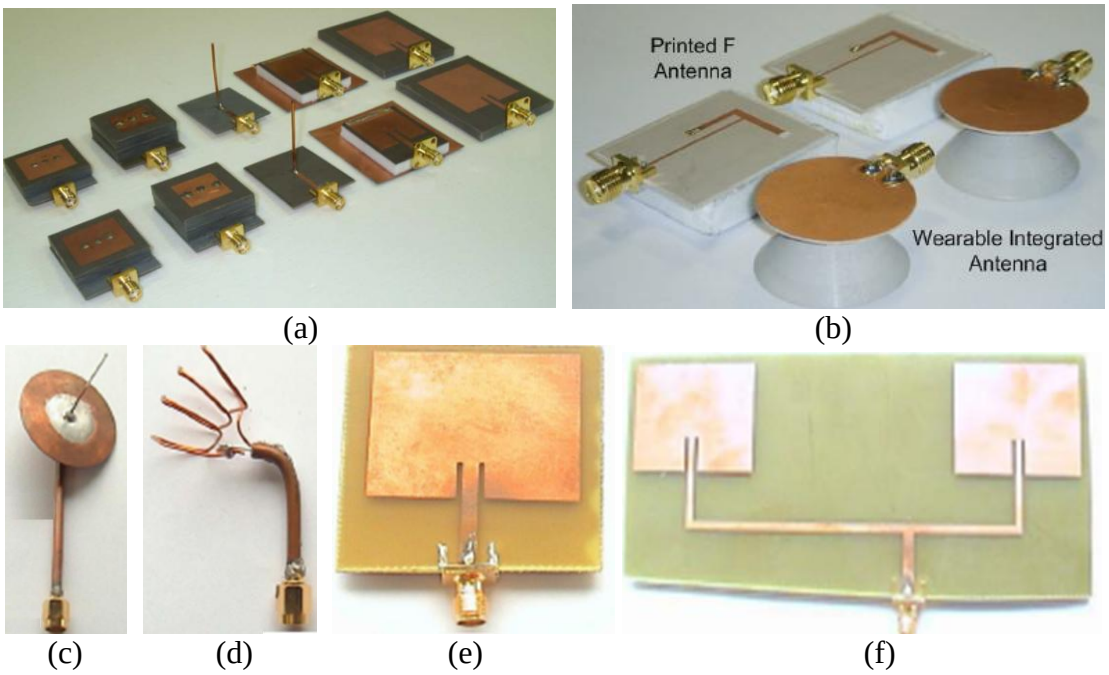

Fig. 2.8.Wearable Antennas designed for the radio channel characterisation of different WBAN links. (a) HMMPA antennas consist of a ground-plane and patch metallization on a dielectric substrate with εr = 2.33 (Taconic TLY-3, PTFE woven glass)[61]; (b) Printed-F antenna is constructed on 0.6 mm thick CER 10 substrate. The wearable integrated antenna (WIA) consists of a 3 mm diameter copper element embedded in a tapered Taconic CER 10 dielectric substrate (εr = 10.2). Dimensions for each antenna can be found in [73]; (c) monopole with a small ground plane, (d) coil with small ground plane, (e) microstrip patch on a small ground plane, (f)Two element patch array with beam at 30 to give a broadside beam. Further details for figures (c)-(f) can be found in [48, 74].

TABLE 2-9
ANTENNA TOPOLOGIES AND THEIR PHYSICAL DIMENSIONS FOR WBAN COMMUNICATIONS EXTRACTED FROM BODY-CENTRIC LITERATURE. THE LISTED BODY-WORN ANTENNAS ARE DESIGNED TO OPERATE AT ISM BAND 2.45 GHZ [48, 61, 73, 74].

Antenna Type	**Size mm**
Monopole (see Fig 2.9c)	H = 31; T = 0.5; D_{ground} = 50 x 0.4
Loop (see Fig 2.9d)	4 turns; D = 19; L = 30
Microstrip Patch (see Fig 2.9e)	W =38; L = 29; Ground Plane = 48 x 48
WIA (see Fig 2.9b)	H= 12.5 x 0.5; Top Plate = 30 x 0.5
HMMPA-10 (see Fig 2.9a)	L_1 = 37; W_1 = 30; h_1 = 1; L_2 = 18; W_2 = 18; h_2 = 9.5
Printed-F (see Fig 2.9b)	30 x 37

Scanlon et al. presented a set of higher mode microstrip patch antennas (HMMPA) operating at 2.45 GHz [62]. The antennas are excited at the higher TM_{21} resonant mode which has the advantage of having a vertical monopole-like radiation pattern. In this way, despite a total antenna height of only $\lambda/20$, the on-body coupling performance is comparable to that achievable with a quarter wavelength monopole and significantly better performance than that measured with a fundamental microstrip patch antenna. The improved performance is achieved thanks to the resonance of higher modes which generates a vertical monopole like radiation.

A cavity slot antenna is proposed in [86] for communication at 2.45 GHz. The polarization of the antenna is normal to the body, thus leading to minimized path loss in the on-body link and relatively high efficiency (50%) when it is body-mounted. In [87], a patch antenna on a ceramic substrate with a high dielectric constant close to the human body was presented by Adel et al. It was concluded that, by choosing a thicker substrate, the radiation efficiency can be improved; and that an improvement of the radiation properties could be accomplished by using a substrate with a lower dielectric constant. Salonen et al. have presented a flexible planar inverted F antenna (PIFA) that can be applied for smart clothing intended for use with wearable computers as part of a WBAN [88].

A full and comprehensive literature review of wearable antennas is not possible due to space constraints. However, the above described some representative WBAN antenna models for different WBAN communication channels.

2.9. Discussion and Conclusion

The chapter presented a brief overview of different communication standards, i.e., Bluetooth, BLE and Zigbee, for body-centric network communications. The advantages and main characteristics of each specification, such as bandwidth, modulation, power consumption, is also addressed, highlighting current regulations and their relevance for present and future WBAN applications.

There will surely be some overlap in application areas, as there is always some tendency to try to broaden the scope of standards, but overall Bluetooth low energy and ZigBee target different areas. They each have their own strengths and weaknesses. BLE will be able to communicate with billions of Bluetooth devices, but

does not support mesh. ZigBee can cover large areas, but is not so well suited to ad-hoc networking.

The standardization of WBAN communications produced by IEEE802.15.6 not only demonstrates the potential of wearable sensors, but it also extends and provides a wide target sector from healthcare to sports, lifestyle and even military. The standard defines and characterises different body-centric topologies, maximizing the benefits and interoperability of different communication standards.

The chapter also described the basics of antennas and radio propagation for BCWC. Propagation models traditionally used in mobile communications are adopted for the characterisation of body-centric communications. The on-body radio channel and fading effects are also described, highlighting several features that need to be studied, such as the dynamic nature of the body, the effect of the indoor environment, and the subject-specificity of the radio channel.

The electromagnetic properties of human tissues and the significance of human body modelling for the study of EM waves alongside the human body were also discussed. This latter task can be accomplished by developing physical phantoms, or digital phantoms loaded in numerical EM codes. In the first case, measurements are performed adopting physical phantoms or real subjects, while in the second case, digital body phantoms are embedded in numerical electromagnetic codes.

A summary of different commercial antenna topologies (which are ready to use) was presented; but they still need additional parametric study for the operation within on-body scenarios.

The last section presented a literature review on the state-of-the-art of wearable antennas for BCWC. On-body antennas are described from simplest structures to the most complex designs, such as textile and EBG antennas.

Chapter 3

Design and Development of Body-Centric Wireless Sensors using the IEEE 802.15.4 Standard

Early research on wireless sensor networking grew out from technologies developed by defence programs and military applications. One of the first platforms targeting wireless sensor networks was TinyOS, which began as a project at UC Berkeley, funded by the Defence Advanced Research Projects Agency program (DARPA) [89, 90]. Other companies, such as Ember, Dust Networks and Sensicast Systems, have also started the development of wireless sensors, extending their applications to simple mesh networks. The high demand of industrial applications created an open market for wireless sensors; however, they were lacking a communication standard. In 2002, Phillips Technologies and Motorola developed the

first communication protocol called ZigBee. The evolution and use of the protocol have created a new area network, the low-power low-data-rate Wireless Personal Area Networks (WPAN), which covers such applications as Home and Building Automation, Smart Energy, and Health Care.

3.1. Understanding the IEEE 802.15.4 standard

An overview of different communication standards for WPAN and WBAN technologies has been given in Chapter 2. One of the aforementioned wireless protocols, the ZigBee specification, is built upon the physical layer (PHY) and medium access control (MAC) defined in IEEE 802.15.4 standard (see Fig. 3.1).

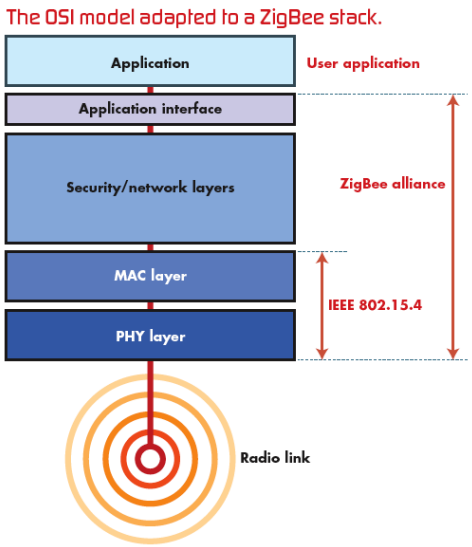

Fig. 3.1.Relation between the ZigBee Alliance specification and IEEE 802.15.4 standard when is compared to the OSI Communication Model.

ZigBee's upper layers manage various communication features, such as the network topology (where the routing protocols are defined), security, authentication, and encryption. The top layer is designated to application services that are driven by an application interface (API). The API is responsible to create applications objects for each end-user application. A predefined number of actions is easily implemented thanks to the ZigBee stack specification, which is recorded in the internal flash memory of the microcontroller. The specification not only yields a quick applications development, but also easily manages multiple sensor nodes (scalable network), thus allowing the functionality and inter-operability between different vendors' products.

Nowadays, highly integrated and compact ZigBee radio modules, housing low-power electronics, can be found in the consumer electronics market. Most of them

integrate a type of microcontroller (e.g., Phillips, Atmel, Microchip) with flash memories between 60 kbytes to 256 kbytes, an RF transceiver (including the associated baseband circuitry) and a type of antenna. The antenna topology is usually small and compact, such as PCB printed (e.g., microstrip path, IFAs, PIFAs) or dielectric chip antennas. Moreover, other wireless modules may include a type of micro-miniature coaxial connector (MMCX) for the connection of an external antenna. A list of different ZigBee-ready solutions, highlighting individual design characteristics (e.g., board size, type of antenna, power consumption) is described in Table 3-1, and Fig. 3.2 illustrates some of those radio-modules.

TABLE 3-1
LOW POWER WIRELESS SSYSTEMS OPERATING AT THE 2.45 GHZ ISM BAND

Manufacturer	SOC/SIP Chip	MCU core	Antenna	TX mA	RX mA	Tx-Power dBm	Sensitivity dBm	PCB Size mm x mm
Atmel [91]	AT86RF230 AT86RF212	8-bit ATmega 1281v	chip antenna or U.FL connector	50	23	20	-104	38 x 13.5
California Eastern Laboratories [92]	Free-Scale MC13224V	32-bit ARM7	PCB Trace Antenna or MMCX connector	193	30	20	-100	25.4 x 36.5
Radiocrafts [93]	Chipcon CC2420	8-bit ATmega 1281L	integrated, MMCX or RF on pin connector	140	28	17	-92	16.5 x 35.6
Jennic [94]	JN5139	32-bit 16 MHz RISC	SMA or U.FL connector	125	45	19	-100	18 x41
ST Microelectronics [95]	SN260 network processor	16-bit XAP2b	Integrated Murata antenna	36	36	3	-95	25 x 13.7
RF Monolithics	Chipcon CC2430	8-bit 8051	RF-IO pad built-in	130	33	17	-95	47 x 21.2
Radios, Inc.	Ember 2420	8-bit ATmega 1281L	RF on pin	17.4	19.7	0	-94	25.4 x 18.4
Radio Pulse	MG2400-F48	8-bit 8051	SMA or receptacle connector	95	29	14	-99	38 x 27
Crossbow Technology [96]	ATmega128L + AT86RF230	8-bit ATmega1281	Internal	10 13 17	16	-17, -3, 3	-101	58 x 32
FlexiPanel Ltd. [97]	Chipcon CC2420	8 bit PIC18LF4620	Internal	25	25	0	-95	60 x30
Panasonic	MC13213	8-bit 16-bit 12 MHz RISC	SMD RF out, ceramic antenna or U.FL	202	45	20	-105	35 x 15
MeshNetics [98]	AT86RF230	8-bit ATmega 1281v	RF output or U.FL connector	50	23	20	-104	38 x 13.5

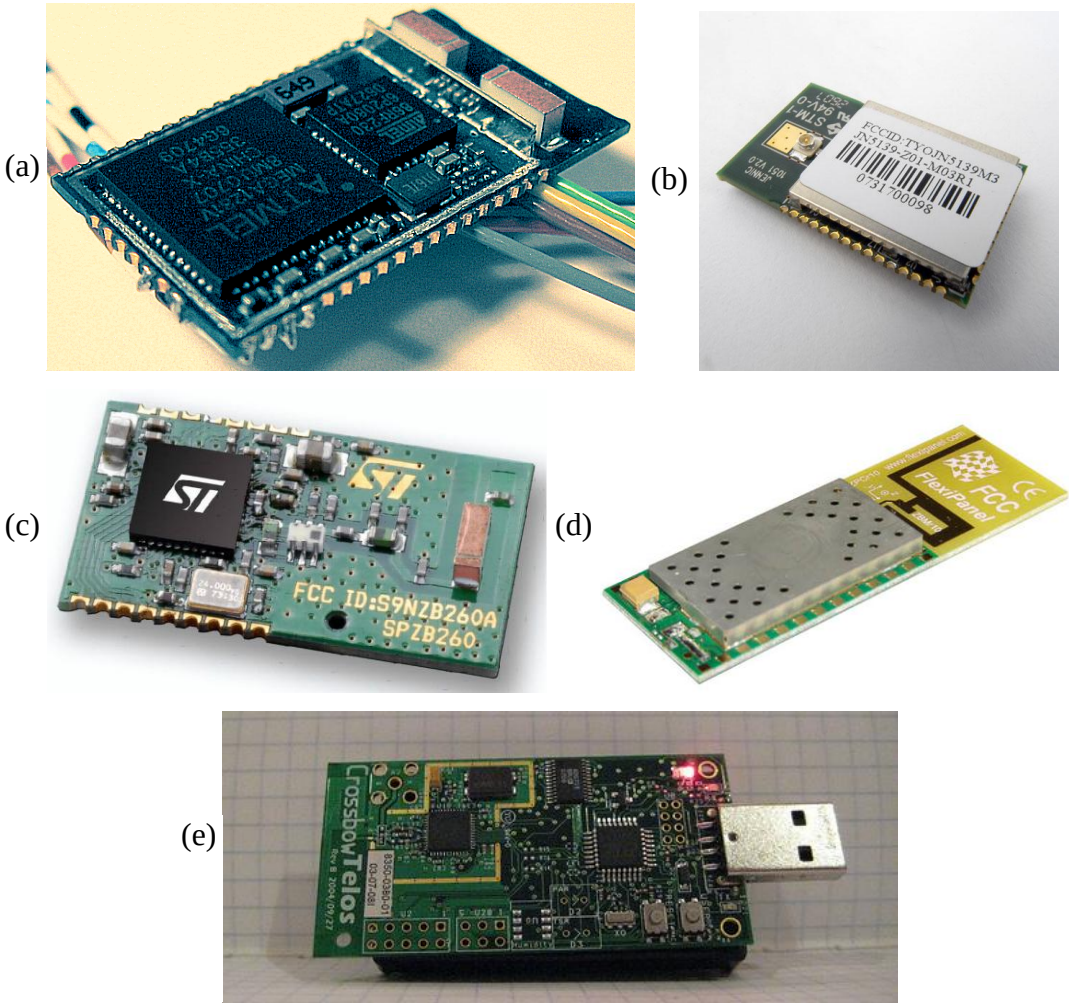

Fig. 3.2.Photograph of commercial wireless modules found in the consumer electronics market: (a) ultra-compact 2.4GHz ZigBee Module from MeshNetics [98]; (b) JN5139 wireless microcontroller from Jenic [94]; (c) SPZB260-ZigBee module from ST [95]; (d) Pixie from FlexiPanel Ltd. [97] and (e) Crossbow's TelosB mote (TPR2400) IEEE 802.15.4/ZigBee compliant platform [96].

Most of the aforementioned commercial radio modules have been designed and optimized to operate on fixed locations for automation and/or control systems. A great majority of ZigBee ready modules, shown in Table 3-1, offer compact designs with simple access routines and flexible programming tools (e.g., Crossbow Technology [96]). The radio-modules usually integrate small radiating elements, with the design structure of the wireless sensor as an essential part of the antenna's radiation performance (see Chapter 2, Table 2-9), which are well described in terms of gain and radiation patterns.

Although ZigBee radios are available for different frequency ranges (2.45 GHz, 915 MHz, 868 MHz and the newly allocated spectrum from 2.36 GHz-2.4 GHz for medical Body Area Network (MBAN) applications), the thesis primarily focuses on the 2.45 GHz ISM band physical layer of the IEEE 802.15.4 standard as a

communication protocol. The frequency band channel structure for 868 MHz, 915 MHz and 2.45 GHz is shown in Fig. 3.3. The core characteristics of the latter were described in Chapter 2, Section 2.1.3.

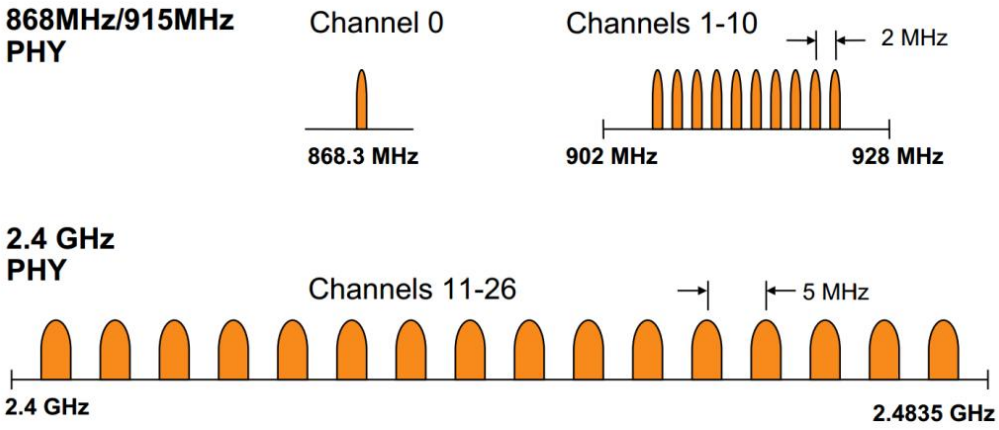

Fig. 3.3.Frequency bands and channel structure for the IEEE 802.15.4 standard.

3.2. Engineering wearable sensors for WBAN communications

Similar to the formerly mentioned wireless solutions, on-body wireless sensors embed a smart core unit (the microcontroller [14, 15]) which drives/controls the RF radio unit (also called radio transceiver) and multiple sensors that monitor specific physiological quantities, such as temperature, cardiac rhythm, blood pressure.

Although previous wireless modules may work in WBAN applications (which is a concept defined under the recently released IEEE 802.15.6 standard [23, 99]), none of them describe or address the effects of the human body in their design specifications. It is implicit that unique areas of the human body are formed by a compound of tissues (a heterogeneous multi-layer dielectric media) with unique properties (see Table 2-6). The effective media not only defines the behaviour of the electromagnetic wave propagation, but also the radio channel characteristics along the human body. Some common locations for WBAN sensors are illustrated in Fig. 3.4.

In order to design wearable devices, a thorough investigation on the causes of inefficiency in WBAN channels, due to antenna performance and the effect of full sensor structures (including ICs and lumped elements) on the wireless sensor operation, is required. For example, wireless modules that exclude the ground

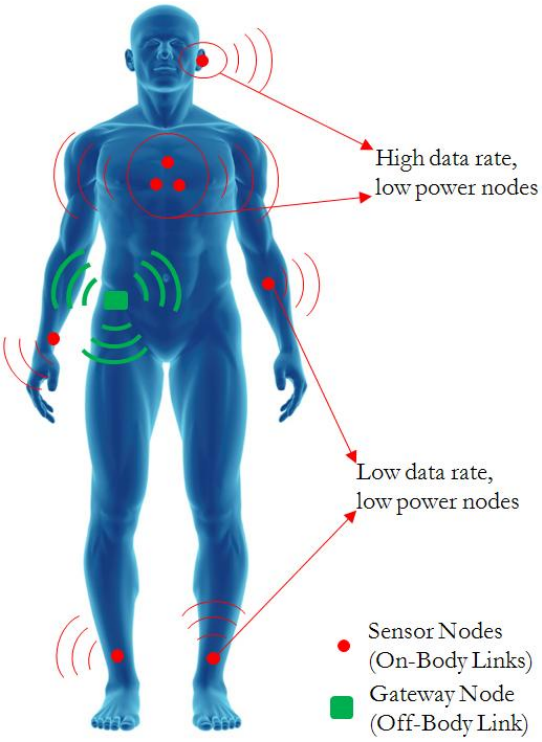

Fig. 3.4.The main concept of Wireless Body Area Networks (WBANs) defined under the IEEE 802.15.6 standard [23].

metallization underneath the antenna like the chip antennas are drastically affected by the human tissue proximity, the user and the application itself, thus hindering the reliability of WBAN communications.

The latter has to be carefully modelled and characterised through simulations and empirical models which account for the resonance shift of the antenna or detuning, the fragmentation of the radiation patterns and the propagation loss due to the body shadowing. The results ought to highlight potential enhancement techniques on the design and manufacturing of forthcoming WBAN sensors. A compact wearable sensor developed by Phillips Research Laboratory is shown in Fig. 3.5.

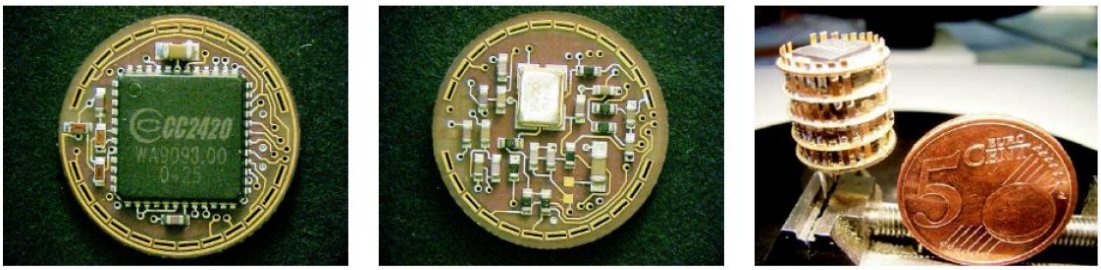

Fig. 3.5.Wireless Sensor prototypes for on-body communications manufactured by Phillips Research Laboratory [100].

Even though wireless sensors using the ZigBee stack specification are directly set to implement end-user applications, the cumbersome access to internal registers, for example changing of communication channel, and tuning of internal parameters (increase/decrease the receiver's sensitivity) made them impractical for the current study.

In addition, it was envisaged a complex process when trying to reproduce the associated antenna as an isolated element (i.e., stand-alone antenna) and evaluate its performance on on-body scenarios. The procedure evidently increases the number of uncertainties not only by the re-manufacturing process, but also by the lack of information on matching network and the losses produced when integrated as a whole wireless sensor. It certainly depicts an uncontrollable environment and hence the qualitative characterisation of on-body channels using wireless sensors.

In order to address these limitations and have a better control of internal parameters of the transceiver, wireless sensor modules operating at the unlicensed frequency band 2.45 GHz were designed and developed as part of this work. Each module embeds a Texas Instruments (TI) transceiver, the CC2420 [101]. A diagram of main digital input/output signalling pins, voltage biasing terminals and antenna connection to/from the CC2420 is shown in the Appendix-Section A.

The radio chip has a programmable RF output power between -25 dBm to 0 dBm, representing the maximum and minimum transmit power, respectively. During transmitting mode, the CC2420 typically consumes currents of 17.4 mA, and 18.8 mA when programmed as a receiver [101]. The transceiver‘s main parameters are controlled and programmed using the Serial Peripheral Interface (SPI) interface, which is managed by a Microchip ultra-low-power microcontroller, the PIC18F2620 [102], in this design. The microcontroller programs the MAC layer of each wireless node according to the guidelines of the IEEE 802.15.4 standard [34]. The radio-modules, which include the microcontroller module and transceiver module, were designed and modelled using Multisim-Circuit Designer Suite 10 and Ultiboard software from National Instruments. Further details of the layout designs can be found in the Appendix-Section A.

Each in-house wireless module is powered by a 3.6V NIMH (Nickel Metal Hydride) battery, 25 mm x 15 mm in size, through external PCB terminals (see Fig. 3.6). The pins serve as a programming interface of the microcontroller and data

retrieval of the recorded RSS levels from the internal flash memory. The manufactured PCB and the assembled prototype are illustrated in Fig. 3.6.

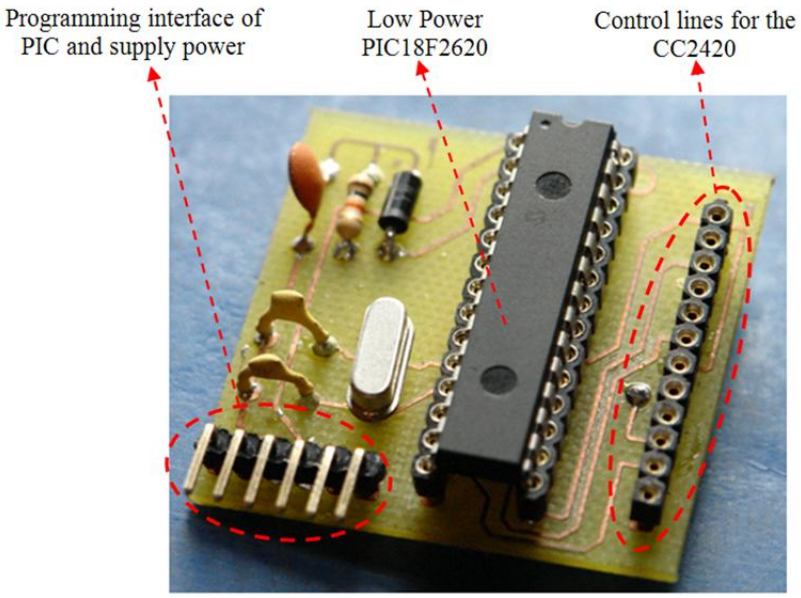

Fig. 3.6.Design and implementation of the Microcontroller module that houses a low power Microchip component, the PIC18LF2620 [102].

3.2.1. Antenna Impedance Matching

The response of the matching network, between the transceiver output impedance and the 50 Ω input impedance of the antenna, impacts on the antenna's radiation performance. Although the power loss is minimized, small reflections are produced in each transitional stage (see Fig.3.7). The CC2420 has a reactive output impedance (Z_{out} = 95+ j187 Ω, value taken from the CC2420 datasheet), so a network of lumped elements is needed to transform the reactive impedance to a real 50 Ω impedance (i.e., the input impedance at the feeding point on the antenna). A passive LC matching network was simulated using Advanced Design Systems software (ADS) from Agilent. Simulation results of a 50 Ω transformer are presented in Fig.3.8.

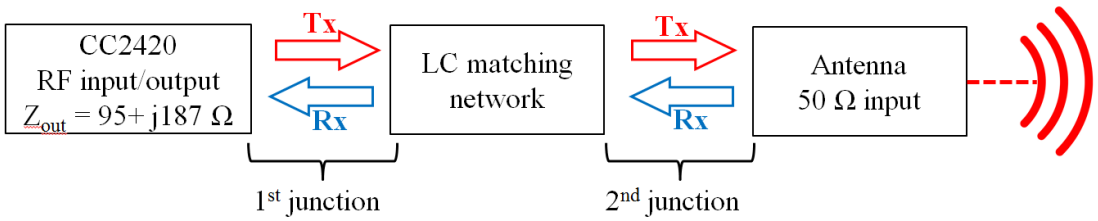

Fig. 3.7.Block diagram representation of the impedance matching network placed between the transceiver output impedance and the 50 Ω input impedance of the antenna.

The maximum power transfer occurs at 2.826 GHz, 0.374 GHz above the desired frequency, with a maximum transmission of -0.28 dB and a reflection coefficient magnitude of 0.25 ($|\Gamma| = 0.25$). At the working frequency, 2.45 GHz, the transmission is -3.37 dB with a reflection coefficient magnitude of 0.73.

The simulated design presented in Fig. 3.8 shows the initial response of the matching circuit, even though it only uses ideal connections (lossless lines). In order to properly assess the frequency performance, it is fundamental to include the transmission lines of each connection, thus the design is the closest to the implemented prototype. The response of the design implemented on each sensor node is shown in Fig. 3.9.

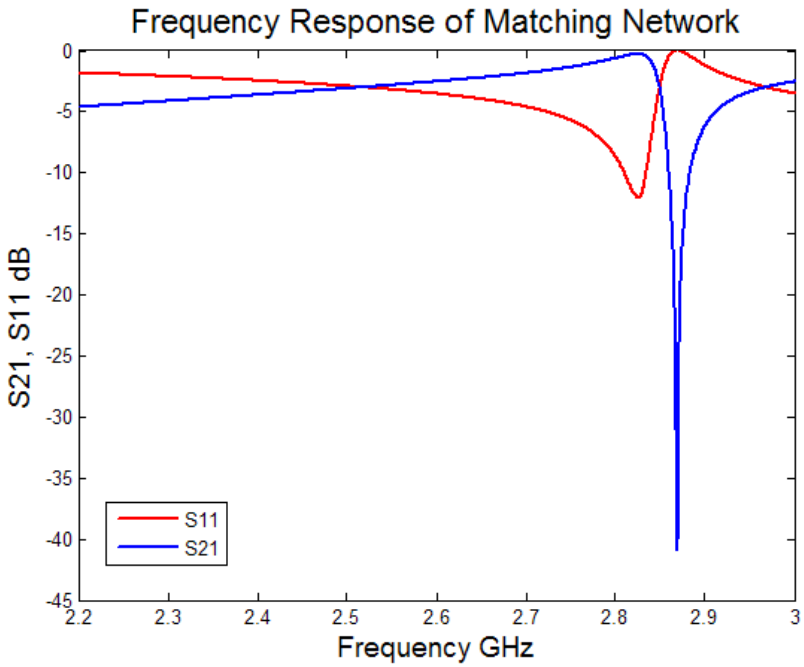

Fig. 3.8.Simulation results of the 50 Ω Matching Network using lossless connections implemented in Advanced Design System (ADS) software from Agilent.

At 2.45 GHz, the reflection coefficient is 0.48 and the maximum power delivered to the antennas is -1.26 dB; however, the best power transfer occurs at 2.48 GHz with a power transmission of -1.15 dB and a return loss of 6.76 dB ($|\Gamma| = 0.49$). Within the whole bandwidth (83.5 MHz), maximum variations of 1 dB and 0.3 dB are observed for return loss (S_{11}) and transmission (S_{21}), respectively. Current results have better performance compared to the initial design, although it is not the best achievable. Moreover, the power provided after the LC matching network (second junction, see Fig. 3.7) is also dissipated at the connection terminal of the 50 Ω

transmission line, in the sensor module, to the antenna's input feeding. The impedance mismatch produced at this point is assumed to be minimal when the antenna S_{11} parameter is below the -10 dB.

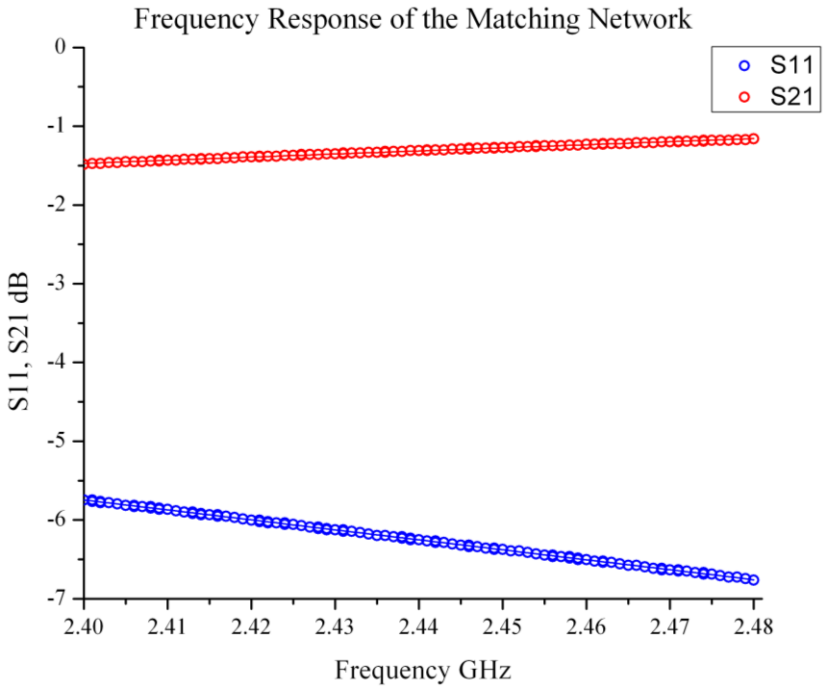

Fig. 3.9.Simulation results of the 50 Ω matching network using transmission lines at the 2.45 GHz ISM band.

3.2.2. Antenna Design and Manufacturing

Despite the fact that other wearable antennas, such as PIFA's, WIAs or monopoles, could be used, microstrip patch antennas still present a favourable choice due to the full ground plane, which not only covers the back of the PCB board, but also provides a good shielding of the radiating element from the lossy human tissues. Wearable antennas with partial ground plane usually experience higher frequency detuning than the antennas with full ground plane.

Moreover, the antenna gain increases in comparison with antennas having partial ground planes which usually are affected by the high power absorption of the reactive human tissues, thus producing a decay of antenna gain. The current study uses a pair of microstrip patch antennas printed on top of a FR-4 substrate layer with thickness of 1.6 mm. Antenna dimensions and prototypes are shown in Fig. 3.10a and Fig. 3.10b, respectively. The analytical description for its design and modelling can be found in the Appendix-Section A.

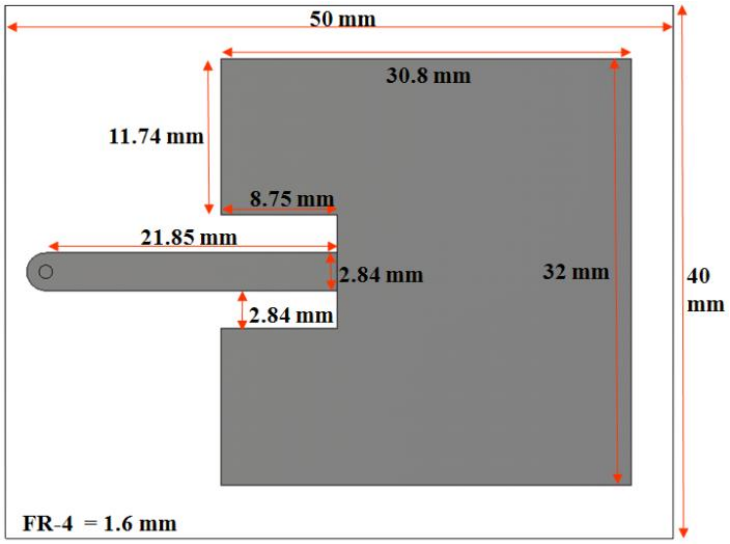

(a)

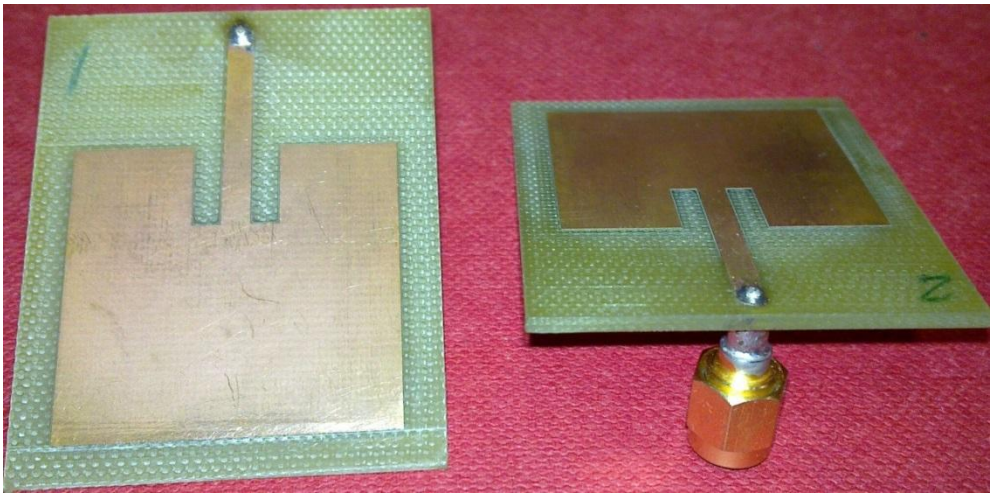

(b)

Fig. 3.10.Antenna used for custom-built wireless sensors and the characterisation of WBAN channels: (a) design layout of a microstrip patch antenna implemented in CST Microwave Studio; (b) manufactured microstrip patch antenna using FR-4 as a base substrate.

The measured and simulated reflection coefficients for transmitter and receiver antennas are depicted in Fig.3.11a. The simulation results were acquired using CST Microwave Studio and the measurements were taken in Queen Mary's Antenna lab using a Hewlett Packard 8720ES S-parameter Vector Network Analyser. The simulated 3D free-space radiation pattern, shown in Fig. 3.11b, proves that the maximum radiation is normal to the patch with no back or side lobes. The radiation is due to the fringing field between the periphery of the patch and the ground plane. The electric field in the centre of the microstrip patch is zero. For the rectangular patch shown in the Fig.3.10, there is no field variation along the width (32 mm) and thickness (FR-4 of 1.6 mm). The amount of the fringing field is a function of the

dimensions of the patch and the thickness of the substrate. Due to the effect of fringing fields waves travel both in substrate and in the air and hence the microstrip patch antenna would look electrically wider compared to its physical dimensions.

A summary of each antenna's radiation performance is presented in Table 3-2. Although each antenna has been manufactured using an identical design layout, it is understandable that the manufacturing and soldering procedure, such as the fitting of the SMA connector, would introduce some systematic errors within the antenna radiation performance. Hence, the two fabricated antennas are characterised individually.

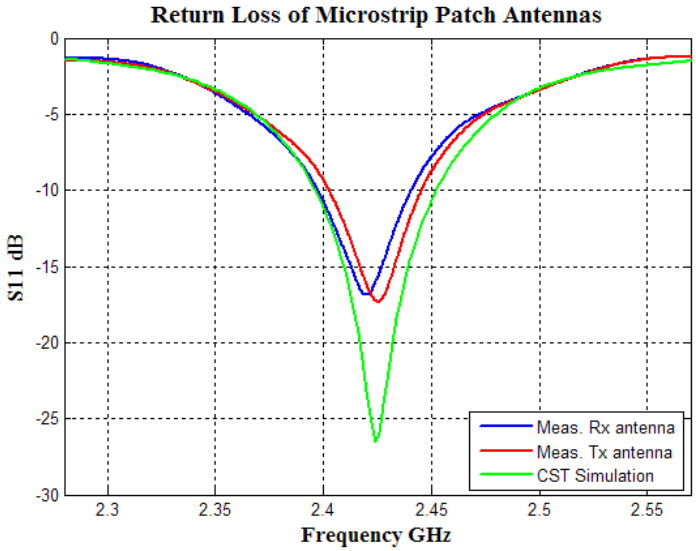

(a)

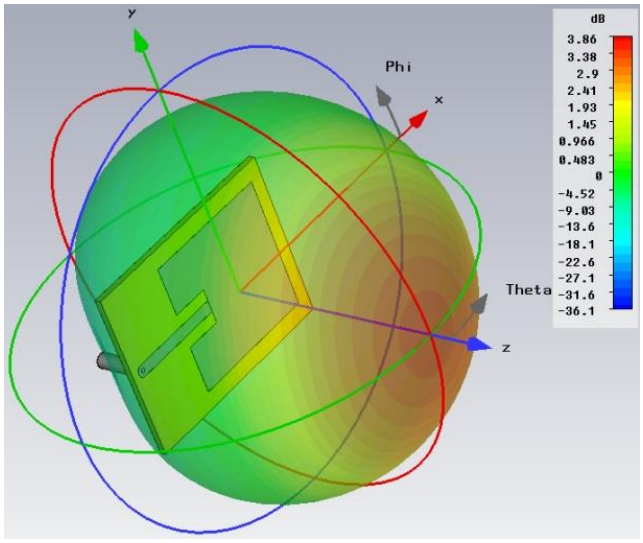

(b)

Fig. 3.11.Simulation and measured results for a pair of patch antennas, one for the Tx. node and the second for the Rx. node. (a) simulated and measured reflection coefficient, S11, for both microstrip patch antennas; (b) 3D free-space radiation pattern of the microstrip patch antenna implemented in CST Microwave Studio

TABLE 3-2
PARAMETRIC COMPARISON BETWEEN ANTENNA DESIGNS IN FREE SPACE SIMULATION AND MEASUREMENTS IN AN ANECHOIC ENVIRONMENT IN QUEEN MARY'S ANTENNA LABORATOY

Antenna Location	Res. Freq. GHz	S11 dB	Gain dBi	BW %
Simulation	2.424	-26.52	3.8	2.39
Measured Rx. Antenna	2.419	-16.87	2.13	1.98
Measured Tx. Antenna	2.425	-17.32	2.15	1.96

3.2.3. Spectral Response of the transceiver modules and Performance of the wireless sensor nodes

In a practical measurement scenario, one module is defined as the transmitter node and the second module is labelled as the receiver node (see Fig. 3.4). In the case of transmitter, the output power defines the amount of energy given to the antenna. For the receiver node, the sensitivity of the transceiver defines the capability to sense RF signals. Each transceiver was programmed to operate with a maximum output power of 0 dBm (output power at the output pins of the transceiver chip); they each have a maximum sensitivity of -95 dBm, with an adjacent channel rejection of 45 dB.

The maximum output power at the antenna port of each wireless sensor was measured by a Rohde & Schwarz FSP 40 Spectrum Analyser while transmitting continuously. The frequency was centred at 2.42 GHz (frequency where is the best S_{11}), with a span of 300 MHz and a resolution bandwidth of 3 MHz.

In the case of the wireless sensor nodes, they were programmed to operate in channel 4; therefore, the operational frequency was effectively 2.42 GHz. This frequency was selected because the manufactured antennas had the best reflection coefficient at the same frequency. The measured power spectrum of each custom-built module (Tx. sensor node and Rx. sensor node) is displayed in Fig. 3.12. A summary of the maximum output power measured using the *max-hold* function of the spectrum analyser over a length of time (~10 minutes) is described in Table 3-3. This enable the best node for transmission to be determined (greatest output power). The acquired results were also compared to Texas Instruments evaluation modules which also embed the CC2420 transceiver.

The use of λ/4 transmission lines for the 50 Ω impedance match on the Texas Instruments modules yields a better output power, -1.05 dBm; in contrast, the purposely-built modules utilize an L-C configuration outputting -3.02 dBm of initial power (see Fig. 3.12 and Table 3-3). Even though L-C networks make use of a smaller area on the PCB, they tend to introduce higher losses, which are consequence of component size, type of dielectric and thermal resistance [103].

The peaks observed below the spectrum envelope show the packet based transmission of each wireless sensor node. A longer measurement (see Fig. 3.12c) or a reduced sampling rate of the spectrum analyser would significantly reduce the number of peaks. However, the latter would not be present if a continuous wave signal was generated in the transceiver module.

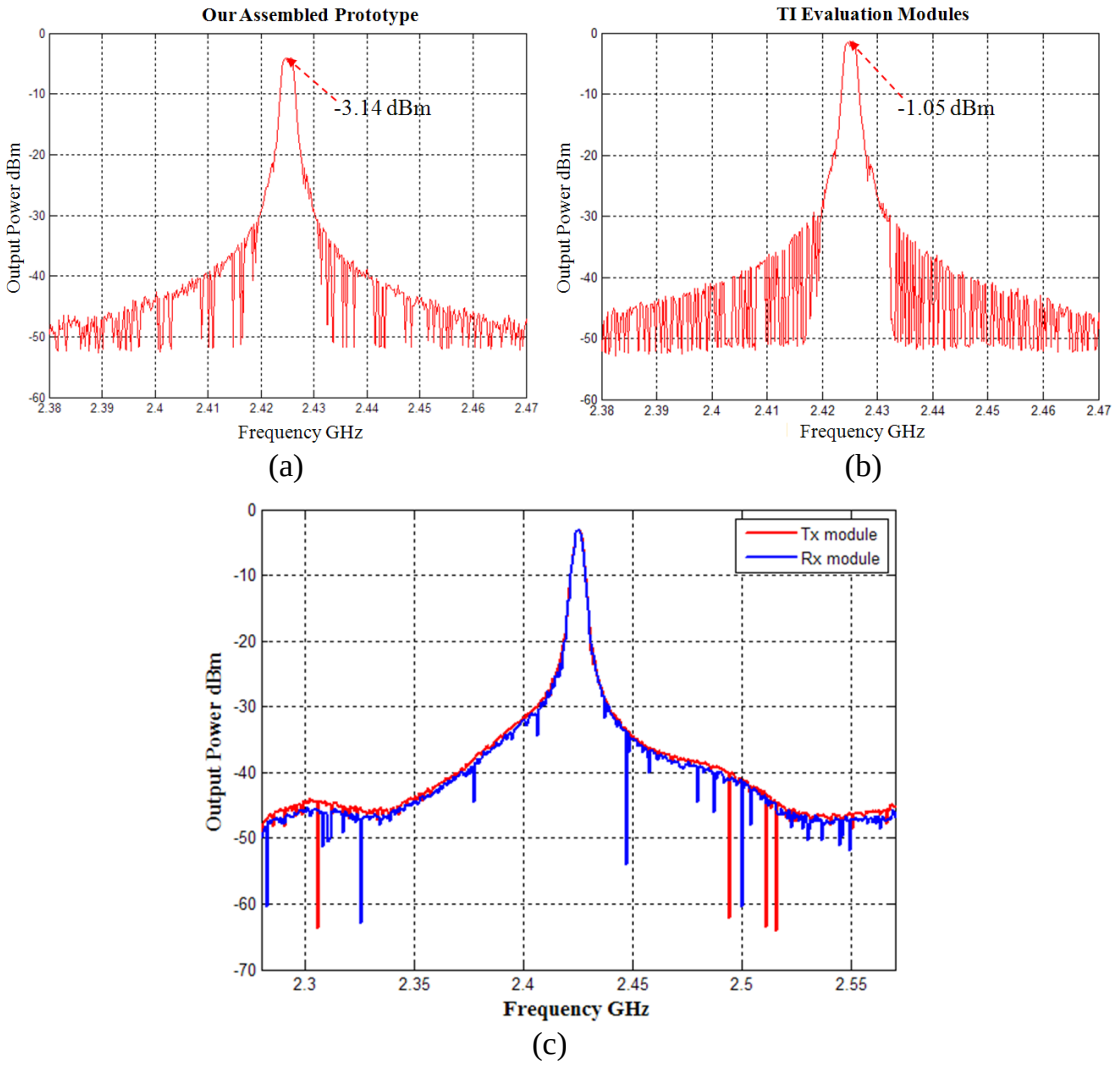

Fig. 3.12.Power spectrum response measured using the *max-hold* function of the Rohde & Schwarz FSP 40 Spectrum Analyser for: (a) custom-built wireless sensor node of a Rx. node, (b) Texas Instrument (TI) evaluation modules; (c) custom-built wireless sensor nodes transmitter and receiver nodes, respectively.

TABLE 3-3
MEASUREMENT OF THE POWER SPECTRUM RESPONSE OF INDIVIDUAL CUSTOM-BUILT WIRELESS SENSOR NODES USED FOR ON-BODY MEASUREMENTS

Wireless Modules	**Max. Output Power dBm**	**Frequency GHz**
In-house Transmitter node	-3.02	2.424
In-house Receiver node	-3.14	2.424
TI Evaluation nodes	-1.05	2.425

A block diagram structure of each wireless module is shown in Fig. 3.13a and Fig. 3.13b shows the implemented wireless sensor node, which was designed and simulated using CST Microwave Studio. The in-house wireless node, showing the battery is depicted in Fig. 3.13c, and Fig. 3.13d displays the TI evaluation module using a CC2420, which was controlled and programed with an in-house control board, and patch antenna.

Each custom built wireless sensor (see Fig. 3.13b) has dimensions of 50 mm length, 40 mm width and 30 mm depth. The later could be significantly reduced if a micro-miniature coaxial connector was used. Nonetheless, the in-house wireless sensor node could still be connected to any type of antenna that has an SMA input connector.

The TI evaluation board served two purposes in this thesis: first, to validate the performance of the in-house custom-built transceiver modules; and second, to provide an alternative system for use in the wireless-sensor-based measurements described in Chapter 4. This allows a degree of verification of the measurement technique: by having two physically-different systems, where differences between the two measurement techniques can be observed, whilst also considering the effects of the physical structure of the specific systems.

The operation of each wireless sensor node is defined by the microcontroller which controls and programs the transmitting or receiving operation mode of the CC2420 transceiver. The receiver node records an average of 8000-10000 samples of the received signal strength (RSS) at a rate of 14 ms per sample. The acquired data was stored in the internal flash memory of the microcontroller which was later extracted and further analysed. The data extraction port was used not only to program and extract data, but also to connect the battery.

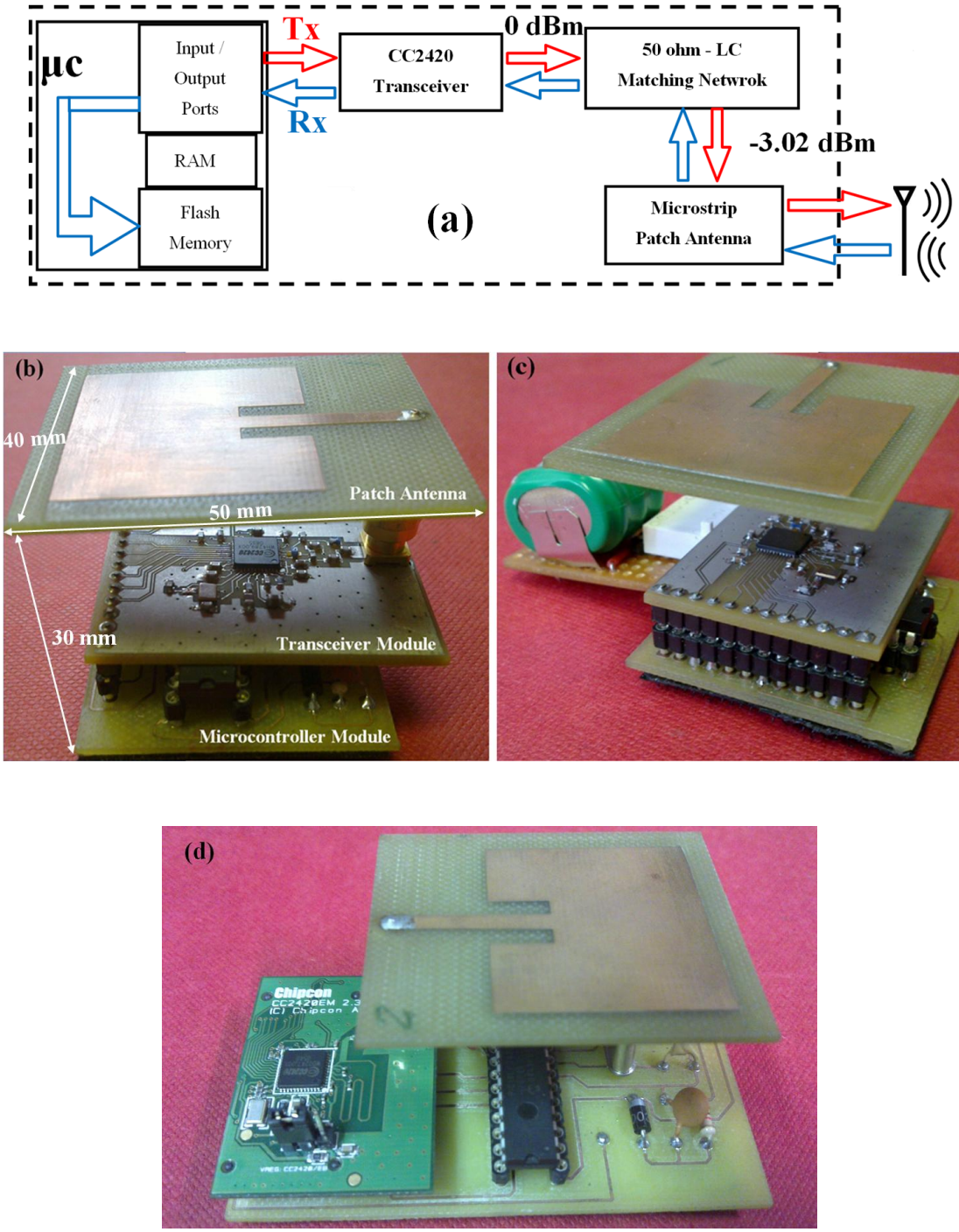

Fig. 3.13.Wireless sensor modules used for WBAN measurements and Data Logging units: (a) internal wireless sensor structure; (b) implemented custom built wireless sensor node using a microstrip patch antenna; (c) custom-built wireless sensor node showing the battery placement; (d) alternative commercial wireless node using CC2420 evaluation modules from TI.

In order to design the communication link between a pair of sensor nodes, it is necessary to quantify the power received by the receiver sensor node when the transmitting sensor node is positioned some distance away transmitting continuously a known amount of power. Mathematically, this is defined by the Friss transmission

equation which gives us the radiated power density as a function of radiated power and distance (see Chapter 2). For this particular test, the separation distance has to be in the far-field region of the designed antenna. In our case, the initial response of purposely-built wireless sensor nodes was evaluated for a separation distance of 30 cm. All the measurements were taken in an Anechoic Chamber (simulated free-space environment) in Queen Mary's Antenna Lab.

The results have been compared with data obtained from the measurements of the microstrip patch antennas (stand-alone) using a Hewlett Packard 8720ES S-parameter Vector Network Analyser (see Fig. 3.14). A summary of obtained results are presented in Table 3-4.

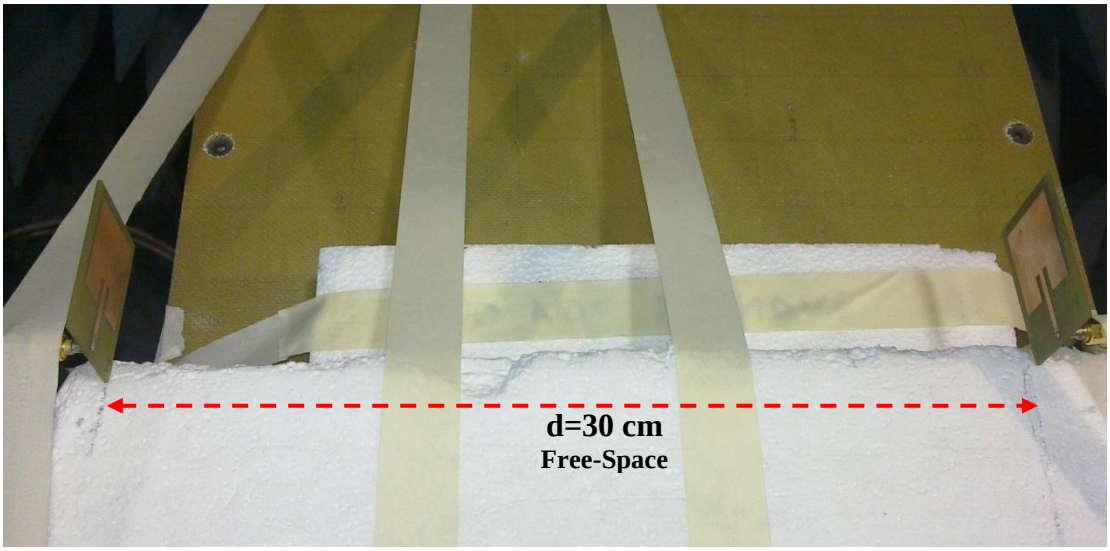

Fig. 3.14.Measurement setup of a pair of microstrip patch antennas separated 30 cm in Queen Mary's Anechoic Chamber Environment.

TABLE 3-4
RESPONSE OF THE WIRELESS SENSORS IN A FREE SPACE ENVIRONMENT AT A DISTANCE OF 30 CM

Measurement Set-up	Antenna Separation cm	Frequency GHz	Output Power dBm	S21 dB	Gain dBi
Antennas CST Sim.	30	2.42	0	-22.02	3.8
Antennas and VNA	30	2.42	0	-24.55	2.13
Custom-Built Wireless Sensors	30	2.419	0	-17.87	2.15

The custom-built wireless nodes were placed on a rotational positioned (i.e., rotating turntable) in order to measure stand alone and on-body radiation patterns. The polar-pattern test setup is shown in Fig. 3.15. The latter was measured in a fully anechoic (simulated free-space) chamber environment with the aid of a Rohde & Schwarz FSP 40 Spectrum Analyzer that was connected to a Diagonal Dual Polarized Horn (i.e., ETS-EMCO Model 3164-04) acting as a receiver. The received power levels were measured as a function of angle and recorded in a personal computer.

The normalized measured radiation patterns of the custom-built wireless sensors and when placed on the body in a free-space environment are shown in Fig. 3.16. It is apparent that the free-space patterns show more radiation in the left-half plane than the on-body results, as would be expected from the increased absorption by the body tissues. Good agreement between the patterns is seen for the right-half plane, for both polarizations. Differences are attributed to the body effect because the antenna is small with respect to the body size. Variations from the standard patch pattern are attributed to the presence of the wireless sensor node.

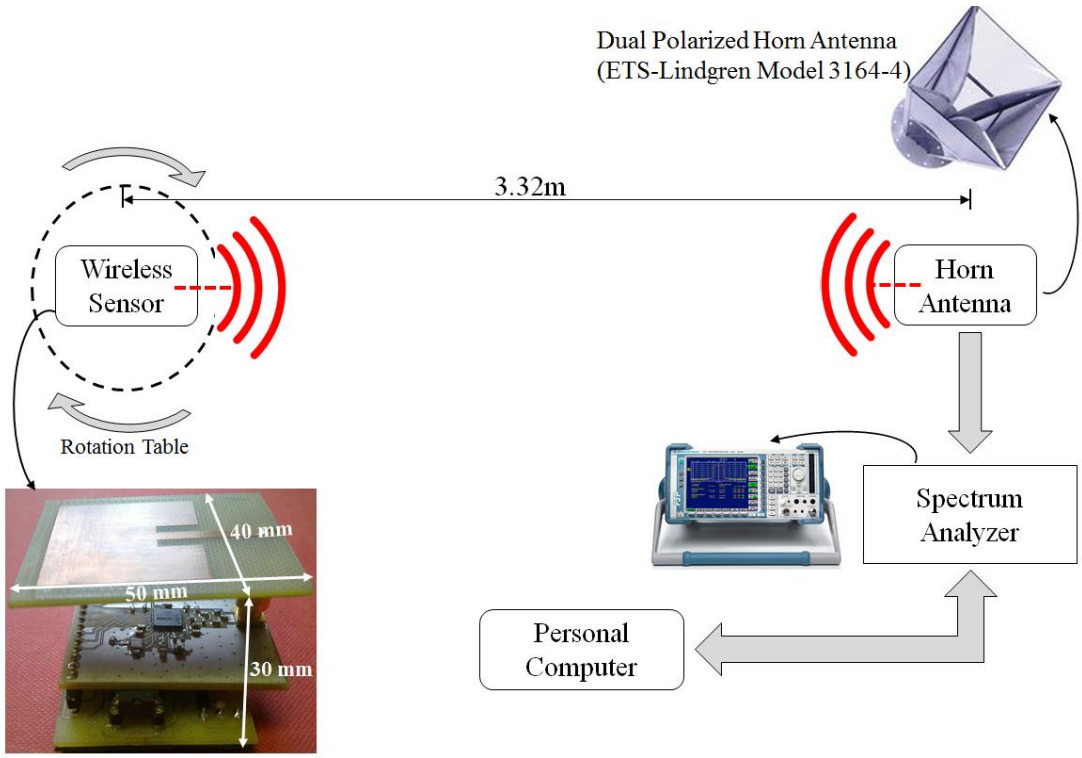

Fig. 3.15.Measurement structure set up for the acquisition of radiation patterns of custom-built wireless sensor nodes. The measurement was performed in Queen Mary's Anechoic Chamber. The wireless node, with dimensions of 50x40x30 mm, was positioned on top a rotational table. The rotational table and data acquisition was controlled by a computer which was synchronized with a Rohde & Schwarz FSP 40 Spectrum Analyser.

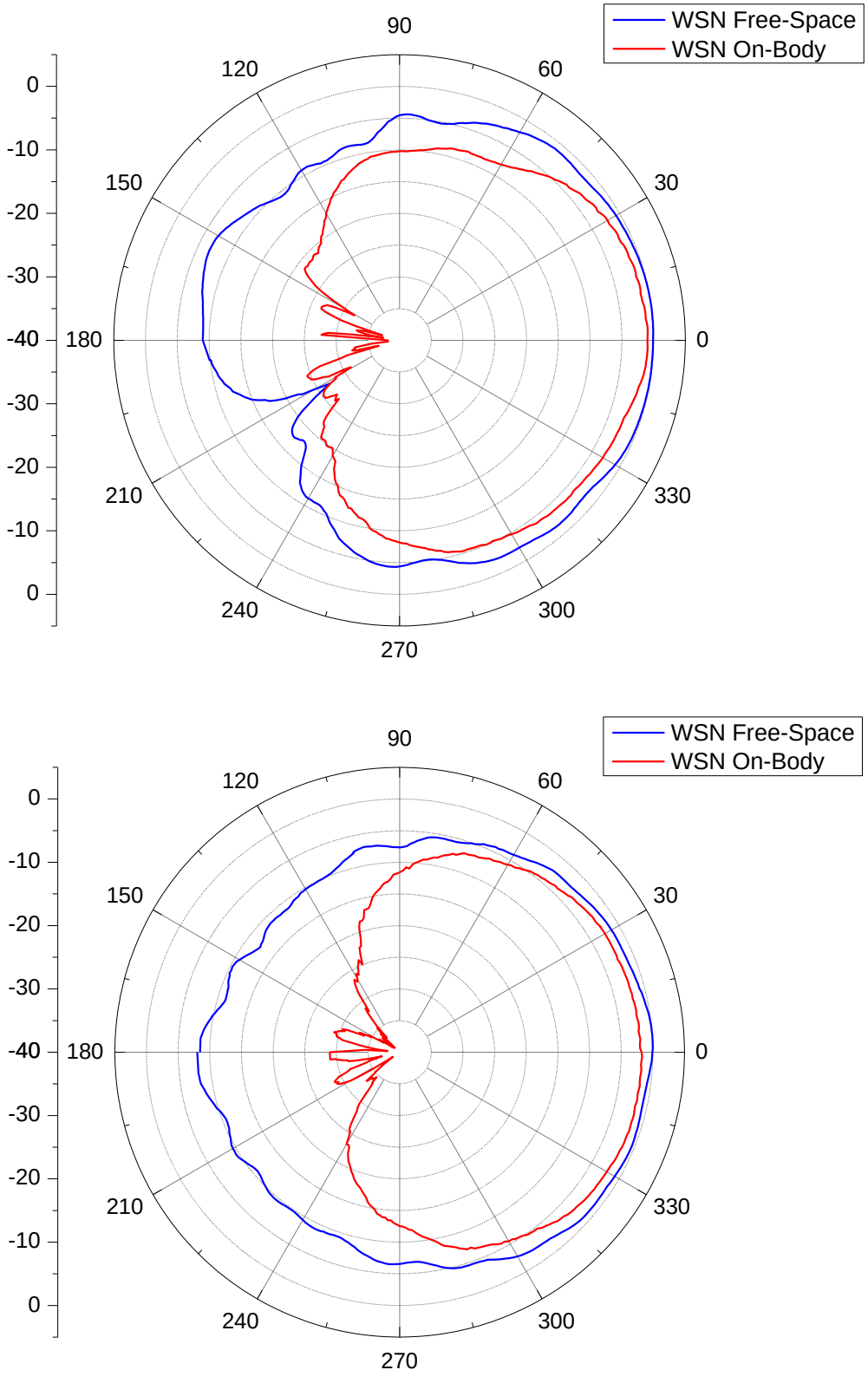

Fig. 3.16.Measured radiation patterns of custom-built wireless sensor nodes and when placed on-body. The measurements were taken in an Anechoic Environment in Queen Mary's Antenna Lab using a Rohde & Schwarz FSP 40 Spectrum Analyser.

3.3. Discussion and Conclusion

In this chapter, a review of low power wireless technology has been presented. Most of them made use of the ZigBee specification as the main communication platform. In addition, different commercial wireless modules have been identified. Nonetheless, it was pointed out that ZigBee-ready solutions are not adequate for body-centric communications (WBAN scenarios), due to the lack of information of the antenna performance (when operating in close proximity to the human body). It also highlights the cumbersome access to different control registers and the high level of uncertainties due to re-manufacturing process which prove to be impractical for the current study.

Purposely-built wireless sensor nodes are designed and implemented using the CC2420 as the core RF transceiver and the PIC28F2620 as a main control, monitor and storage unit. The implemented antenna of each wireless sensor is a microstrip patch design which mitigates the adverse effects of human body proximity such as the detuning of the antenna. The chapter also presented the initial response of each in-house wireless sensor in a free space environment and on-body.

Measurements results show that designed antennas have their best operation at 2.42 GHz. As a result, wireless sensor modules were programed to operate at this frequency band. Spectrum results of individual wireless nodes showed that the best output power to the antenna is -3.02 dB which shows the inherent effect of an LC matching network.

Chapter 4

On-Body Channel Measurement using Wireless Sensors

There has been rapid growth in the number of wireless devices operating in close proximity to the human body in recent years. The design of small antennas that can provide high efficiency, immunity to frequency detuning, immunity to pattern fragmentation and operation at different frequencies whilst close to, on or even within the body, are current topics of active research [15, 56]. Improving our understanding of the on-body propagation channel is central to being able to properly design antennas for the environment.

Thus far, it has proved difficult to separate the observed on-body propagation channel and antenna characteristics, unlike in free-space environments. It has been recognised for some time that operation on or near the human body is far from a free-space environment [56]; hence, to understand on-body behaviour, on-body

measurements must be taken. The standard methods for characterising propagation and antenna performance typically utilise a vector network analyser (VNA), or an RF source and spectrum analyser (SA). To date, most on-body measurements have continued to use the VNA or SA approach (e.g., [51], [104]).

However, the coaxial cable connecting antenna and VNA can often introduce error, due to unwanted radiation from currents flowing on the outer surface of the cable, as well as errors from cable movements. Alternative techniques have been explored to mitigate this 'cable effect', including the use of fibre-optic systems (see, for example, [35, 105]; also [106-108]). Fibre-optic cables are essentially immune to electromagnetic interference (EMI) and radio frequency interference (RFI), which have a major impact on traditional on-body measurements (VNA and coaxial cables). In [109], off-body measurements were performed in an anechoic chamber and indoor environment using a fibre-optic system on a motionless test subject (see Fig. 4.1a-d).

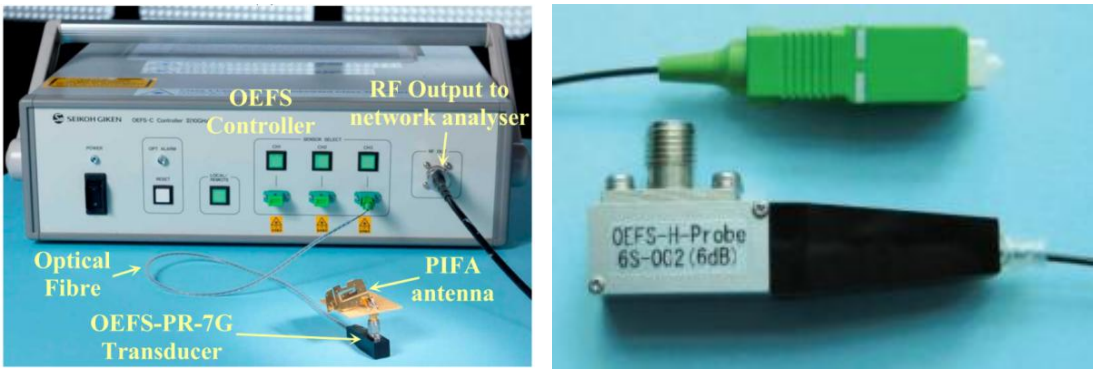

(a)

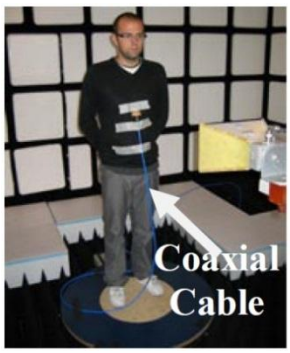

(b)

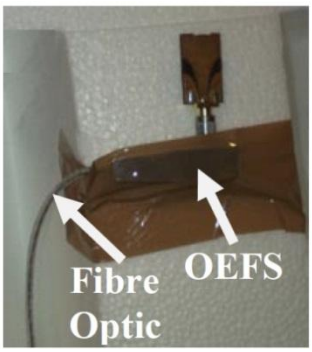

(c)

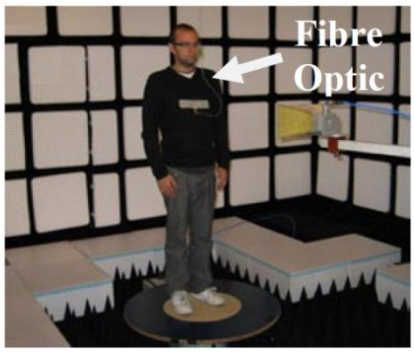

(d)

Fig. 4.1.Fibre-Optic system (a) a PIFA antenna connected directly to the electro-optic Field Sensor (OEFS); (b) a typical measurement set-up using a coaxial cable for body-worn antennas; (c) free-space fibre-optic measurement set-up (close up of antenna taped to underside of foam block); (d) on-body fibre optic measurement set up at the NPL's SMART range facility [35, 105].

The effect on measured data by the method of measuring can still be significant, especially when a dynamic human body scenario is considered (e.g., jogging). The motion may bend the fibre-optic cable, introducing changes in the polarization planes, as well as fluctuations in temperature, leading to changes in the sensitivity of the fibre-mounted sensor [110]. In addition, the fibre optic system usually contains an electrically large optical modulator/demodulator which can cause scattering to on-body radio waves.

Furthermore, the antenna will behave differently when measured in isolation and when integrated with a system, as required in any application (a fact that has influenced mobile phone antenna design for some time; see, for example, [111-113]), due to additional surface currents induced on the system structure. This will, in turn, affect the propagation channel data, due to the difficulty in decoupling the two aspects. In this chapter, a measurement technique is investigated that uses the commonly-available received signal strength (RSS) figure-of-merit to determine propagation characteristics for a number of wireless sensor modules, using two identical microstrip patch antennas to ensure the effect of the antenna is minimized.

These measurements are compared to others made using the conventional VNA technique. The study described below evaluates the channel performance of each frequency carrier for IEEE 802.15.4 sensor nodes operating in the 2.45 GHz ISM band (2.40-2.4835 GHz). The effect of the carrier frequency and antenna radiation performance are also investigated from the system point of view. For this initial study, only a motionless (static) subject was considered; dynamic scenarios are considered in Chapter 6.

4.1. On-Body Communications and Related Work

A noticeable evolution of technique can be traced in the history of on-body propagation channel measurements, whereby the measuring devices become smaller and the complete system is worn on-body. Early research into on-body wireless communications channels used standard measurement techniques, based around a VNA. One of the earliest papers [50] used flexible coaxial cables to connect two patch antennas to the VNA. The variation in cable loss due to body movements was estimated (by replacing the wireless link with semi-rigid coaxial cable) to be 0.1 dB

across the frequency band of interest. No reference was made to the cable effect; the radiation patterns of the two patch antennas used were only characterised off-body.

In order to understand properly the effect of human motion on the channels, measurements were soon made with a Rhode and Schwartz FSH6 spectrum analyser with tracking generator, controlled by a small laptop, both carried by the subject in a small backpack [48, 52]. Flexible coaxial cables were again used to connect the antennas to the measuring equipment, whilst noting the potential for error from the presence of the cables, due to scattering and the potential for surface currents on the outside of the cable. However, neither quantifying nor eliminating the error from the cables was deemed possible. It is noted that the measuring equipment is fairly bulky and prohibits the investigation of some human movement, due to its restrictive position and weight.

In [114-117], on-body propagation models were investigated for indoor and outdoor scenarios, using body-worn sensors communicating at 868 MHz and 2.45 GHz. The use of such sensors removed the need for cables on-body; the size and weight is also significantly less than SAs and laptops. The transmitter was placed at waist level and used a 2.0 dBi gain dipole antenna; the receivers, placed at different points on the body, were either based on Crossbow Mica2Dot wireless sensors (for 868 MHz) [114, 115]; or they were based on Linear Technology LT5504 RF modules (for 2.45 GHz) [116, 117]. Their results show that on-body propagation characteristics are dependent on user state and environment; however, it is noted that the transmitter output power for the experiments at 2.45 GHz was +22 dBm, which is unrealistic for real-world applications.

Furthermore, the transmitter used was a NovaSource G6 synthesized RF signal source, in continuous-wave mode, with an additional Hittite HMC-455LP3 amplifier for the 2.45 GHz experiments, rather than using a solution based purely on packet-radio hardware. The NovaSource G6 is still a relatively bulky item, measuring 70 mm x 102 mm x 19 mm (width by length by height) and weighing 170 g, not including the power supply and cables, with an aluminium case. The effect of this unit on the transmit antenna radiation pattern has not been discussed, either in free-space or on-body.

Other studies have been conducted over the past decade and reported in the literature. Most use either a VNA or Vector Signal Analyzer (e.g., [118-125]), or a source combined with a spectrum analyser (e.g., [126, 127]). In [128], Texas

Instruments wireless nodes embedding CC2510 radio transceiver modules and an RF packet sniffer (i.e., TI smart RF04EB board) were used to characterise the interaction and the performance of the physical layer for on/off-body communication links. A few studies characterised on-body radio links using wireless sensor nodes ([129-133]), but have not compared the obtained results with other measurement techniques, meaning sources of error remain uncertain.

The thesis investigates the potential for improving measurement capabilities on-body, by using small sensor nodes for both transmitter and receiver. A more realistic transmit power of 1mW (0 dBm) will be used and the measurements will be packet-based, rather than continuous-wave. The CC2420 [101], an IEEE 802.15.4-compliant radio transceiver from Texas Instruments, will be used, with the modulation occurring on-chip. Comparisons with conventional measurements using a VNA will be made. One advantage of this approach is that it also provides insight into real-world, rather than laboratory, scenarios.

The current work is focused on the thoracic section of the human body, as it represents the main area for a variety of healthcare applications, such as cardiac monitoring, respiratory sensors, pacemakers, gastric band controllers, bladder implants and others. The trunk includes a great variety of organs, with the associated variability in dielectric characteristics; it is also anticipated to be one of the complex and irregular environment for electromagnetic modelling (because it is formed by heterogeneous multilayer tissues which have different electrical properties, see Table 2-6) and, hence, for on-body radio links. It is noted that the characterisation of low power wireless channels depends upon many factors, some of which are not considered in this present study, for example different test subjects, different antennas or variety of designs (flexible electronics). These include the effect of individual subjects (for instance, short or tall, thin or fat), the surrounding environment, the type of activity and the application.

4.2. Measurement Procedures

Measurements were performed on the trunk section of a male test subject (see Fig. 4.2), measuring 170 cm in height and 78 kg in weight, standing motionless in an anechoic chamber. The transmitter antenna was placed on the right waist section of the body and the receiver antenna moved symmetrically along the trunk section. The

antennas are located 3 cm away from the body's surface. The area was divided into 30 different points (6 × 5 matrix points) using a 5 cm spacing, as shown in Fig. 4.2.

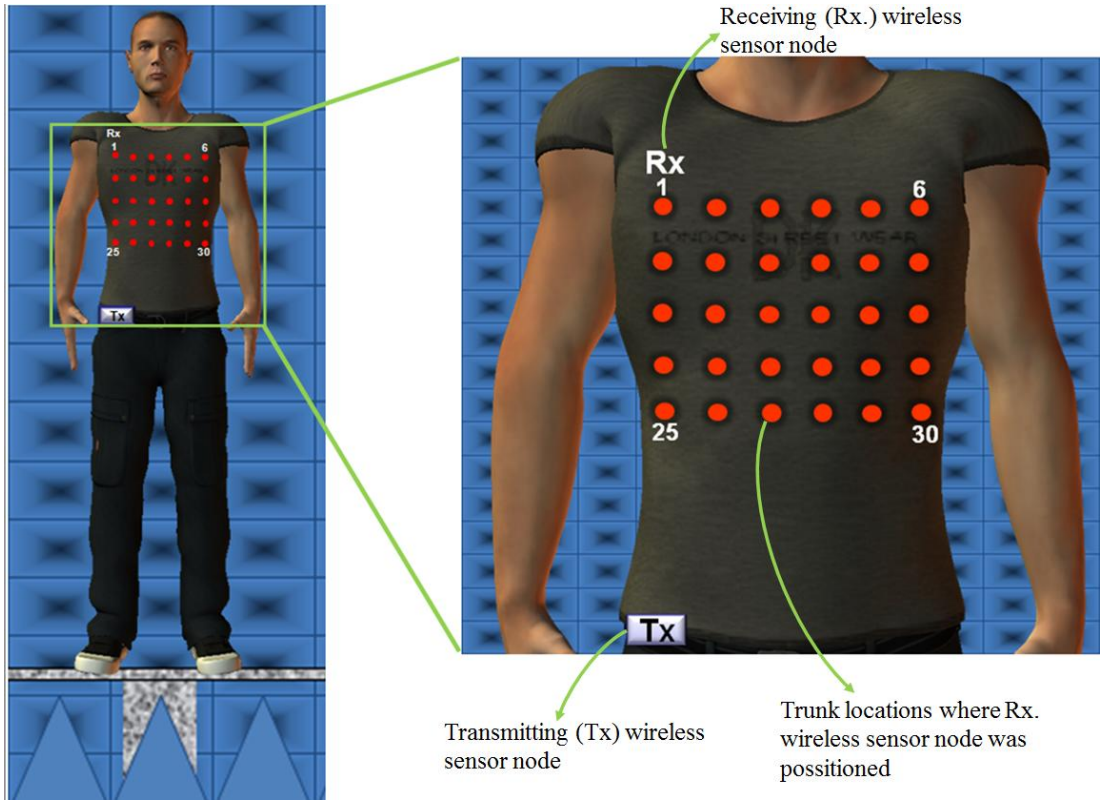

Fig. 4.2.Location of transmitter and receiver antennas used for each on-body measurement in an anechoic environment.

The study uses a pair of microstrip patch antennas. The antenna dimensions, together with and the measured and simulated reflection coefficients for transmit and receive antennas, are depicted in Chapter 3 (Fig. 3.11), and a summary of each antenna's radiation performance is presented in Table 3-2.

A large ground area underneath the patch antenna usually mitigates the effects of the lossy human body tissues. In [134], a patch antenna was fabricated on a RT/Duroid board of dielectric constant $\varepsilon_r = 3$ and thickness 1.524 mm and had a total board size of 60x65 mm^2 (0.49λ× 0.53λ at 2.45 GHz[4]), reporting a 10 MHz detuning when placed on-body. As a result, the initial antenna parameters (antenna alone placed on body in a simulated free-space environment) are influenced by the large volumetric section of the human body, introducing continuous variations in return loss (S_{11} depth) and frequency (detuning). These effects are related not only to on-

[4] The free-space wavelength (λ) at 2.45 GHz is 122.45 mm

body location, but also to mechanical movement of different internal body processes, such as the active cycle of breathing. The absolute variation of the reflection coefficient (S_{11}) of the receiver antenna with respect to its position alongside the trunk section is illustrated in Fig. 4.3. A summary of the mean deviation in S_{11} and frequency, for both transmit and receive antennas is described in Table 4-1.

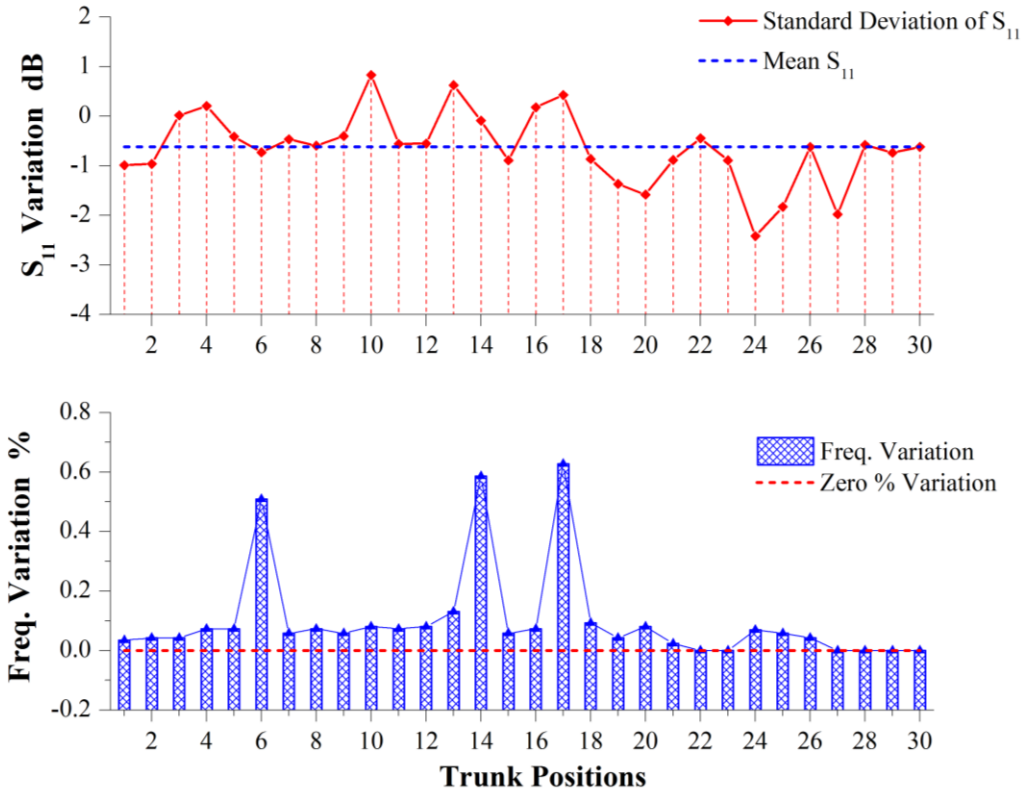

Fig. 4.3.On-body absolute frequency detuning and return loss deviation of the receiver antenna at each point on the trunk section, compared with free-space measurements. Both sets of measurements were taken using a Hewlett Packard 8720ES Vector Network Analyser.

TABLE 4-1
DEVIATION OF ANTENNA PARAMETERS WHEN PLACED ON-BODY

Antenna Location	Freq. Detuning %	S_{11} Mean Deviation dB	BW at -10 dB %
Rx. Antenna	0.001	-0.62	2.16 - 2.36
Tx. Antenna	0.0923	-2.69	2.06

The -10 dB impedance-matched bandwidth of the receiver antenna varies by 2.16% to 2.36%, clearly reflecting the presence of heterogeneous human tissue alongside the trunk. On the other hand, the transmitter antenna, which preserves its location during the measurement procedure, has a maximum detuning of 2.24 MHz

and a 2.06% bandwidth when on-body. It is evident that the variations at this point are lower than the receiver locations. These results are important for understanding the collected measurement data, discussed below.

The wireless on-body radio channel measurements were divided into two groups, discussed below.

4.2.1. First Measurement Setup

The first measurement set was made with the aid of a Hewlett Packard 8720ES S-parameter Vector Network Analyser, calibrated using standard techniques. These measurements were sub-divided in two parts:

- measurement of a stand-alone antenna (Fig. 4.4a), on-body, using coaxial cable (polystyrene foam was used for the mechanical support of the antenna, ensuring its separation is identical to the other tests that included the wireless sensor node);
- measurement of the antenna when in close proximity to the embedded system (i.e., the two are positioned close together, as if connected, but the measurement equipment was still connected with coaxial cable and no direct connection between antenna and embedded system existed; see Fig. 4.4b).

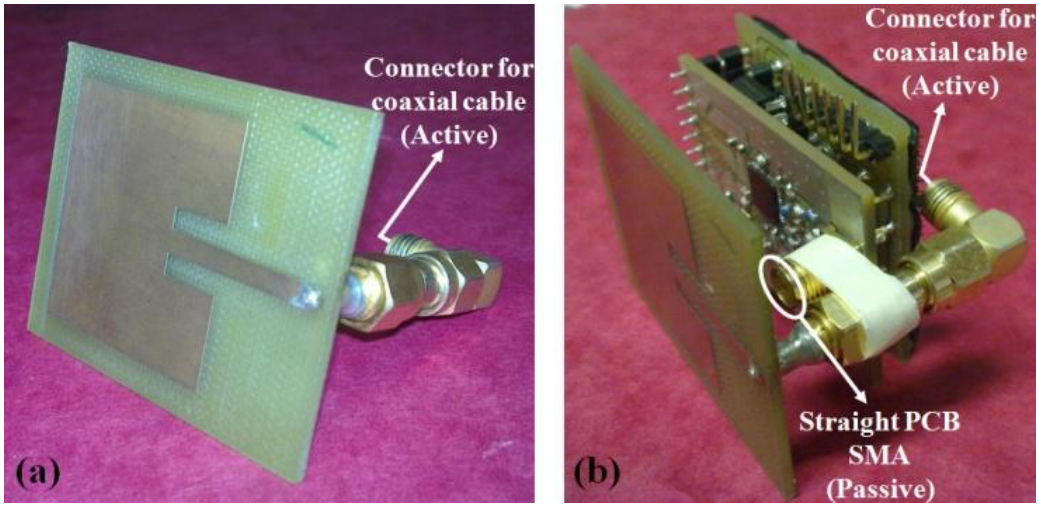

Fig. 4.4.Measurement of the microstrip patch antenna using a Hewlett Packard 8720ES Vector Network Analyser: (a) stand-alone antenna; (b) antenna with close proximity to the in-house wireless node. Note that the PCB SMA is not connected to SMA connector of the antenna (passive SMA).

The frequency sweep was set from 2.4-2.5 GHz, with the maximum number of points (1601). The sweep time was 800 ms, with an output power of 0 dBm (1 mW).

Five different measurements were taken over a period of five days, in order to obtain an averaged response of the measured radiation properties of the antennas, and hence the on-body radio links. In each measurement, two sets of data were recorded. The path loss at each point is calculated from the average of the 10 different samples sets of data.

These results are presented in Section 4.3, where they are combined with those obtained with the second measurement procedure (Section 4.2.2) to aid comparison and understanding.

4.2.2. Second Measurement Setup

Two wireless sensor modules, shown in Fig. 4.5 and with a detailed description presented in Chapter 4, were used for the second measurement campaign.

In order to decrease the error introduced by on-body position displacement (such as that introduced by conducting measurements over a period of five days), each wireless module was fitted using VELCRO tape to the trunk section of the subject; the grid of locations was marked on the T-shirt worn by the test subject, enabling the position to be recaptured reasonably accurately on each subsequent measurement. In each location, the modules acquired an average of 8000 samples of the received signal (RSS), recorded in the internal flash memory of the microcontroller. The obtained data was later extracted and analysed; results are presented in Section 4.3.

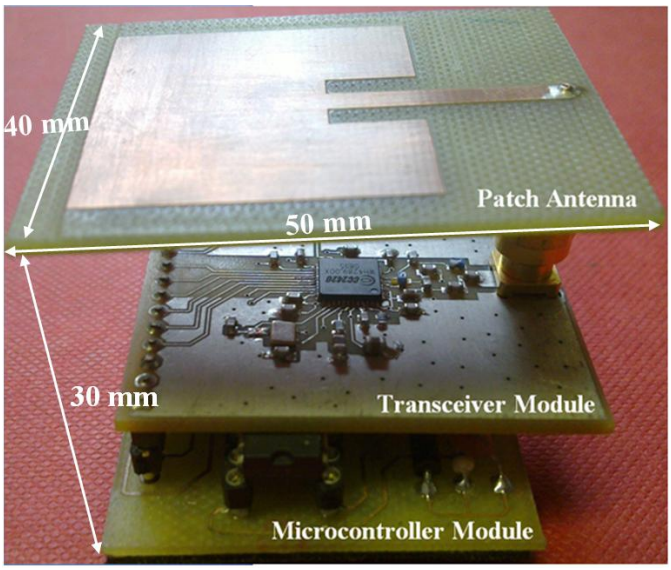

Fig. 4.5.Custom-built wireless sensor node used for WBAN channel characterization. The design and development descriptions are presented in Chapter 3.

4.3. Data Processing

4.3.3. Path Loss Analysis

Analytical and empirical propagation models have been well covered in the literature [14, 44] . Measurements, for both indoor and outdoor environments, have shown that the average received signal decreases logarithmically with distance [45, 46]. The mathematical approximation of power loss as a function of distance was defined by (2.4) in Chapter 2.

For the case of on/off-body communications, (2.4) not only includes antenna characteristics, but also human body shadowing (which depends on the user) and average channel attenuation, which is defined by the surrounding environment [47, 48]. A simplified path loss expression is defined by (4.1):

$$PL(d)_{dB} = PL(d_0)_{dB} + 10\gamma \log\left(\frac{d}{d_0}\right) \qquad (4.1)$$

In our study, γ and $PL_{(d0)dB}$ are derived from measured data considering a reference distance of 15 cm (d_0=15cm). The reference distance should always be in the far field and it should be larger than the wavelength of operational frequency (at 2.45 GHz the wavelength is 12.245 cm) in order to minimise the mutual coupling effect when antennas placed near each other. Recorded data and least square (LS) fitting curves are shown in Fig. 4.6 for both VNA and wireless sensor-based measurements which were taken in an Anechoic Chamber.

The human body torso is formed by curvatures in both longitudinal and horizontal directions, which increase the shadowing effect in the wave propagation (Fig. 4.6); therefore, the use of flat, cylindrical or uniform dielectric phantoms can lead to inaccuracies in the estimation of path loss exponent.

Moreover, the use of directive antennas for on-body communications (microstrip patch antennas in our study) add to the spread of path-loss values around the linear fit (Fig. 4.6); therefore, the more directive the antenna is, the less linear is the relation between $PL_{(d)dB}$ and $\log(d/d_0)$. Important statistical parameters for each on-body setup are presented in Table 4-2.

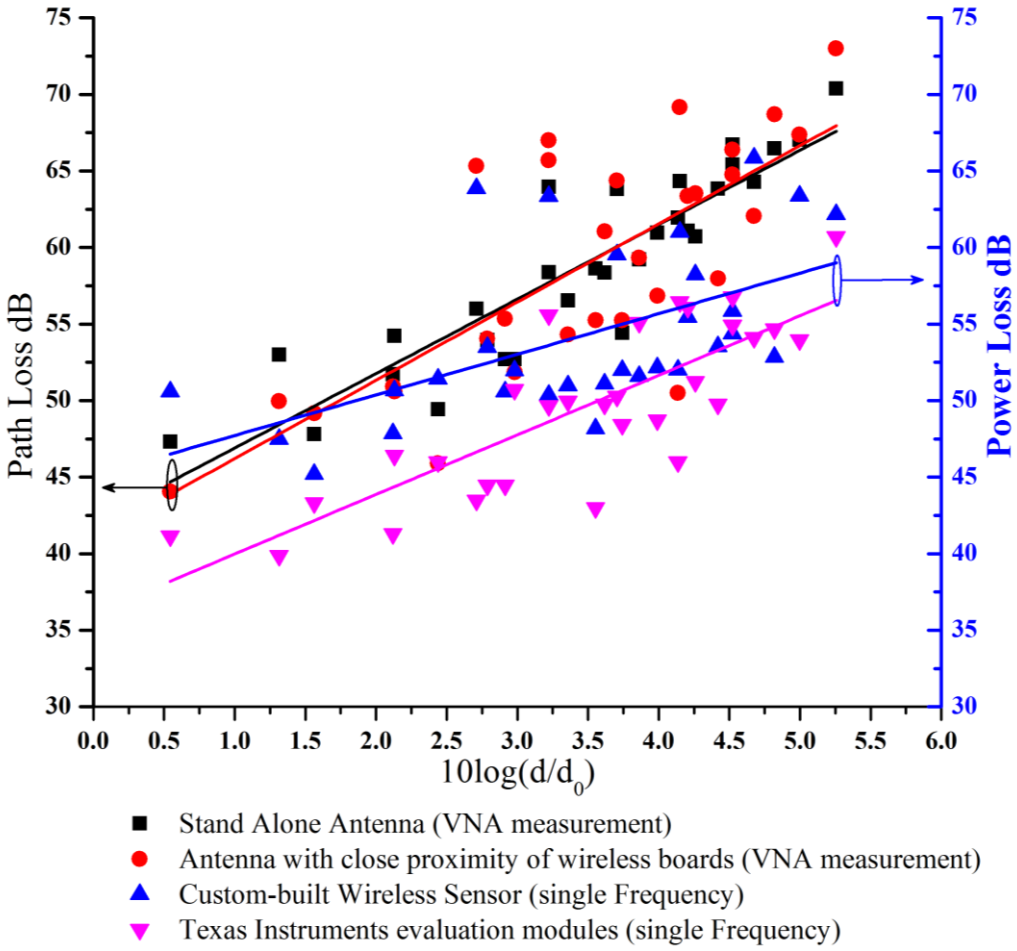

Fig. 4.6.Anechoic Chamber Measured Path and Power Loss values on the trunk section using LS linear fitting for: Stand Alone Antenna (see Fig. 4.4a), Antenna with close proximity to the in-house wireless sensor node (see Fig. 4.4b), in-house wireless sensor node with patch antenna (operating at a single frequency, see Fig. 4.5) and alternative wireless node using Texas Instruments evaluation modules (see Fig. 3.13d).

TABLE 4-2
STATISTICAL PARAMETERS OF MEASURED ON-BODY PATH LOSS AT 2.42 GHZ FOR AN ANECHOIC ENVIRONMENT

Scenario	Median dB	Mean dB	PL(d_0) dB	γ	Root-MSE dB
Stand Alone Antenna (Fig 4.11a)	58.93	58.84	42.03	4.86	2.74
Antenna with In-House System Behind (Fig 4.11b)	58.65	58.77	41.09	5.11	5.06
In-House Embedded Wireless System (Fig 4.11b)	52.09	54.23	45.06	2.65	4.63
Texas Instruments Evaluation modules (Fig 4.11d)	49.74	49.54	36.08	3.89	3.27

The results for all systems show high path-loss components, a product of high electromagnetic absorption along the human trunk tissues and wave propagation alongside a non-uniform curvilinear surface. However, there is a noticeable difference between the results taken with the VNA and those made using the custom-built wireless sensor nodes, discussed below.

Although the projected path loss exponents differ between in-house wireless sensors and TI evaluation modules, 2.65 and 3.89 respectively, the values are comparable to the path loss exponents found by empirical, numerical and analytical methods reported in [135] (pair of microstrip patches), [120] and [136] (pair of dipoles), and [137] (pair of monopoles). Differences are attributed to the differences in size of the two systems (custom-built wireless sensors and TI evaluation boards; see Chapter 3, Fig. 3.13).

The in-house embedded nodes have a better performance with distance (γ=2.65), but have more radiation losses compared to the TI evaluation modules. However, measurements of the stand-alone on-body antennas prove to have higher losses than those integrated with on-body systems. This may be due to measurement uncertainties, such as cable effects (e.g., the presence of common mode currents or reflections from the VNA). It is noticeable that the presence of the system has a minimal effect when using the VNA technique, which may imply that the cable effect dominates.

The results in Fig. 4.6 show some discrepancies between those measured with the VNA and those using the wireless sensor modules, in terms of gradients (see also Table 4-2). It is thought that this difference is partly due to the fact that the wireless nodes operate in a single channel with a maximum bandwidth of 5 MHz, whereas the VNA measurements were performed over the whole ISM bandwidth (80.5 MHz). Other factors include the cable effect, potential scattering from the wireless sensor node structure and the internal bio-mechanical human processes.

In order to further investigate possible causes of this effect, additional on-body measurements with the wireless nodes were performed at location 6 (being the largest distance on the human trunk, d=50.3 cm). The mean and standard deviation of the recorded sensor data, defined by (4.2) with N = 1 and N=2, respectively, are displayed in Fig. 4.7 and a summary is listed in Table 4-3.

$$\sigma_N = \sqrt{\frac{1}{N}\sum_{i=1}^{N}\left(x_i - \bar{x}\right)^2} \qquad (4.2)$$

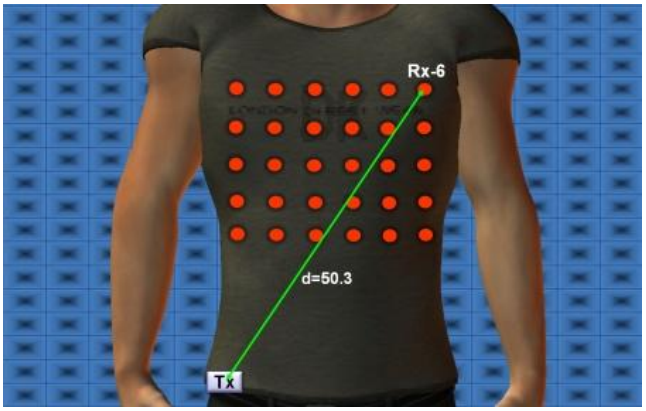

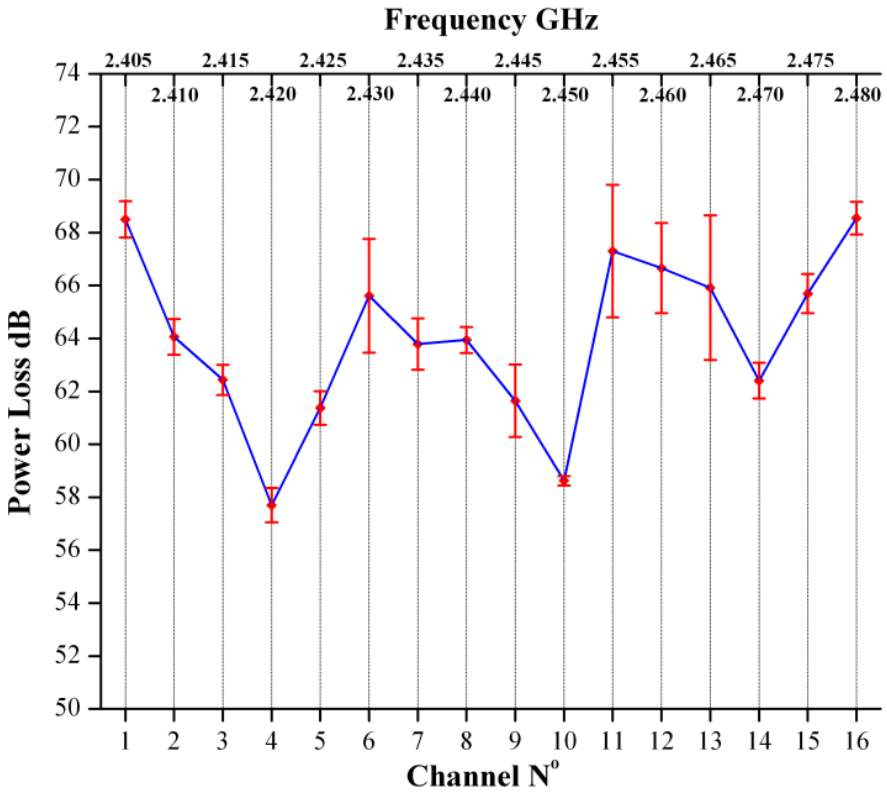

Fig. 4.7.Channel performance of receiving node located at the largest distance (position 6), from the transmitter module. The mean value (line-plot) and standard deviation (red error bars plot) shows the variation of antenna radiation properties is related to long term fading effects, the motion produced by breathing process which also produces movements on the antenna orientation.

Most of the channels experience variations of 0.5 dB to 2 dB on the received signal. Channels 4 and 10, operating at carrier frequencies of 2.42 GHz and 2.45 GHz, respectively, define the best communication links, with the smallest mean path loss values of 57.7 dB and 58.6 dB, respectively (Table 4-3). Although the

antennas have the best power transfer around 2.42 GHz (Chapter 3, Fig. 3.11 and Table 3-2), the performance of channel 10 is still good enough at 30 MHz away from the best radiation performance of the antennas.

TABLE 4-3
MEAN AND STANDARD DEVIATION FOR EACH OF THE 16 CHANNELS IN THE 2.45 GHZ ISM BAND USING IN-HOUSE WIRELESS NODES FOR ON-BODY LOCATION 6

Channel N°	μ dB	σ dB	Channel N°	μ dB	σ dB
1	68.49	0.69	9	61.64	1.37
2	64.05	0.67	10	58.62	0.18
3	62.43	0.57	11	67.29	2.50
4	57.70	0.64	12	66.65	1.70
5	61.37	0.63	13	65.91	2.73
6	65.60	2.15	14	62.40	0.68
7	63.78	0.97	15	65.69	0.74
8	63.94	0.49	16	68.54	0.62

On the other hand, channels 6, 11, and 13 exhibit average variations of 5 dB. For a wireless sensor programmed to operate at 2.43 GHz (channel 6), the variation in antenna radiation properties, such as the 10 MHz detuning observed at point 6 (see Fig. 4.3), have produced a change in the antenna's return loss magnitude, which must contribute to the worse performance in these channels. It is further conjectured that, over a given time frame, the cycle of the breathing process creates both LOS and NLOS propagation; thus, when the subject is stationary, long term fading or shadowing is the dominant fading observed, especially when the largest distance along the trunk is considered. The communication link on channel 6 is comparable to the mean path loss values of channels 1 and 16, despite being only 10 MHz away from the antenna's operating frequency.

In order to have a better understanding of the carrier-frequency dependence, on-body measurements were extended further over 9 different points (Fig. 4.8) using the in-house wireless nodes. The recorded data was used to estimate path loss models for

each carrier frequency. Measured values and least-square (LS) fitted path loss curves are shown in Fig. 4.9a and Fig. 4.9b. Fig. 4.9c shows the performance of each

Fig. 4.8.Different locations used for custom-built wireless sensor nodes to characterize the operation of the sensors at each carrier frequency. The receiver node was moved around trunk locations highlighted in red. The transmitter node was positioned at waist position.

on-body radio channel and the main statistical parameters for each communication channel are described in Table 4-4.

If a static radio propagation analysis is followed, channel 4 provides the maximum and optimum power transfer and, hence, is the best carrier frequency. However, for on-body communications, even when the subject is motionless, channel performance changes dynamically due to small variations caused by internal human body processes. Results show that channels 4 and 9 have the best communication links based on path loss exponents ($\gamma_{CH\text{-}4}$=2.73 and $\gamma_{CH\text{-}9}$=2.38, respectively); on the other hand, channels 6 and 12 have the highest path loss exponents ($\gamma_{CH\text{-}6}$=5.23 and $\gamma_{CH\text{-}12}$=5.98, respectively). If we consider the reference path loss, however, channel 9 exhibits the worst radio link (most loss) and 12 becomes the most suitable channel, in comparison to other adjacent channels.

It is evident that different channels have different characteristics; channel losses are a consequence not only of the presence of tissues with high permittivities, but also of the irregular surface of the torso. When the dynamic nature of the environment is considered, it is evident that optimum performance may require some degree of intelligence, in order to select the most appropriate channel (e.g., in terms of link reliability or minimising energy consumption).

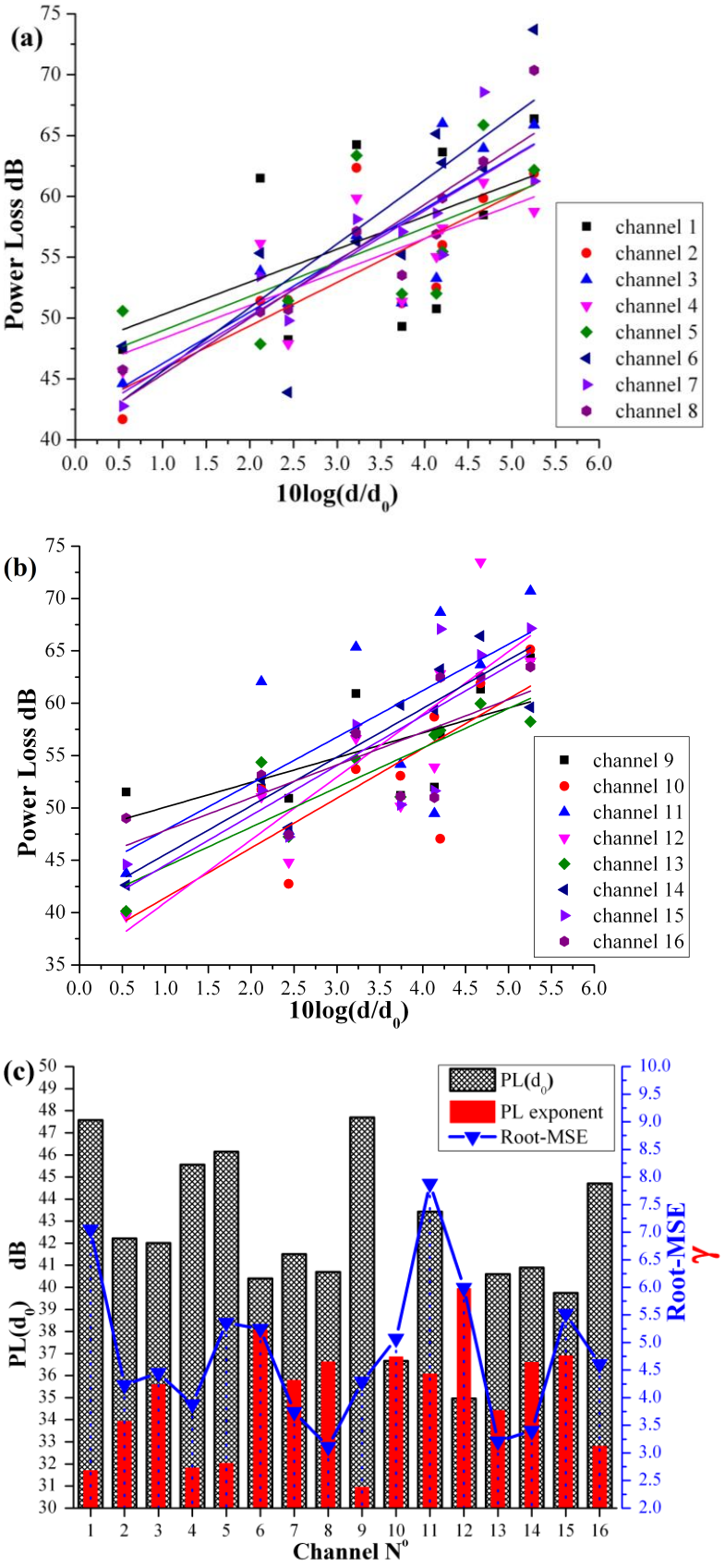

Fig. 4.9.Average Power Loss values using LS linear fitting for each frequency carrier at 2.45 GHz ISM band: (a) response of the first 8 channels; (b) response of the last 8 channels; (c) summary of statistical parameters of each frequency carrier.

TABLE 4-4
SUMMARY OF STATISTICAL PARAMETERS OF 16 DIFFERENT CHANNELS USING LOW POWER SENSORS

Channel N°	Frequency GHz	$PL_{(d0)}$ dB	γ	Root-MSE dB
1	2.405	47.58	2.68	7.05
2	2.410	42.22	3.57	4.23
3	2.415	42.01	4.24	4.45
4	2.420	45.56	2.73	3.88
5	2.425	46.15	2.81	5.36
6	2.430	40.40	5.23	5.25
7	2.435	41.51	4.32	3.74
8	2.440	40.70	4.65	3.11
9	2.445	47.70	2.38	4.29
10	2.450	36.67	4.74	5.07
11	2.455	43.43	4.43	7.88
12	2.460	34.97	5.98	5.99
13	2.465	40.60	3.77	3.21
14	2.470	40.90	4.64	3.40
15	2.475	39.75	4.76	5.52
16	2.480	44.71	3.12	4.61

In order to evaluate the performance of wireless sensors over the whole 2.45 GHz ISM band, the mean power loss was found for the sixteen carrier frequencies. The LS linear fitting of this averaging, compared with the VNA-based measurements is depicted in Fig. 4.10 and Table 4-5 presents the statistical summary.

4.3.4. Cumulative Distribution Function

In this analysis, the two different measurement techniques, using the VNA and using the wireless sensor modules, are compared on the basis of the cumulative distribution functions (CDF) as a function of average received power; these are shown in Fig. 4.11.

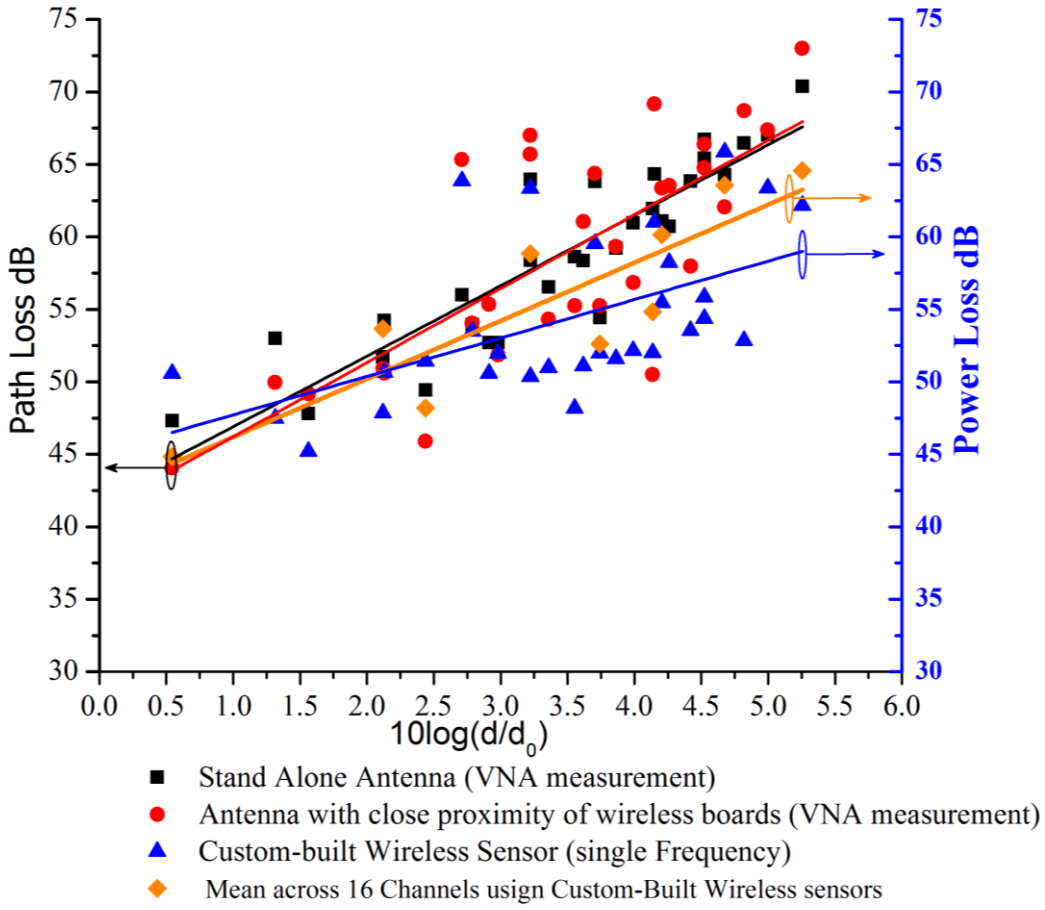

Fig. 4.10. Comparison of average path and power loss of: stand-alone antenna, antenna with close proximity to wireless boards, both measured using VNA equipment, and custom-built wireless sensor nodes operating at a single frequency, and the mean across the 16 channels which was recorded individually and mean was calculated after all channels were recorded.

TABLE 4-5
SUMMARY OF STATISTICAL PARAMETERS FOR PATH AND POWER LOSS MEASURED BY: THE VNA (2.45 GHZ ISM BAND) AND IN-HOUSE WIRELESS NODES (SINGLE CHANNEL 2.42GHZ AND AVERAGE OF ALL 16 CHANNELS)

Scenario	Median dB	Mean dB	$PL_{(d0)}$ dB	γ	Root-MSE dB
Stand Alone Antenna	58.93	58.84	42.03	4.86	2.74
Wireless Sensors (Single Channel)	52.09	54.23	45.06	2.65	4.63
Wireless Sensor (Mean 16-Channels)	54.83	55.69	42.18	4.00	3.4

All parameters were calculated on a 95% confidence interval (CI), according to their maximum-likelihood (ML) estimates. The variation around the mean path loss is best described by a log-normal distribution (4.3) which is commonly used to model long-term fading (shadowing):

$$f(x|\mu,\sigma)=\frac{1}{x\sigma\sqrt{2\pi}}\exp\left\{-\frac{(\ln x-\mu)^2}{2\sigma^2}\right\} \quad (4.3)$$

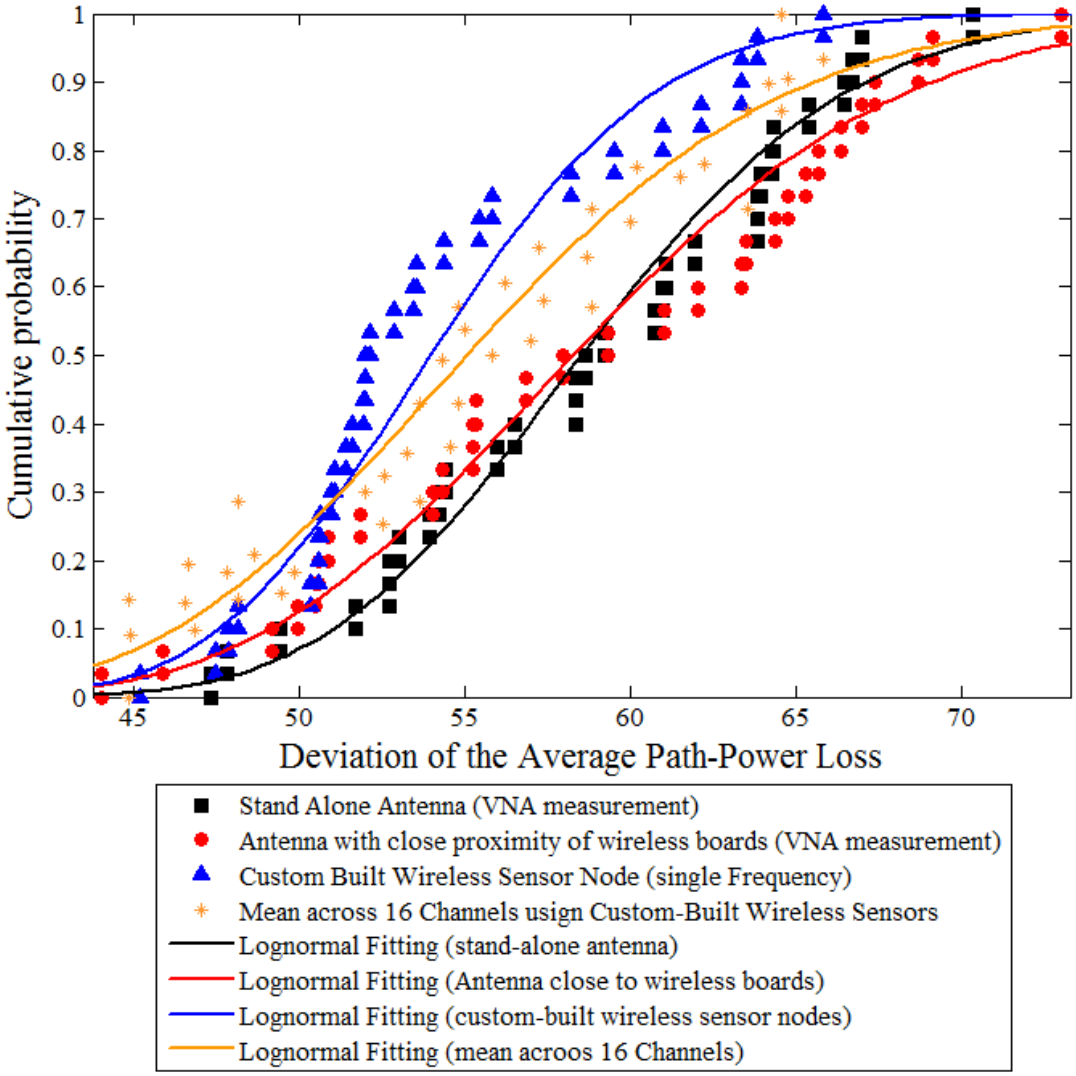

Fig. 4.11.Deviation of measurement from the average path and power loss acquired with VNA and custom-wireless sensor nodes, respectively. A wireless sensor node operating at a single frequency has different radio channel characteristics from a stand-antenna measured by a VNA and characterised over the whole bandwidth of operation.

The mean and variance of the log-normal random variable are denoted μ and σ^2, respectively, and are given in Table 4-6 for each measurement setup. The data acquired by both VNA and wireless sensors shows compact behaviour in the first and third quartiles (below 52.15 dB and above 62.51 dB, respectively). However, the median quartile presents the most spread data.

This trend is caused by two factors: first, the wireless sensor nodes are coupled to an embedded antenna, usually integrated with active and passive elements also assembled on the dielectric substrate; thus, the combination radiates as a whole structure. On the other hand, the stand-alone antennas do not have an adjacent structure that shields the wave propagation from the effects of the human tissue.

Second, the use of semi-rigid coaxial cables in the VNA measurements may introduce errors. For example, the excitation of surface currents on the outer metallic shield of coaxial cables (common mode currents) is unavoidable, causing pattern degradation. Furthermore, the presence of cables in the wave propagation path can scatter or even radiate electromagnetic waves, thus causing fragmentation, distortion of the antenna radiation pattern and signal variation from cable movements, even when not connected to the antenna. These may be exacerbated by the use of unbalanced antennas and designs with small ground planes.

TABLE 4-6
AVERAGE VALUE AND STANDARD DEVIATION OF LOGNORMAL DISTRIBUTION APPLIED TO PATH AND POWER LOSS FOR MEASUREMENTS TAKEN WITH THE VNA (2.45 GHZ ISM BAND) AND IN-HOUSE WIRELESS NODES (SINGLE CHANNEL 2.42GHZ AND AVERAGE OF ALL 16 CHANNELS)

Scenario	**Lognormal Fit**	
	μ dB	**σ dB**
Stand Alone Antenna	4.06	0.106
Antenna with Sensor Behind	4.06	0.133
In-House Wireless Sensor (Single)	3.98	0.098
Wireless Sensor (Mean 16-Channels)	4.00	0.136

4.4. Discussion and Conclusion

On-body communication channels between two low-power IEEE 802.15.4 sensor nodes operating in the 2.45 GHz ISM band (2.40-2.4835 GHz) have been presented. Propagation measurements were performed on the trunk section of the human body in an anechoic environment, where multipath and scattering effects, usually present in an indoor environment, are negligible.

First, measurements were made using a standard VNA connected via coaxial cables. An alternative measurement technique for on-body antennas was then examined, utilising wireless sensors nodes. The latter not only diminished the effect of coaxial cables (scattering or radiation), but also provided a more realistic response of the radio link channel. Moreover, the radio communication for each of the 16 IEEE 802.15.4 channels in the 2.45 GHz ISM band was measured at different points on the torso, using this technique. It was found that the wireless sensors operating at individual carrier frequencies have different responses; hence, system performance is influenced not only by the initial antenna response, but also by the channel selected.

The limitations of the VNA approach are evident when comparing the results shown in Figs. 5.6 and 5.11 (also Tables XV and XIX), where the combination of cable effect and measurement bandwidth dominate over the physical proximity of a realistic system. The VNA measurements usually imply a path loss around 3 dB lower than that using the wireless sensor node approach, with equivalent differences in other measures. The path loss exponent is always found to be greater using the VNA method, often by a factor of 2. Hence, the value of the wireless sensor method can be seen in the more realistic data observed. Thus, the two techniques may be seen as complementary: the VNA approach has the benefits of greater speed and dynamic range, whilst the utilisation of sensor nodes allows a more detailed investigation of real-world scenarios.

Chapter 5

Exploring Dynamic On-Body Radio Channels for Physiological Features

The continuous development of compact and low-power circuits has enabled the miniaturization of hardware systems and, thus, led to wireless pervasive sensing. The connection of different wireless nodes on and around the human body defines a Wireless Body Area Network (WBAN) [14, 25]. It is evident that particular areas of the body have unique characteristics, thereby affecting the performance of the radio channel. Furthermore, external perturbations, such as human mobility and operation in cluttered backgrounds, result in a complex environment for the propagation characteristics of body-worn sensors [138, 139]. Usually, the latter embeds low-power microcontrollers, tiny RF transceivers and compact antennas that have low gain and narrow bandwidth (low-profile antennas).

Different studies have shown the potential use of on-body wireless sensors during the healing process after surgery. Body-worn units housing accelerometers can monitor the level of activity of a patient, indicating an improvement or a decline in recovery process [140, 141]. As a result, the quality of care provided to patients is improved by the continuous monitoring, even those merely indicating general 'well-being'.

The monitoring of human motion is frequently sensed by some combination of accelerometers, gyroscopes and inertial sensors, which are integrated with wireless communication standards, such as ZigBee or Bluetooth. In [142], a footwear-based activity monitor was implemented using accelerometers and pressure sensors to predict the energy expenditure associated with common daily postures and activities.

In [143, 144], the received signal strength (RSS), an internal parameter of RF transceivers, was used to characterise limb movements for kinesiotherapy activities using Crossbow IRIS wireless modules. Their results show that learning techniques, such as a Support Vector Machine (SVM), can determine and classify limb movements based on information from the fading in the propagation signal path.

In recent years, research has been focused on non-invasive technologies and its applications in healthcare environments, so that patients are no longer required to be attached to large, stationary monitoring equipment while their vital signals are recorded. This new trend, and the use of on-body wireless sensors within hospitals and home environments, can reduce healthcare costs and improve daily lifestyles. Many wireless systems have been proposed to accomplish this feat, with diverse solutions shown in [145, 146].

In this chapter, custom-built wireless sensor nodes (described in Chapter 3, Section 4.2.3) are used to evaluate radio propagation characteristics of four on-body channels while different physical activities are executed. In addition, the collected radio propagation data is further post-processed, in order to investigate the ability to identify physiological markers, such as gait pattern, breathing process and heartbeat.

5.1. Measurement Procedure

Measurements were performed on a 168 cm tall, 80 kg male test subject. The transmitter node was fixed in the right waist section and the receiver node was in four different locations in succession: the upper middle section of the thoracic cavity

(chest), the left ankle, the left wrist and the middle back (thoracic spinal cord). These locations were used for each physical activity. The receiver and transmitter locations are shown in Fig. 5.1.

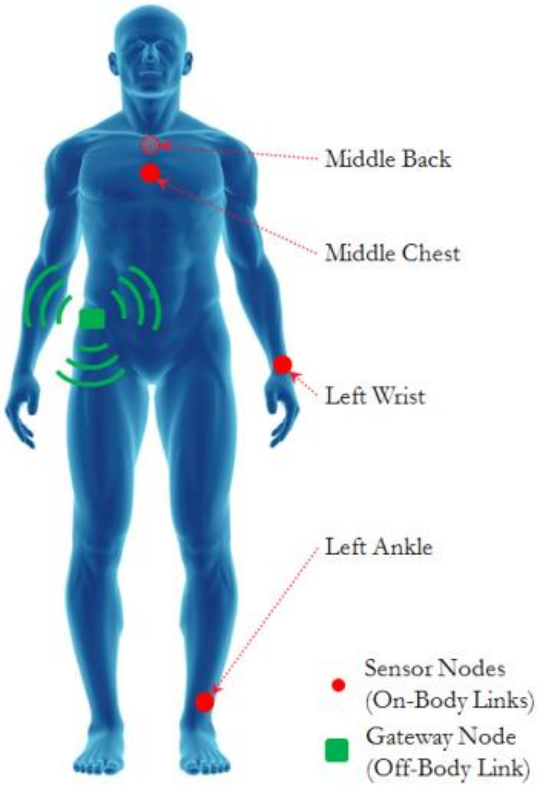

Fig. 5.1.Location of custom-built wireless sensors nodes used for dynamic WBAN radio channel characterization for each athletic activity.

All the measurements were taken in Queen Mary's Human Performance Laboratory (indoor environment). The jogging exercise was performed on a WOODWAY ELG treadmill machine which has a running surface of 70 x 244 cm [147]. The motorized treadmill, shown in Fig 5.2a, is also equipped with a digital display and an electronic console on the front panel. For our experiments, the tilt of the conveyor belt was set flat (no tilt), in order to simulate normal outdoor jogging.

Cycling was carried out on a stationary sport medical training bike, the Lode Excalibur Sport with pedal force measurement [148] depicted in Fig. 5.2b. The resistance of the flywheel attached to the pedals was controlled by a digital control panel on the front of the bike. The test subject was seated with the body leaning forward and hands extended wide on the back part of the handlebar, simulating a normal outdoor pedalling.

In the case of the rowing scenario, a RowPerfect RP3 rowing ergometer was used [149] (see Fig. 5.2c). The rowing machine simulates as closely as possible the

dynamical and mechanical properties of a racing. This ergometer has an air resistance flywheel system called “floating” power head. The footplate with the power head unit and the seat are both mounted on the slide track and are thus free to move independently (see Fig 5.2c). The mass of the power head (about 17 kg) is similar to that of a section of a boat containing one oarsman. To simulate a fixed power head ergometer, the floating head was clamped at one end. The chain was placed on the larger of two cogwheels, and a 39 cm disc was used to set the resistance on the flywheel for all pieces. The rowing equipment is also fitted with a digital console control panel where a user can program different rowing scenarios.

(a) (b)

(c)

Fig. 5.2. Medical Sport Equipment used for the characterization of dynamic WBAN channels using custom-built wireless sensors. (a) WOODWAY ELG treadmill machine [147]; (b) Lode Excalibur Sport bike with pedal force measurement [148], and (c) Rowperfect RP3 rowing ergometer [149].

The channel of operation of each wireless sensor node is programmed according to the performance of the antennas when placed on the body. The radiation properties of each antenna, Tx. antenna and Rx. antenna, were measured using a PNA-L 5230C which recorded the *s* parameters of each antenna for 13 minutes.

The effect of motion on the antenna behaviour was evaluated for the jogging activity. During the first two minutes, the subject was in a resting position (standing on the treadmill); for the next 10 minutes, the subject was moving (jogging at 5 km/h); and for the last minute, the subject was recovering (stop jogging). The performance of the transmit antenna (waist-location) for the aforementioned process is depicted in Fig. 5.3. The main statistical parameters are listed in Table 5-1.

It is apparent that there are small fluctuations in the resonant frequency of the antenna related to the repetitive motion, but these variations are small in magnitude, compared with the bandwidth of the antenna. Additional information of the antenna design, and the spectrum response of each low power wireless sensor can be found in [150, 151].

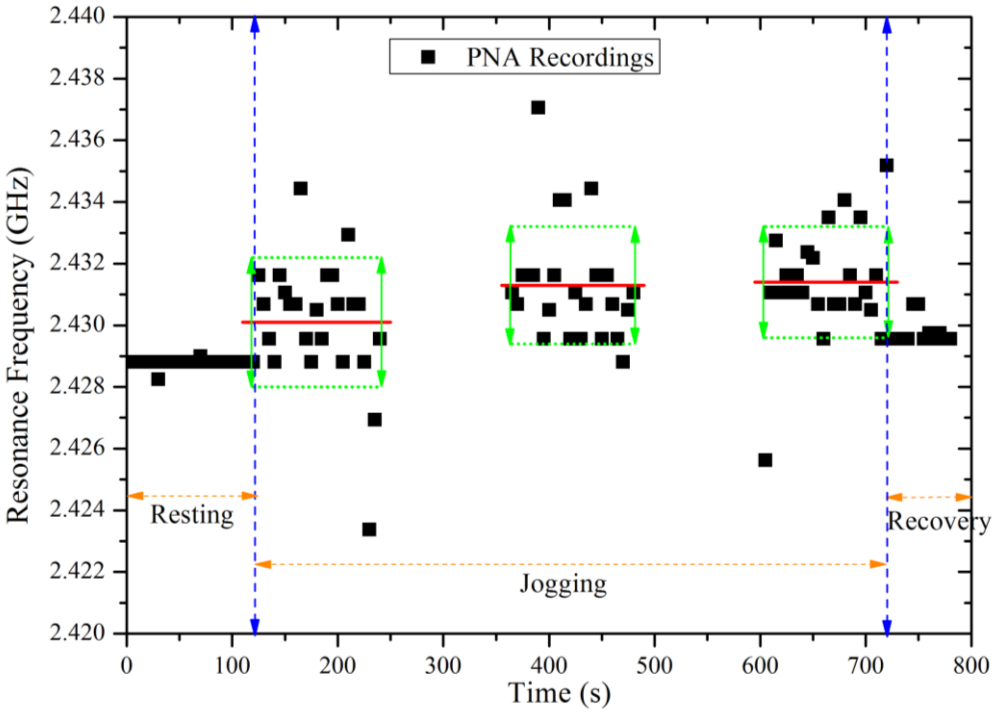

Fig. 5.3. The plot shows the variation of the resonant frequency of the transmitting antenna while the test subject is resting, jogging and in a recovery process.

For each activity, the receiver node records an average of 7000 samples of the received signal strength (RSS) at a rate of 14 ms per sample. In each activity, the

receiver node starts recording data only when the user has a constant speed of 5 km per hour (5 km/h), which was set and controlled by the digital control panel of each sporting machine. Acquired data is stored in the internal flash memory of the microcontroller which was later extracted and further analysed.

In order to decrease location displacement due to the constant movement, VELCRO tape was fitted on the T-shirt and on the wireless sensors, the transmitter and receiver respectively. The performance at different locations (alongside the torso) and the operation at different carrier frequencies (within the 2.45 GHz band) of each custom-built wireless sensor node is described in[151].

TABLE 5-1
VARIATION OF THE S_{11} RECORDED PRIOR THE SELECTION OF THE COMMUNICATION CHANNEL OF THE CUSTOM-BUILT WIRELESS SENSOR NODES

Process	**Duration min**	**Mean μ**	**S.D. σ**
Resting	2	2.4288	0.000122
Jogging	2	2.4301	0.00210
Jogging	2	No recorded Data	No recorded Data
Jogging	2	2.4313	0.00190
Jogging	2	No recorded Data	No recorded Data
Jogging	2	2.4314	0.00180
Recovery	1	2.4298	0.00043

5.2. Data Analysis

5.2.1. Characterisation of On-body Radio Channels for dynamic scenarios

On-body radio models, acquired from simulation and empirical methods, have shown that received signals are the combination of diffracted waves around the human body curvature, decaying creeping wave components and, to a high degree, scattered and reflected contributions (i.e., fast fading, multipath, shadowing) [152, 153].

Initial studies in [50] reported peak-to-peak signal variations of 16 dB between belt and shoulder-worn antennas when changes in body posture occurred. In [154], the walking process in anechoic chamber, open office area and hallway environments was characterised. In the indoor scenarios, their results showed that the signal variations of different on-body channels were best described by a Nakagami-m distribution with a Level Crossing Rate (LCR) threshold of 20 dB below the median signal level.

It is evident that the practice of any sport activity will produce a high level of fluctuations on the received signal, which are the consequence of the continuous movement of the human body. In the case of jogging, our results show these variations are ±15 dB from the average received signal; this is significantly greater than received signals of a motionless user in a free-space environment, where the variations are ±3 dB. The received signal of both scenarios, jogging and motionless is depicted in Fig. 5.4. The graph plots a 45 s window length of a waist-to-chest channel.

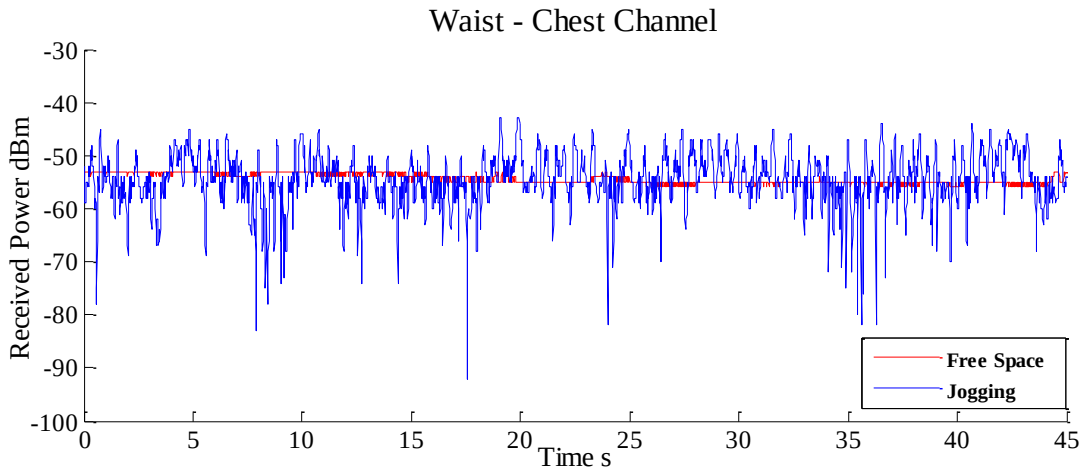

Fig. 5.4.Recorded received signal strength (RSS) for a waist-to-chest channel recorded by custom-built wireless sensor nodes when the test subject is jogging and motionless in Queen Mary's Human Performance Laboratory.

A simplified path loss expression was defined in Chapter 4, Section 4.3.3. In our study, the path loss exponent γ, and the initial path loss $PL(d_0)dB$, are derived from measured data considering a reference distance of 15 cm (d0=15cm). The average power loss for each WBAN channel is described graphically as a function of box plots shown in Fig. 5.5. The non-parametric statistical plot describes the interquartile range of each WBAN activity. The spacing between the different parts of the box

indicates the degree of dispersion (spread) and skewness of logged RSS data. The mean power loss and standard deviation for each on-body channel is summarised in Table 5-2.

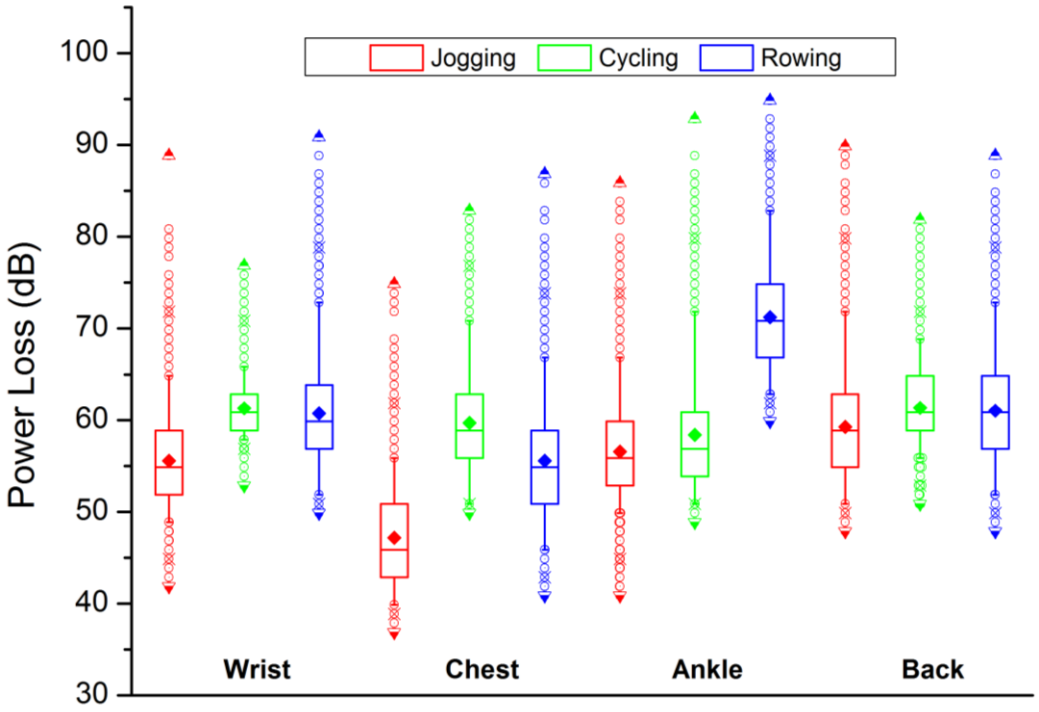

Fig. 5.5.Power loss for different on-body radio channels estimated from recorded RSS while test subject is under physical workout. The spacing between the different parts of the box indicates the degree of dispersion and skewness of the data.

The results demonstrate that dynamic on-body channels present high variation amongst different links; however, the back location presents the most correlated data between different actions. The observed correlation is consequence of the reduced movement, in contrast to wrist and ankle locations.

In the case of the waist–ankle channel, data is highly correlated for two scenarios jogging and cycling, respectively. This behaviour is expected as a consequence of the constant speed of the user (5 km/h).

On the other hand, the rowing scenario is an uncorrelated channel (compared with jogging and cycling), which is the outcome of the constant action of leaning forward and backward. At a given time instant, the legs are totally extended, positioning the receiver at the largest distance from the transmitter; hence, power loss is higher. These results suggest that the combination of data from two or three channels would be sufficient to determine the respective activity. However, the latter requires further investigation.

TABLE 5-2
STATISTICAL SUMMARY OF THE POWER LOSS VARIATION RECORDED BY CUSTOM-BUILT WIRELESS SENSOR NODES

WBAN channel	**Jogging**		**Cycling**		**Rowing**	
Waist-to-	**Mean**	**S.D (σ)**	**Mean**	**S.D. (σ)**	**Mean**	**S.D. (σ)**
Wrist	55.55	5.14	61.27	2.82	60.74	6.16
Ankle	56.57	5.62	58.37	6.26	71.22	5.97
Chest	47.17	5.27	59.66	5.95	55.55	6.32
Back	59.23	6.46	61.31	4.37	61.05	6.23

Second-order statistics are presented from each measurement campaign. The measured received signal was normalized according to the maximum received power. The statistical analysis uses the square root of this normalized receive power in order to find normalized received signal amplitude.

The variation around the recorded received signal is modelled by four statistical distributions (Lognormal, Nakagami, Gamma and Weibull, namely) often used in WBAN communications. All parameters are calculated on a 95% confidence interval (CI) according to their maximum-likelihood (ML) estimates.

In this study, different sports activities are compared. In our data analysis, we consider a time window of 45 s which states approximately 3215 samples ($n \approx 3215$), and all fitted distributions have a coefficient K=2. Estimated distribution parameters according to ML estimates are presented in Table 5-3 for the each sport application.

The log-normal distribution has been commonly applied to describe static and off-body WBAN communication channels [14, 114, 155]. In our study and according to the AICc scores, it was observed that the Nakagami and Weibull distributions, commonly used to model strong fast fading, are in general the best fit to the measured data. Plots of probability distribution functions (PDF) as a function of the normalized received power are shown in Fig. 5.6 and Fig. 5.7. The bin size of the histograms used to describe the PDF of the measured data is chosen according to the "Freedman- Diaconis" rule [156, 157].

TABLE 5-3
ML ESTIMATED DISTRIBUTION PARAMETERS FOR DIFFERENT MOBILE WBAN CHANNELS AND DISTRIBUTIONS

Jogging		
Waist - Wrist	Lognormal	μ=-1.57, σ=0.59
	Nakagami	m=1.03, ω=0.074
	Gamma	a=3.47 , b=0.069
	Weibull	A=0.27 , B=1.96
Waist - Chest	Lognormal	μ=-1.18 , σ=0.61
	Nakagami	m=1.04, ω=0.16
	Gamma	a=3.31 , b=0.11
	Weibull	A=0.40 , B=2.1
Waist - Ankle	Lognormal	μ=-1.81 , σ=0.65
	Nakagami	m=0.89, ω=0.052
	Gamma	a=2.93 , b=0.067
	Weibull	A=0.22 , B=1.79
Waist - Back	Lognormal	μ=-1.31 , σ=0.74
	Nakagami	m=0.79, ω=0.15
	Gamma	a=2.4 , b=0.14
	Weibull	A=0.38 , B=1.73

Cycling		
Waist - Wrist	Lognormal	μ=-0.97, σ=0.32
	Nakagami	m=3.07, ω=0.17
	Gamma	a=10.81, b=0.037
	Weibull	A=0.44, B=3.86
Waist - Chest	Lognormal	μ=-1.13, σ=0.68
	Nakagami	m=0.85, ω=0.21
	Gamma	a=2.67, b=0.15
	Weibull	A=0.44, B=1.79
Waist - Ankle	Lognormal	μ=-1.09, σ=0.72
	Nakagami	m=0.95, ω=0.20
	Gamma	a=2.78, b=0.14
	Weibull	A=0.45, B=2
Waist - Back	Lognormal	μ=-1.20, σ=0.50
	Nakagami	m=1.29, ω=0.14
	Gamma	a=4.45, b=0.076
	Weibull	A=0.38, B=2.22

Rowing		
Waist - Wrist	Lognormal	μ=-1.25, σ=0.71
	Nakagami	m=0.80, ω=0.17
	Gamma	a=2.51, b=0.14
	Weibull	A=0.4, B=1.72
Waist - Chest	Lognormal	μ=-1.69, σ=0.73
	Nakagami	m=0.71, ω=0.079
	Gamma	a=2.31, b=0.1
	Weibull	A=0.26, B=1.57
Waist - Ankle	Lognormal	μ=-1.31, σ=0.69
	Nakagami	m=0.87, ω=0.14
	Gamma	a=2.69, b=0.12
	Weibull	A=0.37, B=1.82
Waist - Back	Lognormal	μ=-1.52, σ=0.72
	Nakagami	m=0.75, ω=0.11
	Gamma	a=2.38, b=0.11
	Weibull	A=0.31, B=1.63

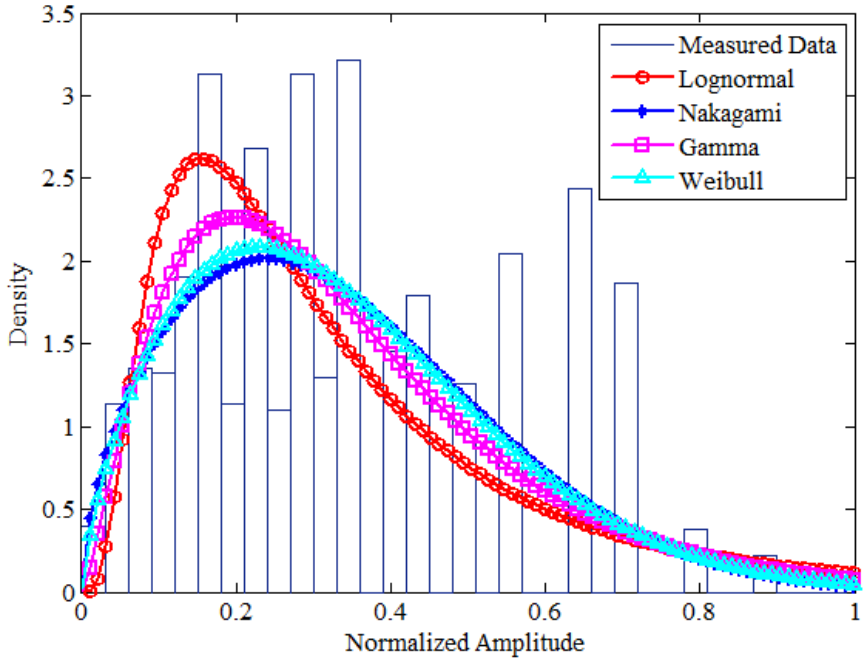

Fig. 5.6.Probability Distribution Function (PFD) for a waist-to-back channel recorded by custom-built wireless sensor nodes operating at 2.45 GHz while the test subject was jogging at a constant speed of 5km/h.

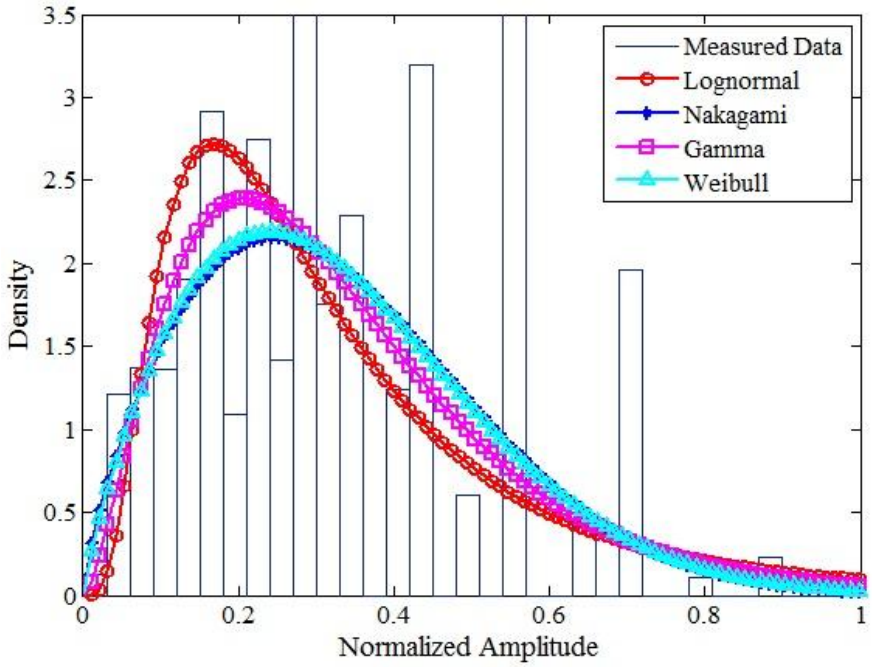

Fig. 5.7.Probability Distribution Function (PFD) for a waist-to-ankle channel recorded by custom-built wireless sensor nodes operating at 2.45 GHz while the test subject was rowing at a constant speed of 5km/h.

5.3. Exploring On-Body Radio Channels for Embedded Physiological Features

The previous section identified two statistical distribution models that describe the behaviour of dynamic on-body radio channels. It also showed that received signals are highly non-stationary due to the constant change of frequency, amplitude and phase with time. Although received signals present high amplitude variance, the use of wireless sensors certainly represents a flexible and sustainable solution for environments where freedom of movement is needed.

The outlook of future infrastructures (hospitals, military services and care centres) supporting wireless sensing technology remains an essential and active part for patient awareness, not only to off-load demand of services, but also to promote autonomous and flexible monitoring solutions, especially for non-stationary scenarios. Active research has shown possible solutions for the latter offering non-invasive sensing capabilities. For example, in 1975, a non-invasive procedure to monitor heartbeat and respiratory movements was introduced by Lin [158-160]. The microwave system transmitted continuous wave (CW) signals from 2.1-2.5 GHz and the periodic displacement of the thoracic cavity was recorded in the reflected wave, which was phase-modulated (PM) by the time-varying position of the chest (concept related to the Doppler Effect).

Further advances in technology made possible the design of compact and lightweight systems, improving not only the detection accuracy, but also reducing the phase-noise of the receiving signal. In [161], Doppler systems operating at different microwave frequencies such as 2.4 GHz, 5.8 GHz, 10 GHz, 26 GHz and 60 GHz, respectively, were considered. The results showed that the use of high frequencies (short wavelengths) vastly improved the sensitivity to small variations exhibited in chest-wall movements.

Other studies made use of double-sideband transmission systems and I/Q modulation (quadrature signals) in order to reduce the number of the null points, a problem in single channel Doppler systems, and enhance the detection of cardiopulmonary movement [162, 163]. Although most of these non-intrusive monitoring systems were studied and implemented in controlled environments using frequency domain techniques, signals recorded in time domain also embed external

information. In this context, the current section explores the on-body electromagnetic (EM) wave propagation, recorded by wireless sensor nodes, as a sensing method.

The transmitting node antenna (at waist level) radiates EM waves that propagate through both free space and human body. The main radiation beam of the patch antenna is normal to the body; however, there are also EM waves travelling along the body's surface that are mainly triggered by the fringing fields and backscattering energy, similar to the operation of radar transceivers. On-body transient simulations were implemented in CST Microwave Studio and the results, shown in Fig. 5.8, verify the aforementioned description.

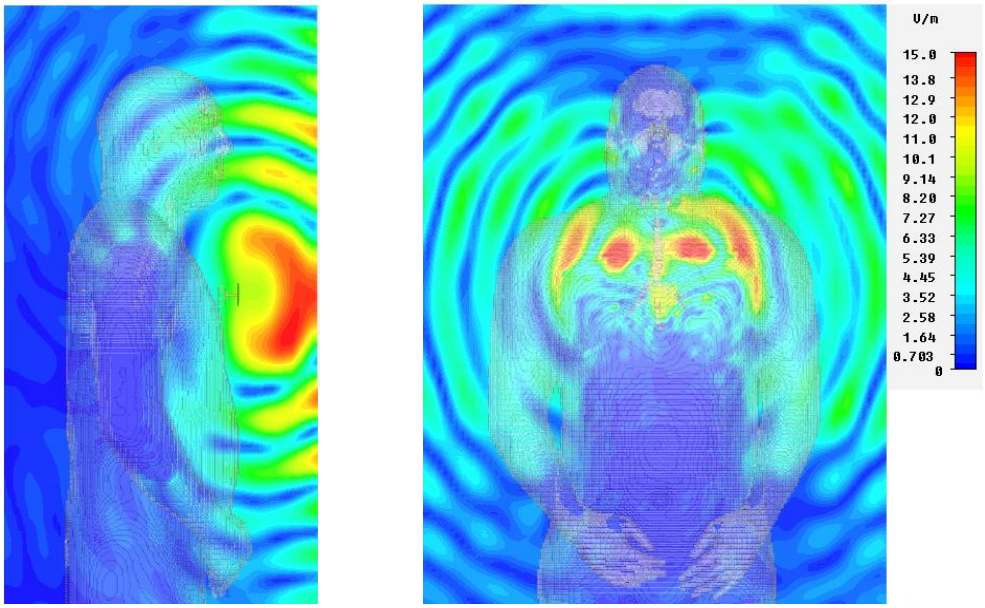

Fig. 5.8.Simulation results of the EM wave propagation alongside the trunk section of the Hugo model implemented in CST Microwave Studio. The radiating element was the designed microstrip patch antenna from Chapter 3

In order to get the best results, the identification and extraction of physiological features, such as motion pattern, respiration rate or heartbeat, the study only considers waist-to-chest channels. The received signal strength for these channels is shown in Fig. 5.9, with mean values of -50.19 dBm, -62.68 dBm and -58.57 dBm, respectively.

The use of powerful and robust digital signal processing techniques (e.g., template matching, blind source separation, wavelet transforms) is undoubtedly advantageous; however, the latter is beyond the current study, and hence a combination of digital filtering and spectral response is presented.

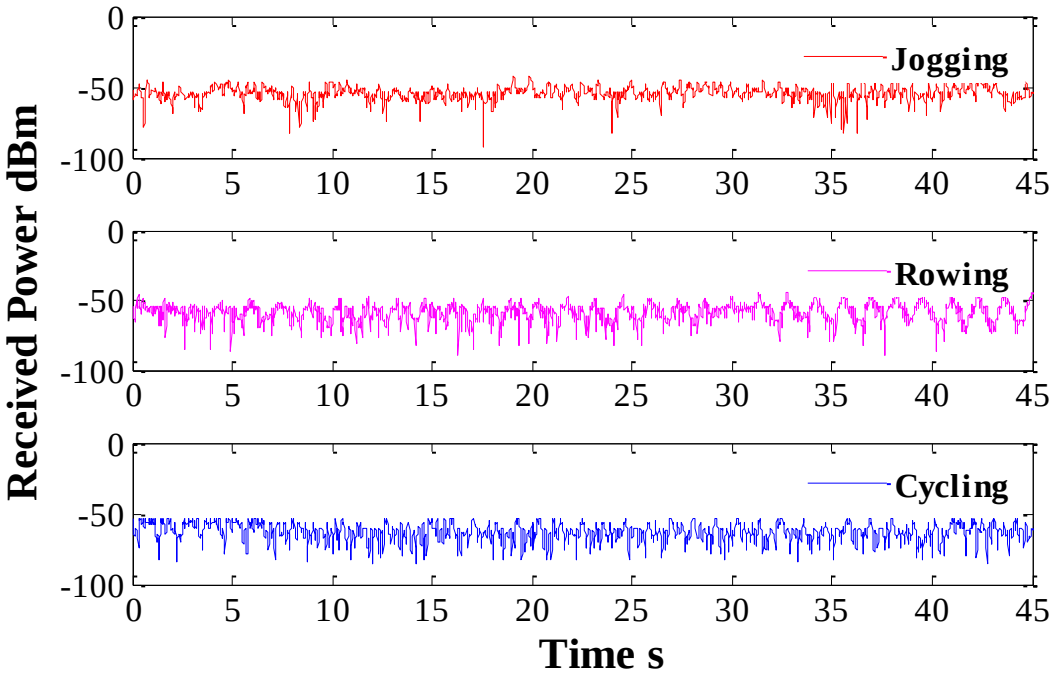

Fig. 5.9.Received Signal Strength (RSS) for waist-chest channels recorded with custom-built wireless sensor nodes from three different activities: (a) jogging; (b) rowing and (c) cycling. The measurements were performed in Queen Mary's Human Performance Laboratory

5.3.2. Physiological Information Parameters

The number of breaths and heart-beats per minute varies with the subject's body mass index (BMI) (i.e., the ratio of body's weight and the square of height), age, gender and, of course, the activity level. The pulse rate of a resting adult has an average frequency of 1 to 1.5 Hz, or 60 to 90 beats per minute (BPM). On the other hand, the resting respiration rate is about 6 - 12 breaths/min [159, 164]. The mechanical processes of the cardiovascular and the respiration cycles produce abdominal displacements of 0.2 - 0.5 mm and 4-12 mm, respectively.

During a normal walk, the pulse increases up to 95 BPM and the respiration rate varies between 12 - 18 breaths/min, while performing other athletic activities (such as running, swimming, rowing or cycling) causes the heartbeat rate to increase to almost twice that of a resting adult: 120 to 190 BPM (2 Hz to 3.1 Hz, respectively) [164].

Considering an average heartbeat frequency of 2.6 Hz ($f_{\text{heart-beat}}$= 2.6 Hz) for a workout activity of an adult, the minimum sampling frequency, defined by Nyquist-Shannon theorem, should be 5.2 Hz (t_s = 192 ms) in order to perfectly reconstruct the original signal. The average sampling rate of custom-built wireless sensors is 14 ms/sample (71.4 Hz), a high margin from the minimum sampling rate.

The exercise testing and data acquisition was validated and executed on a computerised Cortex system that was controlled by a software application called MetaSoft Studio [165]. The application software manages and monitors electrocardiogram (ECG) recordings and jogging speed (5 km/h). The integrated system, shown in Fig. 5.10, was not used for cycling and rowing activities because the amount of cables across the body was restricting the normal workout process.

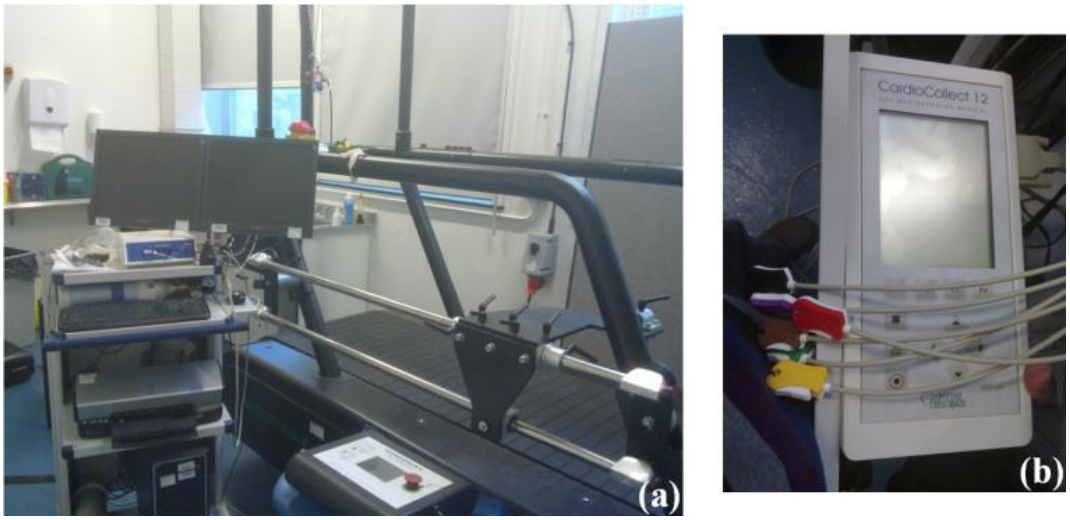

Fig. 5.10.Queen Mary's Human Performance Laboratory, (a) integrated Cortex System synchronized with a treadmill machine and electrocardiograph, (b) 12-Lead electrocardiograph system Cardio-Collect 12.

The ECG recording device was a certified 12-Lead electrocardiograph, the Cardio-Collect 12. The sampling frequency and the ADC resolution of the latter were 500 Hz and 12 bits, respectively. The cardiac recordings were taken for a resting position (standing on the treadmill machine) and jogging (constant speed of 5 km/h) while wireless sensor nodes record RSS values only when constant speed was achieved.

The acquired ECG samples, which served as reference waveforms for cycling and rowing scenarios were described as normal sinus rhythm without any significant arrhythmias. A 10 s ECG sample frame for resting and jogging scenarios is shown in Fig. 5.11Fig. 5.11. In addition, heart rate variability for a time frame of 5 minutes is described in Table 5-4.

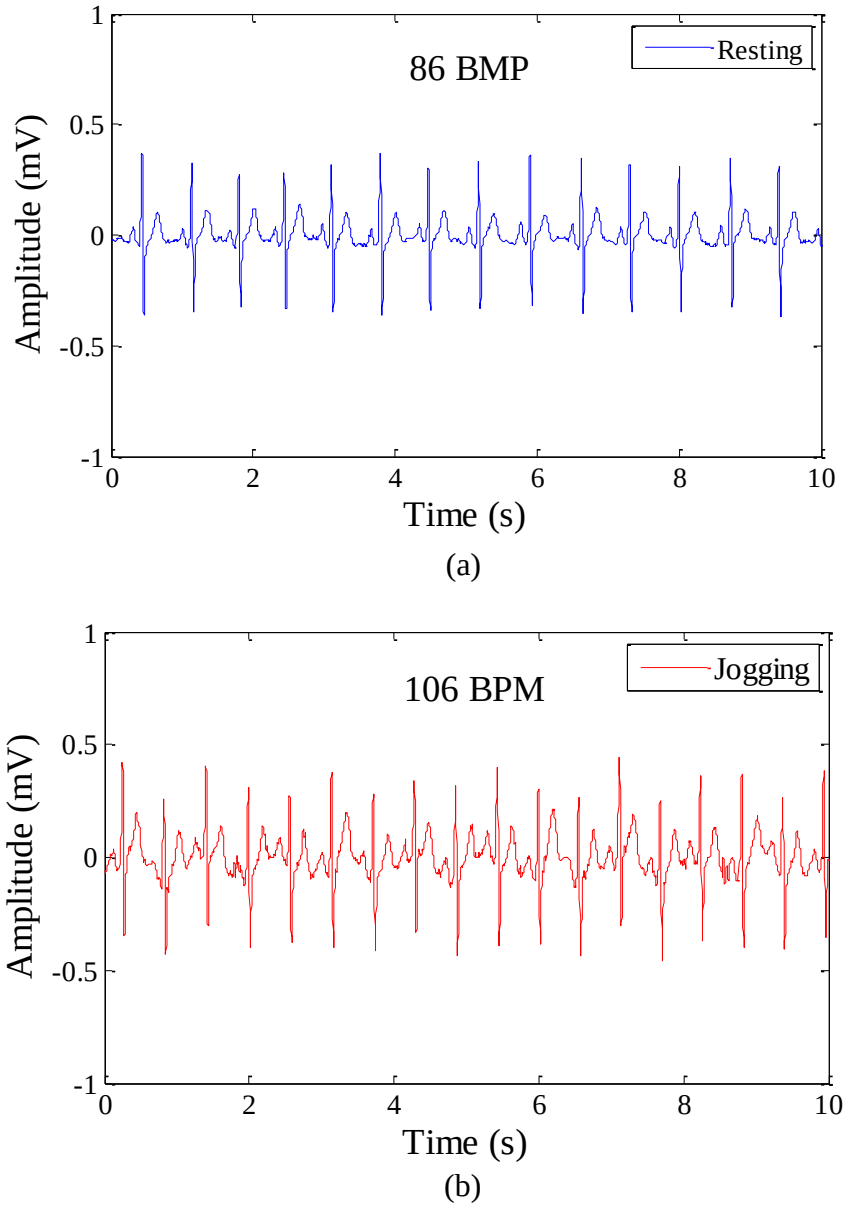

Fig. 5.11.Heartbeat signal of the test subject while is: (a) standing on the treadmill machine (resting stage). The average heartbeat was 86 BPM; (b) jogging at a constant speed of 5 km/h. The heartbeat rate was 106 BPM.

TABLE 5-4
HEART RATE VARIABILITY FOR A RESTING AND JOGGING SCENARIOS CALCULATED FROM A 5 MINUTE SEGMENT FRAME

Scenario	**H.R. Mean**	**H.R. S.D. (σ)**
Resting	86.07	4.83
Jogging at 5 km/h	106.3	4.29

5.3.3. Frequency Analysis of Time-Domain Channel Data

The spectral estimation was performed for four different scenarios resting (0 km/h), jogging, cycling and rowing (each at 5 km/h). Normalized received signals were filtered using a 10th order elliptic band-pass IIR filter (infinite impulse response filter). It was decided not to use FIR filter (finite impulse response filter) because the received data does not contain any phase information, and hence phase linearity was not necessary. The digital filter was computed on data segments of 45 seconds (≈ 3215 samples).

In order to avoid frequency component confusion, two different band-pass filters were implemented: the first filter with cut-off frequencies of the 0.1 Hz (lower frequency) and 0.8 Hz (higher frequency) for breathing analysis and the second filter with cut-off frequencies of 0.8 Hz (lower frequency) and 3 Hz (higher frequency) for heart-beat movement.

The frequency domain analysis was based on the estimation of the power spectrum density (PSD) from filtered data. The PSD evaluation methods can be divided into parametric, e.g., Autoregresice (AR)-model, and non-parametric methods. The non-parametric methods, for example the Welch's periodogram, are, in general, faster to compute and, in the case of a Welch's FFT method, it reduces the variance of the spectral density by averaging. This method divides the time series samples into overlapping sub-sequences. Each sub-sequence is windowed and then the estimated spectral density is averaged (our study uses a Hanning window).

The use of a Hanning window (5.1) smooths uncorrelated data located at the edges, diminishing aliasing of different rooted information and minimizing the amplitude dispersion into other harmonics (reduced spectral leakage). Additionally, the window function limits the extent of the sequence providing a more stationary spectral characteristic. The terms n and N in (5.1) represent the discrete-time index and the length of the window, respectively. The window length was selected such that reasonable spectral performance was achieved. In the data analysis, N was limited to 4096 samples (without zero-padding) with window sections of 1024 and window overlaps of 512.

$$w_n = 0.5\left(1\text{-}\cos\left(2\pi\frac{n}{N}\right)\right) \quad for \quad 0 \le n \le N \qquad (5.1)$$

The spectral content of a resting scenario (test subject standing on the treadmill machine) was taken for five different locations, mainly along the upper chest section. The resulting plot, shown in Fig.5.12, depicts the main component at these locations, which occurs between 0.12 Hz and 0.13 Hz; this would be equivalent to a breathing rate of 7.2-7.8 breaths/min. The spectral results of the second filter (0.8 Hz -3 Hz) did not show any significant harmonics to be related with heart beat movement; therefore, it was not included.

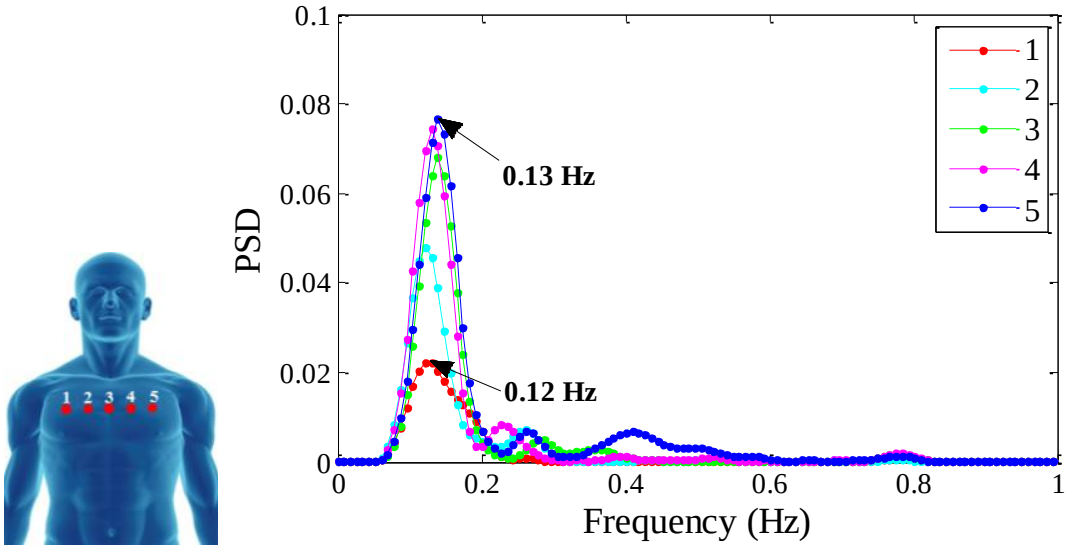

Fig. 5.12.Power spectral response recorded by WSNs for five different positions alongside the trunk section while the test subject is resting (standing on the treadmill machine).

The aforementioned method was also applied to each RSS signal recorded while jogging, rowing and cycling. The spectral response of implemented digital filters is illustrated in Fig. 5.13. The results of a jogging scenario (see Fig. 5.13a) shows a sub-harmonic at 0.14 Hz (lower frequencies), which could be regarded as the thoracic displacement produced by the breathing process (approximately 8.5 breaths/min).

At higher frequencies, two main harmonics are clearly defined: the first at 0.9 Hz and the second at 1.8 Hz. It is known that human locomotion depends on two main factors, stride length and stride frequency, both of which contribute to a jogging activity. The constant speed of 1.38 m/s and the average stride length of 1.5 m give rise to the first harmonic, 0.9 Hz. This is the fundamental component product of the periodic kinematic of the human body which is mainly dominated by the head and the thoracic cavity.

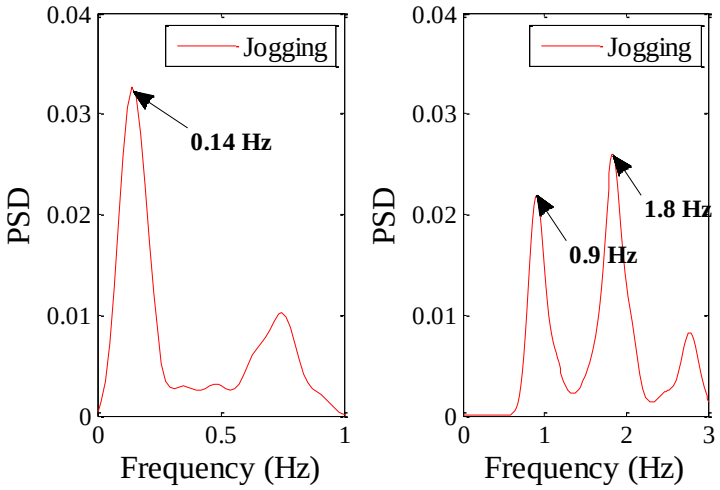

(a)

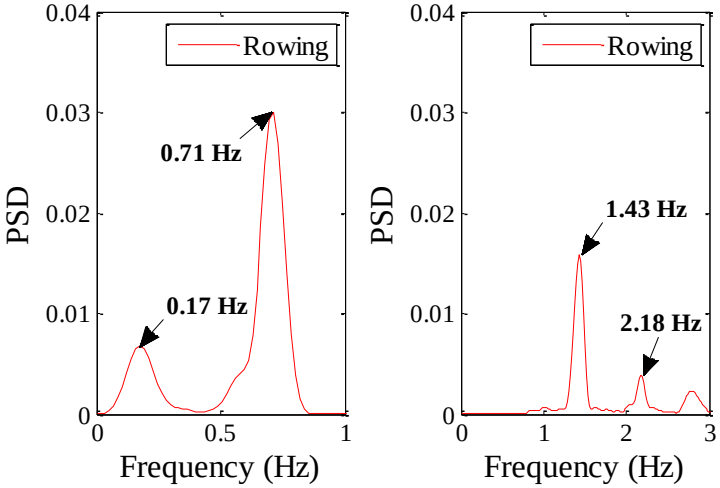

(b)

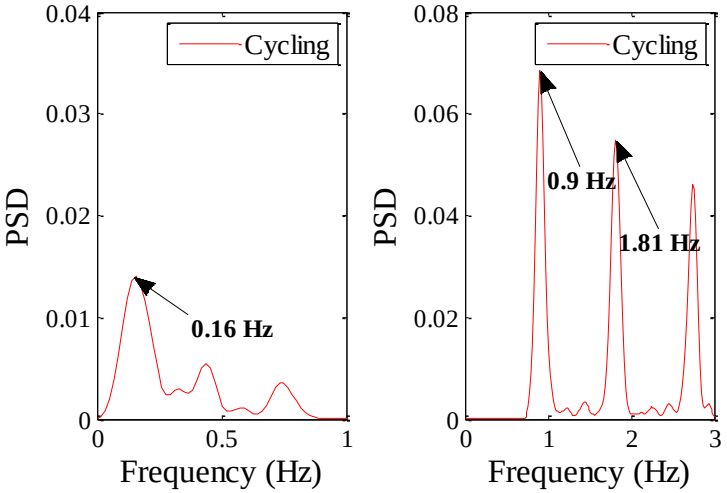

(c)

Fig. 5.13.Power spectral density response using Welch's method for RSS signals while the test subject is (a) jogging; (b) rowing and (c) cycling. All the activities are performed at a constant speed of 5 km/h.

The 1.8 Hz harmonic, which is twice fundamental frequency (0.9 Hz), could also be described by the quasi-synchronous movement of the arms and legs. If we examine the sequence (a)-(b)-(c), depicted in Fig. 5.14, the left-arm and the right-leg go up-front during the initial step succeeded by the right-arm and the left-leg, sequence (d)-(e)-(f), for the following step. The cyclic movement of the extremities, which is repeated during the entire jogging process, shadows the propagation channel, and thus producing a harmonic at 1.8 Hz.

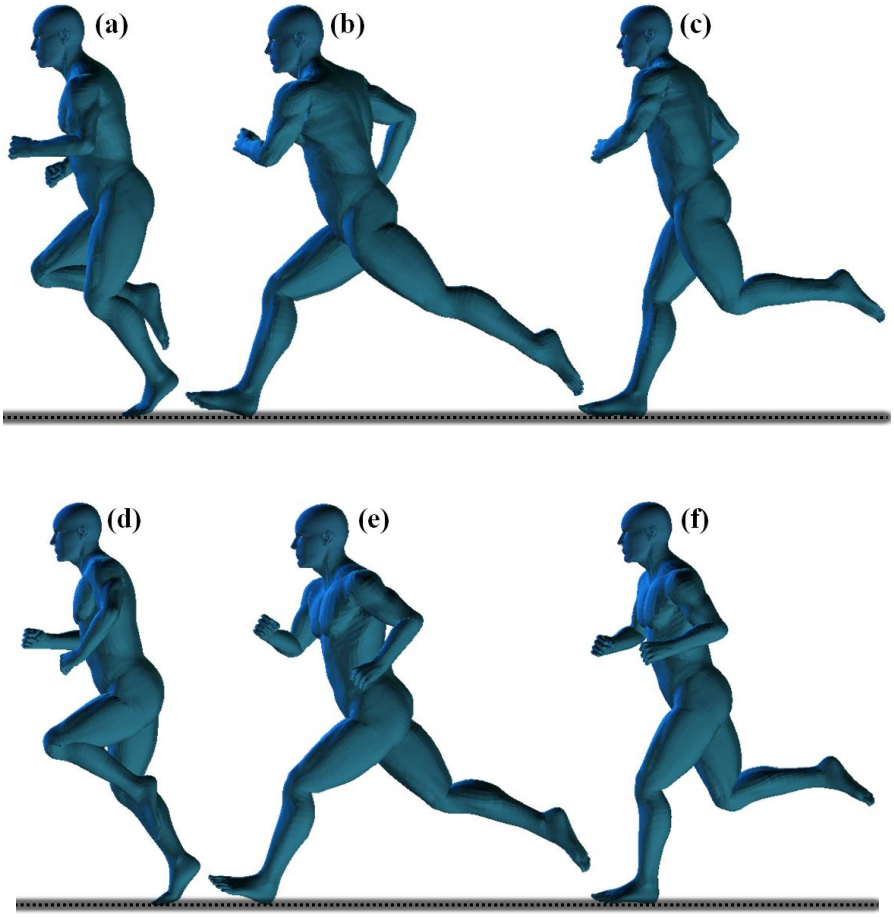

Fig. 5.14.Snapshot sequence of the human body movement during a jogging exercise, modelled in POSER: (a), (b), (c) represent the initial forward step and (d), (e), (f) correspond to the next forward pace.

The frequency domain plot of a rowing activity has two main components at lower frequencies (namely, 0.17 Hz and 0.71 Hz) and two higher harmonics, at 1.43 Hz and 2.18 Hz, respectively (see Fig. 5.13b).

In order to explain the source of each harmonic, it is necessary to unfold the steps of a rowing process. A normal rowing technique is divided into four main phases: the

initial part of a stroke, where the body is pressed up to the legs and shins vertical, thus preparing for the next pull, is regarded as the catch (shown in Fig. 5.15a). The following phase, called the drive (Fig. 5.15b), is initiated when the body's main hip extensors (legs and glutes) push down as the body levers back, but the arms remain straight (transfer of power stage). The next state, where the legs are fully extended and flat, and the rowing handle is located at abdomen position, is defined as the finish position (Fig. 5.15c). The final part of a stroke, called the recovery process (Fig. 5.15d), is a slow slide back to the initial position (actions are in reverse order of the drive phase), thus returning to the catch position (Fig. 5.15e).

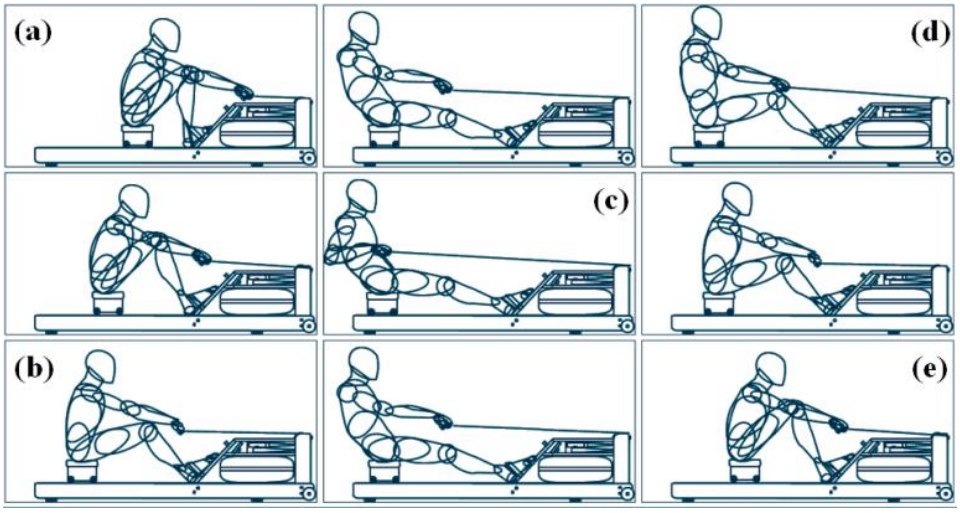

Fig. 5.15.A common sequence during a rowing process: (a) the catch, (b) the drive, (c) the finish, (d) the recovery and (e) the return to catch.

The component at 0.17 Hz is mainly attributed to the thoracic movement produced either by the human motion or the breathing process, which would relate to an average respiration rate of 10.2 breaths/min. During the rowing process, the test subject worked out at a constant speed of 5 km/h, covering an average distance of 1.8 m for each stroke (catch-finish, finish-catch). The continuous levering backward and forward of the body from catch to finish position produces the fundamental component of 0.71 Hz. Similar to a jogging scenario, the 1.43 Hz describes the 2nd harmonic of the fundamental frequency; but, a close examination of the rowing process also shows that, amid each stroke, the rowing handle crosses the transmitter node twice (i.e., shadowing the free-space propagation), the first instance when the

body lays back to the finish stage and the second time when the recovery phase takes place, thus producing a 1.43 Hz component.

The last spectrum plot corresponds to a cycling scenario (see Fig. 5.13c), where main components are observed at 0.16 Hz for the lower frequencies, and 0.9 Hz and 1.81 Hz for the higher frequencies. The cycling process is mainly dominated by the pedalling sequence. Key snapshots of this routine are shown in Fig. 5.16a-c. The movement created by the rotation of the legs around the circumference of the pedal crank is defined by the sprocket-arm (length=0.20 m) and the bike ergometer's speed (5 km/h). The angular movement of the right leg brings about periodic displacements of the transmitter node, which is located on the same side but at waist level, thus defining a cyclic translation of approximately 1.06 Hz and hence an angular speed of 64 rpm. In addition, the link (Tx – Rx) is shadowed twice per cycle, or every π radians, thus defining a frequency of 1.81 Hz.

The motion observed during cycling is mainly dominated by the leg movement, whereas the chest area remains fairly motionless (i.e., leaning forward towards the handle-bar with relaxed arms; see Fig. 5.16Fig. 5.16a-c), in contrast to the other activities. This type of body posture creates a cavity section for the electromagnetic propagation which maximizes the number of waves travelling along the body and hence the 0.16 Hz harmonic is interpreted as a result of the respiration process which would be equivalent to 9.6 breaths/min.

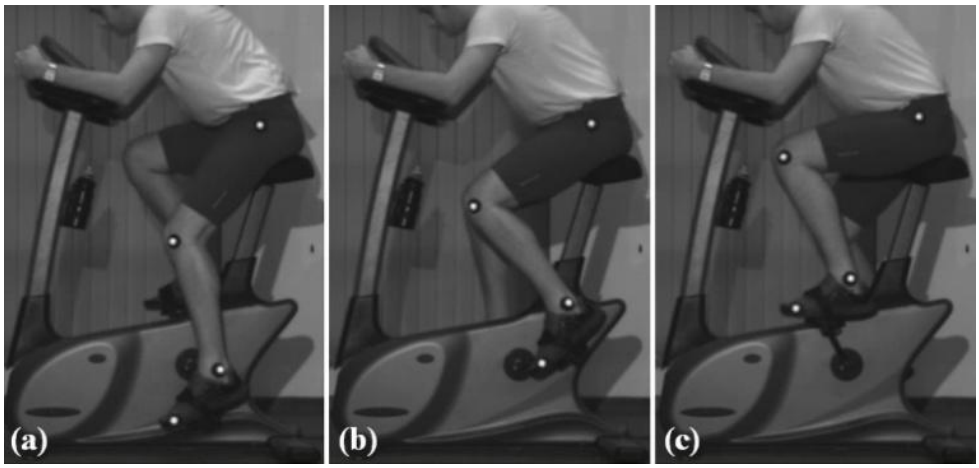

Fig. 5.16.Cycling at a constant speed of 5 km/h, (a)-(c) Snapshots of main movements of the human body while (Images are for illustration purposes only) and (d) normalized spectrum response of the received signal.

The spectral response of recorded ECG signals (resting and jogging scenarios, see Fig. 5.10) are shown in Fig.5.17a-b. In both cases, the noise introduced by the mains was removed using a digital notch filter operating at 50 Hz to 60 Hz.

The resulting plots show a main harmonic at 1.46 Hz (for a resting scenario) which defines a heart rate of 87.6 BPM. By contrast, the ECG from a jogging scenario depicts two main frequency components: the first at 1.04 Hz and the second at 1.71 Hz. The former is mainly attributed to electrode movement due to the constant human motion and the latter may represent the cardiac signal, based on a comparison with the recorded ECG signal; it defines a heart rate of 102.6 BPM.

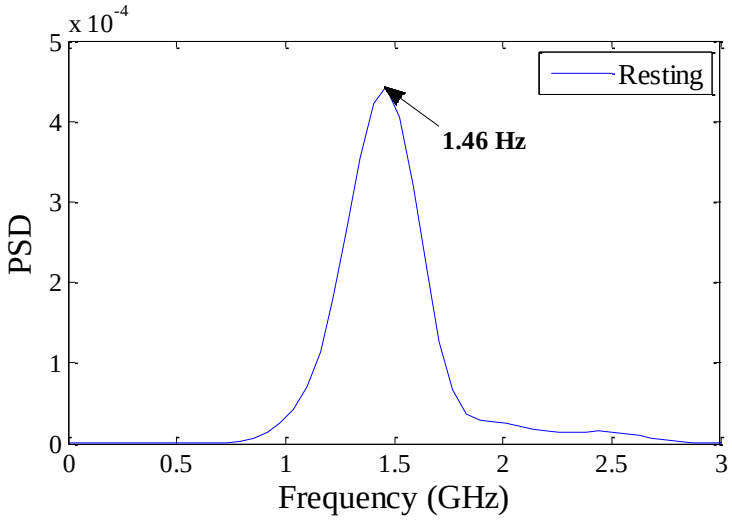

(a)

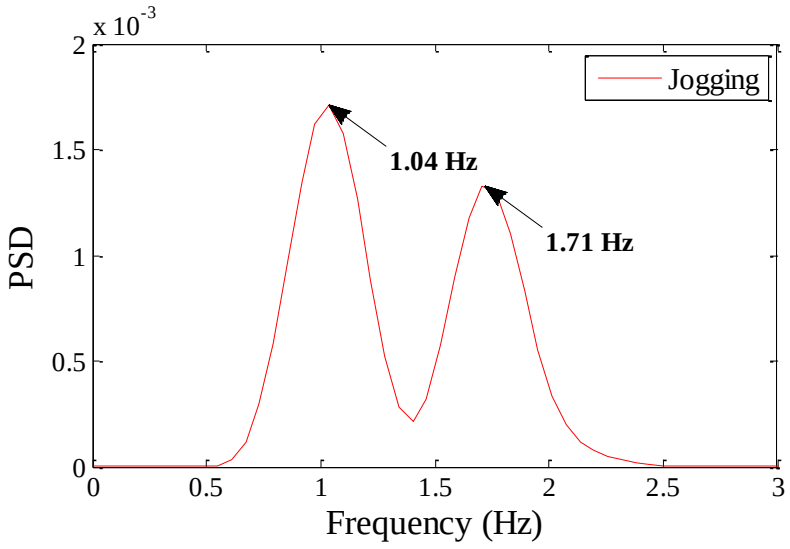

(b)

Fig. 5.17.Power spectral density response using Welch's method for recorded ECG signals while the test subject is (a) standing on the treadmill machine (resting stage); (b) jogging at a constant speed of 5 km/h.

The transformation from time to frequency domain has introduced a HR deviation of 1.77% and 3.4% for resting and jogging scenarios, respectively. This deviation is mainly attributed to the FFT coefficient rounding errors and floating point arithmetic quantization errors.

A summary of the spectral content of each scenario is presented in Table 5-5. The table includes sub-harmonics and main frequencies for each recorded activity, including the spectral components of the electrocardiograph. It can be seen that the 2nd harmonics of jogging and cycling are similar to the main harmonics of the ECG; however, it is difficult to confirm the sensing of the latter. A more rigorous study is required considering important aspects such as different speeds and stride lengths.

It is evident that the spectral content of the electrocardiogram maintains a high level of detail contrary to the spectral plot of the signal recorded by the wireless sensor node. In the case of the ECG, it mainly records electrical variation of the heart over a period of time across the electrodes, whereas the wireless sensor node detects the mechanical movement. Our results have shown that respiration rate could be estimated from the thoracic movement produced over a period of time (see Table 5-5), but not heartbeat.

TABLE 5-5
SUMMARY OF MAIN HARMONICS FOR EACH PERFORMED ACTIVITY AND THE RECORDED ECG

Activity	**Harmonics (Hz)**				
	Low Components (0 Hz - 0.8 Hz)		**High Components (0.8 Hz - 3 Hz)**		**ECG**
	Sub-Harmonics	**1st**	**2nd**	**3rd**	
Resting	0.12-0.13	-	-	-	1.46
Jogging	0.14	-	0.9	1.8	1.71
Rowing	0.17	0.71	1.43	2.18	-
Cycling	0.16	-	0.9	1.81	-

5.4. Discussion and Conclusion

The chapter presented the radio-channel characterisation of different on-body links for assorted body movements. It was first shown that the continuous movement of the human body, trunk and the limbs, for non-stationary scenarios (e.g., jogging exercise) shadows the line-of-sight propagation, thus producing signal fluctuations of ±15 dB (maximum level from the average received signal).

Comparison of the various radio channels considered (which not only include radio propagation characteristics, but also embed biomechanical information, such as the motion pattern and thoracic displacement, for the three activities showed noticeable differences in channel parameters. The fitted statistical distributions for each sport activity showed that dynamic radio channels are best described by Nakagami and Weibull distributions rather than lognormal distributions.

Moreover, the analysis of the spectrum plots, for the waist-to-chest channel, identified distinct frequency components for each recorded exercise. These components are analysed in the context of the activities and physiological signals are observed. Thus, the on-body radio channel provides a model for activity classification and potential physiological feature extraction. The work proposed in this paper may open up a new possibility of non-invasive physiological monitoring based on EM sensing from on-body wireless sensor nodes. One potentially interesting avenue for future research is applying this technique to activities with more complex movements, for instance hurdling or climbing stairs.

Chapter 6

RF Positioning using Body-Centric Low-Power Wireless Sensors

Recent years have seen an increase in the number of wireless communication devices available for a variety of applications, both fixed and mobile. This trend is predicted to continue for the foreseeable future and will result in unprecedented opportunities, as well as considerable challenges [14]. These opportunities are in areas that include some of the more significant fields of our time, including tackling climate change, reducing energy consumption and improving various health and demographic problems [14, 166].

The move towards smart grids, intelligent transportation systems and smart house environments, particularly for assisted living, tele-monitoring and tele-diagnostics, as well as enhanced quality of life, to mention a few areas, is a strong driver in the growth of wireless device usage. The increased availability of such wireless

technologies, including the growth of smart-phone usage, as well as the proliferation of wireless sensor networks (WSNs), offers an opportunity for obtaining valuable localisation information for the efficient provision of services.

In some scenarios, this information is fundamental to the operation of the system; in others, it may be an "optional extra" that provides enhanced quality of service. Body-centric communications has an important role to play in many of the applications discussed above, and it is an additional resource for providing localisation information. For example, in many assisted living and tele-health scenarios, the user will be wearing a device that communicates with an external system, for example a medical alert system where location is critical.

The role of the body in RF positioning systems must, therefore, be understood, particularly in the context of indoor positioning systems. Whilst similar in principle to off-body communications, there are unique characteristics for positioning systems that have yet to be fully analysed in body-centric communications. This chapter discusses the use of WSNs to provide indoor location information, either as their sole function, or as a secondary aspect to their operation.

6.1. Review of Wireless Positioning

There are numerous techniques for determining (and often tracking) the position of a target utilising RF technology. These can cover short distances (a few tens of metres, perhaps with accuracies up to a few millimetres) through to extremely large distances (thousands of miles, although accuracies can still be as high as a metre or even better) [167]. The focus here is on relatively short-range techniques, especially those applicable to indoor applications.

Cellular telephone systems can act as a means of detecting position. First, the network records which base-stations a handset is communicating with; in urban areas, this can give relatively high resolution, as base-stations are more densely clustered, but the resolution in rural areas can be of the order of miles.

Methods to enhance the positioning capability of cellular systems have been proposed, mostly taking advantage of signal timing knowledge; however, indoor positioning is not presently feasible [167].

However, the near-ubiquity of wireless networks (WLANs) in home, office and public places, together with the rise in popularity of smart phones containing WLAN

technology, provides a means of tracking WLAN-enabled assets that can be coupled to cellular technology to obtain near-universal coverage, albeit with differing levels of resolution in position.

The caveat is that WLAN technology is relatively power-hungry, and there is no means of guaranteeing that the WLAN asset being tracked corresponds to the person of interest, in scenarios where that is important [167]. This can include health and assisted-living applications, as well as emergency response scenarios. Despite this, the use of WLAN technology provides a potential pre-built infrastructure for indoor location systems which was shown in [168-171]. In these location systems, a client device measures the RSS from different access points in given positions and uses this information to discover its own location. The estimation process is split into an offline phase (also called location fingerprinting or calibration phase) and an online phase (also called real-time phase). Commercial WLAN-based location and tracking System for indoor environments are RADAR [168] and Ekahau [172].

Another commercially-available tracking system is Ubisense [20], which utilises a form of ultra-wide-band (UWB) technology for extremely accurate positioning by taking advantage of the large bandwidth. These positioning systems transmit ultra-short pulses (typically < 1 ns), with a low duty cycle (typically 1:1000) over multiple bands of frequencies. Ultra-wideband location technologies exploit the characteristics of time-of-arrival techniques and the resilience to multipath propagation within indoor environments [173, 174].

Radio Frequency Identification (RFID) is another technology that offers the potential for tracking objects indoors. There are different types of RFID system, operating at different frequencies. RFID systems can also be classified according to the power source, as active (battery-powered), passive (harvesting energy from the RFID interrogation signal) and semi-passive (battery-powered for all operations apart from communications, which harvests energy as with the passive type). Some popular RFID positioning systems, shown in Fig. 6.1, are SpotON [21] and LANDMARC [175].

Research in [67] has shown that the communication range for an implanted active RFID tag at UHF frequencies (868 MHz) is of the order of 10 m, for a relatively low transmit power of -20 dBm and line-of-sight operation. This used an optimised meandered planar inverted-F antenna (PIFA), with an implanted gain of about -17 dBi at an implant depth of about 7 mm. This corresponds to a subcutaneous implant,

below the skin layer and within the fat layer immediately beneath the skin. A 10 m range is sufficient for indoor positioning and tracking, with a resolution dependent on the number and location of RFID interrogators (also called readers). It can be assumed that a worn RFID tag will have a greater range, as it should experience reduced losses due to the body compared to an implanted tag.

(a) (b)

Fig. 6.1.Commercial RFID tags for indoor location (a) SpotON [21]; (b) LANDMARC [175].

Nonetheless, most of these systems require the target to carry, or wear, a tag that emits RF energy for positioning purposes. Some of these tags are purely used for positioning; other examples may provide positioning as a secondary function, for example an implanted RFID tag may be used for a different primary purpose, such as security, or as a simple wireless sensor for physiological data. In all cases, an understanding of WBANs is required.

6.2. Localization Techniques and Algorithms

In general, location determination comprises two phases, distance estimation, which is commonly referred to as ranging, and position calculation. Distance estimation can be based on different measured parameters such as angle of arrival (AoA, where the direction of incidence, is obtained by the use of directionally sensitive antennas), received signal strength (RSS) and time of arrival (ToA, the absolute travel time of a signal from a transmitter to a receiver is computed which relies on a precise synchronization of transmitter and receiver clocks). Fig. 6.2 shows a basic functional block diagram of wireless positioning system.

Positioning systems using all location metric parameters (e.g., ToA, AoA, RSS) offer high target location accuracy; however, the solution implies having high costs.

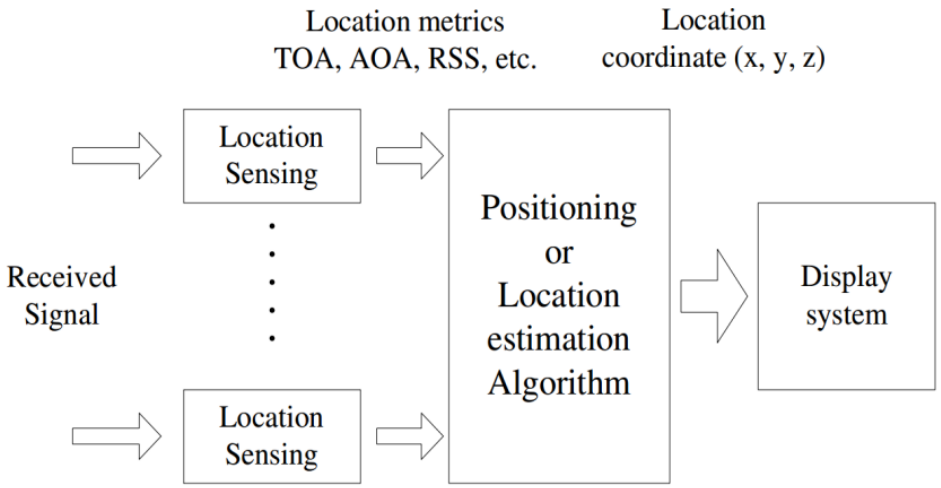

Fig. 6.2.A functional block diagram of positioning system using some location metric parameters which include Time of Arrival (ToA), Angle of Arrival (AoA), RSS for indoor location estimation.

In order to reduce costs, positioning and tracking literature describes different solutions to estimate an object's location, and some of the popular solutions are summarised below [21, 167]:

– Geometry-based techniques (see Fig. 6.3) compute the position from estimated angles or distances using algebraic relationships [176]. The distance estimation can be based on RSS, ToA or AoA of reference signals exchanged between the element to be located and some reference nodes. The most common techniques are triangulation [21] and trilateration[177]; however, other advanced approaches, such as least square minimization [178] and multidimensional scaling [174] are also implemented ;

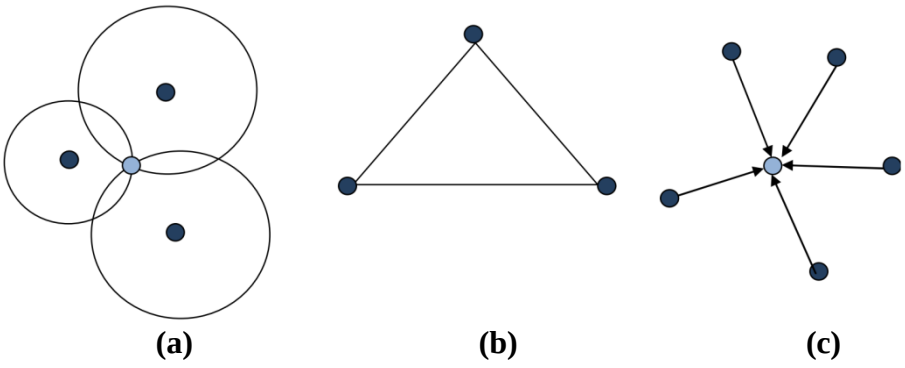

Fig. 6.3.Popular Localization techniques used for tracking and positioning systems (a) trilateration; (b) triangulation; (c) Maximum Likelihood Estimation

- Fingerprint methods rely on a set of location dependent characteristics (e.g., ToA, RSS) available in the radio access database. The number of measured parameters by known access points must be high enough to allow for a unique correspondence with a given location. These parameters must have low variability in time at any given position and they are location dependant; therefore, each RF fingerprint is associated with a specific location. Support vector machine and neural networks are well known database training techniques for fingerprinting-based positioning algorithms [179];
- Bayesian techniques probabilistically estimates the position from past and present measurements using ToA, AoA and statistical models [180] (e.g., particle filters, Kalman filters).

Localization techniques employing ToA and AoA as location-detection signal parameters present some drawbacks within indoor environments. The radio propagation in such environments would suffer from multipath effect, thus a LOS channel between the transmitter and the receiver may be difficult to find. The time and angle of an arrival signals would be affected by the multipath effect; thus, the accuracy of estimated location could be decreased. An alternative approach is to use an RSS-based method which attempt to calculate the effective signal path loss due to propagation. Theoretical and empirical models are used to translate the difference between the transmitted signal strength and the received signal into a range estimate for the object's positioning as shown in Fig. 6.4. The following section aims to investigate and explore the capability of a positioning system based on RSS recordings (i.e. RSS-based indoor location) by low-power wireless sensors using the IEEE 802.15.4 communication standard.

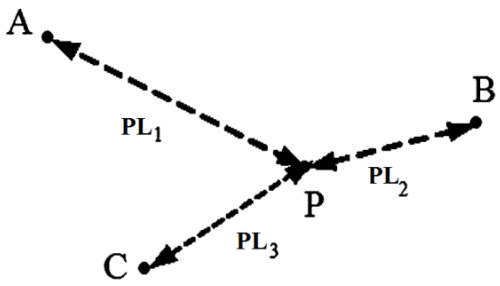

Fig. 6.4.Theoretical and empirical model used to translate the difference between the transmitted signal strength and the received signal into a range estimate for the object's positioning. The positioning is based on RSS, where PL1, PL2, and PL3 denote the measured path loss.

6.3. RSS-based indoor location using low-power wireless sensors

Most on-body research has probably been conducted at narrowband ISM bands which are typically used by communication standards such as Bluetooth and ZigBee. The studies frequently include antenna performance and channel propagation characteristics. In this chapter, most of the experiments are performed using the IEEE 802.15.4 communication standard at 2.45 GHz. The concept behind the empirical study is to use the RSS parameter as means of determining path loss estimation (using a fixed transmit power), which would change according to the distance separation between fixed and body-worn nodes.

The experiment was divided in two scenarios:

- the first scenario made use of custom-built body-worn nodes described in Chapter 3, which can potentially be used to provide positioning information, as a secondary function;
- the second experiment used commercial wireless modules, the TelosB (see Fig. 6.7a). This experiment was sub-divided in two additional scenarios: (a) empty indoor environment and (b) occupied environment in which a person is standing in the middle of the room.

Both experiments were performed in order to determine the expected path loss, multipath components and body-shadowing effects in an indoor environment. The results assess the performance of generic low-power WBAN wireless nodes for RF positioning systems.

6.3.1. First Experiment - Feasibility study using custom-built wireless sensors

This experiment was performed using three fixed nodes which were wall mounted nodes and one body-worn node. The nodes were designed and fabricated in-house, rather than commercially-obtained. Each module used the same Texas Instruments CC2420 transceiver [101]. The transceivers are programmed and controlled by an ultra-low-power microcontroller, the PIC18F2620 [102] (see Chapter 3). The custom-built low power wireless sensor node is shown in Fig. 6.5a. Each wall mounted node recorded the RSSI value from a transmitting node that was placed on-body (the data was transmitted at 14 ms per sample). The data was stored in the internal memory of each wall mounted sensor for a later retrieval and processing.

The nodes used channel 4 of the IEEE 802.15.4 communication standard, with a centre-frequency of 2.42 GHz. A simplified representation of the indoor layout is shown in Fig. 6.5b. Additional information is given in Table 6-1.

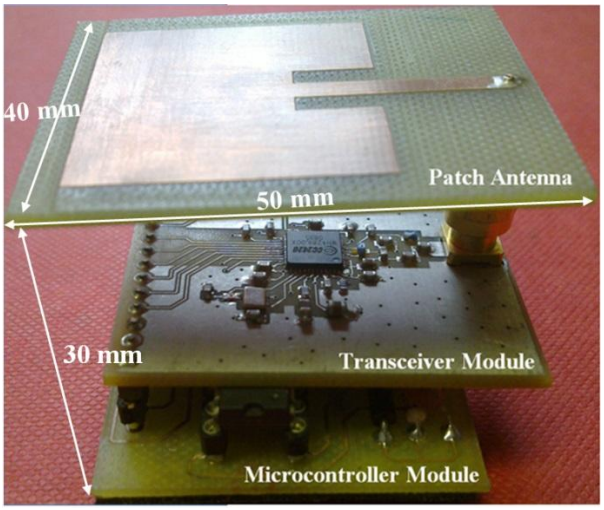

(a)

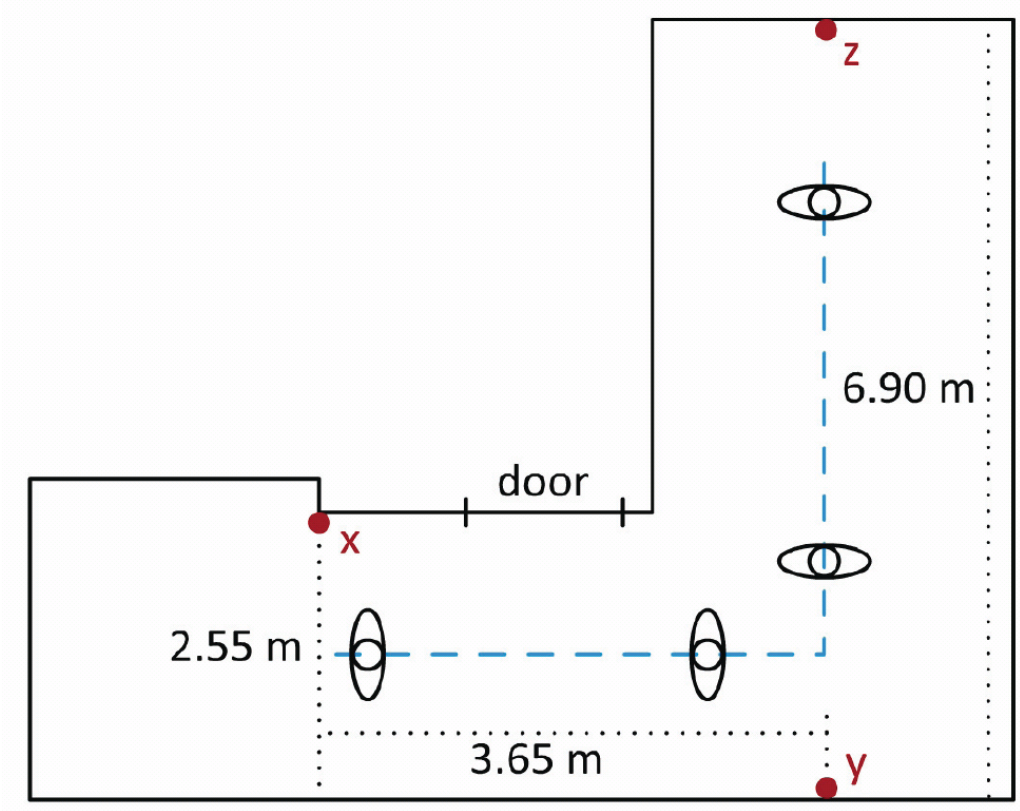

(b)

Fig. 6.5. (a) Implemented wireless nodes using a microstrip patch antenna; (b) simplified floor-plan of the Body-Centric Lab, with node positions and separations shown. Note the assumed orientations of the body along the path.

TABLE 6-1
SUMMARY OF INFORMATION FOR THE FIRST EXPERIMENT (FEASIBILITY STUDY)

Property	Nodes			
	x	**y**	**z**	**On-Body**
Height from the floor (m)	1.25	1.15	1.15	1.21
Radiating Element	Patch	Patch	Printed IFA	Patch
Gain (dBi)	2.13	2.13	1.1	2.15
S_{11} (dB)	16.9	-16.8	-15	-17.3
Transmit Power (dBm)	N/A	N/A	N/A	-3.02
Rx Sensitivity (dB)	-95	-95	-95	N/A

The test subject followed an L-shaped path (dashed blue line in Fig. 6.5b), beginning near *x* and walking straight ahead, towards the end of the room containing *y* and *z*, before turning left when adjacent to *y*, and approximately 1.27 m away from it. The subject then walked until approximately 1 m from *z*, before turning and retracing the route. The walking process was repeated three times. The smoothed RSS in dBm for each communication link (on-body node to fixed node) is depicted in Fig. 6.6, where a moving-average filter was used with a window size of 50 samples.

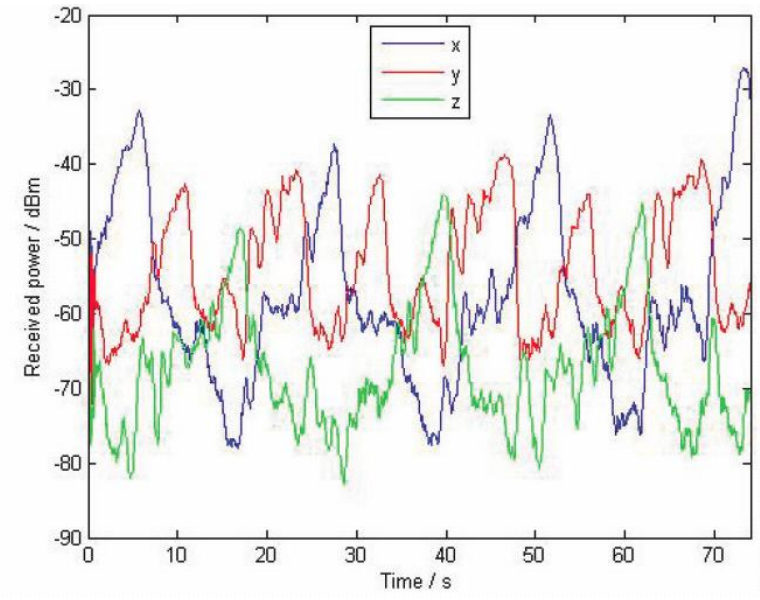

Fig. 6.6 Smoothed received power in dBm for each node: x in blue; y in red; z in green. Sampling period was 14 ms; window-size for moving average filter was 50 samples.

To evaluate the potential of this approach in determining the range to the user, equation (6.1) was solved for the position at the "corner" of the path (i.e., closest to

y), as this allowed line-of-sight between all three fixed nodes and the user. The terms P_r and P_t represent the received and transmit power, G_t and G_r are transmit and receive antenna gains, all are in decibels, and γ is the unknown path loss exponent.

$$R=\frac{\lambda}{4\pi 10^{(P_r-G_t-G_r-P_t)/10\gamma}} \tag{6.1}$$

This was done by identifying the samples where the received power at *y* was at its maximum and assuming this was equivalent to the corner position. The received powers for all three fixed nodes were then used to solve for the unknown γ values, for the known distances to the corner of the path. The mean of the path loss exponent (γ) was then found for each link and used to estimate the position of the user, given the same received powers, using (6.1). Selected results are summarised in Table 6-2.

TABLE 6-2
SUMMARY OF CALCULATED PATH-LOSS EXPONENTS AND ESTIMATED POSITIONS
(NOTE: NEGATIVE ERRORS INDICATE UNDER-ESTIMATES; POSITIVE ERRORS INDICATE OVER-ESTIMATES.)

Parameter	**Nodes**		
	x	**y**	**z**
Sample 1 - Path loss exponent (γ)	2.52	2.07	2.50
Sample 2 - Path loss exponent (γ)	2.39	2.02	2.76
Sample 3 - Path loss exponent (γ)	2.29	1.90	2.76
Mean path loss exponent $(\bar{\gamma})$ for all six samples	2.44	2.01	2.65
Parameter	**Distance (m)**		
	x	**y**	**z**
Known separation / m	3.87	1.28	5.63
Sample 1 - Estimated separation using $(\bar{\gamma})$	4.72	1.50	3.92
Sample 2 - Estimated separation using $(\bar{\gamma})$	3.46	1.32	7.34
Sample 3 - Estimated separation using $(\bar{\gamma})$	2.64	0.98	7.46
Parameter	**Error (%)**		
	x	**y**	**z**
Sample 1	22.1	17.7	-30.2
Sample 2	-10.6	3.3	30.6
Sample 3	-31.6	-23.6	32.6

It was observed that the error in estimated position varies between around 3% and 60%, for this first experiment. The real position is always within the error bounds, however, sources of error include the antenna positions (in particular, the variation in gain due to off-bore-sight operation and the differences in height has not been accounted for), as well as fading due to multi-path scattering and body shadowing. Obviously, this must be examined more systematically and rigorously before any firm conclusions may be drawn. The effect of multi-path scattering from the environment, as well as shadowing from the body, must be taken explicitly into account. Separating these two effects will aid in the design of such systems.

6.3.2. Second Experiment using Commercial Wireless Modules TelosB

Commercial wireless sensor nodes, the TelosB [96], were used. The nodes are based around a low-power microcontroller and an IEEE-802.15.4-compatible radio transceiver, the CC2420 [101]. The board module integrates a printed IFA (PIFA), but the design allows an alternative antenna to be connected externally by attaching an SMA connector. The device can be powered by two AA-batteries or via USB. The wireless module is shown in Fig. 6.7a, together with a simplified CST Microwave Studio model of the wireless sensor node (Fig. 6.7b). The 3D antenna radiation pattern at 2.4GHz is shown in Fig. 6.8. The patterns show a peak gain of 3.1 dBi at 2.42 GHz (elevation plane) with significant variation in gain with respect to angle. The azimuthal plane presents a fragmented radiation pattern which may be due to the battery socket.

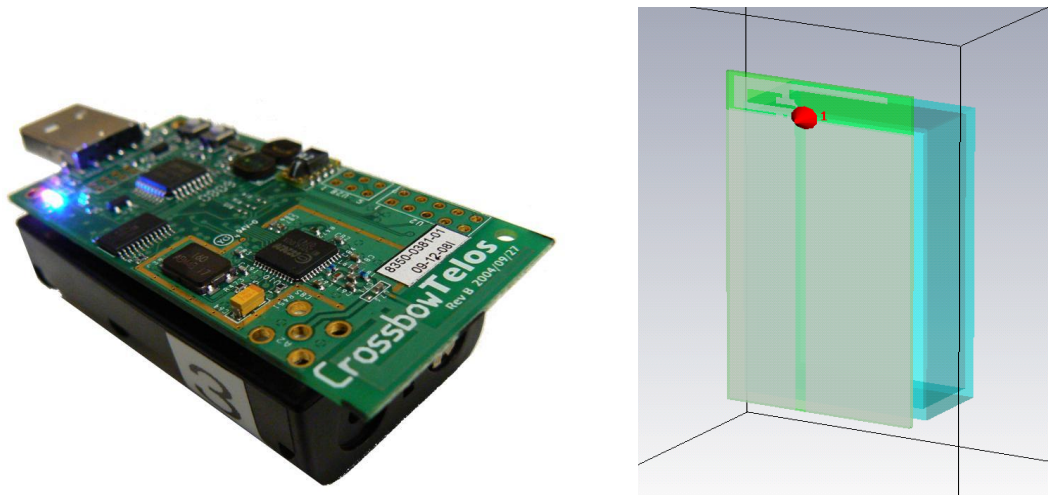

(a) (b)

Fig. 6.7 (a) The Telos B sensor board, with integrated printed IFA, battery-pack, USB connector, and temperature and humidity sensors [96]; (b) simplified CST model of the TelosB wireless sensor.

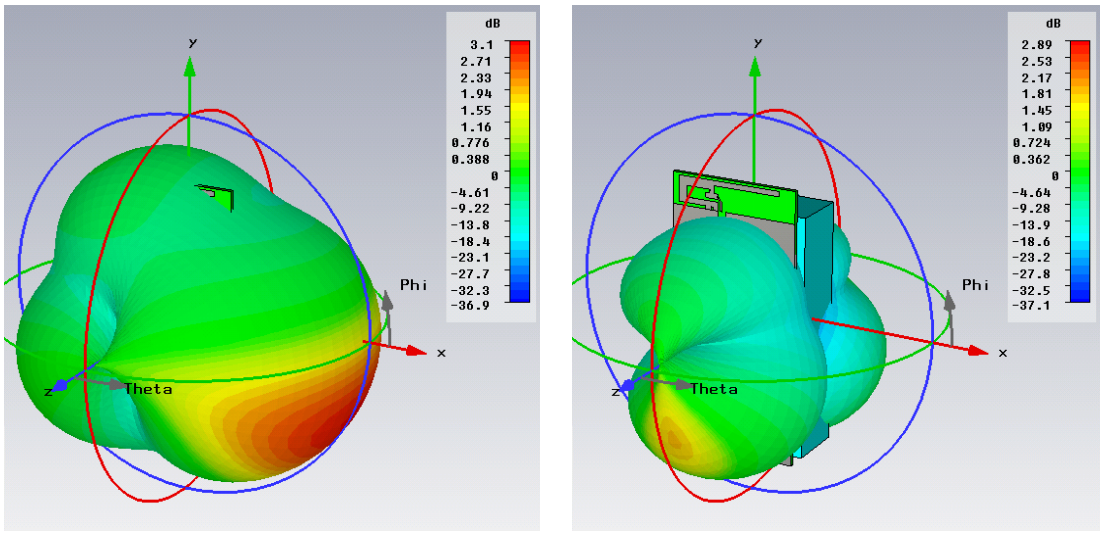

(a) (b)

Fig. 6.8. Free-space radiation patterns from CST Microwave Studio: (a) Gθ plane and (b) Gφ plane.

Simulated results give an initial overview of the radiation performance of the integrated antenna. These factors must be considered in the analysis and post-processing of the recorded radio channels.

A representation of the experimental area is shown in Fig. 6.9. The latter was defined in the Body-Centric Laboratory at QMUL. Blue circles denote wireless nodes used as RF position and tracking sensors; the yellow circle denotes the master wireless node, used to control the experiment and collect the data. The dashed black line denotes a temporary partition, used to make a square cross-sectional area.

The nodes run custom programs written for the experiment, based around the TinyOS embedded operating system [96, 181]. Each fixed and mobile node listened to the transmissions from the other nodes and recorded the RSS value for that packet. When it was allocated a transmission slot, a given node broadcasted a custom packet containing the most recent RSSI values for all other nodes, together with the associated node ID. The master node (see Fig. 6.9) was connected to a PC and listened to all packets transmitted by the fixed and mobile nodes, allowing RSS data to be recorded in real time. The characteristics of the experimental setup are:

- Fixed node position – 16 nodes wall mounted;
- Body-worn devices – 4 wearable nodes;
- Frequency channel – channel 4 in the IEEE 802.15.4 communication standard for 2.45 GHz;
- Transmit power – 0 dBm (i.e., maximum transmit level);

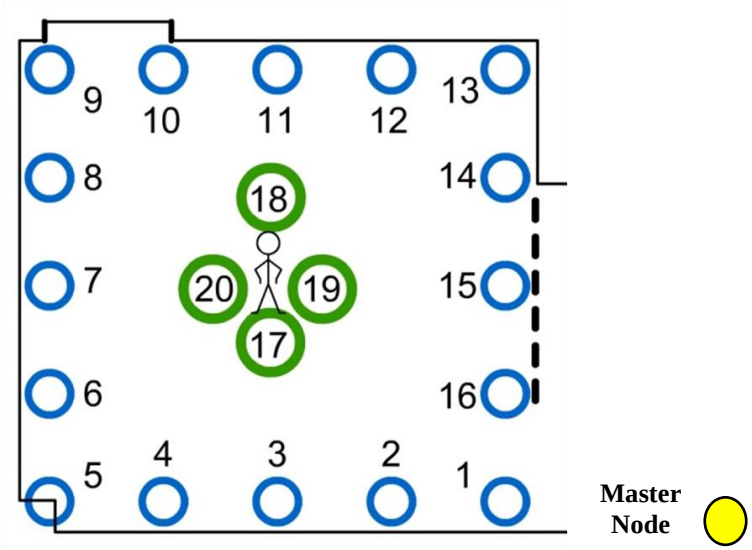

(a)

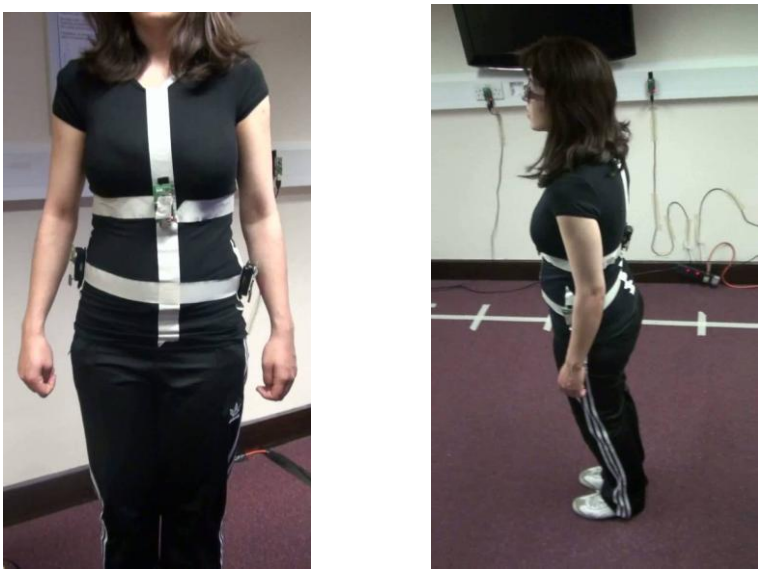

(b)

Fig. 6.9. Second experiment setup based on commercial wireless sensor nodes, TelosB. (a) Experimental arrangement: the blue circles denote the positions of the fixed wireless sensor nodes; the green circles denote the positions of the on-body nodes; (b) wireless sensor nodes on the test subject

- Receiver sensitivity – -95 dBm (i.e., maximum sensitivity level);
- Antenna type – integrated Printed IFA (i.e., PIFA);
- Distance from the floor (fixed nodes) – 112 cm to the centre of the TelosB board;
- Floor-to-ceiling height – 330.5 cm;
- Length and width of the experimental area – L=300 cm; W=332 cm.

The initial experiment involved the test subject standing in the centre of the monitored zone. Representative time-series plots of the recorded RSS are shown in

Fig. 6.10 where the effects of the human body are explicit. The LoS *node 2* is essentially unaffected, but the obscured *node 10* shows greater variation (i.e., ±5 dB from the average received signal) and lower mean received power. Off-body radio links (i.e., body-to-wall and wall-to-body channels) are measured with the aim to inspect the relative received signal and the effects of multipath on the communication channel to each sensor node. The mean path loss for each off-body link is shown in Fig. 6.11, for both transmit and receive scenarios, taking *nodes 17, 18 and 19* as the reference. The variation in mean path loss (see Fig. 6.11a and Fig. 6.11b) is related to the separation between nodes, but also includes multipath effects and body shadowing.

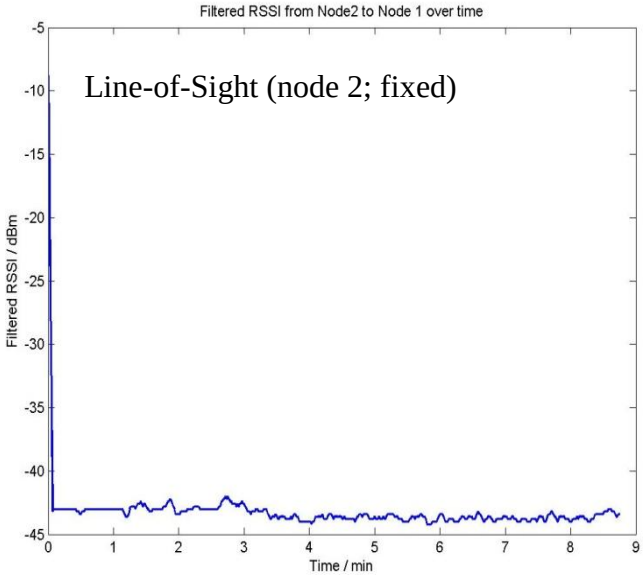

(a)

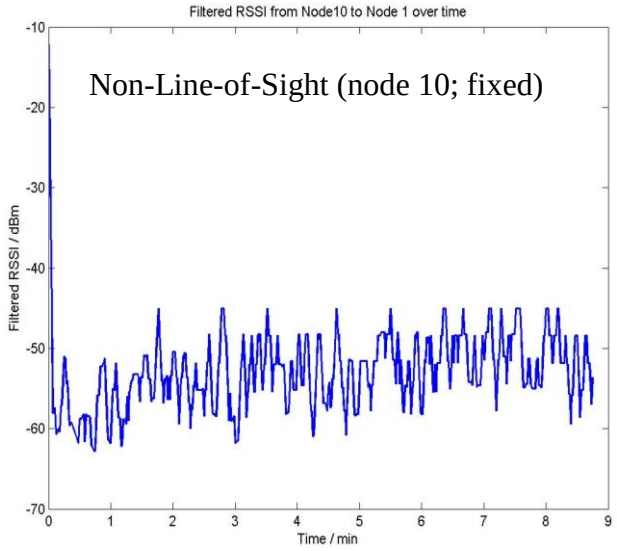

(b)

Fig. 6.10.Representative RSS time-series plots (a) node 1-to- node 2; (b) node 1-to-node 10

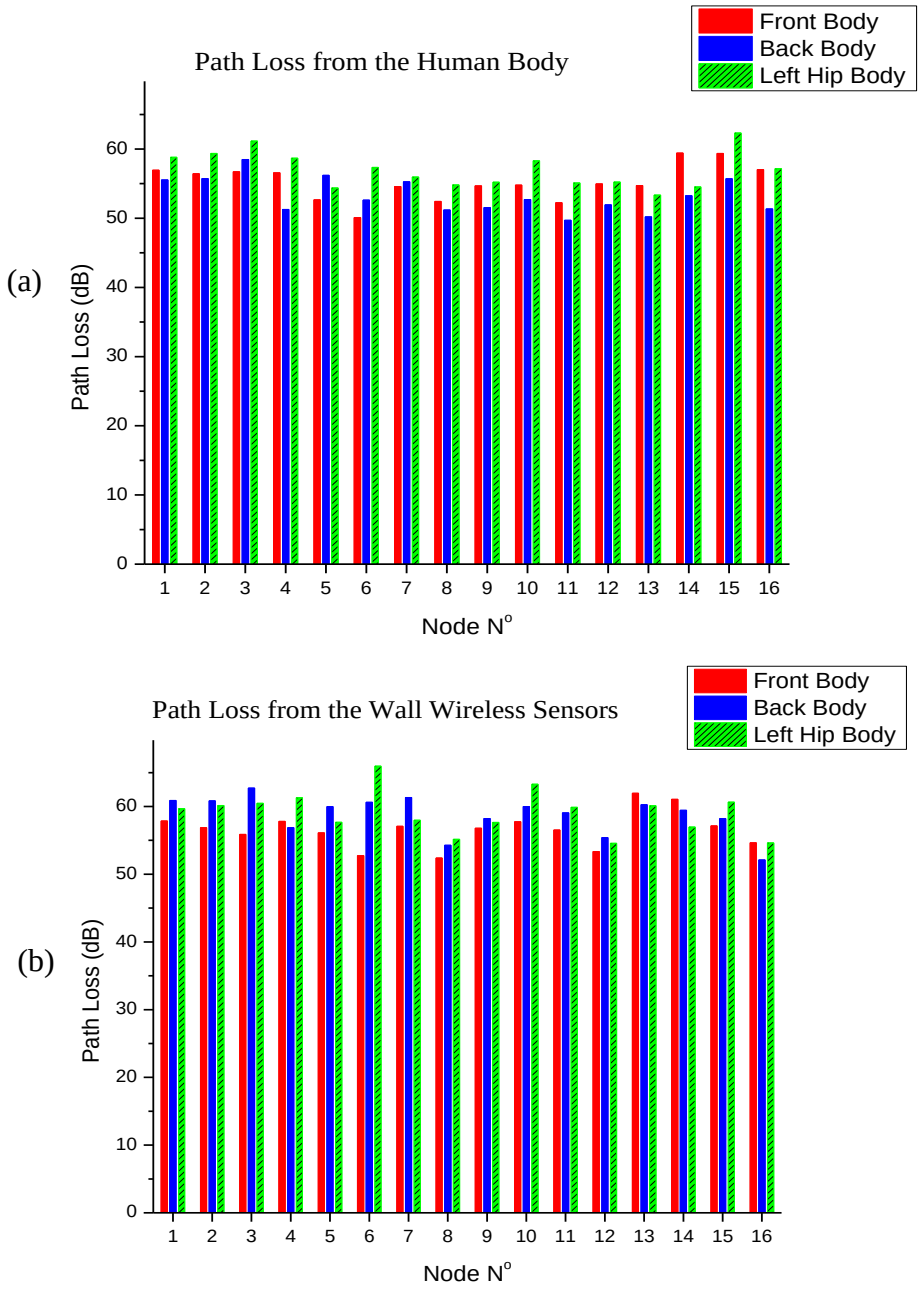

Fig. 6.11.Mean Path Loss values for off-body links in transmit and receive modes. (a) Path loss from the human body, (b) path loss from the wall mounted wireless sensors.

The mean path-loss values also show that wireless nodes located on-body have different radiation performance when compared to wall mounted sensor nodes (i.e., fixed nodes). This effect is more evident on the sensor nodes located in the back and the left hip of the test subject. However, the radio channel performance of the module located in front of the test subject presented a similar behaviour in both scenarios (i.e., transmit and receive modes). The results showed that the wave propagation, namely free space and surface waves, is heavily affected by the surrounding media (i.e. human body and wall surfaces). Additionally, the strong

multipath propagation mechanisms including diffraction, refraction, reflection and scattering, and the radiation properties of the integrated antenna, which present variation in gain with respect to angle, mitigate the performance of different WBAN radio channels.

Although previous results highlighted the effects of the human presence in indoor environments, they only show vague information of the subject positioning. In order to have qualitative results, it is important to characterise and understand the behaviour of the radio propagation when the indoor section to be monitored is without human presence (empty scenario), so that variations of the received signal can be compared to populated environments. A statistical analysis of individual radio channels (when a given sensor node is in transmitting mode) can point out which other sensor node(s) are greatly affected by the human presence.

The mean path loss and standard deviation for a receiving and a transmitting mode of *node 1* is listed in Table 6-3 and Table 6-4. The tables include experimental data for both scenarios empty and occupied environments. Differences are observed on both operating modes (i.e. transmit and receive modes). The largest variations, for an empty scenario, are accounted for *nodes 4*, *8* and *15* with $\sigma = 3.92$, $\sigma = 2.8$ and $\sigma = 2.5$, correspondingly. Significant differences are also accounted for when both scenarios are compared. For instance, in Table 6-3, where *node 1* is programmed in receiving node, the transmitting *nodes 9* and *15* have standard deviations of $\sigma = 2.96$ and $\sigma = 2.69$, respectively; whereas in Table 6-4, where *node 1* is programmed in transmitting node, the receiving *nodes 4*, *13* and *15* have the largest received signal variations with $\sigma = 3$, $\sigma = 3.06$ and $\sigma = 3.92$, respectively.

However, the listed results also show some ambiguity on mean path loss (PL) values. For example: in Table 6-4 (column for empty room), *node 3* has a PL=58.54 and *node 4* has a PL=56.54 dB; however, *node 3* is closer in distance than *node 4* to the transmitting *node 1*. Similarly, Table 6-3 (column for empty room) show that *node 9* (PL=57.85 dB) has reduced power loss than *node 10* (PL=60.02 dB) even though node 9 has longer distance than *node 10* to the transmitting *node 1*. These observed variations are a consequence of the reflected EM waves, within the indoor test-room, which create constructive and destructive signals which arrive to the receiving node from various paths.

Although Table 6-3 and Table 6-4 give an initial knowledge of the indoor radio propagation, the behaviour of other radio-links (other transmitting nodes) ought to

contribute additional information of the overall EM propagation. Path loss plots for an empty and occupied environment when *nodes 3*, *7*, *11* and *15* are operating as transmitting nodes are shown in Fig. 6.12 and the received signal variation for each receiving node is depicted in Fig. 6.13.

TABLE 6-3
MEAN PATH LOSS AND STANDARD DEVIATION FOR NODE 1 WHEN IT IS OPERATING IN A RECEIVING MODE

Transmitting Nodes	**Mean Path Loss (dB)**		**Standard Deviation (σ)**
	Occupied	**Empty**	**Node 1 (Receiving mode)**
2	42.22	40.85	0.97
3	59.28	56.69	1.83
4	57.83	56.13	1.21
5	57.66	58.89	0.87
6	56.57	55.93	0.46
7	55.98	56.46	0.34
8	53.47	51.67	1.27
9	62.03	57.85	2.96
10	57.91	60.02	1.49
11	54.54	55.10	0.40
12	56.13	56.30	0.12
13	62.81	63.91	0.78
14	65.51	63.09	1.71
15	59.74	55.94	2.69
16	48.17	49.14	0.69

TABLE 6-4
MEAN PATH LOSS AND STANDARD DEVIATION FOR NODE 1 WHEN IT IS OPERATING IN A TRANSMITTING MODE

Receiving Nodes	**Mean Path Loss (dB)**		**Standard Deviation (σ)**
	Occupied	**Empty**	**Node 1 (Transmitting mode)**
2	42.26	40.44	1.28
3	60.14	58.54	1.13
4	52.29	56.54	3.00
5	60.44	63.53	2.18
6	56.46	55.78	0.48
7	56.67	57.23	0.39
8	49.51	52.80	2.33
9	62.72	59.87	2.02
10	60.02	64.08	2.87
11	53.07	53.54	0.33
12	58.38	56.70	1.19
13	63.09	67.41	3.06
14	63.72	61.80	1.36
15	61.95	56.40	3.92
16	51.76	51.07	0.49

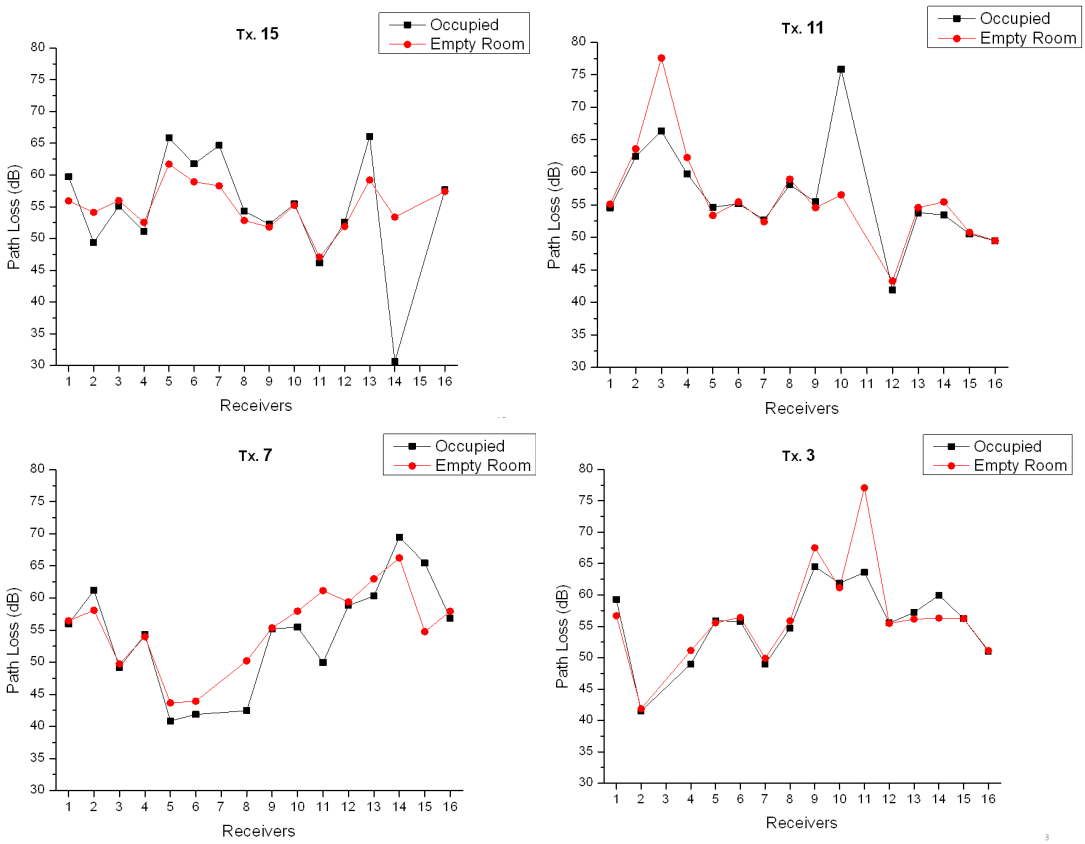

Fig. 6.12.Path loss comparison plots for an empty and occupied environment while sensor nodes 3, 7, 11 and 15 are transmitting.

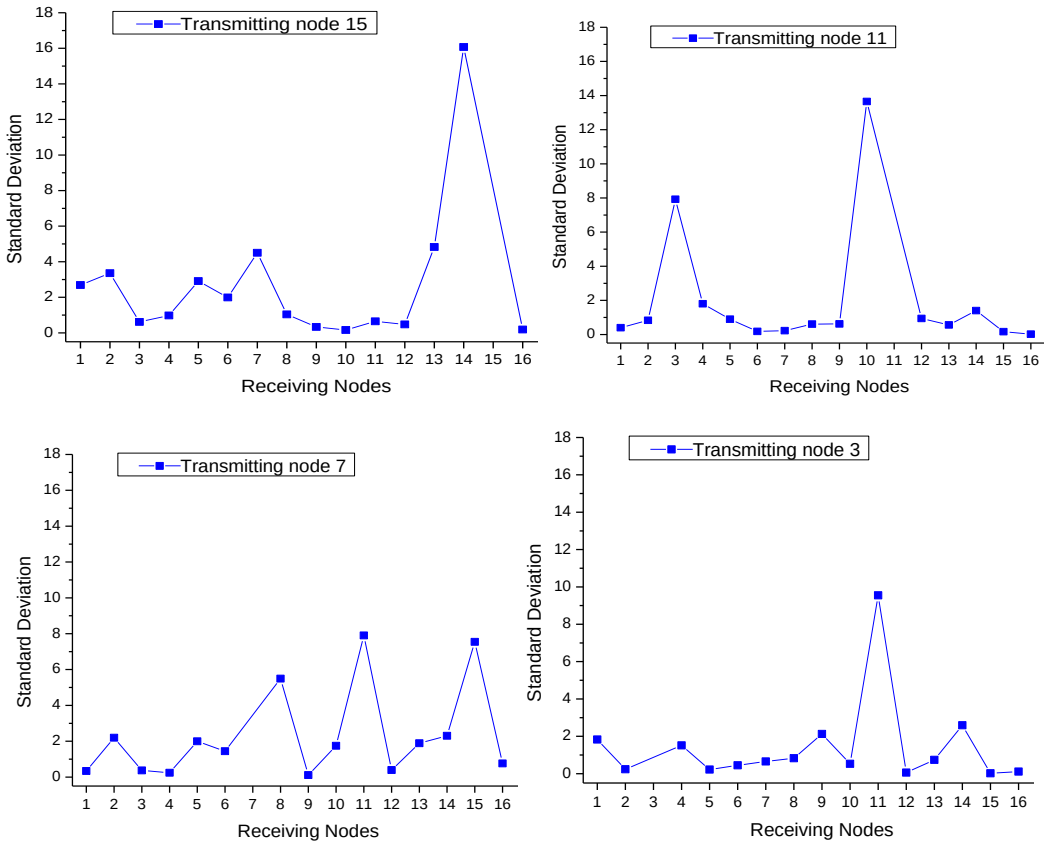

Fig. 6.13.Standard deviation for transmitting nodes 3, 7 11 and 15 (the remaining nodes are operating as receivers).

The graphs show low received signal variation for receiving *nodes 1-7* ($\sigma \ll 3$) and high variations for *nodes 10*, *11* and *14* with σ = 9.87, σ =14 and σ=16.2, respectively. These results, together with previous suggest that an obstructing object, in this case the presence of a human subject, is expected within the local area.

A more descriptive distribution of the path loss alongside the experimental area can be found by combining the Friss equation (Chapter 2) with indoor radio propagation models. Therefore, distances within the vicinity can be estimated using the prior knowledge of the received signal alongside the perimeter (i.e., trilateration concept using RSS values). Trilateration requires the coordinates of at least three reference nodes (x_i, y_i) and the distances between pre-positioned reference nodes (neighbour nodes). The distance between measured and estimated distances is defined by (6.2) where d_i is the distance between sensor node i and the target. Depending on the number of nodes equation (6.2) can be expanded to (6.3) where the term α represents the weight applied to each f_i. The target's position (x_0, y_0) is estimated using minimum mean square error (MSE) of a system of f_i equations (6.3).

$$f_i(x_0,y_0)=d_i-\sqrt{(x_i-x_0)^2+(y_i-y_0)^2} \tag{6.2}$$

$$F(x_0,y_0)=\sum_{i=1}^{N}\alpha_i^2(f_i)^2 \tag{6.3}$$

Moreover, the system of equations can be linearized so that a matrix solution can together with path loss and empirical indoor propagation models (e.g., path loss exponents derived from individual sensors) can be used to estimate the relative position of an object. In order to put in practice the concept, let's consider *node 1* as:

- the reference point defined at position x = 0 and y = 0, and
- the unique wireless sensor that is the source of radio signals.

A matrix map of the different distances between *node 1* and the neighbour nodes is shown in Fig. 6.14 (all the distances are represented in centimetres). The highlighted region (Fig. 6.14b and Fig. 6.14c) is the area that would require distance interpolation which can easily be found using geometry based calculations based on the outer distance values. The interpolated distance matrix (see Fig. 7.14c) yields estimated distance positions which could be described as empirical test points in the overall RF positioning system.

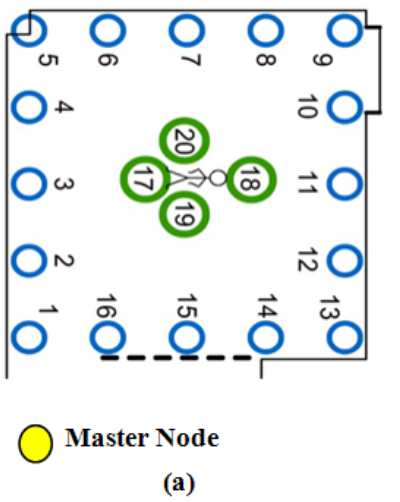

(b)

291.50	320.00	351.00	396.00	447.50
228.50	**0**	**0**	**0**	420.00
148.50	**0**	**0**	**0**	371.00
68.50	**0**	**0**	**0**	344.00
0	90.00	170.00	250.50	330.00

(c)

291.50	320.00	351.00	396.00	447.50
228.50	**245.59**	**284.80**	**339.06**	420.00
148.50	**173.64**	**225.73**	**291.21**	371.00
68.50	**113.10**	**183.28**	**259.70**	344.00
0	90.00	170.00	250.50	330.00

Fig. 6.14.Representation of (a) monitoring area layout; (b) distance matrix between neighbour nodes in cm and (c) interpolated distances.

Initial calculations takes initial path loss exponent (γ) and reference path loss ($PL_{(d0)dB}$) from indoor radio propagation literature [182-184] which yields $\gamma = 3$ and $PL_{(d_0)dB} = 40$. The estimated path loss within the highlighted area can be pre-computed using as a reference the mean path loss values listed in Table 6-4.

The estimated path loss values are depicted in Fig. 6.15 and a colour map plot, shown in Fig. 6.16, is computed for an empty and occupied environment. The initial results show the difference between both scenarios. It can be seen that an occupied scenario is perturbed by the human body presence (subject standing in the centre of the monitoring area) which not only shadows some of the communications links, but also creates additional multipath signals that mitigates some of the radio channels.

63.53	55.78	57.23	52.80	59.87
56.54	60.74	62.67	64.94	64.08
58.54	56.22	59.64	62.96	53.54
40.44	50.64	56.92	61.46	56.70
0.00	51.07	56.40	61.80	67.41

(a)

60.44	56.46	56.67	49.51	62.72
52.29	64.04	61.17	60.40	60.02
60.14	58.42	59.64	62.11	53.07
42.26	52.84	56.92	63.76	58.38
0.00	51.76	61.95	63.72	63.09

(b)

Fig. 6.15.Estimated path loss values acquired from pre-calculated distances (a) empty room and (b) occupied room.

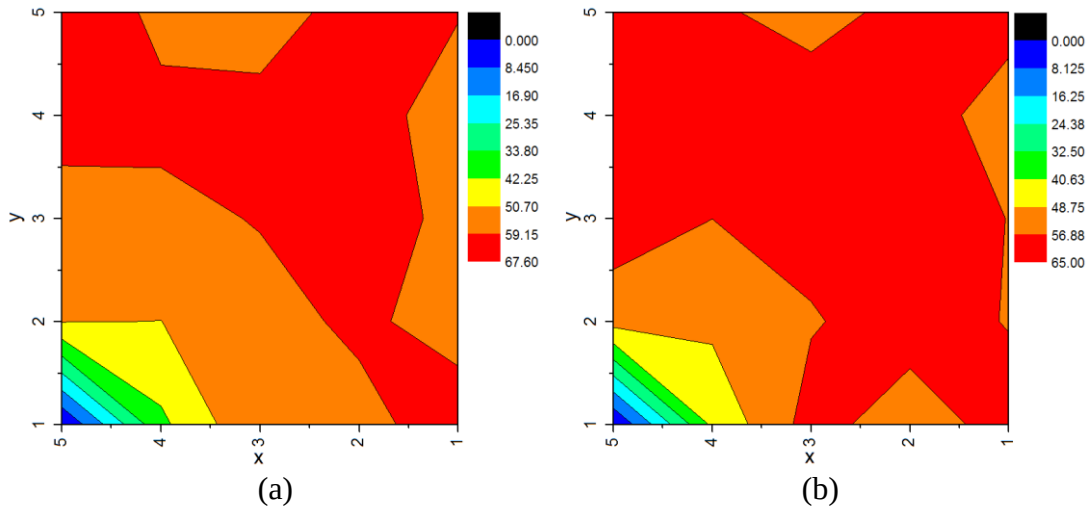

Fig. 6.16.Colour map contour plots of estimated path loss values. (a) empty indoor environment; (b) a test subject standing in the centre of the monitoring area.

In our study, γ and $PL_{(d0)dB}$ were assumed from indoor radio propagation literature. Nonetheless, they can be derived from our own empirical data considering a reference distance of 50 cm (d_0 = 50 cm). Recorded data and least square (LS) fitting curves are shown in Fig. 6.17 and a summary of the path loss exponent and the reference path loss for both scenarios is described in Table 6-5.

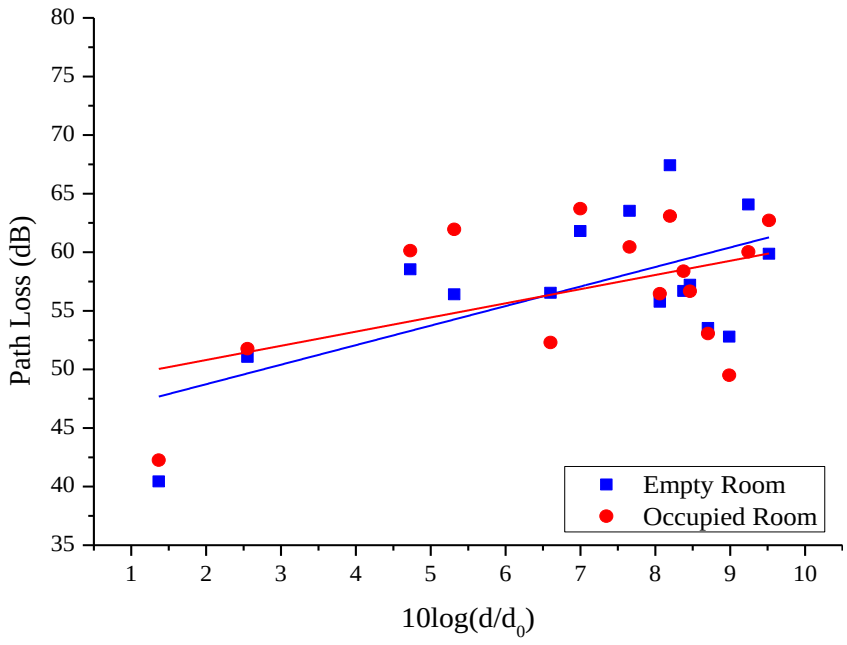

Fig. 6.17.Measured Path values for an empty and occupied room using LS linear fitting

TABLE 6-5
STATISTICAL PARAMETERS OF MEASURED PATH LOSS AT 2.42 GHZ FOR AN INDOOR ENVIRONMENT

Scenario	**PL(d_0) dB**	**γ**
Empty Room	45.40	1.67
Occupied Room	48.39	1.20

Results show that an occupied environment has a better radio communication performance based on path loss exponent (γ = 1.20); on the other hand, an empty indoor environment presents lower reference path loss ($PL_{(d0)dB}$ = 45.40 dB) than a populated scenario ($PL_{(d0)dB}$ = 48.39 dB).

The obtained radio propagation parameters are used to estimate path loss distributions within the monitoring area (see Fig. 6.18). Updated colour map plots are illustrated in Fig. 6.19. The latter shows highest changes in the areas nearest the Tx. and Rx. (*nodes 3-5*) and next highest changes in the line between Tx. and Rx. (*nodes 8-9*). The RF attenuation plots not only show the path loss variation, but also the use of the radio channel measurements to infer the presence and position of the test subject.

63.53	55.78	57.23	52.80	59.87
56.54	56.94	58.02	59.28	64.08
58.54	54.43	56.33	58.18	53.54
40.44	51.32	54.82	57.35	56.70
0.00	51.07	56.40	61.80	67.41

(a)

60.44	56.46	56.67	49.51	62.72
52.29	59.68	62.46	58.37	60.02
60.14	59.78	62.25	59.57	53.07
42.26	61.64	55.16	56.98	58.38
0.00	51.76	61.95	63.72	63.09

(b)

Fig. 6.18.Updated path loss matrix using information from the fitted path loss curves (a) empty room; (b) occupied indoor environment.

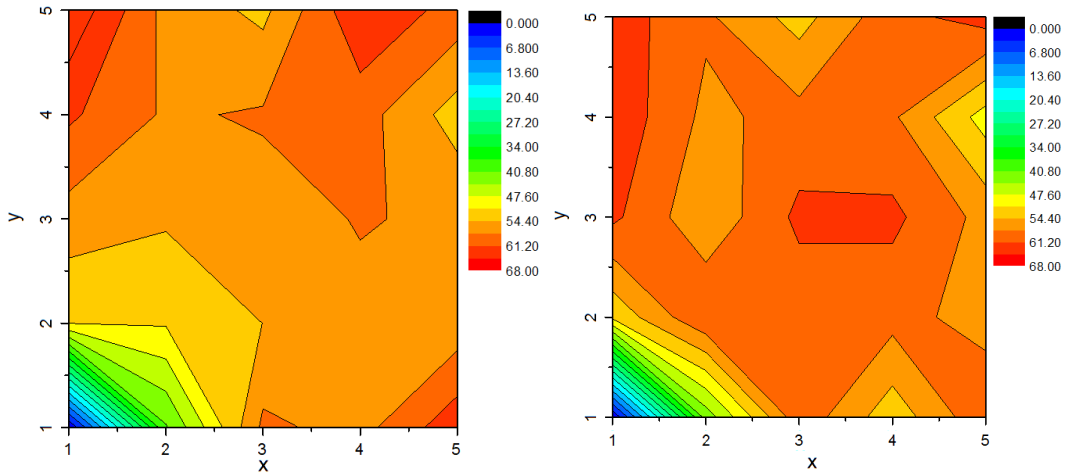

Fig. 6.19.Colour map contour for calculated path loss values. (a) empty indoor environment; (b) a test subject in the centre of the monitoring area.

6.4. Discussion and Conclusion

This chapter discussed the need for, and opportunities to provide, greater positioning information. Some of the available technologies for obtaining this information in an indoor environment have been reviewed, before a proposed measurement campaign was described. This is designed to assess the performance of generic low-power WBAN sensors as an RF positioning system, in order to gain an understanding as to the potential for such devices (expected to become more prevalent in coming years for various reasons, including the changing health needs of the population). Results from two different experiments were presented, indicating that indoor positioning using RSS-based and trilateration is viable, however various factors require further study.

Chapter 7

Conclusions and Future Work

7.1. Discussion and Conclusion

The thesis presented significant advancements in the characterisation and modelling of WBAN propagation channels (motionless and dynamic scenarios). In particular, the importance of developing flexible and more realistic modelling tools was highlighted, to be used in conjunction with simulations and measurements using standard RF instrumentation, for a comprehensive understanding of the propagation mechanisms of body area communications.

From the empirical radio models of different on-body channels communicating at 2.45 GHz, it was concluded that utilising wireless sensors nodes not only diminished the effect of coaxial cables (scattering or radiation), but also provided a more realistic response of the radio link channel. The limitations of the VNA approach are evident when comparing the results shown in Figs. 5.6 and 5.11 (also Tables XV and

XVIII), where the combination of cable effect and measurement bandwidth dominate over the physical proximity of a realistic system.

The VNA measurements usually imply a path loss around 3 dB lower than that using the wireless sensor node approach, with equivalent differences in other measures. The path loss exponent is always found to be greater using the VNA method, often by a factor of 2. Hence, the value of the wireless sensor method can be seen in the more realistic data observed. Thus, the two techniques may be seen as complementary: the VNA approach has the benefits of greater speed and dynamic range, whilst the utilisation of sensor nodes allows a more detailed investigation of real-world scenarios. Moreover, the performance of the antenna (i.e., stand-alone antenna) differs when it is integrated in compact wireless modules

Mean path loss values for a motionless test subject are dependent on the curvature of the human torso, which is subject-specific (and, for instance, can vary considerably between fat and thin subjects); this impedes LOS signals (strong signals) and, hence, the path-loss characteristics exhibit dominant shadowing effects (weak signal).

During the measurement campaign of dynamic environments, the use of coaxial cables and VNA introduced a high degree of discomfort not only restricting the normal activity, but also the quality of the measuring procedure. On-body propagation models have been characterised using wireless sensor nodes which prove to be more flexible and easy to wear.

The comparison of static and dynamic environments reported variations of ±15 dB from the average received signal. Moreover, dynamic scenarios were best fit by a lognormal distribution (i.e., the variation in the coefficients is relatively small), which has been commonly applied to static communications for on-body propagation links.

The results also showed the potential use of on-body radio propagation models between low-power wireless sensor as a non-invasive technology to identify physiological features, such as gait pattern, and thoracic movement which embeds breathing process and heartbeat.

Following the concept of healthcare applications, a low-power RSS-based for indoor location system is introduced for tele-monitoring and tele-diagnostics purposes. Initial measurements suggest that directive antennas are desirable, because of large changes in the received signal amplitude (see Fig. 7.6 and Table XXVI)

Furthermore, the miniaturization of wearable systems increases the fluctuations of individual radio links, due to small and compact antenna designs. The new trend of wireless sensors with channel-sensing capabilities and radio performance algorithms are promising solutions; thus, channel and system performance can be optimized by dynamic scans between different channels linking different on-body nodes.

7.2. Key Contributions

The major contributions in this thesis are described below:

- An alternative measurement technique for on-body radio channels is introduced, utilising wireless sensors nodes. The latter not only diminished the effect of coaxial cables (scattering or radiation), but also provided a more realistic response of the radio link channel.

- A comprehensive, in-depth examination of the physical layer behaviour of low-power IEEE 802.15.4-based wireless sensors operating at the 2.45 GHz ISM band. The study uses packet-based received signal strength (RSS) figure-of-merit to determine propagation characteristics on all the channels of the IEEE 802.15.4 standard (i.e., 16 channels at the 2.45 GHz band). It also makes observations on the temporal trends of received signal, channel effects (i.e., fading and shadowing), and performance of IEEE 802.15.4 links.

- It is shown that the response at individual carrier frequencies is dependent not only on the initial antenna response, as determined by the on-body measurement in isolation, or the on-body location, but also by the channel selected (i.e., one of the 16 channels), and hence system performance is influenced.

- Empirical and statistical models of narrowband (i.e., 2.40-2.48 GHz) on-body radio communication channels are characterised for motionless and dynamic environments using custom-build wireless sensors. In the case of

dynamic scenarios, three different sport activities, jogging, rowing and cycling were modelled using statistical distributions.

- Identification of biomechanical features from dynamic on-body radio channels. Frequency domain plots, spectrograms and multi-resolution analysis of the received signal acquired in the time domain embed gait pattern and thoracic movement produced by the human motion, the breathing process and the heart-beat.

- Introduction of a low-power RSS-based indoor location system using IEEE 802.15.4 for tele-monitoring and tele-diagnostic purposes. Firstly, attenuation factors (due to human presence) and indoor radio propagation models from multiple sensors estimate the relative position of an object. Secondly, it addresses the effects of multipath on different receivers and their implications on the positioning system.

7.3. Future Work

The work presented in this thesis focused on the use of wireless sensors, operating on the IEEE 802.15.4 communication standard, for the measurement and characterisation of different WBAN channels (i.e., motion-less, dynamic, free-space, indoor, RF indoor positioning). There is still a lot of scope for further work, in terms of the research carried out and the limitations of the work presented. The following research aspects are described as a potential and natural progression to previous work:

- Optimization and miniaturization of custom-built wireless sensors for the connection of different wearable antennas, together with the design of compact and low-profile antennas; thus, the best body-worn antenna can be identified. Previous studies have demonstrated that body-worn antennas suffer of reduced efficiency, impedance mismatch, and frequency detuning. The nature of these drawbacks depends on the frequency of operation, the polarisation, and the physical constraints of the antenna itself. A parametrical and statistical analysis of these effects can help on the development of wearable sensor nodes.

- Extending the narrowband (i.e. 2.45 GHz ISM band) on-body propagation measurements to cover various common frequency bands (e.g., UWB) where the sensor nodes can be adapted to implement the concept of diversity antennas.

- Design of antennas that radiate tangentially to the human skin surface, consequently strong surface waves propagate along the body (i.e., confining the radiated power in proximity of the body surface) which not only reduce the external interference (S/N ratio), but also improve the detection of thoracic movements (i.e., breathing process and heartbeat). The same concept can be extended to higher frequencies so the sensitivity is improved (e.g., 5.8 GHz, 10 GHz).

- Design of wireless sensors using textile and fabric antennas, which exploits the potential of conductive and insulating materials; thus, the whole design is integrated in everyday clothing. Different combinations of e-textiles, substrate/conductor, etc., need to be investigated for providing optimised antennas with constant radiation characteristics.

- The accuracy of the low-power RF positioning can be enhanced by implementing the radio channel models of the remaining nodes; therefore, updated path loss distributions and indoor propagation models will yield a much better localization result. Moreover, the post-processing of the data can be done directly in each sensor node producing a self-organizing and self-calibrating radio positioning system.

- The localization technique can also be extended to dynamic scenarios where the test subjects would be moving continuously. To enhance the localization technique, fingerprinting models using MSE weights can be implemented and post-processed in each microcontroller of each sensor node. The results are expected to have significant improvement when compared to previous work.

References

[1] Cobham Antenna Systems and Microwave Antennas. (2008). *Body worn camera and antenna system.* Available: http://www.european-antennas.co.uk/2008-10domo.php

[2] R. S. Hornung, R. F. Mahler, and E. B. Raftery, "Ambulatory Blood Pressure and Heart Rate in Diabetic Patients: an Assessment of Autonomic Function," *Diabetic Medicine,* vol. 6, pp. 579-585, 1989.

[3] B. Gyselinckx, C. Van Hoof, J. Ryckaert, R. F. Yazicioglu, P. Fiorini, and V. Leonov, "Human++: autonomous wireless sensors for body area networks," in *Custom Integrated Circuits Conference, 2005. Proceedings of the IEEE 2005*, 2005, pp. 13-19.

[4] A. D. Joseph, "Energy harvesting projects," *Pervasive Computing, IEEE,* vol. 4, pp. 69-71, 2005.

[5] L. Xin and Y. Shuang-Hua, "Thermal energy harvesting for WSNs," in *Systems Man and Cybernetics (SMC), 2010 IEEE International Conference on*, 2010, pp. 3045-3052.

[6] ABI Research. (2009). *Wearable Wireless Sensors*. Available: http://www.abiresearch.com/research/1004149

[7] S. R. Forrest, "The path to ubiquitous and low-cost organic electronic appliances on plastic," *Nature,* vol. 428, pp. 911-918, 2004.

[8] L. Y. Chi, L. R. Prada Gomez, R. A. Ryskamp, and S. G. Mavinkurve, "Wearable heads-up display with integrated finger-tracking input sensor.," United States Patent, 2011.

[9] Queen's University Human Media Lab. (2011). *E-paper for computer interface in the pipeline*. Available: http://www.plusplasticelectronics.com/consumerelectronics/e-paper-for-computer-interface-in-the-pipeline-33610.aspx

[10] W. A. MacDonald, "Engineered films for display technologies," *Journal of Materials Chemistry,* vol. 14, pp. 4-10, 2004.

[11] B. Lamontagne, P. Barrios, C. Py, and S. Nikumb, "The next generation of switchable glass : the Micro-Blinds," *Proceedings of the Glass Performance Days,* pp. 637–639, 2009.

[12] C. E. Smith, "Human Microchip Implantation," *Journal of Technology Management & Innovation,* vol. 3, pp. 151-160, 2008.

[13] J. T. Santini, A. C. Richards, R. A. Scheidt, M. J. Cima, and R. S. Langer, "Microchip technology in drug delivery," *Annals of medicine,* vol. 32, pp. 377-379, 2000.

[14] P. S. Hall and Y. Hao, *Antennas and propagation for body-centric wireless communications*: Artech House, 2006, ISBN: 9781580534932.

[15] G. Z. Yang, *Body sensor networks*: Springer-Verlag New York Inc, 2006, ISBN: 1846282721.

[16] K. Aminian and B. Najafi, "Capturing human motion using body-fixed sensors: outdoor measurement and clinical applications," *Computer Animation and Virtual Worlds,* vol. 15, pp. 79-94, 2004.

[17] S. J. Morris and J. A. Paradiso, "Shoe-integrated sensor system for wireless gait analysis and real-time feedback," in *Engineering in Medicine and Biology, 2002. 24th Annual Conference and the Annual Fall Meeting of the Biomedical Engineering Society EMBS/BMES Conference, 2002. Proceedings of the Second Joint*, 2002, pp. 2468-2469 vol.3.

[18] M. Pacelli, G. Loriga, N. Taccini, and R. Paradiso, "Sensing Fabrics for Monitoring Physiological and Biomechanical Variables: E-textile solutions," in *Medical Devices and Biosensors, 2006. 3rd IEEE/EMBS International Summer School on*, 2006, pp. 1-4.

[19] T. Arampatzis, J. Lygeros, and S. Manesis, "A Survey of Applications of Wireless Sensors and Wireless Sensor Networks," in *Intelligent Control, 2005. Proceedings of the 2005 IEEE*

International Symposium on, Mediterrean Conference on Control and Automation, 2005, pp. 719-724.

[20] L. Schwiebert, S. K. S. Gupta, and J. Weinmann, "Research challenges in wireless networks of biomedical sensors," presented at the Proceedings of the 7th annual international conference on Mobile computing and networking, Rome, Italy, 2001.

[21] J. Hightower and G. Borriello, "Location systems for ubiquitous computing," *Computer*, vol. 34, pp. 57-66, 2001.

[22] IEEE 802.15. (2011). *Working Group for Wireless Personal Area Networks (WPAN)*. Available: http://grouper.ieee.org/groups/802/15/

[23] IEEE 802.15 WPAN. (2011). *Task Group 6 (TG6) Body Area Networks (BAN)*. Available: http://www.ieee802.org/15/pub/TG6.html

[24] A. Alomainy, "Antennas and Radio Propagation for Body-Centric Wireless Network," Doctor of Philosophy, Electronic Engineering, Queen Mary, University of London, London, 2007.

[25] Y. Hao and R. Foster, "Wireless body sensor networks for health-monitoring applications," *Physiological Measurement*, vol. 29, p. R27, 2008.

[26] Federal Communications Commission (FCC) rules and regulations. (2009). *MedRadio transmitters*. Available: http://www.gpo.gov/fdsys/pkg/CFR-2009-title47-vol5/pdf/CFR-2009-title47-vol5-part95.pdf

[27] Texas Instruments. (2005). *Application Report: ISM-Band and Short Range Device Regulatory Compliance Overview*. Available: http://www.ti.com/lit/an/swra048/swra048.pdf

[28] Federal Communications Commission (FCC) rules and regulations. (2011). *Title 47: Telecommunication, Part 15: Radio Frequency Devices, Subpart F: Ultra Wideband Operation*. Available: http://hraunfoss.fcc.gov/edocs_public/attachmatch/FCC-02-48A1.pdf

[29] The European Conference of Postal and Telecommunications Administrations. (2006). *ECC Decision of 1 December 2006 on the harmonised conditions for devices using Ultra-Wideband (UWB) technology with Low Duty Cycle (LDC)*. Available: http://www.erodocdb.dk/Docs/doc98/official/pdf/ECCDEC0612_old_version.PDF

[30] K. Hachisuka, A. Nakata, T. Takeda, Y. Terauchi, K. Shiba, K. Sasaki, H. Hosaka, and K. Itao, "Development and performance analysis of an intra-body communication device," in *TRANSDUCERS, Solid-State Sensors, Actuators and Microsystems, 12th International Conference on, 2003*, 2003, pp. 1722-1725 vol.2.

[31] T. G. Zimmerman, "Personal Area Networks: Near-field intrabody communication," *IBM Systems Journal*, vol. 35, pp. 609-617, 1996.

[32] Bluetooth Special Interest Group (SIG). (2010). *Bluetooth Specification Version 4.0 Vol 0*. Available: https://www.bluetooth.org/Technical/Specifications/adopted.htm

[33] Forum-Nokia. (2003). *Bluetooth Technology Overview Version 1.0*. Available: http://lms.uni-mb.si/~meolic/ptk-seminarske/bluetooth2.pdf

[34] IEEE 802.15.4 Standard. (2006). *Wireless Medium Access Control (MAC) and Physical Layer (PHY) Specifications for Low Rate Wireless Personal Area Networks (LR-WPANs)*. Available: http://standards.ieee.org/getieee802/download/802.15.4-2006.pdf

[35] T. H. Loh, M. Alexander, F. Widmer, P. Miller, and D. Knight, "Validation of a new small-antenna radiated testing range," in *Antennas and Propagation, 2009. EuCAP 2009. 3rd European Conference on*, 2009, pp. 699-703.

[36] M. G. DiBenedetto, *Home Automation and Power Conservation Using ZigBee®*: Florida Atlantic University, 2009.

[37] Nick Hunn, *Essentials of Short-Range Wireless*: Cambridge University Press, ISBN: 9781139488945.

[38] WG802.15 - Wireless Personal Area Network (WPAN) Working Group. (2012). *802.15.6-2012 - IEEE Standard for Local and metropolitan area networks - Part 15.6: Wireless Body Area Networks*. Available: http://standards.ieee.org/findstds/standard/802.15.6-2012.html

[39] S. Ullah, H. Higgins, B. Braem, B. Latre, C. Blondia, I. Moerman, S. Saleem, Z. Rahman, and K. S. Kwak, "A Comprehensive Survey of Wireless Body Area Networks : On PHY, MAC, and Network Layers Solutions," *Journal of Medical Systems*, Aug 19 2010.

[40] Z. N. Chen, *Antennas for portable devices*: John Wiley, 2007, ISBN: 9780470030738.

[41] Y. T. Lo and S. W. Lee, *Antenna Handbook: Applications*: Van Nostrand Reinhold, 1993, ISBN: 9780442015947.

[42] C. A. Balanis, *Antenna theory : analysis and design*, 3rd ed. ed. Hoboken, N.J.: [Great Britain] : Wiley-Interscience, 2005, ISBN: 047166782X (cased).

[43] S. R. Saunders, *Antennas and propagation for wireless communication systems*: John Wiley & Sons, 1999, ISBN: 9780471986096.

[44] T. S. Rappaport, *Wireless communications : principles and practice*. Upper Saddle River, N.J.: Prentice Hall PTR ; London : Prentice-Hall International, 1996, ISBN: 0133755363.

[45] A. Goldsmith, *Wireless communications*. Cambridge: Cambridge University Press, 2005, ISBN: 9780521837163 (hbk.), 0521837162 (hbk.).

[46] T. S. Rappaport, *Wireless communications : principles and practice*, 2nd ed. ed. Upper Saddle River, N.J. ; [Great Britain]: Prentice Hall PTR, 2002, ISBN: 0130422320 : No price.

[47] S. L. Cotton and W. G. Scanlon, "An experimental investigation into the influence of user state and environment on fading characteristics in wireless body area networks at 2.45 GHz," *Wireless Communications, IEEE Transactions on,* vol. 8, pp. 6-12, 2009.

[48] P. S. Hall, H. Yang, Y. I. Nechayev, A. Alomalny, C. C. Constantinou, C. Parini, M. R. Kamarudin, T. Z. Salim, D. T. M. Hee, R. Dubrovka, A. S. Owadally, S. Wei, A. Serra, P. Nepa, M. Gallo, and M. Bozzetti, "Antennas and Propagation for On-Body Communication Systems," *Antennas and Propagation Magazine, IEEE,* vol. 49, pp. 41-58, 2007.

[49] S. L. Cotton, W. G. Scanlon, and J. Guy, "The kappa-mu Distribution Applied to the Analysis of Fading in Body to Body Communication Channels for Fire and Rescue Personnel," *Antennas and Wireless Propagation Letters, IEEE,* vol. 7, pp. 66-69, 2008.

[50] P. S. Hall, M. Ricci, and T. M. Hee, "Measurements of on-body propagation characteristics," in *Antennas and Propagation Society International Symposium, 2002. IEEE*, 2002, pp. 310-313 vol.2.

[51] Z. H. Hu, M. Gallo, Q. Bai, Y. I. Nechayev, P. S. Hall, and M. Bozzettit, "Measurements and Simulations for On-Body Antenna Design and Propagation Studies," in *Antennas and Propagation, 2007. EuCAP 2007. The Second European Conference on*, 2007, pp. 1-7.

[52] Z. H. Hu, Y. I. Nechayev, P. S. Hall, C. C. Constantinou, and H. Yang, "Measurements and Statistical Analysis of On-Body Channel Fading at 2.45 GHz," *Antennas and Wireless Propagation Letters, IEEE,* vol. 6, pp. 612-615, 2007.

[53] Y. I. Nechayev, P. S. Hall, and Z. H. Hu, "Characterisation of narrowband communication channels on the human body at 2.45 GHz," *Microwaves, Antennas & Propagation, IET,* vol. 4, pp. 722-732, 2010.

[54] M. O. Munoz, R. Foster, and Y. Hao, "Physiological Features from an On-Body Radio Propagation Channel," in *Wearable and Implantable Body Sensor Networks (BSN), 2012 Ninth International Conference on*, 2012, pp. 52-57.

[55] H. Akaike, "A new look at the statistical model identification," *Automatic Control, IEEE Transactions on,* vol. 19, pp. 716-723, 1974.

[56] P. S. Hall and Y. Hao, *Antennas and propagation for body-centric wireless communications*. Boston, Mass. ; London: Artech House, 2006, ISBN: 9781580534932 (cased), 1580534937 (cased).

[57] S. Gabriel, R. W. Lau, and C. Gabriel, "The dielectric properties of biological tissues: II. Measurements in the frequency range 10 Hz to 20 GHz," *Physics in Medicine and Biology,* vol. 41, p. 2251, 1996.

[58] Camilia Gabriel, "Compilation of the Dielectric Properties of Body Tissues at RF and Microwave Frequencies," Radiofrequency Radiation Division Brooks Air Force Base, Ed., ed. Texas, United States, 1996.

[59] C. Gabriel, S. Gabriel, and E. Corthout, "The dielectric properties of biological tissues: I. Literature survey," *Physics in Medicine and Biology,* vol. 41, p. 2231, 1996.

[60] Institute for Applied Physics - Italian National Research Council. (2007). *Calculation of the Dielectric Properties of Body Tissues*. Available: http://niremf.ifac.cnr.it/tissprop/htmlclie/htmlclie.htm#atsftag

[61] G. A. Conway and W. G. Scanlon, "Low-Profile Patch Antennas for Over-Body-Surface Communication at 2.45 GHz," in *Antenna Technology: Small and Smart Antennas Metamaterials and Applications, 2007. IWAT '07. International Workshop on*, 2007, pp. 416-419.

[62] G. A. Conway and W. G. Scanlon, "Antennas for Over-Body-Surface Communication at 2.45 GHz," *Antennas and Propagation, IEEE Transactions on,* vol. 57, pp. 844-855, 2009.

[63] J. Garcia, A. Arriola, G. Sasiain, D. Valderas, J. I. Sancho, and X. Chen, "Characterization of phantom size and link budget for off-body communications," in *Antennas and Propagation (EuCAP), 2010 Proceedings of the Fourth European Conference on*, 2010, pp. 1-5.

[64] K. T. Karathanasis, I. A. Gouzouasis, I. S. Karanasiou, M. I. Giamalaki, G. Stratakos, and N. K. Uzunoglu, "Noninvasive Focused Monitoring and Irradiation of Head Tissue Phantoms at Microwave Frequencies," *Information Technology in Biomedicine, IEEE Transactions on,* vol. 14, pp. 657-663, 2010.

[65] L. Roelens, S. Van den Bulcke, W. Joseph, G. Vermeeren, and L. Martens, "Path loss model for wireless narrowband communication above flat phantom," *Electronics Letters,* vol. 42, pp. 10-11, 2006.

[66] K. Wake, H. Hongo, S. Watanabe, T. Masao, Y. Kamimura, Y. Yamanaka, T. Uno, M. Kojima, I. Hata, and K. Sasaki, "Development of a 2.45-GHz Local Exposure System for <emphasis emphasistype="italic">In Vivo</emphasis> Study on Ocular Effects," *Microwave Theory and Techniques, IEEE Transactions on,* vol. 55, pp. 588-596, 2007.

[67] A. Sani, M. Rajab, R. Foster, and H. Yang, "Antennas and Propagation of Implanted RFIDs for Pervasive Healthcare Applications," *Proceedings of the IEEE,* vol. 98, pp. 1648-1655, 2010.

[68] J. C. Hebden, D. J. Hall, M. Firbank, and D. T. Delpy, "Time-resolved optical imaging of a solid tissue-equivalent phantom," *Appl. Opt.*, vol. 34, pp. 8038-8047, 1995.

[69] A. Lea, H. Ping, J. Ollikainen, and R. G. Vaughan, "Propagation Between On-Body Antennas," *Antennas and Propagation, IEEE Transactions on,* vol. 57, pp. 3619-3627, 2009.

[70] W. D. Waddoup, "Multi-Element Antenna Techniques for Remote Monitoring of Wireless-Equipped On-Body Medical Sensors," Master of Philosophy (MPhil.), School of Electronic Engineering and Computer Science, Queen Mary, University of London, 2011.

[71] A. Ltd. (2009). *Rufa 2.4 GHz SMD Antenna*. Available: http://www.antenova.com/Product%20Specs/AE020157-N-Product-Specification-Rufa.pdf

[72] A. Alomainy, H. Yang, and D. M. Davenport, "Parametric Study of Wearable Antennas with Varying Distances from the Body and Different On-Body Positions," in *Antennas and Propagation for Body-Centric Wireless Communications, 2007 IET Seminar on*, 2007, pp. 84-89.

[73] G. Conway, S. Cotton, and W. Scanlon, "An Antennas and Propagation Approach to Improving Physical Layer Performance in Wireless Body Area Networks," *Selected Areas in Communications, IEEE Journal on,* vol. 27, pp. 27-36, 2009.

[74] M. R. Kamarudin, Y. I. Nechayev, and P. S. Hall, "Antennas for on-body communication systems," in *Antenna Technology: Small Antennas and Novel Metamaterials, 2005. IWAT 2005. IEEE International Workshop on*, 2005, pp. 17-20.

[75] A. Alomainy, Y. Hao, A. Owadally, C. G. Parini, Y. Nechayev, C. C. Constantinou, and P. S. Hall, "Statistical Analysis and Performance Evaluation for On-Body Radio Propagation With Microstrip Patch Antennas," *Antennas and Propagation, IEEE Transactions on,* vol. 55, pp. 245-248, 2007.

[76] P. Salonen, Y. Rahmat-Samii, and M. Kivikoski, "Wearable antennas in the vicinity of human body," in *Antennas and Propagation Society International Symposium, 2004. IEEE,* 2004, pp. 467-470 Vol.1.

[77] J. Wang, O. Fujiwara, S. Watanabe, and Y. Yamanaka, "Computation with a parallel FDTD system of human-body effect on electromagnetic absorption for portable telephones," *Microwave Theory and Techniques, IEEE Transactions on*, vol. 52, pp. 53-58, 2004.

[78] B. Sinha, "Numerical modeling of adsorption and scattering of EM energy radiated by cellular phones by human arms," in *TENCON '98. 1998 IEEE Region 10 International Conference on Global Connectivity in Energy, Computer, Communication and Control*, 1998, pp. 261-264 vol.2.

[79] K. I. Ziri-Castro, W. G. Scanlon, and N. E. Evans, "Indoor radio channel characterization and modeling for a 5.2-GHz bodyworn receiver," *Antennas and Wireless Propagation Letters, IEEE*, vol. 3, pp. 219-222, 2004.

[80] C. Hertleer, H. Rogier, L. Vallozzi, and L. Van Langenhove, "A Textile Antenna for Off-Body Communication Integrated Into Protective Clothing for Firefighters," *Antennas and Propagation, IEEE Transactions on*, vol. 57, pp. 919-925, 2009.

[81] P. Salonen and Y. Rahmat-Samii, "Textile antennas: Effects of antenna bending on input matching and impedance bandwidth," in *Antennas and Propagation, 2006. EuCAP 2006. First European Conference on*, 2006, pp. 1-5.

[82] P. Salonen and Y. Rahmat-Samii, "Textile Antennas: Effects of Antenna Bending on Input Matching and Impedance Bandwidth," *Aerospace and Electronic Systems Magazine, IEEE*, vol. 22, pp. 18-22, 2007.

[83] S. Zhu and R. Langley, "Dual-band wearable antennas over EBG substrate," *Electronics Letters*, vol. 43, pp. 141-142, 2007.

[84] Z. Shaozhen and R. Langley, "Dual-Band Wearable Textile Antenna on an EBG Substrate," *Antennas and Propagation, IEEE Transactions on*, vol. 57, pp. 926-935, 2009.

[85] K. Jaehoon and Y. Rahmat-Samii, "Exterior antennas for wireless medical links: EBG backed dipole and loop antennas," in *Antennas and Propagation Society International Symposium, 2005 IEEE*, 2005, pp. 800-803 vol. 2B.

[86] N. Haga, K. Saito, M. Takahashi, and K. Ito, "Characteristics of Cavity Slot Antenna for Body-Area Networks," *Antennas and Propagation, IEEE Transactions on*, vol. 57, pp. 837-843, 2009.

[87] H. Adel, R. Wansch, and C. Schmidt, "Antennas for a body area network," in *Antennas and Propagation Society International Symposium, 2003. IEEE*, 2003, pp. 471-474 vol.1.

[88] P. Salonen and J. Rantanen, "A dual-band and wide-band antenna on flexible substrate for smart clothing," in *Industrial Electronics Society, 2001. IECON '01. The 27th Annual Conference of the IEEE*, 2001, pp. 125-130 vol.1.

[89] J. Polastre, R. Szewczyk, C. Sharp, and D. Culler, "The mote revolution: Low power wireless sensor network devices," in *Proceedings of Hot Chips 16: A Symposium on High Performance Chips*, 2004.

[90] J. Hill, R. Szewczyk, A. Woo, S. Hollar, D. Culler, and K. Pister, "A System Architecture for Networked Sensors," in *UC Berkeley*, N. DARPA NEST program, Intel, CITRIS and California MICRO, Ed., ed. California, United States, 2000.

[91] Atmel Corporation. (2009). *Low Power 2.4 GHz Transceiver for ZigBee, IEEE 802.15.4, 6LoWPAN, RF4CE and ISM Applications AT86RF230*. Available: http://www.atmel.com/dyn/products/product_card.asp?part_id=3941

[92] Freescale Semiconductor. (2010). *MC1322x Advanced ZigBee™ - Compliant Platform-in-Package (PiP) for the 2.4 GHz IEEE802.15.4 Standard*. Available: http://www.freescale.com/webapp/sps/site/prod_summary.jsp?code=MC13224V

[93] Radiocrafts Embedded Wireless Solutions. (2008). *ZigBee Ready RF Transceiver*. Available: http://www.radiocrafts.com/index.php?sideID=243&ledd1=33

[94] Jenic. (2010). *JN5139 Wireless Microcontroller IEEE802.15.4/ZigBee Module Family*. Available: http://www.jennic.com/products/wireless_microcontrollers/jn5139

[95] STMicroelectronics. (2009). *ZigBee 802.15.4 network processor SN260*. Available: http://www.st.com/stonline/books/pdf/docs/12972.pdf

[96] Crossbow Technology. (2004). *Telos B Mote Platform*. Available: http://bullseye.xbow.com:81/Products/Product_pdf_files/Wireless_pdf/TelosB_Datasheet.pdf

[97] FlexiPanel Ltd. (2008). *Pixie-PIC microcontroller with 2.4GHz IEEE 802.15.4 transceiver and ZigBee stack*. Available: http://www.flexipanel.com/Docs/Pixie%20DS481.pdf

[98] MeshNetics. (2008). *Ultra-Compact 2.4GHz 802.15.4/ZigBee Modules for Wireless Networking Applications*. Available: http://www.meshnetics.com/netcat_files/Image/M-251~01-(ZigBit%20OEM%20Module%20Product%20Datasheet).pdf

[99] "IEEE Standard for Local and metropolitan area networks Part 15.6: Wireless Body Area Networks," *IEEE Std 802.15.6-2012*, pp. 1-271, 2012.

[100] A. Alomainy, H. Yang, and F. Pasveer, "Numerical and Experimental Evaluation of a Compact Sensor Antenna for Healthcare Devices," *Biomedical Circuits and Systems, IEEE Transactions on*, vol. 1, pp. 242-249, 2007.

[101] Texas Instruments. (2007). *2.4 GHz IEEE 802.15.4 / ZigBee-ready RF Transceiver*. Available: http://focus.ti.com/lit/ds/symlink/cc2420.pdf

[102] Microchip. (2008). *PIC18F2620 28-Pin Enhanced Flash Microcontrollers with 10-Bit A/D and NanoWatt Technology*. Available: http://ww1.microchip.com/downloads/en/DeviceDoc/39626e.pdf

[103] C. A. Balanis, *Antenna theory: analysis and design*: John Wiley, 2005, ISBN: 9780471667827.

[104] M. Gallo, P. S. Hall, and M. Bozzetti, "Simulation And Measurement Of Body Dymamics For On-Body Channel Characteirisation," in *Antennas and Propagation for Body-Centric Wireless Communications, 2007 IET Seminar on*, 2007, pp. 71-74.

[105] M. Alexander, G. Palikaras, A. Sani, and M. Rajab, "Characterisation of low reflectivity antenna supports for electrically small antennas, and pattern measurement via optical fibre to eliminate common mode current errors," *Automated RF & Microwave Measurement Society (ARMMS)*, 20-21 April 2009.

[106] L. Kin Seong, N. Mun Leng, and P. H. Cole, "Investigation of RF cable effect on RFID tag antenna impedance measurement," in *Antennas and Propagation Society International Symposium, 2007 IEEE*, 2007, pp. 573-576.

[107] P. J. Massey and K. R. Boyle, "Controlling the effects of feed cable in small antenna measurements," in *Antennas and Propagation, 2003. (ICAP 2003). Twelfth International Conference on (Conf. Publ. No. 491)*, 2003, pp. 561-564 vol.2.

[108] S. Saario, D. V. Thiel, J. W. Lu, and S. G. O'Keefe, "An assessment of cable radiation effects on mobile communications antenna measurements," in *Antennas and Propagation Society International Symposium, 1997. IEEE., 1997 Digest*, 1997, pp. 550-553 vol.1.

[109] P. A. Catherwood and W. G. Scanlon, "Measurement errors introduced by the use of co-axial cabling in the assessment of wearable antenna performance in off-body channels," in *Antennas and Propagation (EUCAP), Proceedings of the 5th European Conference on*, 2011, pp. 3787-3791.

[110] A. D. Olver, *Microwave and optical transmission*: Wiley, 1992, ISBN: 047193478X, 047193416X (pbk).

[111] I. L. Chun and W. Kin-Lu, "Printed Monopole Slot Antenna for Internal Multiband Mobile Phone Antenna," *Antennas and Propagation, IEEE Transactions on*, vol. 55, pp. 3690-3697, 2007.

[112] L. Chung-Huan, E. Ofli, N. Chavannes, and N. Kuster, "SAr and efficiency performance of mobile phone antenna with different user hand positions," in *Antennas and Propagation Society International Symposium, 2009. APSURSI '09. IEEE*, 2009, pp. 1-4.

[113] A. Ikram, C. Beckman, and S. Irmscher, "Design and development of a multiband loop antenna for cellular mobile handsets," in *Antenna Technology (iWAT), 2011 International Workshop on*, 2011, pp. 251-254.

[114] S. L. Cotton and W. G. Scanlon, "Statistical characterisation for a mobile bodyworn personal area network in an indoor multipath environment at 868 MHz," in *Antennas and Propagation, 2006. EuCAP 2006. First European Conference on*, 2006, pp. 1-7.

[115] S. L. Cotton and W. G. Scanlon, "Characterization and modeling of on-body spatial diversity within indoor environments at 868 MHz," *IEEE Transactions on Wireless Communications,* vol. 8, pp. 176-185, 2009.

[116] S. L. Cotton and W. G. Scanlon, "Characterization of the on-body channel in an outdoor environment at 2.45 GHz," in *Antennas and Propagation, 2009. EuCAP 2009. 3rd European Conference on*, 2009, pp. 722-725.

[117] S. L. Cotton and W. G. Scanlon, "An experimental investigation into the influence of user state and environment on fading characteristics in wireless body area networks at 2.45 GHz," *IEEE Transactions on Wireless Communications,* vol. 8, pp. 6-12, 2009.

[118] Z. Jian, D. B. Smith, L. W. Hanlen, D. Miniutti, D. Rodda, and B. Gilbert, "Stability of Narrowband Dynamic Body Area Channel," *IEEE Antennas and Wireless Propagation Letters,* vol. 8, pp. 53-56, 2009.

[119] E. Reusens, W. Joseph, B. Latre, B. Braem, G. Vermeeren, E. Tanghe, L. Martens, I. Moerman, and C. Blondia, "Characterization of On-Body Communication Channel and Energy Efficient Topology Design for Wireless Body Area Networks," *IEEE Transactions on Information Technology in Biomedicine,* vol. 13, pp. 933-945, 2009.

[120] E. Reusens, W. Joseph, G. Vermeeren, L. Martens, B. Latre, I. Moerman, B. Braem, and C. Blondia, "Path loss models for wireless communication channel along arm and torso: measurements and simulations," in *IEEE Antennas and Propagation Society International Symposium*, 2007, pp. 345-348.

[121] D. Smith, L. Hanlen, Z. Jian, D. Miniutti, D. Rodda, and B. Gilbert, "Characterization of the Dynamic Narrowband On-Body to Off-Body Area Channel," in *IEEE International Conference on Communications, 2009. ICC '09*, 2009, pp. 1-6.

[122] D. Smith, L. Hanlen, D. Miniutti, Z. Jian, D. Rodda, and B. Gilbert, "Statistical characterization of the dynamic narrowband body area channel," in *First International Symposium in Applied Sciences on Biomedical and Communication Technologies, ISABEL '08.* , 2008, pp. 1-5.

[123] D. B. Smith, Z. Jian, L. W. Hanlen, D. Miniutti, D. Rodda, and B. Gilbert, "A simulator for the dynamic on-body area propagation channel," in *IEEE Antennas and Propagation Society International Symposium, 2009. APSURSI '09*, 2009, pp. 1-4.

[124] D. B. Smith, J. Zhang, L. W. Hanlen, D. Miniutti, D. Rodda, and B. Gilbert, "Temporal correlation of dynamic on-body area radio channel," *Electronics Letters,* vol. 45, pp. 1212-1213, 2009.

[125] D. B. Smith, D. Miniutti, L. W. Hanlen, D. Rodda, and B. Gilbert, "Dynamic Narrowband Body Area Communications: Link-Margin Based Performance Analysis and Second-Order Temporal Statistics," in *IEEE Wireless Communications and Networking Conference (WCNC)*, 2010, pp. 1-6.

[126] Y. I. Nechayev, P. S. Hall, and Z. H. Hu, "Characterisation of narrowband communication channels on the human body at 2.45 GHz," *IET Microwaves, Antennas & Propagation,* vol. 4, pp. 722-732, 2010.

[127] Y. I. Nechayev, Z. H. Hu, and P. S. Hall, "Short-term and long-term fading of on-body transmission channels at 2.45 GHz," in *LAPC Antennas & Propagation Conference, Loughborough*, 2009, pp. 657-660.

[128] S. F. Heaney, W. G. Scanlon, E. Garcia-Palacios, and S. L. Cotton, "Fading characterization for Context Aware Body Area Networks (CABAN) in interactive smart environments," in *Loughborough Antennas and Propagation Conference (LAPC)*, 2010, pp. 501-504.

[129] V. G. Chaganti, D. B. Smith, and L. W. Hanlen, "Second-Order Statistics for Many-Link Body Area Networks," *IEEE Antennas and Wireless Propagation Letters,* vol. 9, pp. 322-325, 2010.

[130] A. Guraliuc, A. A. Serra, P. Nepa, G. Manara, F. Potorti, and P. Barsocchi, "Body posture/activity detection: Path loss characterization for 2.4GHz on-body wireless sensors," in *IEEE Antennas and Propagation Society International Symposium, APSURSI '09*, 2009, pp. 1-4.

[131] A. R. Guraliuc, A. A. Serra, P. Nepa, and G. Manara, "Channel model for on body communication along and around the human torso at 2.4GHz and 5.8GHz," in *International Workshop on Antenna Technology (iWAT 2010)*, 2010, pp. 1-4.

[132] L. W. Hanlen, D. Miniutti, D. Rodda, and B. Gilbert, "Interference in body area networks: Distance does not dominate," in *IEEE 20th International Symposium on Personal, Indoor and Mobile Radio Communications*, 2009, pp. 281-285.

[133] A. Zhang, L. W. Hanlen, D. Miniutti, D. Rodda, and B. Gilbert, "Interference in body area networks: Are signal-links and interference-links independent?," in *IEEE 20th International Symposium on Personal, Indoor and Mobile Radio Communications*, 2009, pp. 456-460.

[134] A. Alomainy, Y. Hao, A. Owadally, C. G. Parini, Y. Nechayev, C. C. Constantinou, and P. S. Hall, "Statistical Analysis and Performance Evaluation for On-Body Radio Propagation With Microstrip Patch Antennas," *IEEE Transactions on Antennas and Propagation*, vol. 55, pp. 245-248, 2007.

[135] A. Sani, Z. Yan, H. Yang, A. Alomainy, and C. Parini, "An Efficient FDTD Algorithm Based on the Equivalence Principle for Analyzing Onbody Antenna Performance," *IEEE Transactions on Antennas and Propagation*, vol. 57, pp. 1006-1014, 2009.

[136] E. Reusens, W. Joseph, G. Vermeeren, and L. Martens, "On-Body Measurements and Characterization of Wireless Communication Channel for Arm and Torso of Human," in *4th International Workshop on Wearable and Implantable Body Sensor Networks (BSN 2007)*. vol. 13, S. Leonhardt, T. Falck, and P. Mähönen, Eds., ed: Springer Berlin Heidelberg, 2007, pp. 264-269.

[137] G. A. Conway, W. G. Scanlon, S. L. Cotton, and M. J. Bentum, "An analytical path-loss model for on-body radio propagation," in *International Symposium on Electromagnetic Theory (EMTS), URSI* 2010, pp. 332-335.

[138] Z. H. Hu, M. Gallo, Q. Bai, Y. I. Nechayev, P. S. Hall, and M. Bozzettit, "Measurements and Simulations for On-Body Antenna Design and Propagation Studies," in *The Second European Conference on Antennas and Propagation, EuCAP 2007*, 2007, pp. 1-7.

[139] M. Gallo, P. S. Hall, and M. Bozzetti, "Simulation And Measurement Of Body Dymamics For On-Body Channel Characteirisation," in *IET Seminar on Antennas and Propagation for Body-Centric Wireless Communications, 2007* 2007, pp. 71-74.

[140] O. Aziz, B. Lo, R. King, A. Darzi, and Y. Guang-Zhong, "Pervasive body sensor network: an approach to monitoring the post-operative surgical patient," in *International Workshop on Wearable and Implantable Body Sensor Networks, BSN 2006.*, 2006, pp. 4 pp.-18.

[141] L. Atallah, B. Lo, R. King, and Y. Guang-Zhong, "Sensor Placement for Activity Detection Using Wearable Accelerometers," in *International Conference on Body Sensor Networks (BSN), 2010*, 2010, pp. 24-29.

[142] N. Sazonova, R. C. Browning, and E. Sazonov, "Accurate Prediction of Energy Expenditure Using a Shoe-Based Activity Monitor," *Med Sci Sports Exerc*, Dec 1 2010.

[143] A. R. Guraliuc, P. Barsocchi, Potorti, x, F., and P. Nepa, "Limb Movements Classification Using Wearable Wireless Transceivers," *IEEE Transactions on Information Technology in Biomedicine*, vol. 15, pp. 474-480, 2011.

[144] A. R. Guraliuc, A. A. Serra, P. Nepa, G. Manara, and F. Potorti, "Detection and classification of human arm movements for physical rehabilitation," in *IEEE Antennas and Propagation Society International Symposium (APSURSI), 2010* 2010, pp. 1-4.

[145] P. Frehill, D. Chambers, and C. Rotariu, "Using Zigbee to Integrate Medical Devices," in *Engineering in Medicine and Biology Society, 2007. EMBS 2007. 29th Annual International Conference of the IEEE*, 2007, pp. 6717-6720.

[146] C. Shih-Lun, L. Ho-Yin, C. Chiung-An, H. Hong-Yi, and L. Ching-Hsing, "Wireless Body Sensor Network With Adaptive Low-Power Design for Biometrics and Healthcare Applications," *Systems Journal, IEEE*, vol. 3, pp. 398-409, 2009.

[147] WOODWAY USA. Inc. (2011). *WOODWAY ELG Treadmill for Sports Medicine*. Available: http://medical.woodway.com/literature/ELGspec.pdf

[148] Lode B.V. (2008). *Excalibur Sport with Pedal Force Measurement*. Available: http://www.lode.nl/en/product/excalibur-sport-mit-pedalkraftmessung/194/id_segment/1#

[149] Rowperfect from Casper Rekers. (2012). *Rowperfect RP3 rowing ergometer* Available: http://www.rowperfect.co.uk/rowperfect/rowperfect-specifications/#.UfS2uY04t8E http://www.row-ware.com/html/rp3w.html http://www.rowperfect3.com/

[150] M. Munoz, R. Foster, and Y. Hao, "On-body performance of wireless sensor nodes using IEEE 802.15.4," in *Antennas and Propagation (EUCAP), Proceedings of the 5th European Conference on*, 2011, pp. 3783-3786.

[151] M. O. Munoz, R. Foster, and H. Yang, "On-Body Channel Measurement Using Wireless Sensors," *Antennas and Propagation, IEEE Transactions on*, vol. 60, pp. 3397-3406, 2012.

[152] G. A. Conway and W. G. Scanlon, "Antennas for Over-Body-Surface Communication at 2.45 GHz," *IEEE Transactions on Antennas and Propagation*, vol. 57, pp. 844-855, 2009.

[153] A. Lea, H. Ping, J. Ollikainen, and R. G. Vaughan, "Propagation Between On-Body Antennas," *IEEE Transactions on Antennas and Propagation*, vol. 57, pp. 3619-3627, 2009.

[154] S. L. Cotton, W. G. Scanlon, and J. Guy, "The kappa-mu Distribution Applied to the Analysis of Fading in Body to Body Communication Channels for Fire and Rescue Personnel," *IEEE Antennas and Wireless Propagation Letters*, vol. 7, pp. 66-69, 2008.

[155] Y. I. Nechayev, Z. H. Hu, and P. S. Hall, "Short-term and long-term fading of on-body transmission channels at 2.45 GHz," in *Antennas & Propagation Conference, 2009. LAPC 2009. Loughborough*, 2009, pp. 657-660.

[156] L. Birgé and Y. Rozenholc, "How many bins should be put in a regular histogram," *ESAIM: Probability and Statistics*, vol. 10, pp. 24-45, 2006.

[157] D. Freedman and P. Diaconis, "On the histogram as a density estimator: L 2 theory," *Probability theory and related fields*, vol. 57, pp. 453-476, 1981.

[158] J. C. Lin, "Noninvasive microwave measurement of respiration," *Proceedings of the IEEE*, vol. 63, pp. 1530-1530, 1975.

[159] J. C. Lin, "Microwave sensing of physiological movement and volume change: a review," *Bioelectromagnetics*, vol. 13, pp. 557-65, 1992.

[160] J. C. Lin, J. Kiernicki, M. Kiernicki, and P. B. Wollschlaeger, "Microwave Apexcardiography," *Microwave Theory and Techniques, IEEE Transactions on*, vol. 27, pp. 618-620, 1979.

[161] A. Pantelopoulos and N. G. Bourbakis, "A Survey on Wearable Sensor-Based Systems for Health Monitoring and Prognosis," *Systems, Man, and Cybernetics, Part C: Applications and Reviews, IEEE Transactions on*, vol. 40, pp. 1-12, 2010.

[162] L. Changzhi, X. Yanming, and J. Lin, "Experiment and Spectral Analysis of a Low-Power K*a*-Band Heartbeat Detector Measuring From Four Sides of a Human Body," *Microwave Theory and Techniques, IEEE Transactions on*, vol. 54, pp. 4464-4471, 2006.

[163] A. D. Droitcour, O. Boric-Lubecke, V. M. Lubecke, J. Lin, and G. T. A. Kovacs, "Range correlation and I/Q performance benefits in single-chip silicon Doppler radars for noncontact cardiopulmonary monitoring," *Microwave Theory and Techniques, IEEE Transactions on*, vol. 52, pp. 838-848, 2004.

[164] P. J. Maud and C. Foster, *Physiological assessment of human fitness*: Human Kinetics Publishers, 2006, ISBN: 073604633X.

[165] CORTEX Medical - Sports - Fitness. (2012). *CORTEX centrepiece: MetaSoft® Studio*. Available: http://www.cortex-medical.de/software_mss_sp_en.htm

[166] European Commision. (2010). *Digital Agenda for Europe (DAE)*. Available: http://europa.eu/legislation_summaries/information_society/strategies/si0016_en.htm

[167] R. Mannings, *Ubiquitous positioning*: Artech House, 2008, ISBN: 1596931043.

[168] P. Bahl and V. N. Padmanabhan, "RADAR: an in-building RF-based user location and tracking system," in *INFOCOM 2000. Nineteenth Annual Joint Conference of the IEEE Computer and Communications Societies. Proceedings. IEEE*, 2000, pp. 775-784 vol.2.

[169] L. Chin-Heng, W. Yahong, B.-P. Ng, and C. M. S. See, "A Real-Time Indoor WiFi Localization System Utilizing Smart Antennas," *Consumer Electronics, IEEE Transactions on*, vol. 53, pp. 618-622, 2007.

[170] C. Komar and C. Ersoy, "Location tracking and location based service using IEEE 802.11 WLAN infrastructure," in *European Wireless*, 2004, pp. 24-27.

[171] D. Madigan, E. Einahrawy, R. P. Martin, W. H. Ju, P. Krishnan, and A. S. Krishnakumar, "Bayesian indoor positioning systems," in *INFOCOM 2005. 24th Annual Joint Conference of the IEEE Computer and Communications Societies. Proceedings IEEE*, 2005, pp. 1217-1227 vol. 2.

[172] Ekahau. (2011). *Ekahau Real Time Location System (RTLS),*. Available: http://www.ekahau.com/products/real-time-location-system/overview.html

[173] R. J. Fontana, "Recent system applications of short-pulse ultra-wideband (UWB) technology," *Microwave Theory and Techniques, IEEE Transactions on*, vol. 52, pp. 2087-2104, 2004.

[174] W. He-Wen, W. Qun, C. Zhang-Xin, and Y. Shang-Fu, "A Novel Weighted Multidimensional Scaling Analysis for Time-of-Arrival-Based Mobile Location," *Signal Processing, IEEE Transactions on*, vol. 56, pp. 3018-3022, 2008.

[175] L. M. Ni, L. Yunhao, L. Yiu Cho, and A. P. Patil, "LANDMARC: indoor location sensing using active RFID," in *Pervasive Computing and Communications, 2003. (PerCom 2003). Proceedings of the First IEEE International Conference on*, 2003, pp. 407-415.

[176] F. Seco, A. R. Jimenez, C. Prieto, J. Roa, and K. Koutsou, "A survey of mathematical methods for indoor localization," in *Intelligent Signal Processing, 2009. WISP 2009. IEEE International Symposium on*, 2009, pp. 9-14.

[177] Z. Da, X. Feng, Y. Zhuo, Y. Lin, and Z. Wenhong, "Localization Technologies for Indoor Human Tracking," in *Future Information Technology (FutureTech), 2010 5th International Conference on*, 2010, pp. 1-6.

[178] K. W. Cheung, H. C. So, W. K. Ma, and Y. T. Chan, "Least squares algorithms for time-of-arrival-based mobile location," *Signal Processing, IEEE Transactions on*, vol. 52, pp. 1121-1130, 2004.

[179] C. Steiner, *Location Fingerprinting for Ultra-wideband Systems: The Key to Efficient and Robust Localization*: Logos Verlag Berlin GmbH, 2010, ISBN: 9783832525675.

[180] D. Fox, J. Hightower, L. Lin, D. Schulz, and G. Borriello, "Bayesian filtering for location estimation," *Pervasive Computing, IEEE*, vol. 2, pp. 24-33, 2003.

[181] TinyOS website. (2011). Available: http://www.tinyos.net/

[182] F. Mikas, S. Zvanovec, and P. Pechac, "Measurement and prediction of signal propagation for WLAN systems," *Department of Electromagnetic Field, Czech Technical University, Prague*, 2003.

[183] R. Oy and J. Tamminen, "2.4 GHz WLAN Radio Interface," 2002.

[184] S. Zvanovec, M. Valek, and P. Pechac, "Results of indoor propagation measurement campaign for WLAN systems operating in 2.4 GHz ISM band," in *Antennas and Propagation, 2003.(ICAP 2003). Twelfth International Conference on (Conf. Publ. No. 491)*, 2003, pp. 63-66.

[185] M. Akay, *Time-frequency and wavelets in biomedical signal processing*. New York: IEEE Press, 1998, ISBN: 0780311477.

[186] L. Cohen, *Generalized Phase-Space Distribution Functions* vol. 7: AIP, 1966.

[187] L. Cohen, "Time-frequency distributions-a review," *Proceedings of the IEEE*, vol. 77, pp. 941-981, 1989.

Appendix A

Prototyping a Wireless Sensor Node

A.1. The microstrip patch antenna

This type of antenna is mainly affected by two factors: design topology and substrate material. In order to assess the influence of substrate layers on the antenna design, a microstrip patch is designed, printed onto a single substrate layer. The antenna topology for 2.45 GHz ISM band is shown in Fig. A.1.

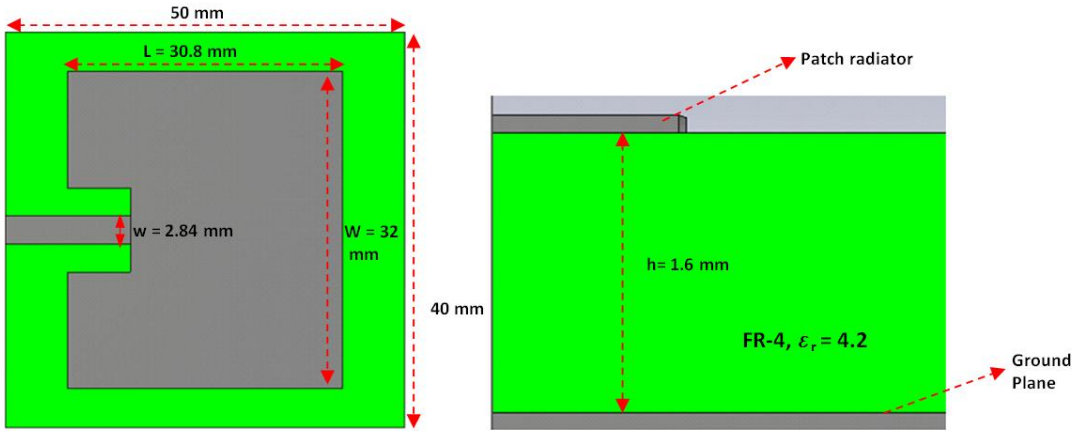

Fig. A.1 Microstrip Patch Antenna on an FR-4 substrate

The main design parameters to be considered for a successful prototype are:

- width (**W**) of the radiator,
- length (**L**) of the radiator,
- thickness (**h**) of the substrate, and
- the relative permittivity ($\boldsymbol{\varepsilon_r}$) of the substrate.

The feed of the current design is matched to a 50 Ω transmission line of width ‘w’. The radiator width (W) and the effective permittivity (ε_{eff}) are calculated using (A.1) and (A.2), respectively.

$$W=\frac{1}{2f_r\sqrt{\mu_0\varepsilon_0}}\sqrt{\frac{2}{\varepsilon_r+1}}=\frac{c}{2f_r}\sqrt{\frac{2}{\varepsilon_r+1}} \qquad (A.1)$$

$$\varepsilon_{reff}=\frac{\varepsilon_r+1}{2}+\frac{\varepsilon_r-1}{2}\left[\frac{1}{\sqrt{1+12\frac{h}{W}}}\right] \text{ only when } W/h > 1 \qquad (A.2)$$

Additionally, if the design considers the effects of fringing fields on the microstrip patch, the effective length of the antenna is calculated using (A.3) and (A.4). The ratio of change of ‘W/h’, in (A.4), causes alterations on the calculated value of the effective permittivity

$$L_{eff}=L+2L \quad \text{,where} \qquad (A.3)$$

$$L=0.412 * h\frac{(\varepsilon_{reff}+0.3)\left(\frac{W}{h}+0.264\right)}{(\varepsilon_{reff}-0.2582)\left(\frac{W}{h}+0.8\right)} \qquad (A.4)$$

Therefore, the previous analysis only defines the effective permittivity for a microstrip printed on a single substrate layer. If the antenna is on top of a multi-layer substrate for example, a stacked patch or a loaded patch antenna, equation (A.4) is no longer valid and does not represent a correct approximation for the effective permittivity.

A.2. CC2420 from Texas Instruments

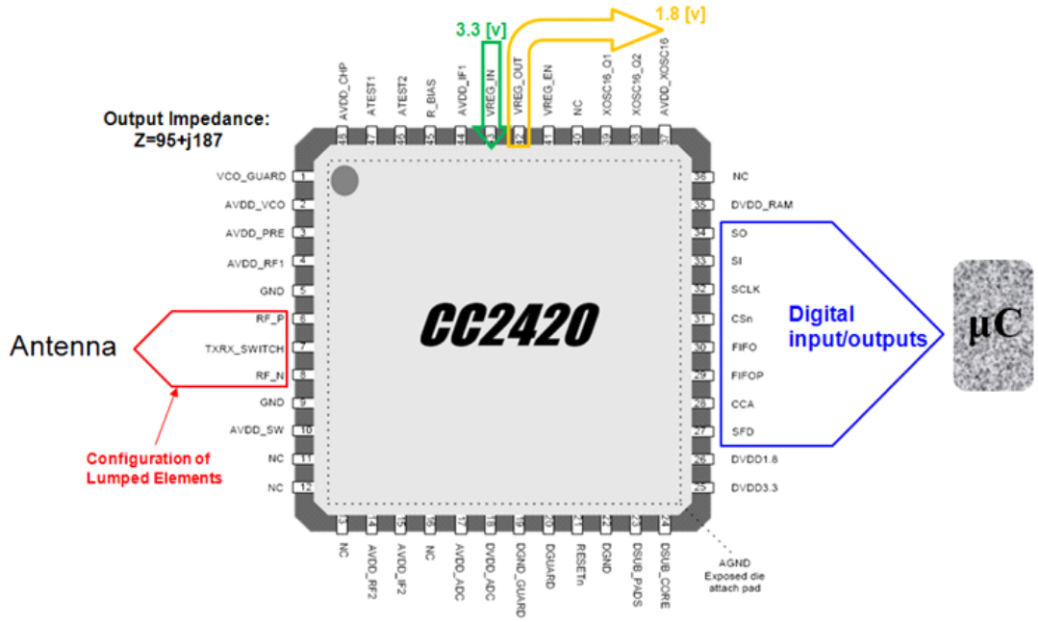

Fig. A.2. CC2420 core transceiver pin out [101].

A.3. Microcontroller board design and manufactured module

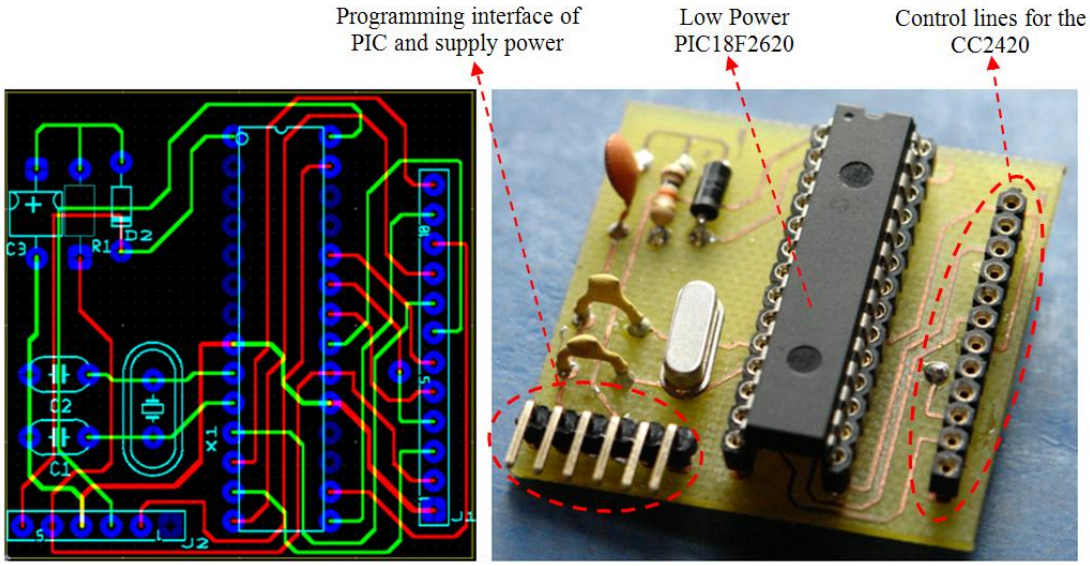

Fig.A.3.Design and implementation of the Microcontroller module that houses a low power Microchip component, the PIC18LF2620.

A.4. Radio transceiver (CC2420) board design and manufactured module.

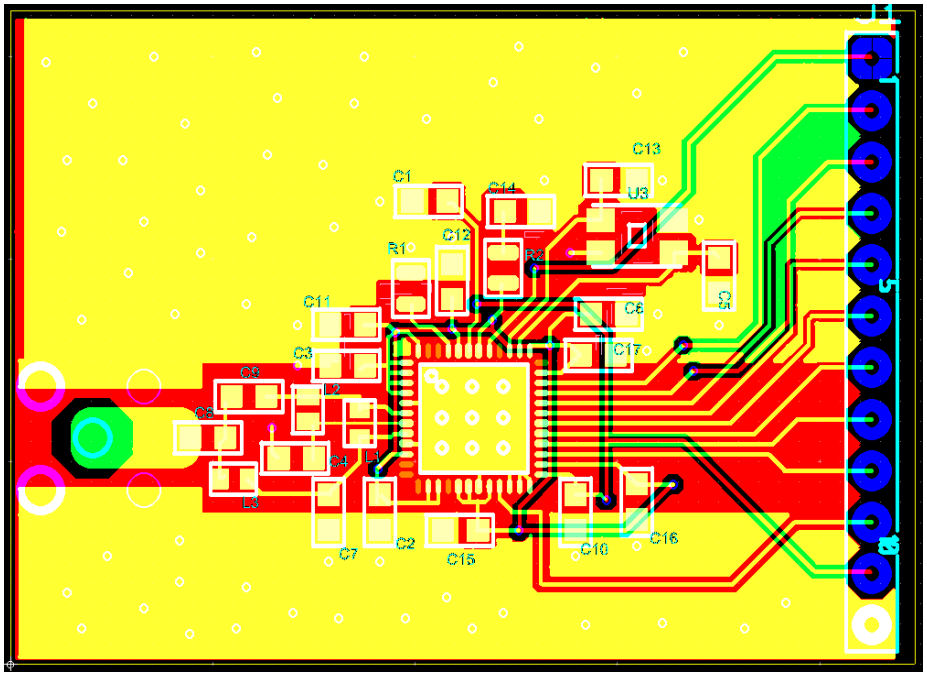

(a)

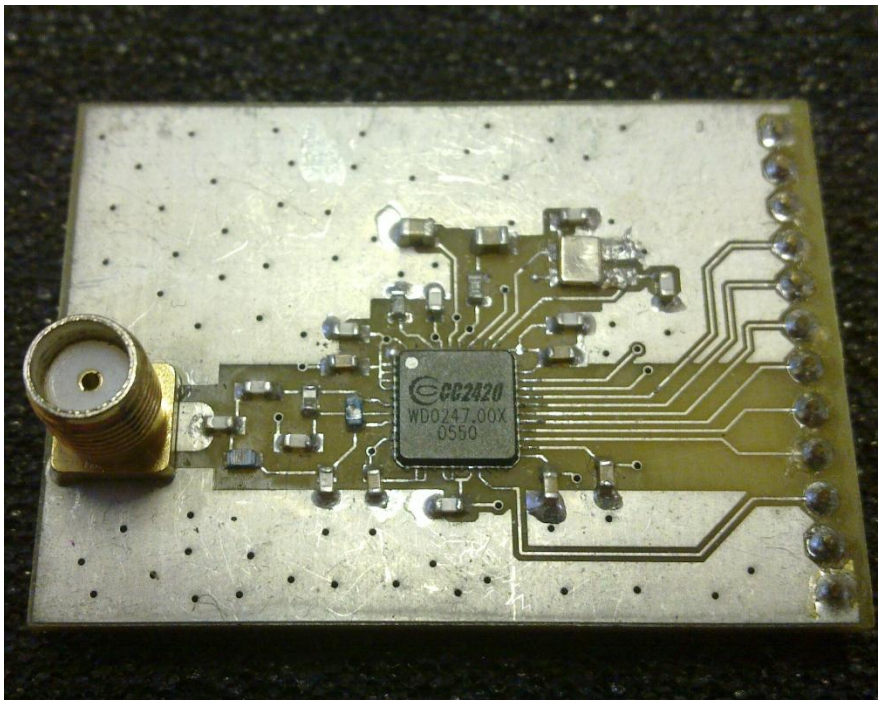

(b)

Fig.A.4.Design and implementation of the RF radio transceiver boar module that houses a Texas Instruments transceiver, the CC2420. (a) design implemented using Ultiboard software from National Instruments; (b) manufactured and assembled module

A.5. Simulation models for the impedance matching network

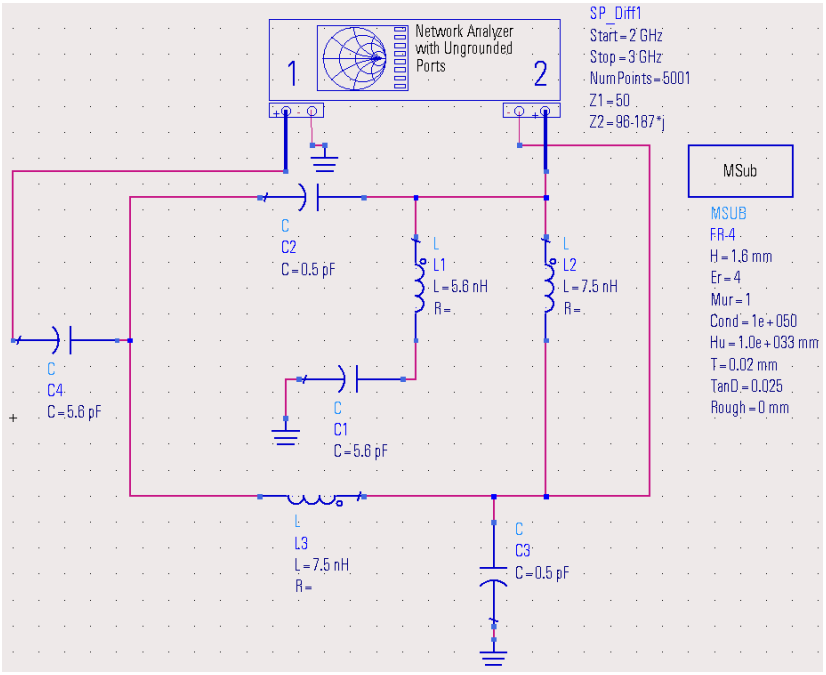

(a)

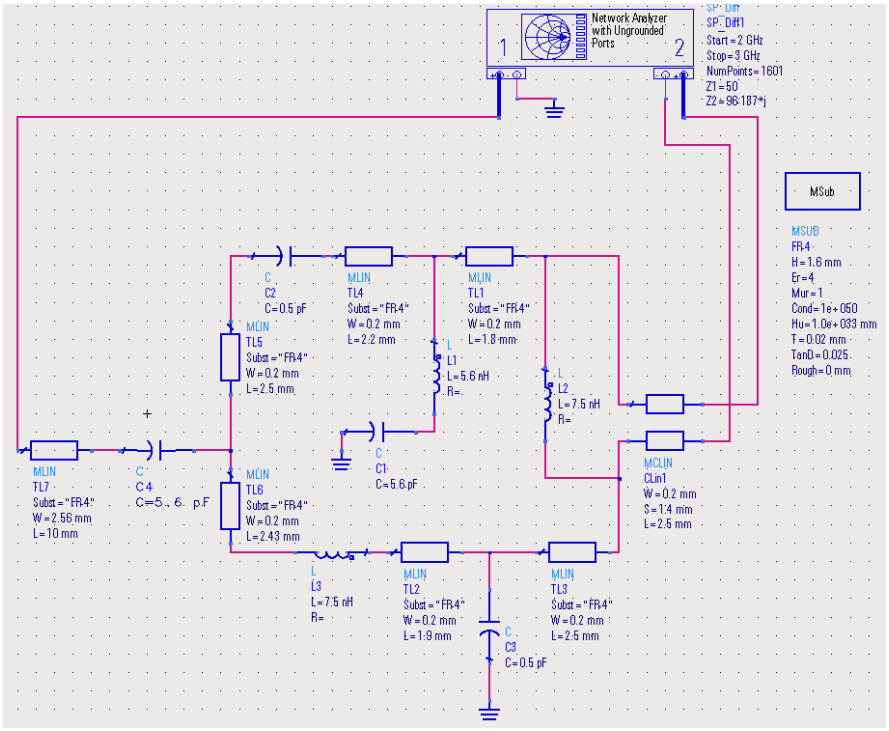

(b)

Fig.A.5. (a) Implemented design using ideal transmission lines (losless) modelled and simulated in Advanced Design System (ADS) software from Agilent; (b)implemented design using transmission lines model between passive components.

Appendix B

The IEEE 802.15.4 MAC Frame Format

B.1. The IEEE 802.15.4 MAC Frame Format

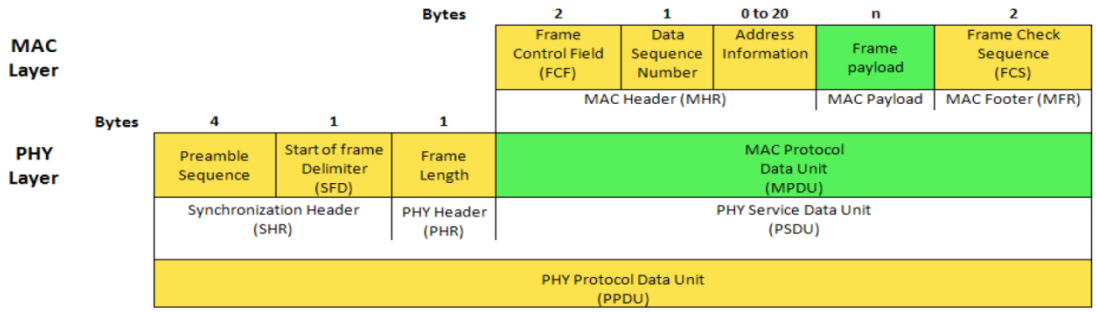

Fig. B.1.Schematic view of the IEEE 802.15.4 Frame Format.

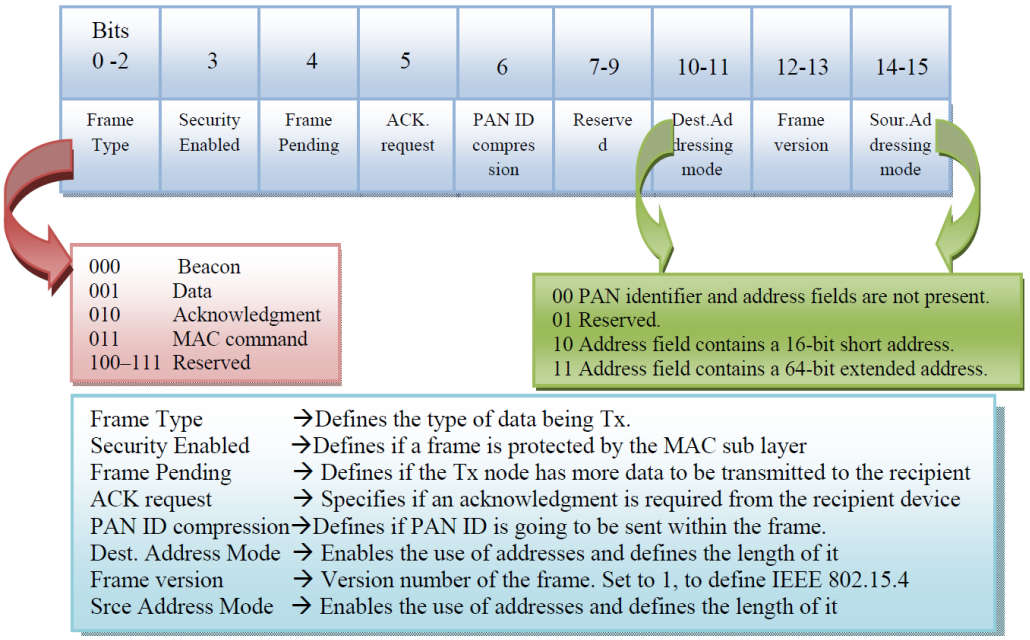

Fig. B.2.Format of the Frame Control Field (FCF).

B.2 Steps to Configure CC2420 in transmitting mode

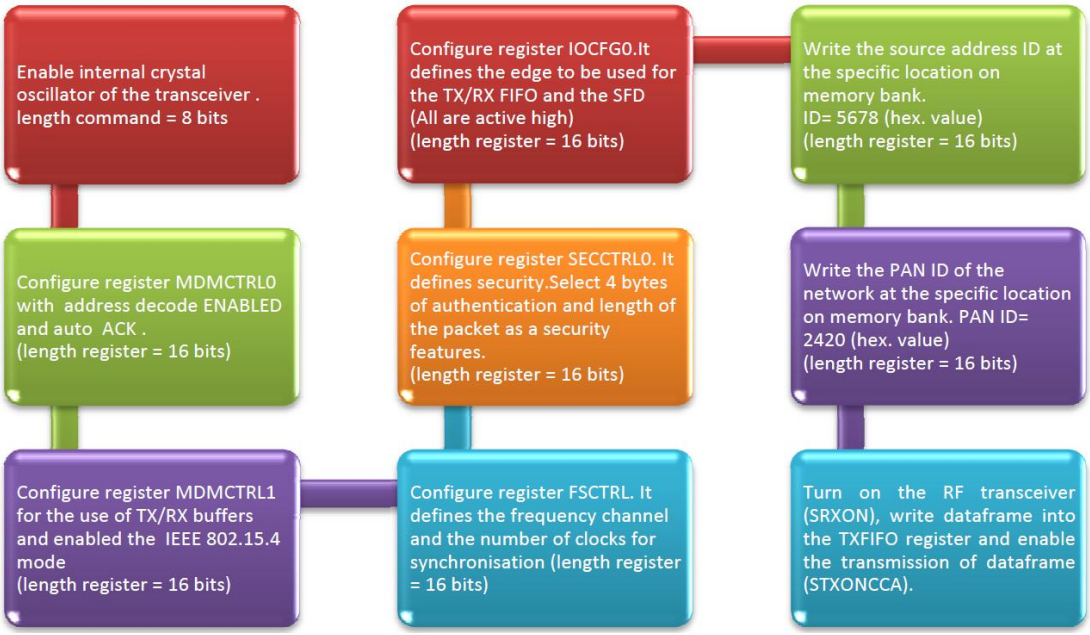

Fig.B.3.Sequential steps for a successful configuration of the CC2420 in transmitting mode.

B.3 Steps to Configure CC2420 in receiving mode

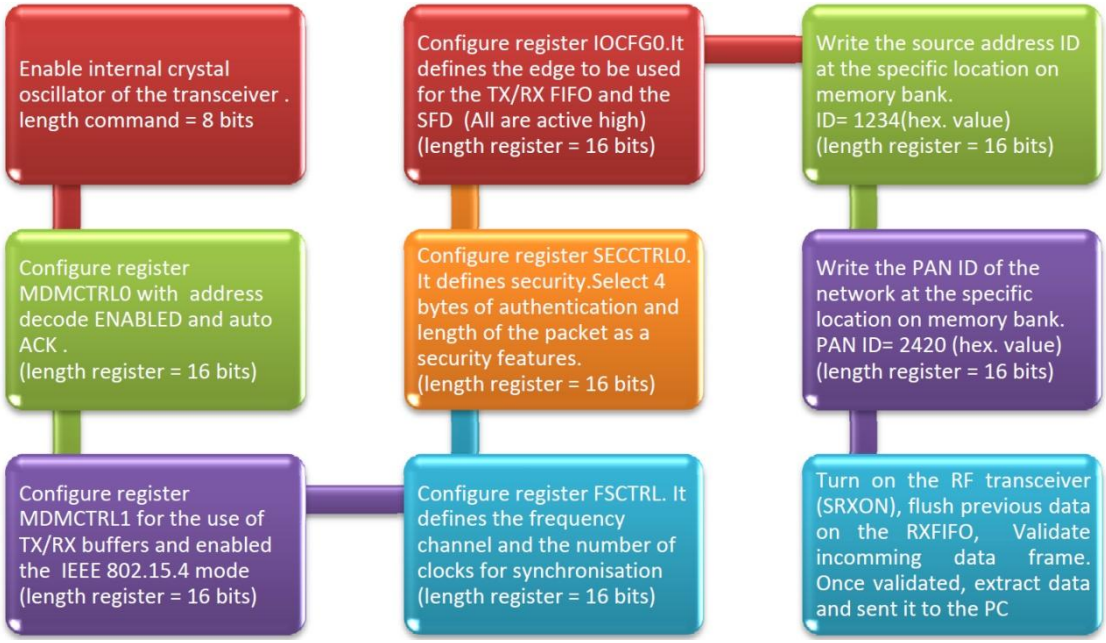

Fig.B.4.Sequential steps for a successful configuration of the CC2420 in receiving mode.

Appendix C

Short-Time Fourier Transform for Non-Stationary Signals

In chapter 6, FFT methods were used to describe the behaviour of the signal in the spectral domain; nonetheless, the truncation limits of the FFT integral and the integration over the whole time domain highlight the inherent drawback of the algorithm: the absence of the time information (local information).

Although the FFT algorithm gives an initial representation of the frequency domain, it remains unsuitable for non-stationary signals, since it is difficult to discriminate frequencies that occur at different times. A qualitative representation of the spectrum response is acquired when the FFT is screened through a short-time window where the signal's behaviour is assumed to be stationary or quasi-stationary. The screening of the FFT is accomplished by a Short-Time Fourier Transform (STFT), which for a continuous time-signal, $x(t)$, with a real window, $w(t)$is defined by (C.1):

$$STFT_x(t,\omega)=\frac{1}{\sqrt{2\pi}}\int_{-\infty}^{+\infty} x(\tau)\,w(\tau-t)\,e^{-j\omega t}d\tau \qquad (C.1)$$

The terms 't' and 'ω' in (C.1) represent the translation and modulation parameters. The observation window, $w(t)$, allows the localization of the spectrum in time, but it also smears the spectrum in frequency. The discretization of a continuous signal over a period of time is given by the sampling theorem (C.2):

$$x(t) \approx \hat{x}(t)=\sum_{n}^{N-1} x(n)\delta(t-n\tau_s) \qquad (C.2)$$

where τ_s is the sampling period. Therefore, the discrete STFT is defined by (C.3)

$$STFT_i(n,k)=\sum_{m=0}^{N-1} x(m-n)w_i(m)e^{-j2\pi mk/N} \qquad (C.3)$$

where the discrete spectrogram window is denoted as $w_{i(n)}$ and the discrete time signal as $x_{(n)}$. The implementation of STFT facilitates the analysis of variations of the signal spectrum as a function of time which are typically represented by time-frequency plots called spectrograms which are denoted as Cohen's class distributions [185-187].

The time-varying spectral representation shows an intensity plot of the STFT's magnitude. The resolution depends on the length of the window, a short time window provides good time resolution but poor frequency resolution, and a long time window provides good frequency resolution but poor time resolution; thus, the best representation depends on a trade-off of both.

The time-frequency distributions for the radio channel of different sport activities from Chapter 6 are shown in Fig. C.1. The spectrogram of a recorded ECG when the test subject was jogging is depicted in Fig. C.1a. The plot shows high intensities (resonant frequencies) around 3.3 s, 6.1 s and 7.1 s and weak energy content at other times (e.g., 0.5 s, 2s, 5 s). These show the effects of the human motion; however, the combination of weak and strong energy contours over the 8 s window still identifies heart beats.

In the case of the radio channel data recorded by custom-built wireless sensors, jogging and cycling spectrograms (see Fig. C.1b and Fig. C.1d, respectively) have

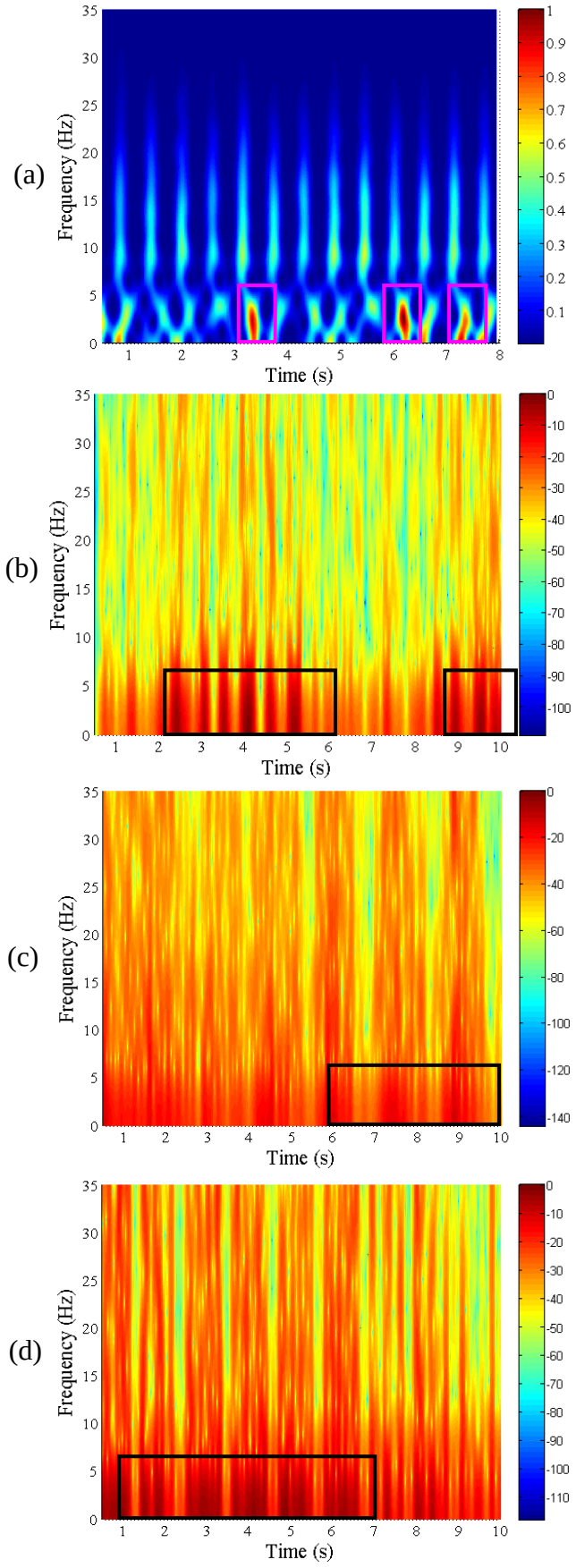

Fig. C.1. Spectrogram results while exercising at a constant speed of 5 km/h: (a) ECG recording, (b) jogging, (c) rowing and (d) cycling using a window size of (a) 256 and (b)-(d) 128

strong energy contours in the lowest frequency band with relative continuous harmonic change within 1–5 Hz. On the contrary, the recorded radio channel of a rowing scenario, shown in Fig. C.1c), indicates large amplitude variations, which are evenly distributed through both low and high frequencies (large frequency variation and time smear).

The spectrogram plots of ECG and wireless sensor recordings for a jogging scenario have shown how the energy amplitude of the harmonics gradually decays at high frequencies. In a similar way, the spectrogram plot of a jogging scenario shows that most of the energy content is evenly distributed below 5 Hz, whereas rowing and cycling scenarios have complex energy contour distributions due to the large frequency variations.

Spectrogram plots have shown the non-stationary behaviour of the recorded signals, which are accounted by the human motion including trunk and limb movement, breathing and muscle contractions of the heart. Although the time-frequency plots of wireless sensor data identify peaks of energy content at different times, it is still complex to differentiate heart movement, thus it is necessary to employ other non-linear DSP methods. Time-frequency literature describes different digital signal processing (DSP) techniques that characterise and classify non-stationary signals, such as the independent component analysis (ICA), the reduced interference distribution (RID), exponential distributions (ED) and wavelet-transforms (WT).

Appendix D

Wavelet Transform

This section use wavelet-transform (WT) for de-noising purposes on received signals acquired by custom-built wireless sensors for different sports applications. The method uses variable frequency and time resolutions to different components, also known as multi-resolution analysis, thus reducing the interference factors (de-noising). The analysis of the signal at multiple scales (variable time-frequency resolution) allows not only signal de-noising, but also pattern recognition. The multi-resolution analysis relies on being able to dilate (squeeze or expand) and translate the wavelet function derived from a basis function called the *mother wavelet* mathematically represented by (D.1):

$$\Psi_{a,b}(t)=\frac{1}{\sqrt{a}}\Psi\left(\frac{t-b}{a}\right) \qquad (D.1)$$

The terms ‘a’ and ‘b’ represent the scale and translation parameters, respectively. In the case of a discrete time-sampled signal, the *mother wavelet* is represented by (D.2). The values of ‘a’ and ‘b’ are expressed by $a = 2^j$ and $b = k * 2^j$ for $(j,k) \in \mathbb{Z}^2$.

$$\Psi_{j,k}[n]=\frac{1}{\sqrt{a_o^j}}\Psi\left(\frac{n - kb_o a_o^j}{a_o^j}\right) \qquad (D.2)$$

The discrete wavelet-transform (DWT) of a time-sampled signal $x_{(n)}$ is separated into a pair of transforms: the coarse coefficients or scaling coefficients which are related to low-frequencies and the detail coefficients, also known as wavelet coefficients for the high-frequencies. These terms are defined by (D.3) and (D.4), respectively. The term 'N' represents the length of the sample data, *j* is the level of the detail and approximation coefficients ($j \geq j_o$), 'k' is the scale index and $\phi_{j_o,k}$, $\psi_{j,k}$ are the set of orthogonal functions.

$$W_{\phi}[j_{\circ},k] = \frac{1}{\sqrt{N}} \sum_{n} x[n] \phi_{j_o,k}[n] \qquad (D.3)$$

$$W_{\psi}[j,k] = \frac{1}{\sqrt{N}} \sum_{n} x[n] \psi_{j,k}[n] \qquad (D.4)$$

This section evaluates a one-dimensional DWT for de-noising and detection of any additional feature embedded in the radio channel of custom-built wireless sensors, specifically for sports applications. The process decomposes the signal into its orthogonal functions$(\phi_{j_o,k},\ \psi_{j,k})$. The detail coefficients are compared against a fixed-form threshold, T_x, denoted by (C.5), which mitigates noise coefficients. The quantification analysis uses a hard-threshold method, where coefficients below 'T_x' are described as noise and they are set to zero (D.6).

$$T_x = \sigma\sqrt{2 \log (N)} \qquad (D.5)$$

$$W_{\psi}[j,k] = \begin{cases} W_{\psi}[j,k] & \text{if } |W_{\psi}[j,k]| > T_x \\ 0 & \text{if } |W_{\psi}[j,k]| \leq T_x \end{cases} \qquad (D.6)$$

The de-noising process is applied to each recorded activity. The results of the numerical DSP method are shown in Fig. D.1. It can be observed that each synthesized signal contains a series of energy peaks over the entire time window analysis. It is conjectured that the short peak-trains characterise the mechanical activity of the heart; even though, the beat-to-beat periods are consistent on small

time-frames (highlighted window size of 4 s, resulting in approximately 7 heartbeats).

The discontinuities on the retrieved signal are highly dependent on the quantification threshold. Hard-thresholding yields sharp transitions on signal levels, thus creating gaps in the reconstructed signal. Moreover, the human motion creates friction and, in many cases, a discontinuous attachment of the wireless sensor module from the human body.

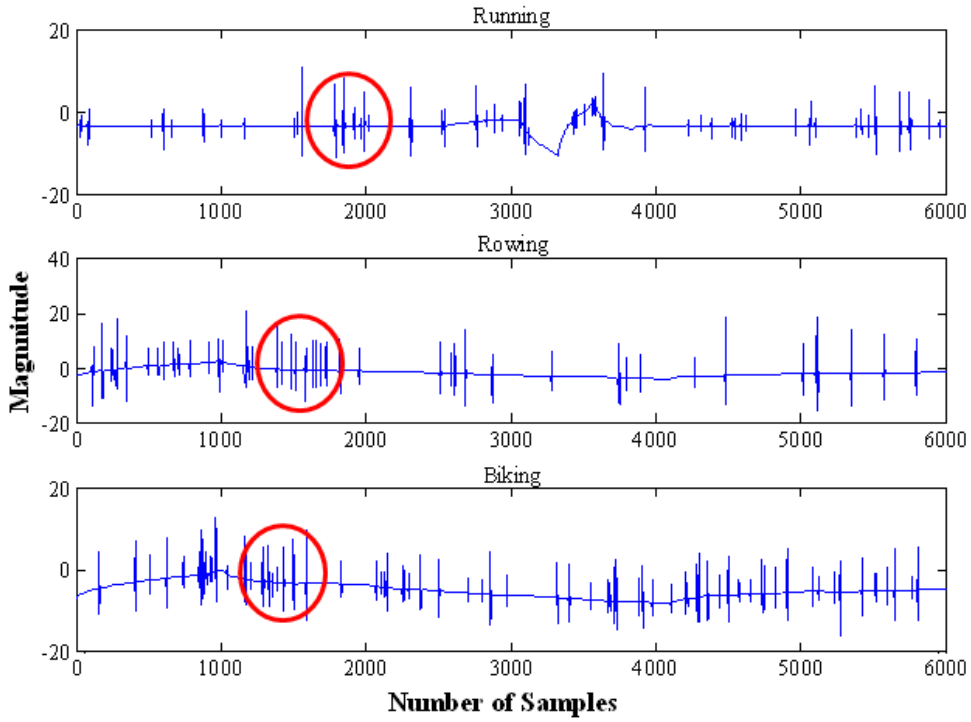

Fig. D.1.De-noising of the received signal using a one dimensional wavelet function for a) jogging, b) rowing, c) cycling.